

Nuffield Department of Clinical Neurosciences

Structural, quantitative, and functional brain MRI findings in MOGAD: a comparison with NMOSD-AQP4 and MS

A thesis submitted for the degree of Doctor of Philosophy (DPhil) in Clinical Neurosciences

Silvia Messina

St Cross College, University of Oxford

Trinity Term, 2021

Supervisors

Prof Jacqueline Palace

Prof Mark Jenkinson

In loving memory of my Father

A mio padre

Acknowledgements

This thesis would have not been possible without the support of all the people who supported me over these years in Oxford.

I will always be extremely grateful to my supervisor, Prof Palace, for giving me the opportunity to pursue my DPhil in the stimulating and nurturing environment of the University of Oxford. She shared her clinical and research expertise with me and gave me the possibility to grow as a clinician and a researcher.

I'm particularly grateful to my supervisor Prof Mark Jenkinson for sharing part of his immense knowledge of MRI analysis with me and for teaching me through his example, the scientific rigour and the passion for imaging analysis.

A special thanks to Prof Isabel Leite. She has been for me an example of a caring clinician and a passionate researcher, and I will always be grateful for her support, especially during the most difficult times.

An immense thank you to the wonderful NMO team at the John Radcliffe Hospital in Oxford. The administrative team: Alix Platt, Ralitsa Mileva, James Moore; the clinical team: Rosie Everett, Sandra Reeve, Cheryl Perkins, and Yvonne Sharawakanda; Nina Eagle, Kay Day, Annamaria Feroleto, who have been working with me through these years. The teamwork and the love for our clinical work have been our strength, especially through the difficult time of the pandemic.

I would also like to thank the OUH MS clinical trials team: Dr Matt Craner, Ana Cavey, Helen Birmingham, Christina Abarno, Joy Hodder, Sadia Ahmad, and Julia Goodgame. Their support has been crucial over these years and I'm now very proud to be part of their team with my new role. A special thanks also to the OUH MS clinical team: Prof Gabriele DeLuca, the nurses Pete Monaghan and Chris Rigozzi, for their help in recruiting the MS participants.

I would like to acknowledge the amazing WIN team in FMRIB, for giving me the opportunity to carry on my research MRI project and for their help in imaging analysis. A special thanks to the radiographers, Michael Sanders, Jon Campbell, and David Parker. Thank you to Dr Michael Cottar and Dr Hanna Nowicka for their support on diffusion analysis and Dr Fidel Alfaro Almagro for his insight on the FreeSurfer software.

A special thanks to Dr Ludovica Griffanti, not only for her insight on the MRI analysis, but most of all for her friendship over these years.

I was fortunate enough to share these years with a great group of colleagues, who became friends: Dr Romina Mariano, Adriana Roca-Fernandez, Dr Ruth Geraldes, Dr Maciej Jurynczyk, and Dr Pedro Cruz. I will always be grateful for their support and their friendship.

This research project would have not been possible without the NMOSD/MOG/MS patients and their relatives who donated their time for research. To them my greatest thank you.

I would also like to thank my friends (London-based and Italy-based), for always being there for me and supporting my decision to pursue a DPhil as a mature student and in another country.

Finally, I would like to thank my family. My mother Anna, for always supporting me over these years, since my first exam at the University to my decision to purse a DPhil, and my brother Sandro, for being family in UK and for always supporting us.

Thank you to my father, Salvatore who would have been immensely proud of this achievement, for pushing me to follow my path since I was a child.

Abstract

Structural, quantitative, and functional brain MRI findings in MOGAD: a comparison with NMOSD-AQP4 and MS

Silvia Messina, St Cross College

In the past fifteen years two new antibody mediated Central Nervous System (CNS) diseases, have been identified as distinct from multiple sclerosis (MS): Aquaporin-4-antibody (AQP4-Ab) and the more recently discovered myelin oligodendrocyte glycoprotein antibody-associated disorder (MOGAD).
Although conventional brain MRI may help distinguish MS from antibody-mediated diseases, the use of quantitative and non-conventional imaging may give more pathological information and explain the clinical differences.
This thesis comprises a clinical study, describing the main clinical characteristics of MOGAD, and a cross sectional MRI study that compares structural, quantitative and functional brain MRI findings across MOGAD, NMOSD-AQP4, MS and healthy controls.

The principal clinical finding is:

- MOGAD patients have a good recovery from visual and physical disability compared to NMOSD-AQP4, although some of them can be left with sphincter, erectile dysfunction, and cognitive impairment.

The main MRI study findings are:

- In MOGAD most of the white matter lesions tend to resolve, but patients are left with grey matter damage, and this may be related to persistent white matter lesions. Despite the greater residual disability, NMOSD-AQP4 patients showed a relative sparing of deep grey matter volumes.

- Non-lesional tissue fractional anisotropy (FA) was only reduced in MS, although focal reductions were noted in NMOSD-AQP4 patients, reflecting mainly optic nerve and corticospinal tract pathways. In MOGAD there is no abnormal non-lesional tissue FA.

- Disability (EDSS) in NMOSD-AQP4 is associated with NAWM FA alone, with deep grey matter atrophy and female sex in MS, and with brainstem volume in MOGAD. Visual acuity was associated with optic chiasm volume in NMOSD-AQP4 disease and with thalamic volume and female sex in MOGAD.

- in MOGAD, despite the good visual recovery, and the absence of structural and microstructural tissue damage, there is a reduced functional connectivity in the primary visual cortex. In NMOSD-AQP4 there is a broader involvement of the large brain networks (visual, salience, sensorimotor, default mode network), possibly related to the higher level of disability (and tissue damage), while in MS, a preferential involvement of subcortical network was found (i.e., basal ganglia).

- Cognitive performance is influenced by fatigue and depression in MOGAD and NMOSD-AQP4 but not in MS. Low cognitive score is associated with low deep grey matter volume in MOGAD and MS, while is mainly driven by cortical volume in NMOSD-AQP4.

The clinical and MRI studies from this thesis, represent some of the earliest studies directed at better understanding the MRI changes behind the clinical recovery and outcome in MOGAD. The comprehensive clinical and MRI approach, investigating not only physical disability, but also the often-neglected cognitive function, added novelty to this body of work and can open to future larger studies.

Publications related to this thesis

The use of the content of the publications related directly to this thesis is referenced in all the relevant chapters. I confirm that all the written content, figures and tables used in this thesis from these publications was produced by me and presented here with the permission of all co-authors.

Papers

Clinical presentation and prognosis in MOG-antibody disease: a UK study. Jurynczyk M*, **Messina S***, Woodhall MR*, Raza N, Everett R, Roca-Fernandez A, Tackley G, Hamid S, Sheard A, Reynolds G, Chandratre S, Hemingway C, Jacob A, Vincent A, Leite MI, Waters P, Palace J. Brain. 2017 Dec 1; 140(12):3128-3138.
* These authors equally contributed to the study

Part of the results of this paper are presented in Chapter 2.

Contrasting the brain imaging features of MOG-Antibody disease, with AQP4-Antibody NMOSD and Multiple Sclerosis. Messina S, Mariano, Roca-Fernandez A, Cavey A, Jurynczyk M, Leite MI, Calabrese M, Jenkinson M, Palace J.

Part of the results of this paper are presented in Chapter 4-6.

Abstract

Contrasting brain MRI features in Ab-mediated demyelinating diseases and MS: understanding the pathogenesis of brain damage.
S. Messina. Poster presentation, ISMRM April 2020 (Virtual)
2nd place for best poster presentation ISMRM 2020 White matter study group

Lesions distribution and normal appearing white matter in demyelinating diseases. S. Messina.
Poster presentation, Charcot Foundation meeting November 2019, Baveno, Italy.

Normal appearing white matter and lesional integrity in MOG-Ab disease and MS: a diffusion-weighted imaging study. ECTRIMS Online Library.
S. Messina. 09/11/19; 278888; P528.
Poster presentation ECTRIMS September 2019, Stockholm, Sweden.

Clinical Outcome In MOG-Antibody Disease: A Large Single Site Cohort.
S. Messina. J Neurol Neurosurg Psychiatry October 2018 Vol 89 No 10.
Oral presentation at Association of British Neurologist 2018.

Publications indirectly related to this thesis

An In-vivo 1H-MRS short-echo time technique at 7T: Quantification of metabolites in chronic multiple sclerosis and neuromyelitis optica brain lesions and normal appearing brain tissue. Tackley G, Kong Y, Minne R, **Messina S,** Winkler A, Cavey A, Everett R, DeLuca GC, Weir A, Craner M, Tracey I, Palace J, Stagg CJ, Emir U. Neuroimage. 2021 Sep; 238:118225.

Elucidating distinct clinico-radiologic signatures in the borderland between neuromyelitis optica and multiple sclerosis. Juryńczyk M, Klimiec-Moskal E, Kong Y, Hurley S, **Messina S,** Yeo T, Jenkinson M, Leite MI, Palace J. J Neurol. 2021 May 27.

The influence of smoking on the pattern of disability and relapse risk in AQP4-postitive neuromyelitis optica spectrum disorder, MOG-Ab disease and multiple sclerosis. **Messina S*,** Mariano R*, Geraldes R, et al. Mult Scler Relat Disord 2021 Apr; 49:102773.

Quantitative spinal cord MRI in MOG-antibody disease, neuromyelitis optica and multiple sclerosis. Mariano R, **Messina S,** Roca-Fernandez A, Leite MI, Kong Y, Palace JA. Brain. 2021 Feb 12;144(1):198-212.

Spinal cord and brain MRI should be routinely performed during follow-up in patients with NMOSD - No. Juryńczyk M, **Messina S,** Palace J. Mult Scler. 2021 Jan;27(1):15-16.

Prevalence and incidence of neuromyelitis optica spectrum disorder, aquaporin-4 antibody-positive NMOSD and MOG antibody-positive disease in Oxfordshire, UK. O'Connell K, Hamilton-Shield A, Woodhall M, **Messina S,** Mariano R, Waters P, Ramdas S, Leite MI, Palace J. J Neurol Neurosurg Psychiatry. 2020 Oct;91(10):1126-1128.

Seasonal distribution of attacks in aquaporin-4 antibody disease and myelin-oligodendrocyte antibody disease. Dos Passos GR, Elsone L, Luppe S, Kitley J, **Messina S**, Rodríguez Cruz PM, Harding K, Mutch K, Leite MI, Robertson N, Jacob A, Palace J. J Neurol Sci. 2020 Aug 15;415:116881.

Prodromal headache in MOG-antibody positive optic neuritis. Asseyer S, Hamblin J, **Messina S,** Mariano R, Siebert N, Everett R, Küker W, Bellmann-Strobl J, Ruprecht K, Jarius S, Leite MI, U Brandt A, Paul F, Palace J. Mult Scler Relat Disord. 2020 May; 40:101965.

Factors associated with fatigue in CNS inflammatory diseases with AQP4 and MOG antibodies. Yeo T, Dos Passos GR, Muhammed L, Everett R, Reeve S, **Messina S,** Probert F, Leite MI, Palace J. Ann Clin Transl Neurol. 2020 Mar;7(3):375-383.

The frequency of longitudinally extensive transverse myelitis in MS: A population-based study. Asnafi S, Morris PP, Sechi E, Pittock SJ, Weinshenker BG, Palace J, **Messina S,** Flanagan EP. Mult Scler Relat Disord. 2020 Jan; 37:101487.

Comparison of Clinical Outcomes of Transverse Myelitis Among Adults With Myelin Oligodendrocyte Glycoprotein Antibody vs Aquaporin-4 Antibody Disease. Mariano R, **Messina S,** Kumar K, Kuker W, Leite MI, Palace J. JAMA Netw Open. 2019 Oct 2;2(10): e1912732.

Outcome prediction models in AQP4-IgG positive neuromyelitis optica spectrum disorders. Palace J, Lin DY, Zeng D, Majed M, Elsone L, Hamid S, **Messina S,** Misu T, Sagen J, Whittam D, Takai Y, Leite MI, Weinshenker B, Cabre P, Jacob A, Nakashima I, Fujihara K, Pittock SJ. Brain. 2019 May 1;142(5):1310-1323.

Long-term disability in neuromyelitis optica spectrum disorder with a history of myelitis is associated with age at onset, delay in diagnosis/preventive treatment, MRI lesion length and presence of symptomatic brain lesions. Mealy MA, Mossburg SE, Kim SH, **Messina S,** Borisow N, Lopez-Gonzalez R, Ospina JP, Scheel M, Yeshokumar AK, Awad A, Leite MI, Arango JJ, Paul F, Palace J, Kim HJ, Levy M. Mult Scler Relat Disord. 2019 Feb; 28:64-68.

Area postrema syndrome: Frequency, criteria, and severity in AQP4-IgG-positive NMOSD. Shosha E, Dubey D, Palace J, Nakashima I, Jacob A, Fujihara K, Takahashi T, Whittam D, Leite MI, Misu T, Yoshiki T, **Messina S,** Elsone L, Majed M, Flanagan E, Gadoth A, Huebert C, Sagen J, Greenberg BM, Levy M, Banerjee A, Weinshenker B, Pittock SJ. Neurology. 2018 Oct 23;91(17): e1642-e1651.

Endocrinopathies in paediatric-onset neuromyelitis optica spectrum disorder with aquaporin 4 (AQP4) antibody. Hacohen Y, **Messina S,** Gan HW, Wright S, Chandratre S, Leite MI, Fallon P, Vincent A, Ciccarelli O, Wassmer E, Lim M, Palace J, Hemingway C. Mult Scler. 2018 Apr;24(5):679-684.

Abbreviations

CNS - Central Nervous System

MS – Multiple Sclerosis

DMT – Disease Modifying Therapy

RRMS – Relapsing Remitting Multiple Sclerosis

CIS – Clinically Isolated Syndrome

HC – Healthy control

AQP4-Ab – Aquaporin-4 Antibody

NMO – Neuromyelitis Optica

NMOSD-AQP4 – Neuromyelitis Optica Associated with Aquaporin-4 antibody

MOG-Ab – Myelin Oligodendrocytes Glycoprotein Antibody

MOGAD - Myelin Oligodendrocytes Glycoprotein Antibody Associated Disease

ON – Optic Neuritis

TM – Transverse Myelitis

LETM – Longitudinally Extensive Transverse Myelitis

ADEM – Acute Diffuse Encephalomyelitis

APS – Area Postrema Syndrome

MRI – Magnetic Resonance Imaging

DTI- Diffusion Tensor Imaging

NAWM – Normal Appearing White Matter

f-MRI – Functional MRI

RS – Resting State

RSN – Resting State Network

List of Figures

Figure 1.1 A graphic representation of the immunopathogenesis of demyelinating diseases..... 26
Figure 1.2 Examples of MRI images in MOGAD 38
Figure 1.3 Examples of MRI images in NMOSD-AQP4. 39
Figure 1.4 Examples of MRI images in MS 39
Figure 1.5 Examples of cord MRI images in MOGAD 43
Figure 1.6 Examples of cord MRI images in NMOSD-AQP4. 44
Figure 1.7 Examples of cord MRI images in MS 44
Figure 1.8 Graphical representation of the main clinical and demographic differences across MOGAD, NMOSD-AQP4 and MS. 50
Figure 2.1 Graphical representation of the different clinical features analysed in the two cohorts 65
Figure 2.2 Distribution of age at onset in Oxford MOGAD patients 67
Figure 2.3 Percentage comparison of the onset attack phenotype between female and male patients with MOGAD in the Oxford Total cohort. 70
Figure 2.4 A) density plot of age at onset in distinct MOGAD phenotype. B) percentage comparison of onset phenotype between age-class. 72
Figure 2.5 Examples of MRI brainstem lesions adjacent to 4th ventricle 74
Figure 2.6 Kaplan Meier curve showing the cumulative probability over time to remain relapse free 75
Figure 2.7 Kaplan-Meier curves showing the cumulative probability over time to remain relapse free, depending on the duration of the immunosuppression 76
Figure 2.8 Kaplan-Meier curves showing the cumulative probability over time to remain non visually disabled. 78
Figure 2.9 Kaplan-Meier curves showing the cumulative probability over time to remain non mobility disabled 79
Figure 2.10 Kaplan-Meier curves showing the cumulative probability over time to remain bladder disability free. 80
Figure 3.1 Outline of the study workflow. 88
Figure 4.1 T2 lesion analysis pipeline. 112
Figure 4.2 Pearson correlation between grey matter volumes obtained with FIRST and FreeSurfer 114
Figure 4.3 Volumetric analysis pipeline 115
Figure 4.4 A) Lesion volume across group and B) association with disease duration. 117
Figure 4.5 A) Lesion probability maps in NMOSD-AQP4, MS and MOGAD; B) Subtraction maps: MS-AQP4-Ab disease, MS-MOGAD, AQP4-Ab disease-MOGAD. 119
Figure 4.6 Voxel-wise comparison across groups 120
Figure 4.7 A) ovoid cortical lesion in an MS patient; B) an ovoid cortical/juxtacortical lesion in an MS patient; C-D) curvilinear juxtacortical lesions in two MOGAD patients. 122
Figure 4.8 The brain volume A), the white matter fraction B) and grey matter fraction C) comparison between disease groups. 123
Figure 4.9 Total deep grey matter volumes A), basal ganglia, hippocampus, and brainstem volumes B-I) between disease groups. 127
Figure 4.10 Cortex measures between groups 128
Figure 4.11 A) Optic chiasm (mm3) and B) corpus callosum (mm3) volumes between disease groups. 130
Figure 4.12 Comparison of hippocampus volumetric measures for patients with MOGAD and either a monophasic, relapsing with a brain relapse or relapsing with a non-brain relapse phenotype. 132

Figure 5.1 Study flow-chart and diffusion pipeline..... 140
Figure 5.2 tract based spatial statistics FA in NMOSD-AQP4 vs HC A), MS vs HC B), NMOSD-AQP4 vs MOGAD C), and MOGAD vs HC D) 148
Figure 0.1 FA, MD RD, and AD T2 lesion and NAWM comparison in the four groups (A-D) 142
Figure 5.4 MD in the cortex (A) and in the deep grey matter structures (B) between groups.. 149
Figure 5.5 FA in the optic radiation tract (left and right sides averaged) between groups. 150
Figure 6.1 graphical representation of the key findings 168
Figure 7.1 Resting-state analysis pipeline. 176
Figure 7.2 Resting state networks (RSNs). 181
Figure 7.3 Voxel-wise between-group difference (MOGAD<HC) in the occipital pole visual network (represented in red-yellow)..... 182
Figure 7.4 Voxel-wise between-group differences (AQP4-Ab<HC) in various networks (represented in red-yellow)..... 183
Figure 7.5 Voxel-wise between-group difference (MS<HC) in the medial visual and basal ganglia networks (represented in red-yellow) 184
Figure 7.6 Voxel-wise between-group difference (AQP4-Ab<MOGAD) in the salience, executive function and sensorimotor networks (represented in red-yellow)..... 185
Figure 7.7 Voxel-wise between-group difference in the executive function (AQP4-Ab<MS) and frontostriatal networks (MS<MOGAD) (represented in red-yellow 185
Figure 7.8 Medial (A), lateral (B) and occipital pole (C) visual cortex network WNC between disease group. 189
Figure 7.9 Medial (A), lateral (B) and occipital pole (C) visual cortex WNC between participants with normal and impaired VA. 191
Figure 7.10 visual cortex network WNC between participants with normal and impaired VA in the three disease groups. 193
Figure 7.11 WNC in the medial visual network (A), lateral visual network (B) and occipital pole visual network (C) between participants with or without at least one episode of ON in the NMOSD-AQP4 and MOGAD group. 197
Figure 7.12 WNC in the medial visual network (A), lateral visual network (B) and occipital pole visual network (C) between the NMOSD-AQP4-ON and MOGAD-ON participants, based on the time from the last episode of ON..... 199
Figure 7.13: WNC in the medial visual network (A), lateral visual network (B) and occipital pole visual network (C) between the NMOSD-AQP4-ON and MOGAD-ON participants, based on the time from the last episode of ON..... 200
Figure 7.14 Salience network WNC between disease groups. 201
Figure 7.15 Salience network WNC between “pain” and “no pain” groups. 202
Figure 7.16 Salience network WNC between “pain’ and “no pain” participants in the three disease groups..... 203
Figure 7.17 Sensorimotor network average WNC between disease groups..... 205
Figure 7.18 Sensorimotor network WNC between the high disability (EDSS≥4) and the low disability (EDSS<4 groups)..... 207
Figure 7.19 Sensorimotor network WNC between the high disability subgroup (EDSS≥4) and the low disability subgroup (EDSS<4) across disease groups. 208
Figure 7.20 Auditory network WNC between disease groups 210
Figure 8.1 Outline of this chapter workflow 225
Figure 8.2 Cognitive test score between disease groups (A-J). 233
Figure 8.3 Brain MRI of the participants classified as cognitively impaired (four MOGAD, two NMOSD-AQP4 and two MS, as an example). 237
Figure 8.4 The association between cognitive index and the grey matter structure measures in the three disease groups. 239
Figure 8.5 representation of the significant association between the cognitive index/cognitive domain scores and the grey matter structure measures in the three disease groups..... 240
Figure 8.6 The association between fatigue score and grey matter volume measures. 243
Figure 8.7 The association between cognitive index and fatigue score 246

List of Tables

Table 1.1 Neuromyelitis Optica Diagnostic Criteria. Table adapted from Wingerchuk et al 2015 with permission. All rights reserved. 21
Table 2.1 Demographics and clinical features of the Oxford Prevalent and Incident Cohorts ... 67
Table 2.2 Comparison of demographics and clinical features in female and male patients with MOGAD in the Oxford Total cohort. 68
Table 2.3 Comparison of demographics and clinical features in Caucasians and Non-Caucasians 70
Table 3.1 MRI imaging protocol 100
Table 3.2 Clinical and demographic characteristics of the studied cohort. 102
Table 4.1 Clinical and demographic characteristics of the studied cohort. 109
Table 4.2 Cortical/juxtacortical lesion number across the disease groups. 121
Table 4.3 Brain volume, white and grey matter fraction estimates, SE and p-value across groups 123
Table 4.4 Third and fourth ventricle volume estimates, SE and p-value across groups. 123
Table 5.1 Clinical and demographic characteristics of the studied cohort. 140
Table 5.2 Summary of the key-findings. 150
Table 6.1 Final model after multivariate linear regression across the disease groups (MOGAD, NMOSD-AQP4, MS); EDSS: dependent variable. CI=95% confidence intervals 160
Table 6.2 Final model after multivariate linear regression in the NMOSD-AQP4 group; EDSS: dependent variable. CI=95% confidence intervals 161
Table 6.3 Final model after multivariate linear regression in the MOGAD group; EDSS: dependent variable. CI=95% confidence intervals 161
Table 6.4 Final model after multivariate linear regression in the MOGAD group; EDSS: dependent variable. CI=95% confidence intervals 161
Table 6.5 Final model after multivariate linear regression in the whole disease group (MOGAD, NMOSD-AQP4 and MS); Visual Acuity: dependent variable. CI=95% confidence intervals. 162
Table 6.6 Final model after multivariate linear regression in the NMOSD-AQP4 group; Visual Acuity: dependent variable. CI=95% confidence intervals 163
Table 6.7 Final model after multivariate linear regression in the MOGAD group; Visual Acuity: dependent variable. CI=95% confidence intervals 163
Table 6.8 Final model after multivariate linear regression in the MS group; Visual Acuity: dependent variable. CI=95% confidence intervals 163
Table 7.1 Clinical and demographic characteristics of the RS-fMRI cohort 171
Table 7.2 RSNs obtained from group-ICA. 178
Table 7.3 Statistical peaks of significant resting state networks (RSNs) across groups (TFCE corrected p-values), organized by contrast (voxel-wise analysis). Coordinates are reported in mm in Montreal Neurological Institute (MNI) space. When more clusters were significant, the largest was represented in the table 185
Table 7.4 Age and sex adjusted comparisons of within network connectivity (WNC) values, Bonferroni corrected, across groups. 188
Table 7.5: multiple linear regression model for WNC, age and sex adjusted, between optic chiasm and the visual networks in the three disease groups 193
Table 7.6: multiple linear regression model for WNC, age and sex adjusted, between thalamus volume and the visual networks in the three disease groups 193
Table 7.7: multiple linear regression model for WNC, age and sex adjusted, between optic radiation FA and the visual networks in the three disease groups 194
Table 7.8 Age and sex adjusted comparisons of WNC, Bonferroni corrected, in the NMOSD-AQP4 and MOGAD, based on the occurrence of at least one episode of ON, and HC. 196
Table 7.9 : Age and sex adjusted comparisons of WNC, Bonferroni corrected, in the four groups. 199

Table 7.10 Multiple linear regression model, age and sex adjusted, between pain score the WNC in and the salience network in the three disease groups. 202
Table 7.11 Age and sex adjusted comparisons of WNC, Bonferroni corrected, in the four groups. 204
Table 7.12 Multiple linear regression model of WNC, age and sex adjusted, between pain score and the sensorimotor network in the three disease groups. 207
Table 7.13 Age and sex adjusted comparisons of WNC, Bonferroni corrected, in the four groups. 209
Table 7.14 Multiple linear regression model of WNC, age and sex adjusted, between pain score and the auditory network in the three disease groups..... 210
Table 7.15 Summary of the key-findings. Voxel-wise analysis results of disease group vs HC. 218
Table 8.1 Clinical and demographic characteristics of the studied cohort. 229
Table 8.2 Raw scores of the cognitive assessment in the studied cohorts..... 232
Table 8.3 Age, sex and education adjusted comparisons of the cognitive scores, Bonferroni corrected, across groups. 233
Table 8.4 Fatigue score comparisons, Bonferroni corrected, across groups. 239
Table 8.5 Cognitive fatigue score comparisons, Bonferroni corrected, across groups 239
Table 8.6 Physical fatigue score comparisons, Bonferroni corrected, across groups 240
Table 8.7 Psychosocial fatigue score comparisons, Bonferroni corrected, across groups 240
Table 8.8 Summary of the key-findings 245
Table 9.1 : Summary of the key MRI findings. 256

Table of Contents

1 Chapter 1 Introduction and Background 19

1.1 The spectrum of demyelinating diseases 19

1.2 A focus on MOGAD: a comparison with NMOSD-AQP4 and MS 23

1.2.1 Immunopathology 23
1.2.2 Pathology 26
1.2.3 Epidemiology 28
1.2.4 Clinical features 31
1.2.5 Disease course and prognosis 34
1.2.6 Conventional brain MRI findings 35
1.2.7 Other conventional MRI findings 40
1.2.8 Other investigations 45
1.2.9 Treatment 46
1.2.10 Understanding MOGAD: knowledge gap and challenges 48

1.3 Non-conventional brain MRI in MOGAD: a comparison with NMOSD-AQP4 and MS 51

1.3.1 Structural MRI 51
1.3.2 Advanced Quantitative MRI 53
1.3.3 Resting State MRI 57

1.4 Thesis overview 58

1.4.1 The main aims of the thesis 58
1.4.2 Structure of the thesis 59

2 Chapter 2 Clinical presentation and prognosis in MOGAD: The Oxford cohort 61

2.1 Introduction and background 61

2.1.1 Objectives 62
2.1.2 Hypothesis 62

2.2 Material and methods 63

2.2.1 Ethics 63
2.2.2 Cohorts 63
2.2.3 Oxford total cohort 63
2.2.4 Oxford incident cohort 64

2.3 Statistical Analysis 65

2.4 Results 65

2.4.1 Demographic Data 65
2.4.2 Disease presentation – Oxford Total cohort 70
2.4.3 Disease course – Oxford Incident cohort 73
2.4.4 Second attack – Oxford Total cohort 74
2.4.5 Treatment and relapse risk – Oxford Incident cohort 74
2.4.6 Disability outcome – Oxford Total cohort 75
2.4.7 Poor outcome predictors - Oxford Total cohort 80
2.4.8 Acute brain MRI involvement 81

2.5 Discussion 81

2.6 Conclusion 85

3 Chapter 3 MRI study overview: methods, clinical assessment, and cohort 86

3.1 Introduction and Background 86

3.2 Study design 87
3.2.1 Ethics 88
3.2.2 Consideration for powering the study 88
3.2.3 Study participants recruitment 89
3.3 Study visits and clinical data 90
3.3.1 Motor disability 91
3.3.2 Visual Disability 91
3.3.3 Cognitive function 92
3.3.4 Pain score 94
3.3.5 Fatigue Score 95
3.3.6 Anxiety and Depression scores 95
3.4 MRI hardware and acquisition protocol 96
3.4.1 Brain imaging hardware 96
3.4.2 Sequence Development 96
3.4.3 Structural MRI sequences 98
3.4.4 Diffusion Imaging sequence 98
3.4.5 Resting state imaging sequence 99
3.4.6 Double Inversion Recovery sequence 99
3.4.7 Brain Imaging Protocol 99
3.5 Data collection 101
3.5.1 Data protection 101
3.6 Analysis overview 101
3.7 The study cohort 103
3.7.1 Disability and disease activity outcomes 103
3.7.2 Pain score 104
3.7.3 Fatigue scores 104
3.7.4 Anxiety and Depression scores 105
3.8 Limitations 106
3.9 Conclusions 106
4 Chapter 4 Lesion distribution and volumetric changes in demyelinating disease: a structural MRI study 107
4.1 Introduction and Background 107
4.1.1 Objectives 108
4.1.2 Hypotheses 108
4.1 Material and Methods 108
4.1.3 Subjects 108
4.1.4 MRI images 109
4.1.5 MRI Analysis 110
4.1.6 Statistical Analysis 114
4.2 Results 115
4.2.1 Lesion number and lesion volume 116
4.2.2 Lesion probability maps 117
4.2.3 Cortical lesion analysis 120
4.2.4 Volumetric analysis 122
4.2.5 Lesion volume and grey matter volumes in NMOSD-AQP4, MOGAD and MS 130
4.2.6 Monophasic and relapsing MOGAD 130
4.3 Discussion 131
4.4 Conclusions 135

5 Chapter 5 Lesional and non-lesional tissue integrity in demyelinating diseases: a diffusion MRI study ... 136

5.1 Introduction and Background ... 136
5.1.1 Objectives ... 137
5.1.2 Hypothesis ... 138

5.2 Methods ... 139
5.2.1 Subjects ... 139
5.2.2 Statistical Analysis ... 140

5.3 MRI Imaging protocol ... 141
5.3.1 Image Analysis ... 141

5.4 Results ... 144
5.4.1 Tract-based spatial statistics of NAWM FA ... 144
5.4.2 ROI analysis ... 146

5.5 Discussion ... 149

5.6 Conclusions ... 154

6 Chapter 6 Clinical outcomes and their association with structural and diffusion imaging findings in demyelinating diseases ... 156

6.1 Introduction and Background ... 156
6.1.1 Objective ... 157
6.1.2 Hypothesis ... 158

6.2 Methods ... 158
6.2.1 Subjects and clinical measures ... 158
6.2.2 MRI measures ... 158
6.2.3 Statistical Analysis ... 159

6.3 Results ... 160
6.3.1 Disability – EDSS ... 160
6.3.2 Disability - Visual acuity ... 162

6.4 Discussion ... 164

6.5 Conclusions ... 166

7 Functional connectivity analysis in the spectrum of demyelinating diseases: the sensory and motor networks ... 167

7.1 Introduction and Background ... 167
7.1.1 Objectives ... 169
7.1.2 Hypothesis ... 170

7.2 Methods ... 170
7.2.1 Subjects ... 170
7.2.2 MRI RS-sequence ... 171
7.2.3 MRI preprocessing ... 172
7.2.4 RSNs analysis ... 173
7.2.5 Statistical analysis ... 175

7.3 Results ... 176
7.3.1 Identifying the main RSNs ... 176
7.3.2 Comparing the RSNs across the groups using voxel-wise analysis ... 179
7.3.3 WNC analysis of the sensory/motor RSNs of interest ... 186

7.4 Discussion ... 211

7.5 Conclusions ... 218

8 Chapter 8 The "invisible" symptoms in CNS demyelinating disorders: cognition and fatigue, and their imaging correlates ... 220

8.1 Introduction ... 220
8.1.1 Objectives ... 222
8.1.2 Hypothesis ... 222

8.2 Methods ... 223
8.2.1 Subjects ... 223
8.2.2 Cognitive Assessment ... 224
8.2.3 MRI measures ... 225
8.2.4 Statistical Analysis ... 226
8.2.5 Analysis of imaging data ... 228

8.3 Results ... 228
8.3.1 Cognitive function ... 230
8.3.2 Cognition: the role of the grey matter ... 236
8.3.3 Fatigue ... 238
8.3.4 Fatigue: the role of grey matter ... 240
8.3.5 The influence of fatigue, depression, and anxiety on cognition ... 243

8.4 Discussion ... 244

8.5 Conclusion ... 251

9 Chapter 9 Discussion ... 253

9.1 Introduction ... 253

9.2 Aims and key findings of the thesis ... 253

9.3 Towards a better understanding of MOGAD: filling the gaps ... 258

9.4 Future steps: translating the findings into clinical practice ... 260
9.4.1 Integrating clinical management and research ... 263

9.5 Conclusions ... 264

10 Bibliography ... 266

11 Appendix ... 286

1 Chapter 1 Introduction and Background

1.1 The spectrum of demyelinating diseases

In recent years the understanding of central nervous system (CNS) inflammatory demyelinating diseases has grown exponentially and has led to the discovery of two conditions, different from Multiple Sclerosis (MS).

MS is the most common demyelinating disease of the CNS, thus the most studied. The clinical picture is heterogeneous and the patients can present with symptoms affecting the visual, motor, sensory and cerebellar systems (Compston and Coles, 2008). Since Charcot first described the MS pathological findings, the understanding of the pathogenesis, diagnosis and treatment have grown considerably (Charcot and Oliver, 1876). Pre-Disease modifying therapy (DMT)-era natural history studies have shown that around 85% of patients presented with a relapsing course (RRMS) and that around 40% of them after 10 years would switch towards a progressive stage (Weinshenker et al., 1989).

Neuromyelitis Optica (NMO) is a severe relapsing inflammatory disease of the CNS that can mimic MS, with a predisposition to affect the optic nerve and the spinal cord. In 1894, Eugene Devic and Fernand Gault described a series of patients with optic neuritis and acute myelitis, and they used for the first time the term "*neuro-myélite optique aiguë*" (English translation: acute neuromyelitis optica)(Jarius and Wildemann, 2013). This led to the eponymous naming of this condition as "Devic's disease"(Devic, 1894).

For many years "Devic's disease" was considered as a severe variant of MS due to the similarity in clinical presentation (Mandler et al., 1993). In 1999, Wingerchuk and colleagues described NMO as more severe compared to MS and often associated with other autoimmune conditions (Wingerchuk et al., 1999). In addition, pathology studies

revealed a vasculocentric immunoglobulin and complement deposition in the demyelinating lesions. In light of these findings, a central role of B cells in the pathogenesis of NMO was suggested (Lucchinetti et al., 2002).

The discovery of the pathogenic antibodies (Ab) to aquaporin-4 (AQP4) water channels in 2004, confirmed what the clinical and pathological observations suggested: NMO associated with AQP4-Ab, is distinct from MS, and the demyelination is secondary to the astrocytes damage induced by the presence of the antibodies (Lennon et al., 2004; Lennon et al., 2005).

In 2006 the diagnostic criteria were updated including the presence of AQP4 antibodies in serum. Patients were required to have both optic neuritis and acute myelitis and at least two of three supportive criteria: (1) A contiguous spinal cord MRI lesion extending over >3 vertebral segments (2) Brain MRI not meeting diagnostic criteria for MS and (3) NMO-IgG seropositive status (Wingerchuk et al., 2006). In recent years, the recognition of an antibody-positive limited form of NMO (i.e. isolated optic neuritis or transverse myelitis) and brain/brainstem syndrome, led to the use of a unifying term, NMO spectrum disorder (NMOSD) which encompass all different presentations (Wingerchuk et al., 2007a). The term NMOSD and the MRI findings to support the diagnosis were included in the updated 2015 diagnostic criteria, together with the definition of seronegative NMOSD (Wingerchuk et al., 2015)(see Table 1.1).

Table 1.1 Neuromyelitis Optica Diagnostic Criteria. *Table adapted from Wingerchuk et al 2015 with permission. All rights reserved.*

Diagnostic criteria for NMOSD with AQP4-IgG
1. *At least 1 core clinical characteristic* *2. Positive test for AQP4-IgG using best available detection method (cell-based assay strongly recommended)* *3. Exclusion of alternative diagnoses*
Diagnostic criteria for NMOSD without AQP4-IgG or NMOSD with unknown AQP4-IgG status
1. At least 2 core clinical characteristics occurring as a result of one or more clinical attacks and meeting all of the following requirements: *a. At least 1 core clinical characteristic must be optic neuritis, acute myelitis with LETM, or area postrema syndrome* *b. Dissemination in space (2 or more different core clinical characteristics)* *c. Fulfilment of additional MRI requirements, as applicable* *2. Negative tests for AQP4-IgG using best available detection method, or testing unavailable* *3. Exclusion of alternative diagnoses*
Core clinical characteristics
1. *Optic neuritis* *2. Acute myelitis* *3. Area postrema syndrome: episode of otherwise unexplained hiccups or nausea and vomiting* *4. Acute brainstem syndrome* *5. Symptomatic narcolepsy or acute diencephalic clinical syndrome with NMOSD-typical diencephalic MRI lesions* *6. Symptomatic cerebral syndrome with NMOSD-typical brain lesions*
Additional MRI requirements for NMOSD without AQP4-IgG and NMOSD with unknown AQP4-IgG status
1. *Acute optic neuritis: requires brain MRI showing (a) normal findings or only nonspecific white matter lesions, OR (b) optic nerve MRI with T2-hyperintense lesion or T1-weighted gadolinium enhancing lesion extending over >1/2 optic nerve length or involving optic chiasm* *2. Acute myelitis: requires associated intramedullary MRI lesion extending over ≥3 contiguous segments (LETM) OR ≥3 contiguous segments of focal spinal cord atrophy in patients with history compatible with acute myelitis (figure 1)* *3. Area postrema syndrome: requires associated dorsal medulla/area postrema* *4. Acute brainstem syndrome: requires associated periependymal brainstem lesions*

A new pathogenic antibody directed against the myelin oligodendrocytes glycoprotein (MOG) expressed on the outer surface of the myelin sheet, has been identified in ADEM (initially mostly in the paediatric patients) and AQP4-Ab negative NMOSD (Brilot et al.,

2009; Kitley et al., 2012b) and patients with atypical MS findings (Berger et al., 2003; Klawiter et al., 2010).

Recently, the development of a cell-based assay (CBA) directed against the conformational epitope of MOG, led to the identification of a demyelinating disease associated with MOG antibodies (MOGAD) as distinct from MS (Waters et al., 2015).

When the research presented in this thesis was conducted, the understanding of MOGAD was very limited and most of the clinical and MRI findings described here were not known.

The main aim of this chapter is to set the scene for the results presented in the following chapters. First, the main clinical, MRI and pathology characteristics of MOGAD and the comparison to NMOSD associated with AQP4-Ab (NMOSD-AQP4) and MS, will be described. The existing literature of non-conventional MRI use applied to demyelinating disease and the knowledge gap will be described. Finally, the thesis structures and the main research questions will be outlined. As most of the early studies focused on both AQP4-Ab positive and negative NMOSD, the term NMOSD will be used in this chapter, to include both.

The findings presented in this thesis have improved the clinical understanding of MOGAD and are among the first studies using non-conventional MRI as a tool to better understand the pathogenesis of this condition.

1.2 A focus on MOGAD: a comparison with NMOSD-AQP4 and MS

In this section MOGAD will be described and compared to NMOSD-AQP4 and MS, focussing on the distinctive features and the common findings.

1.2.1 *Immunopathology*

MOG is a glycoprotein of 218 amino acids and is expressed in oligodendrocytes of the CNS of mammals (Brunner et al., 1989; Linington et al., 1988), but account only for a small portion of all myelin proteins. MOG has been detected in humans in the corpus callosum at the time of birth (Kang et al., 2011). As the expression of MOG starts later, compared to the other myelin protein, it has potential as a marker of myelin maturation and structure (Reindl and Waters, 2019). In primates, there are different isoforms of MOG (α isoform or β isoform), based on their intracellular c-terminal amino acids (Boyle et al., 2007). Although the biological role of MOG in the CNS is not clear, it is known that it can trigger a demyelinating response in experimental models of inflammatory demyelinating disease (Iglesias et al., 2001; Peschl et al., 2017).

Early studies, using immunoblots or an enzyme-linked immunosorbent assay (ELISA), suggested that MOG-Ab were present in a proportion of patients with MS (Lindert et al., 1999; Reindl et al., 1999). However, the high percentage of MOG-Ab in the healthy controls (>10% in some studies) and other demyelinating diseases, highlighted the inconsistency of these findings.

Following studies, using more specific radioimmunoprecipitation assays (RIA) did not find an association between MOG and MS, demonstrating that immunoblots and ELISA were inconsistent methods to define a clinical entity, as they used the linear and refolded short isoform of MOG as a substrate for the assay, thus detecting the non-specific, non-

native MOG epitopes, which can be present in healthy controls and other diseases (Lampasona et al., 2004; O'Connor et al., 2005).

The use of the natively folded MOG as a substrate for an RIA assay showed that MOG-Ab were present in 19% of children with ADEM, and only in 1% of other diseases and 2% of MS. This work showed for the first time that MOG-Ab were associated with a phenotype different from MS and represented a stepping-stone towards a better understanding of MOGAD as a distinct clinical entity (O'Connor et al., 2007).

Cell-based assays (CBA), where the cells expressing the protein of interest are incubated with the patients' sera, were also used in MOG-Ab disease studies, showing differing results (Haase et al., 2001; Lalive et al., 2006; Zhou et al., 2006).

The use of an IgG1-specific secondary antibody increased the specificity of the assay and enabled the detection of MOG-Ab in patients with ADEM, isolated optic neuritis, isolated transverse myelitis and AQP4-Ab negative NMOSD, and more recently cortical encephalitis with seizures (Hardy et al., 2016; Kitley et al., 2014b; Ogawa et al., 2017; Waters et al., 2015).

The live CBA with IgG1 as a secondary antibody is currently the most accurate assay for the detection of MOGAD and all MOGAD participants in this thesis have been tested with this assay.

As shown in the previous section, the presence of AQP4-Ab enabled the definition of NMOSD as an entity distinct from MS (Lennon et al., 2004). The AQP4 is a water channel and is localised in perivascular and peripial astrocytic end-feet, in contact with the endothelium and the pia, respectively, and it is also present in the ependymal cells (Jarius et al., 2008). Two isoforms are relevant in human, the "a" isoform (M1) and the

"c" isoform (M23). The M23 homotetramers and M1/M23 heterotetramers can assemble and form orthogonal arrays of particles. (Amiry-Moghaddam and Ottersen, 2003; Rossi et al., 2012).

In NMOSD, the presence of the antibody directed against the AQP4 water channel, cause an astrocytopathy, where demyelination is a secondary event. The antibodies are present in up to 70% of patients, and as illustrated above, they are part of the diagnostic criteria (Wingerchuk et al., 2015). CBA assay is the most sensitive and specific to detect AQP4-Ab and has been used to test the NMOSD-AQP4 participants included in this thesis (Waters et al., 2012; Wingerchuk and Weinshenker, 2014). The antibody-negative NMOSD is a heterogeneous group, which likely include patients with atypical MS or other undiscovered antibodies (Juryńczyk et al., 2021). Given the difficulty in defining this group, antibody negative NMOSD patients were not included in the studies of this thesis.

MS is a chronic, immune-mediated disease, where demyelination, inflammation and oligodendrocytes damage can be present (Filippi et al., 2018). MS has been considered for a long time a predominantly T cells mediated disease, where aberrant activated T cells pass the blood-brain (BBB) barrier to damage the oligodendrocytes directly in the CNS. In the last years, the role of B cells and myeloid cells, and their interaction with T cells, have been recognised (Dendrou et al., 2015). Additionally, B cell depletion therapies have shown a beneficial effect in both the relapsing and the progressive stage of the disease (Hauser et al., 2017; Rose and Cohen, 2020). Myelin antigens are suspected to be involved and several antibodies (including MOG-Ab) and potential antigens have been proposed as involved in the pathogenesis of the disease (Yu et al., 2020). However, none

of them has shown a clear association with MS (see Figure 1.1 for a graphic representation of the different disease targets).

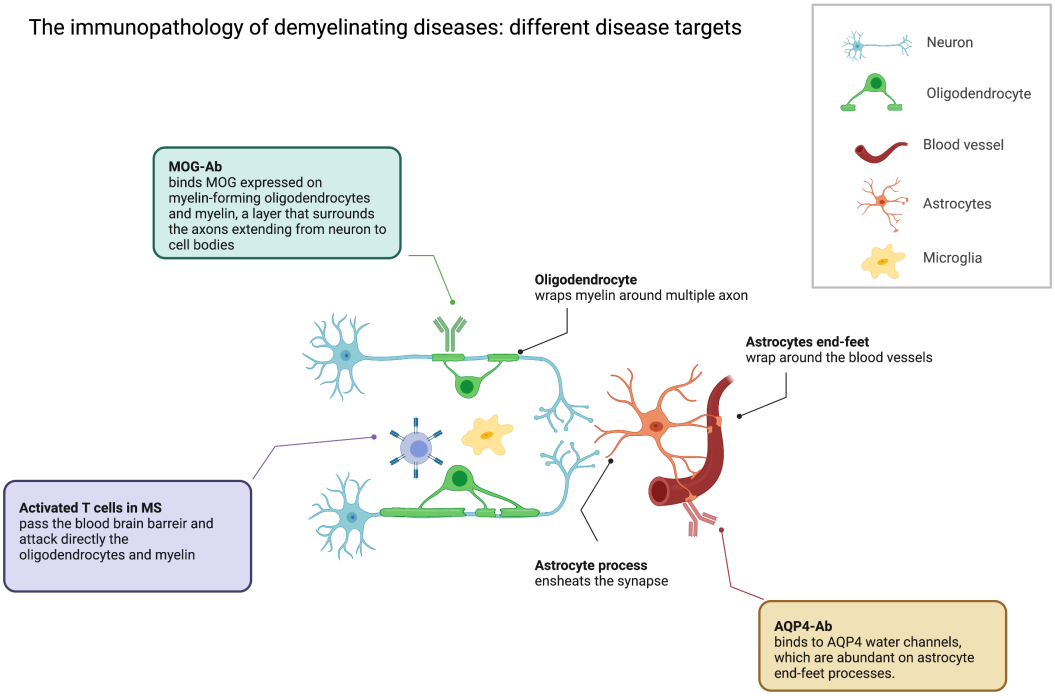


Figure 1.1 A graphic representation of the immunopathogenesis of demyelinating diseases. *The AQP4-Ab binds to the AQP4 water channel, localised in the end-feet of the astrocytes. Specific MOG-Ab binds to MOG, which is expressed on the outermost myelin sheet in the oligodendrocytes. In MS, activated T cells, together with B cells and Natural Killers (not represented), pass the blood-brain barrier, and together with the resident microglia and the astrocytes, contribute to the oligodendrocyte's injury. Created with BioRender.com*

1.2.2 *Pathology*

Early pathology studies in MOGAD described perivascular demyelination with partial axonal preservation and complement activation in the active lesions, in keeping with the features described in humoral immune-mediated MS demyelination (MS pathology pattern II) (Jarius et al., 2016b; Körtvélyessy et al., 2017; Spadaro et al., 2015a). The presence of confluent lesions, similar to those seen in MS, has been described in a

subgroup of ADEM and in a recent study of brain biopsies (Höftberger et al., 2020; Young et al., 2010).

However, recently a predominance of perivascular ADEM-like demyelination in MOGAD and lack of complement deposition was observed, suggesting that possibly confluent lesions and complement activation are seen in the later stage of the disease (Takai et al., 2020). Infiltrates of lymphocytes in the wall of small vessels, mimicking a vasculitis, has been described in two brain biopsy of MOGAD patients, although fibrinoid necrosis, an hallmark of small vessel vasculitis, was not present (Patterson et al., 2019). The lymphocyte infiltration of the vessel in MOGAD can result in perivascular contrast enhancement on MRI (Komatsu et al., 2019), mimicking Chronic lymphocytic inflammation with pontine perivascular enhancement responsive to steroids (CLIPPERS) appearance (Obeidat et al., 2021).

Lymphocyte perivascular cuffing, associated with the lack of a demyelination pattern, have been also described in the unilateral cortical encephalitis, a recently identified MOGAD phenotype, presenting clinically with seizure and cortical hyperintensity visible on FLAIR MRI (Ikeda et al., 2018).

NMOSD-AQP4 is an autoimmune astrocytopathy where demyelination is a secondary event. The key findings in NMOSD are the loss of AQP4 immunoreactivity on the astrocytes and the perivenular complement and immunoglobulin deposition (Takai et al., 2021). Antibody-dependent cell-mediated cytotoxicity, complement-dependent cytotoxicity and internalisation of AQP4-channels may also play a role in the pathogenesis of lesion (Bennett et al., 2009; Hinson et al., 2012; Zhang and Verkman, 2013). AQP4 channels are expressed in the diencephalon, the area postrema, and at a higher proportion in the optic nerve and spinal cord. The lesion distribution mirror the localisation of the AQP4 water channel in the CNS (Pittock et al., 2006b).

Clinical observations and natural history studies have shown that in MS the inflammatory component is common in the early relapsing stage of the disease; while neurodegeneration plays a more prominent role in the progressive stage, when physical disability and cognitive impairment are more evident (Hemmer et al., 2015). The hallmarks of MS pathology are focal demyelinating lesions, typically located around postcapillary venules, associated with a dysregulation of the BBB. The aberrant B and T cells, pass through the abnormal BBB, causing further demyelination, oligodendrocytes loss and neuro-axonal degeneration (Frohman et al., 2006; Lucchinetti et al., 2000). Lesions can occur in both white and grey matter, throughout the CNS. Although the anatomical location is associated with symptoms, the white matter lesion volume is moderately associated with disability and cognitive impairment, suggesting that other pathological mechanisms, such as cortical lesion and normal-appearing white/grey matter coexist (Calabrese et al., 2010b; DeLuca et al., 2015; Lassmann, 2018; Rocca et al., 2015; Sormani et al., 2009).

1.2.3 *Epidemiology*

1.2.3.1 Incidence and prevalence

MOGAD has been recently recognised as a distinct clinical condition, therefore the real frequency in the population is largely unknown.

NMOSD epidemiology studies have shown in Spain and Denmark a prevalence ranging from 0.89-1.09/100,000, and an incidence ranging from 0.07 and 0.63 million persons-year (Papp et al., 2018; Sepúlveda et al., 2018). A recent Dutch nationwide study reported an incidence of 1.6/million person-years (de Mol et al., 2020).

A comparison of incidence and prevalence between MOGAD and NMOSD-AQP4 in Oxfordshire showed that MOGAD was almost twice more common than NMOSD-AQP4 with a prevalence of 2.0/100 000 in MOGAD versus 1.2/100 000 in NMOSD-AQP4, and an incidence of 3.4/million person-years in MOGAD versus 2.0/million person-years in NMOSD-AQP4 (O'Connell et al., 2020).

The prevalence and incidence of NMOSD vary based on ethnicity (Hor et al., 2020). A recent worldwide systematic review found the highest incidence and prevalence in the Afro-Caribbean region (0.73/100 000 person-years and 10/100 000 persons) and the lowest incidence and prevalence in Australia and New Zealand (0.037/100 000 person-years and 0.7/100,000 persons) (Papp et al., 2021).

Despite being more frequent than NMOSD-AQP4, MOGAD is rarer than MS, which has a prevalence ranging from 8.62/100 000 in South-East Asia, to 142.81/100 000 in Europe. According to Public Health England figures released in 2020, the current prevalence in England is 190/100 000 (Walton et al., 2020).

1.2.3.2 Environmental and genetic factors

MOGAD studies exploring environmental risk factors are scarce. Recently, a detrimental effect of smoking on recovery from onset attack, especially after transverse myelitis, has been shown (Messina et al., 2021a). Infections and vaccinations have been reported as preceding an attack, however further studies are needed to clarify the association (Jarius et al., 2016c).

One study, investigating the HLA alleles in MOGAD, did not find any significant association, while in the most recent study a weak protective association of HLA-C*03:04 was observed (Bruijstens et al., 2020b; Grant-Peters et al., 2021).

In NMOSD, among the environmental factors, a potential protective role of infection in early life has been postulated, while smoking has been associated with attack severity and disability (Graves et al., 2014; Laurent Kremer, 2015; Messina et al., 2021a; Varela F). Other environmental factors, such as diet, low vitamin D, infection and vaccination preceding the attack, have been proposed, but further studies are needed to confirm the association and the causality (Eskandarieh et al., 2018; Gao et al., 2019; Jarius et al., 2012; Mealy et al., 2018). Several studies, in different ethnic groups, have found associations with HLA alleles (Asseyer et al., 2020), which are in line with a genome-wide association study, suggesting that the genetic variance of the MHC is a risk factor for NMOSD-AQP4 in people with European ancestry (Estrada et al., 2018).

Migration studies, showing that the risk of MS for those who migrated from low-risk areas to high-risk areas before adolescence, is similar to that of those who were born in the high-risk countries, highlighted the role of environmental risk factors in MS. Early life infection (i.e. EBV), smoking, and metabolic factors such as low vitamin D and adolescent obesity, are among the most studied risk factors in MS, where a complex interplay with genetic factors may contribute to the aetiology (Marrie, 2011). In particular, a recent study showed that smoking in MS, can increased the risk of progression, but not the risk of relapse (Messina et al., 2021a).

1.2.3.3 Demographics

Large national studies showed a preponderance of the female sex in MOGAD ranging from 49% to 57%. The ethnicity breakdown appears to mirror the ethnic background of the studied population. In the UK, with a prevalent white local population (87.1%), 85.7% of MOGAD patients were white, while in Sri Lanka, with a local population of 75% of

Sinhalese, 85% of MOGAD patients were Sinhalese. The mean age at onset in MOGAD is 26-37 years (Cobo-Calvo et al., 2018; Jurynczyk et al., 2017b; Senanayake et al., 2019). NMOSD-AQP4 is more common in non-white ethnicity (i.e., Asian and Afro-Caribbean) with a mean age at onset of 40 years and a female preponderance of 9:1 (Kitley et al., 2012a).

MS is more common in the white population, with a female sex ratio of 2:1 and a younger age at onset (~20-30 years old), compared to NMOSD-AQP4 (Compston and Coles, 2008).

1.2.4 *Clinical features*

Over the time in which the studies presented in this thesis were conducted, no large studies exploring the clinical, demographic features and clinical outcome of MOGAD were published. Most of the clinical presentation and disease course features presented in this introductory chapter were derived from the clinical study presented in Chapter 3, and the other larger studies which followed (Cobo-Calvo et al., 2018; Jurynczyk et al., 2017b). MOGAD encompass a spectrum of different phenotypes, which includes optic neuritis (unilateral or bilateral), transverse myelitis, acute demyelinating encephalomyelitis (ADEM), neuromyelitis optica, and more recently cortical encephalitis. It can affect both children and adult and can be monophasic or relapsing (Jurynczyk et al., 2019).

The most common onset phenotype is optic neuritis (31% unilateral optic neuritis and 24% bilateral optic neuritis) (Jurynczyk et al., 2017b). Optic neuritis in MOGAD is typically anterior, can present with papillitis, although a long lesion of the optic nerve, with occasional involvement of the chiasm, can be present (Ramanathan et al., 2016). It can be preceded by intense migraine-like pain, more frequently than in NMOSD-AQP4 (Asseyer et al., 2020). Transverse myelitis represents 14% of the onset phenotype.

Classically, it presents as a longitudinal extended transverse myelitis and the conus involvement is common (Kitley et al., 2014a). An incomplete cord syndrome, mostly associated with short cord lesions has also been described, especially with older age at presentation (Jurynczyk et al., 2017b).

The ADEM, ADEM-optic neuritis and the monophasic ADEM (MDEM), are more common in children, while ADEM-like presentation (i.e., brainstem attack and no features of encephalopathy) are more common in adult patients (Hennes et al., 2017; Jurynczyk et al., 2017b).

Recently, a purely cortical encephalitis has been described associated with MOG-Ab. Unilateral/bilateral cortical encephalitis can present with seizures, sometimes behavioural changes, and focal neurological symptoms (Ikeda et al., 2018; Ogawa et al., 2017).

NMOSDA-AQP4 presents more commonly with optic neuritis and transverse myelitis, although some patients can present with brainstem, brain involvement and less commonly encephalopathy secondary to large brain lesions. Optic neuritis is more commonly unilateral and preceded or associated with pain on eye movement (Jarius et al., 2012; Jarius et al., 2016c). A transverse myelitis can present with symptoms ranging from mild sensory symptoms to a severe complete cord syndrome, and can be isolated or associated with optic neuritis (Jarius et al., 2020a). Persistent sphincter dysfunction associated with conus lesions are less common in NMOSD-AQP4 than in MOGAD (Mariano et al., 2019). Lesions in the area postrema can present with intractable nausea, hiccups and vomiting and can precede the onset of other neurological symptoms (i.e., ON or LETM) (Wingerchuk et al., 2015). The involvement of the diencephalon can cause narcolepsy, anorexia, inappropriate diuresis, hypothermia, and hypersomnia (Dutra et al., 2018; Tsagkas et al., 2021). The large brain lesions causing encephalopathy are more common

in NMOSD-AQP4 children (McKeon et al., 2008). Other common symptoms of brain involvement are hemiparesis or cerebellar symptoms (Jarius et al., 2020a).

In MS, the clinical presentation depends on the location of the demyelinating lesions in the CNS. The symptom onset is usually acute/subacute and generally less severe than NMOSD-AQP4 and MOGAD (Filippi et al., 2018; Jarius et al., 2020a).

1.2.4.1 Brain involvement and cognition

Brain involvement can leave patients with cognitive deficit, fatigue, and mood disturbance.

The cognitive function has not been fully studied in MOGAD, although ADEM studies have documented cognitive deficits, especially in children (Armangue et al., 2020; Bruijstens et al., 2020a; Hacohen et al., 2018b).

Some case reports have shown progressive cognitive impairment in MOGAD children with progressive leukodystrophy-like demyelinating pattern (Hacohen et al., 2018a; Yazbeck et al., 2021), in MOGAD children with atypical brain demyelination associated with NMDAR-Ab (Nan et al., 2021), and MOGAD adult with a vasculitis-like pathology and/or brain cortical involvement (Baba et al., 2019; Jain et al., 2021). Recently, a paediatric study using the academic performance as a proxy of cognitive impairment, showed that cognition is affected in 26% of MOGAD children, was more frequent in younger children (≤10 years-old) and associated with deep grey matter lesions on MRI (Deiva et al., 2020).

To date there are no studies, systematically investigating the cognitive function in adult MOGAD, therefore it plausible that the burden of cognitive impairment in the adult MOGAD population with brain involvement is largely underestimated.

One recent study has correlated cognitive scores with MRI features and the methods and results will be discussed in Chapter 8 (Zhuo et al., 2020).

The presence of cognitive impairment in NMOSD-AQP4 is still a matter of debate. It is not clear if cognitive impairment is a general feature of NMOSD patients, or if it is only observed in those with brain involvement. Additionally, it is difficult to compare the existing studies, as different cognitive batteries have been used and on mixed cohorts, where both AQP4-Ab positive and negative patients were assessed (Oertel et al., 2019).

Cognitive impairment has been extensively studied in MS and has been described in up to 65% of patients (Messina and Patti, 2014). Cognitive impairment in MS is a dynamic process, where abnormal information processing speed is present in the earlier stage, and memory and executive dysfunction are prevalent at a later stage (Wojcik et al., 2021).

MRI studies have shown that deep grey matter pathology is the main imaging correlate of cognitive performance in MS, while cortex volume is a predictor of cognitive decline (Eijlers et al., 2018).

1.2.5 *Disease course and prognosis*

Despite similar attack severity, MOGAD patients have a better recovery with a lower risk of long-term disability compared to NMOSD-AQP4 (Jurynczyk et al., 2017b; Kitley et al., 2012a).

In MOGAD disability is relapse related and appear to be mainly driven by the recovery from the onset attack, although longer follow up data are needed. MOGAD can be monophasic or relapsing. Early studies showed a bias towards a more relapsing phenotype, due to the inclusion of non-incident retrospectively collected cohorts, since patients presenting after onset will be biased towards those with relapses (Jurynczyk et al., 2017b).

The long-term clinical outcome, together with the effect of long-term steroids on relapse risk, will be analysed and discussed in Chapter 2.

In NMOSD-AQP4, the presence of AQP4-Ab is a prognostic factor for a relapsing course, and patients will relapse if left untreated (Tackley et al., 2016; Weinshenker et al., 2006). Also, in NMOSD-AQP4 disability is relapse-related, and progressive phenotype are extremely rare (Wingerchuk et al., 2007b). Patients of African origin may have a higher risk of further attack, especially cerebral attack, with younger patients having a higher risk of visual disability and older patients a higher risk of motor disability (Palace et al., 2019).

In MS, most of the patients present with relapses, with 40% of relapsing-remitting MS becoming secondary progressive after 10 years (Vukusic and Confavreux, 2003). However, DMTs may reduce this percentage (Rollot et al., 2021). A minority of patients (~13%) present with a progressive disease since onset (primary progressive disease).

1.2.6 *Conventional brain MRI findings*

MRI plays a fundamental role in the diagnosis, and monitoring of long-term outcome and disease activity in demyelinating diseases (Gasperini et al., 2019). Conventional MRI refers to the sequences commonly used in clinical practice, namely T1, FLAIR, T2 and PD.

Despite MOGAD and NMOSD-AQP4 are both antibody-mediated disease with two different cells targets (i.e., oligodendrocytes in MOGAD and astrocytes in NMOSD-AQP4), conventional brain and spinal cord MRI features may overlap (Jurynczyk et al., 2017a). About 45% of MOGAD patients at onset present with brain lesions (Cobo-Calvo et al., 2018; Ramanathan et al., 2018). The most common brain MRI finding in MOGAD is “fluffy” (poorly demarcated) (Figure 1.2 A), and infratentorial lesions (cerebellum,

cerebellar peduncle) often adjacent to the 4th ventricle (see Figure 1.2 D-F). However typical NMOSD lesions (close to the 3rd ventricle, periaqueductal and area postrema lesions) have also been described (Jurynczyk et al., 2017c). Cases of unilateral cortical encephalitis, presenting with seizures and cortical hyperintensities on MRI (FLAIR) (see Figure 1.2 B, showing a cortical lesion on T2), and thalamus lesions (see Figure 1.2 C) in the acute stage (Cobo-Calvo et al., 2018), have been described, suggesting a preferential involvement of the grey matter in MOGAD (Ikeda et al., 2018). A recent clinical MRI study showed that temporal lobe lesions, and mostly the cerebellar peduncle lesions are more frequent in MOGAD than NMOSD-AQP4 (Matsumoto et al., 2021).

In paediatric MOGAD, ADEM is the most common phenotype, and the MRI typically shows large (>2 cm) T2 lesions, poorly demarcated, affecting the subcortical area, the deep white and the deep grey matter (Baumann et al., 2018; Konuskan et al., 2018). In younger children (<7 years), diffuse, symmetrical T2 lesions, mimicking a leukodystrophy disease, have been described (Baumann et al., 2020; Hacohen et al., 2018a).

Although it was thought that the brain is relatively spared in NMOSD (Wingerchuk et al., 1999), brain lesions have been reported in up to 60% of NMOSD patients (Pittock et al., 2006a). NMOSD lesions show a different distribution compared with MS, mirroring the expression of AQP4 in astrocyte end-feet, as demonstrated by immunopathological and MRI studies (Pittock et al., 2006b; Roemer et al., 2007). NMOSD lesions in the brain occur adjacent to the ventricular system around the third and fourth ventricle and the aqueduct of Sylvius, and the area postrema (see Figure 1.3 A-C). However, “MS-like” brain lesions (10-42% of NMOSD-AQP4 patients) and non-specific brain lesions (see Figure 1.3 D) have been described (Asgari et al., 2011; Matthews et al., 2013; Pittock et al., 2006a).

The distribution of MS lesions in the brain on MRI follows the distribution of the demyelinating plaques, as described in histopathology studies. MS lesions in the brain are ovoid, with a periventricular location, often perpendicular to the corpus callosum (Dawson's fingers), reflecting the perivenular distributions of demyelinating plaques (Jurynczyk et al., 2019) (Barkhof et al., 1997; Cerqueira et al., 2018) (see Figure 1.4 A-C). The presence of lateral and inferior temporal lobe lesions, or Dawson's fingers or U/S shaped juxtacortical lesions have been described as the main discriminant between MS and Ab-mediated diseases (Jurynczyk et al., 2016; Jurynczyk et al., 2017a; Matthews et al., 2013). Additionally, the absence of typical MS lesions (cortical/juxtacortical lesions, absence of periventricular lesions, absence of Dawson's fingers), the presence of long transverse myelitis lesions and periependymal lesions along the lateral ventricle, can discriminate NMOSD-AQP4 from MS with even a higher sensitivity and specificity (Cacciaguerra et al., 2019).

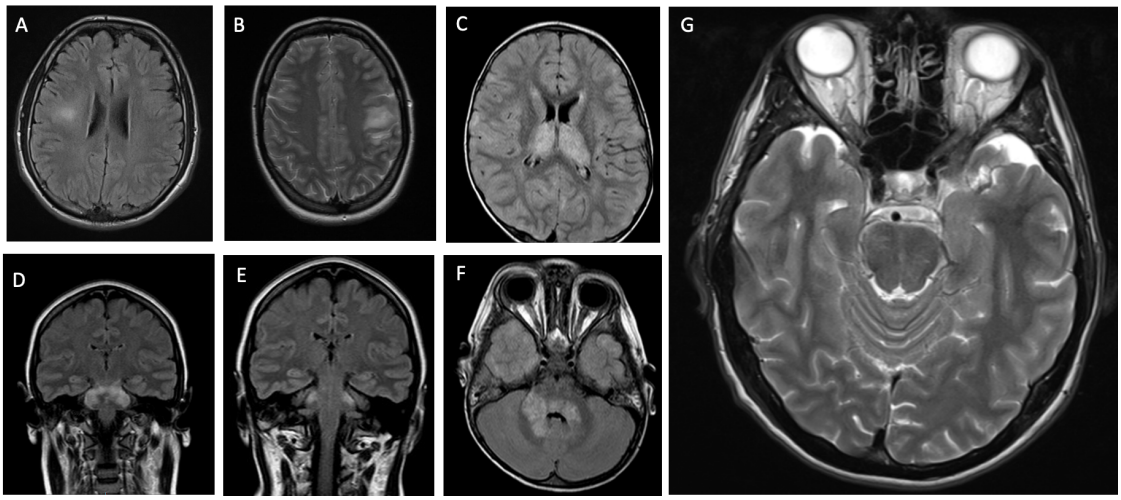


Figure 1.2 Examples of MRI images in MOGAD. *A) Axial FLAIR showing "fluffy" parenchymal lesion, B) Axial T2 showing cortical/subcortical lesion. C) Axial FLAIR showing a basal ganglia lesion D) Coronal FLAIR showing a pons lesion E) Coronal FLAIR image showing bilateral cerebellar peduncle lesion F) Axial FLAIR showing a "fluffy" cerebellar peduncle lesion, adjacent to the 4th ventricle. G) Axial T2 showing anterior hyperintensity in the optic nerves bilaterally. (NHS MRI, patients consented under Tissue Bank Ref: 10/H0606/56).*

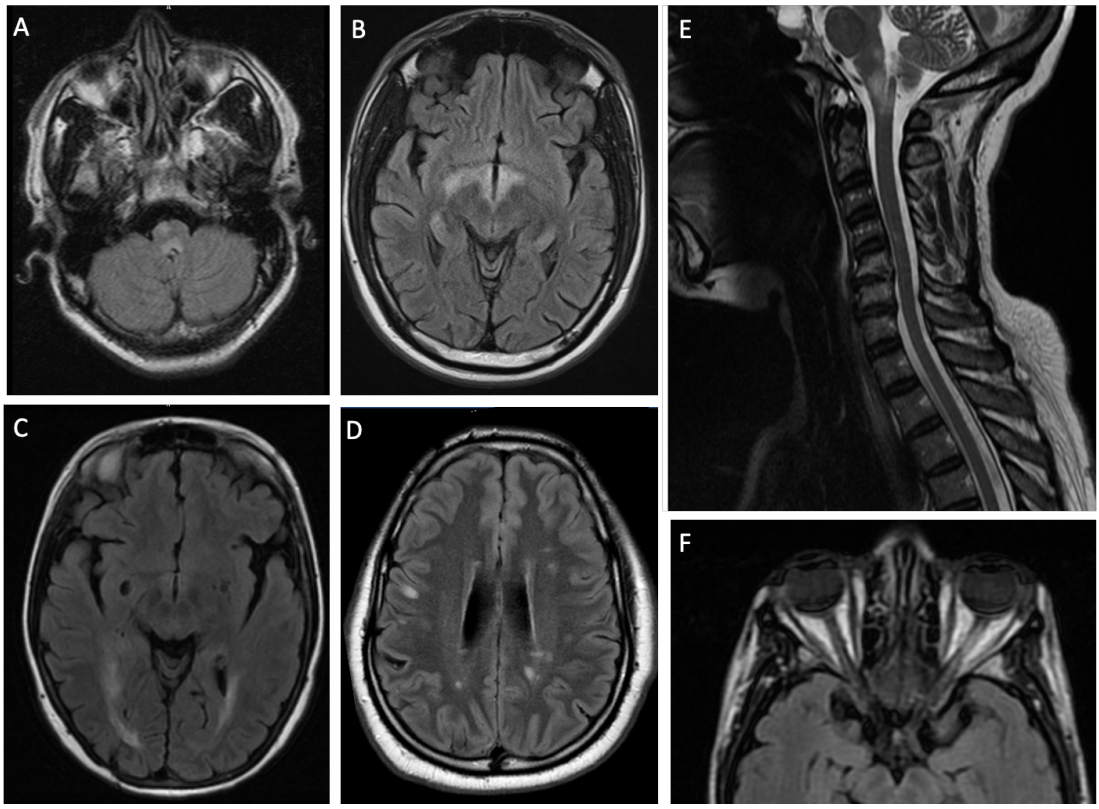


Figure 1.3 Examples of MRI images in NMOSD-AQP4. *A) Axial FLAIR showing an area postrema lesion, B) Axial FLAIR showing a lesion adjacent to the 3rd ventricle. C) Axial FLAIR showing periependymal lesions adjacent to both lateral ventricles, D) Axial FLAIR showing non-specific deep white matter and subcortical lesions E) Sagittal T2 cord image showing a posterior medulla lesion extending down to the upper cervical cord F) Axial FLAIR showing a long left optic nerve lesion involving the left side of the chiasm. (NHS MRI, patients consented under Tissue Bank Ref: 10/H0606/56).*

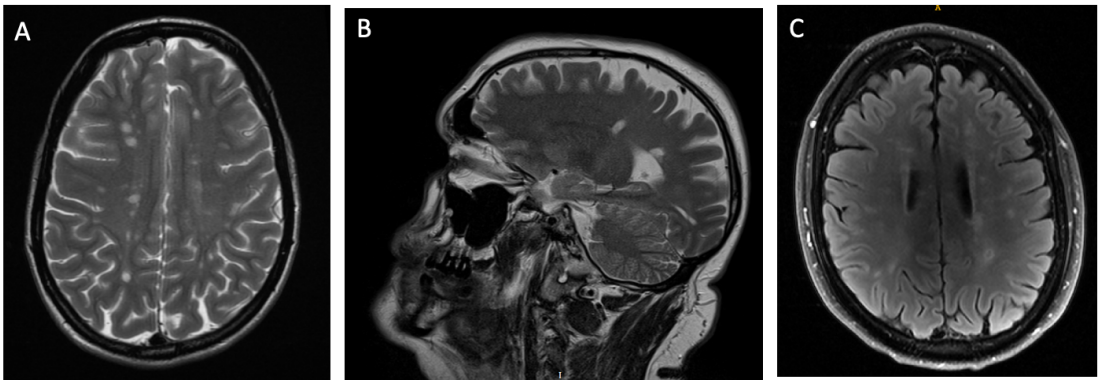


Figure 1.4 Examples of MRI images in MS. *A) Axial T2 showing juxtacortical lesions, B) Axial T2 showing lesions perpendicular to the corpus callosum (Dawson's fingers) C) Axial FLAIR showing juxtacortical and periventricular lesions. (NHS MRI, patients consented under Tissue Bank Ref: 10/H0606/56).*

1.2.7 *Other conventional MRI findings*

1.2.7.1 Optic nerve imaging findings

Optic neuritis is a common presenting symptom of demyelinating diseases. Comparative studies of MOGAD and NMOSD-AQP4 optic neuritis, showed severe optic nerve swelling and contrast enhancing lesions of the optic nerve more frequently in MOGAD. In addition, the inflammation of the periorbital tissue surrounding the intra orbital portion of the optic nerve was also noted, which may explain the severe pain accompanying, and often preceding, most of the MOGAD optic neuritis (Asseyer et al., 2020; Biotti et al., 2017) (see Figure 1.2 G). Both NMOSD-AQP4 and MOGAD showed long lesion in the Short TI inversion recovery (STIR) sequence involving different tracts of the optic nerve. The optic chiasm was more often affected in NMOSD-AQP4, suggesting more posterior involvement (Akaishi et al., 2016; Ramanathan et al., 2016) (see Figure 1.3 F). A more recent large study found similar optic nerve involvement in MOGAD and NMOSD-AQP4 (16% and 20%), challenging this assumption. However, the characteristic of the chiasmatic involvement was different. In MOGAD the chiasmal involvement is part of the longitudinally extensive optic nerve lesion, while in NMOSD-AQP4 the posterior chiasmal involvement is more likely, also without long optic nerve lesion (Tajfirouz et al., 2021). Unilateral optic neuritis with short segment optic nerve involvement is more common in MS. Optic nerve head-swelling and chiasm involvement are usually less common in MS, compared to NMOSD-AQP4 and MOGAD (Ramanathan et al., 2016).

1.2.7.2 Spinal cord imaging findings

Initial studies on MOGAD were focussed on the NMOSD phenotype, therefore LETM appeared as the most common imaging findings. Larger studies have shown that short cord lesions can be present, especially with older age at onset (Jurynczyk et al., 2017b). Lesions are more frequently seen in the thoracic cord and the conus involvement is a prominent feature (Kitley et al., 2014b) (see Figure 1.5 A-B). On axial view the cord lesion in MOGAD tend to be central and selectively involving the grey matter. The "H sign" (T2 hyperintensity highly restricted to the grey matter on the axial view) and a linear sagittal hyperintensity have been described as characteristics of MOGAD (Dubey et al., 2019) (see Figure 1.5 C). Recently symptomatic myelitis with negative MRI have been described. It is possible that inflammatory change restricted to the grey matter may not always be visible on conventional MRI sequences, however, more technical issues, as the timing and the quality of the MRI scans, should also be considered.

In NMOSD-AQP4 the spinal cord MRI typically shows long lesions (> 3 vertebral segments), a central location on axial view, and a predominance of lesions in the cervical and upper thoracic cord (Kim et al., 2015a; Tackley et al., 2014) (see Figure 1.6 A-D). The cord appears swollen on sagittal view and the post contrast enhancement is more frequently seen in NMOSD-AQP4 than MOGAD and MS (Dubey et al., 2019), and is mostly patchy and irregular. The lesions are hyperintense on T2 and sometimes hypointense in T1 (see Figure 1.6 C). "Bright spotty lesions", defined as areas of strong T2 hyperintensity within the lesions, has been described in NMOSD-AQP4 (Yonezu et al., 2014).

In MS cord lesions are usually short (less than one segment) and peripheral on the axial view, can also be asymptomatic and may occur in up to 80% of relapsing remitting MS patients (Bot et al., 2004) (see Figure 1.7 A-C).

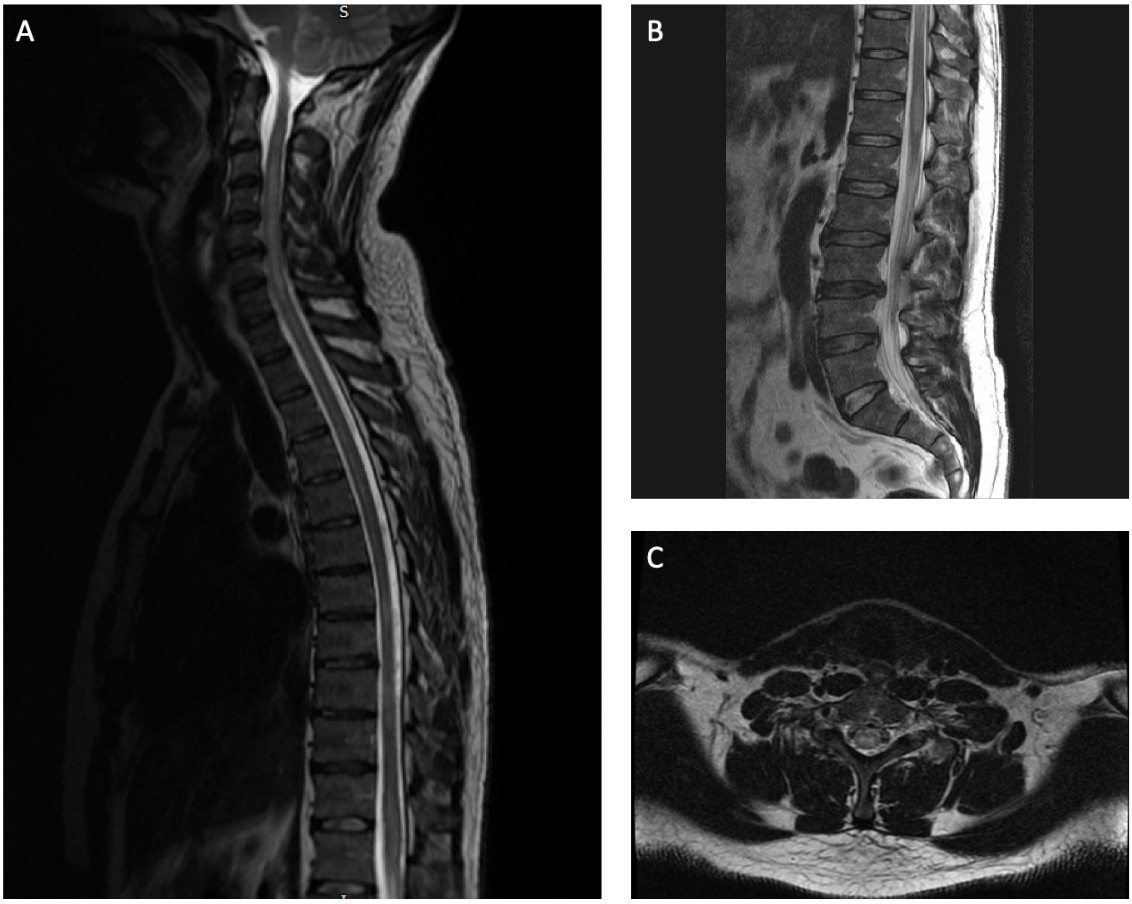


Figure 1.5 Examples of cord MRI images in MOGAD. *A) Sagittal T2 image showing an LETM, B) Sagittal T2 image showing a conus lesion. C) Axial T2 image showing a central cord lesion. Legend: LETM=longitudinally extensive transverse myelitis. (NHS MRI, patients consented under Tissue Bank Ref: 10/H0606/56).*

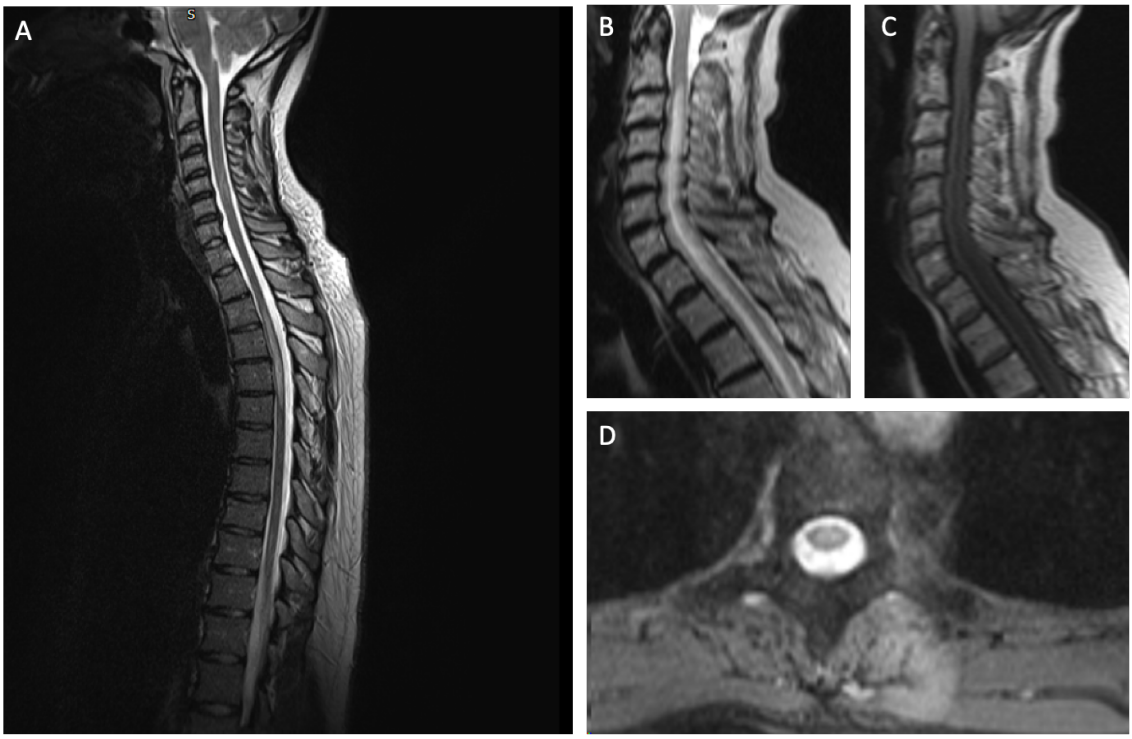


Figure 1.6 Examples of cord MRI images in NMOSD-AQP4*. A) Sagittal T2 image showing an LETM, B) Sagittal T2 image showing an LETM and swollen cord C) Sagittal T1 image showing a hypointense cord lesion D) Axial T2 image showing a central cord lesion. Legend: LETM=longitudinally extensive transverse myelitis. (NHS MRI, patients consented under Tissue Bank Ref: 10/H0606/56).*

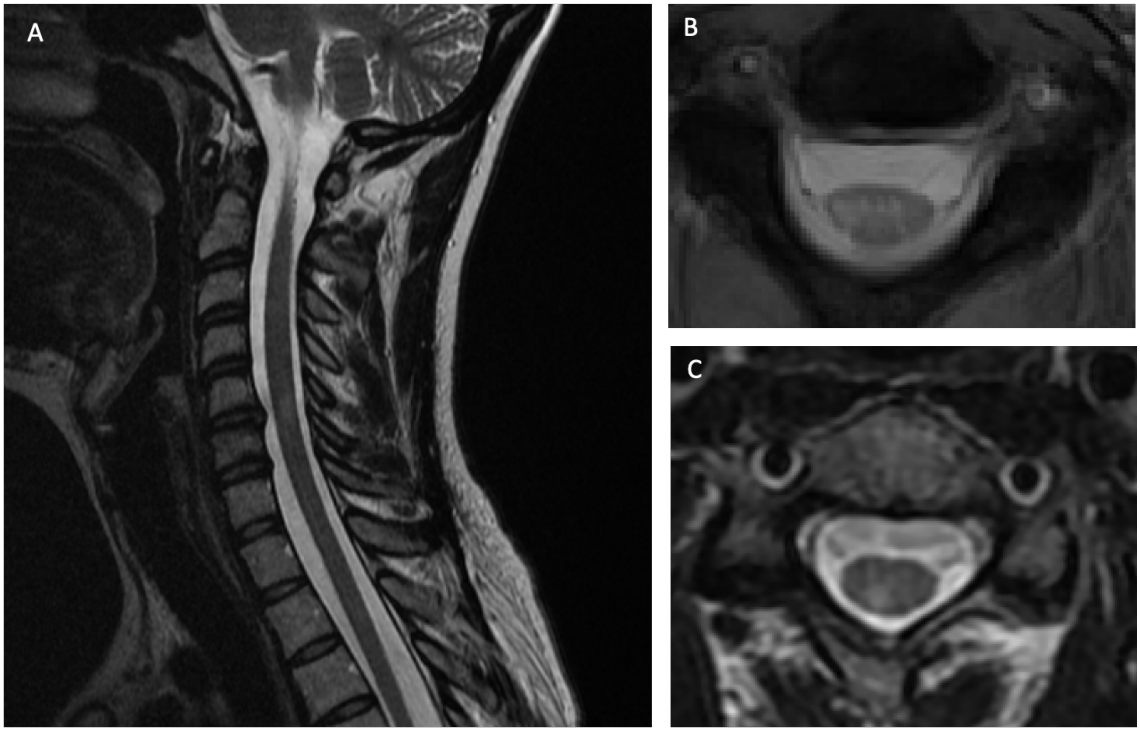


Figure 1.7 Examples of cord MRI images in MS. *A) Sagittal T2 image showing a cervical short lesion B) Axial T2 image showing an asymmetric cord lesion C) Axial T2 image showing an asymmetric cord lesion. (NHS MRI, patients consented under Tissue Bank Ref: 10/H0606/56).*

1.2.8 *Other investigations*

The MRI has a prominent role in the diagnosis and the long-term follow-up of demyelinating disease. However, other investigations are useful in differentiating across disease, especially when the antibody results are not available and to rule out differential diagnoses.

The analysis of cerebrospinal fluid (CSF) is a particularly useful tool to exclude other autoimmune conditions or infective aetiologies. In 38-55% of MOGAD patient cells in the CSF are elevated (3-306), with lymphocytes predominance (Jarius et al., 2020b; Kitley et al., 2014b). Total CSF protein are elevated in 46-48% of cases (Jarius et al., 2020b; Jurynczyk et al., 2017b). Oligoclonal bands, which are a marker of intrathecal inflammation, are rare and can be present in 6-12% of MOGAD patients, especially during the acute attack (Cobo-Calvo et al., 2018; Jarius et al., 2020b; Jurynczyk et al., 2017b). In NMOSD-AQP4 the CSF analysis usually show elevated cells and protein in ~50% of samples (Jarius et al., 2011). Additionally, eosinophils, which are absent in MS and very rare in MOGAD, are present in about 10% of NMOSD-AQP4 CSF samples (Correale and Fiol, 2004). Oligoclonal bands can be present in 16% of NMOSD-AQP4 CSF sample. In MS cell count and protein levels are usually normal or slightly elevated, while oligoclonal bands can be present ~88% of MS cases and ~69% of clinically isolated syndrome (first demyelinating event). Given their high prevalence in MS and their predictive value for conversion to defined MS, oligoclonal bands have been included in the updated MS diagnostic criteria as a marker of dissemination in time (Thompson et al., 2018).

Electrophysiology studies, used to detect abnormal conduction along the optic nerve (visual evoked potentials) and along the somatosensory pathways (somatosensory evoked potentials), in the last years have been replaced by MRI for the diagnosis of demyelinating diseases. However, they still have a role in the monitoring of visual and cord symptoms recovery. The visual and sensory evoked potentials are usually delayed after an optic neuritis and transverse myelitis attack, in about 72% of MOGAD and 42% of NMOSD (mostly AQP4-Ab positive). Unlike MS, in MOGAD and NMOSD-AQP4, the delayed conduction is associated with reduced amplitude, or absent response, suggesting a more severe axonal loss (Jarius et al., 2016c; Ringelstein et al., 2014).

Unlike NMOSD-AQP4, in MOGAD the recovery is often associated with a normalisation of the evoked potentials (Kitley et al., 2014b). In MS, evoked potentials are able to capture silent CNS lesions, supporting the presence of subclinical pathology in this condition (Pisa et al., 2021).

Optical coherence tomography (OCT) is an imaging technique that can assess the retinal damage, measuring the retinal nerve fibre layers (RNFL), among other measures. In MOGAD, despite the usual good visual outcome, OCT studies showed a retinal damage similar to that found in NMOSD-AQP4, where the visual function is worse (Filippatou et al., 2020). In MS retinal damage has been described, is usually less severe than NMOSD-AQP4, and may be present in the not affected eye (Bennett et al., 2015).

1.2.9 *Treatment*

In MOGAD the treatment is empirical and derived from the NMOSD-AQP4 and other neurological autoimmune diseases management. To date there are no universally accepted treatment algorithms and clinical trials are lacking (Whittam et al., 2020b). This

section is a general overview of the treatment choices in MOGAD and reflects the common clinical practice in the main specialist services.

The standard treatment for relapse is high dose steroids (3-5 days of intravenous methylprednisolone - IVMP) followed by an oral prednisolone tapering dose. At the time of the starting of this thesis project, there were no clear guidelines regarding the timing of the prednisolone dose. In Chapter 2 the effect of steroids tapering dose on the risk of following relapse has been studied and will be discussed.

The rescue therapy for those patients with an incomplete recovery after IVMP, include plasma exchange (PLEX) and intravenous immunoglobulin (IVIG) (Kleiter et al., 2016). Although large phase III clinical trials are lacking, the use of the following immunosuppressants as long-term treatment is common: azathioprine, mycophenolate, methotrexate and recently rituximab; however a recent study showed that rituximab may be not as effective as it is in NMOSD-AQP4 and MS (Jurynczyk et al., 2019; Whittam et al., 2020a).

In NMOSD-AQP4 the attacks are treated with high dose steroids and the low dose oral prednisolone is maintained long-term. As for MOGAD the long-term treatments are azathioprine, mycophenolate, methotrexate and rituximab (Palace et al., 2012; Whittam et al., 2019). Recently immunological studies elucidating the immune system mechanism behind AQP4-Ab disease, have identified the complement system, the IL-6 pathway, and the B cells as possible new therapeutic targets. These findings prompted to three new therapies for NMOSD-AQP4, such as eculizumab, a complement inhibitor, satralizumab, an anti-IL-6 receptor monoclonal antibody and inebilizumab, an anti-CD-19 monoclonal antibody (Cree et al., 2019; Pittock et al., 2019; Traboulsee et al., 2020; Yamamura et al., 2019). In the last years the MS treatment armamentarium has grown, with the approval of several monoclonal antibodies which have changed the long-term prognosis of the MS

patients. A comprehensive description of all the available DMTs in MS is out of the scope of thesis, however it is important to note that most of the DMT can be harmful or ineffective in NMOSD-AQP4 and MOGAD (Cobo-Calvo et al., 2019; Kira, 2017; Munot et al., 2010; Reindl and Waters, 2019).

1.2.10 *Understanding MOGAD: knowledge gap and challenges*

Since 2010, when the MOG-Ab was first described as associated with a disease different from MS, our understanding of MOGAD as a new and distinct clinical entity, has grown significantly.

MOGAD is a primary demyelinating autoimmune condition where the disability is related to relapses, and a progressive phase has not been described, except for rare case report (Baba et al., 2019). The recovery is usually good and is associated with improvement and/or resolution of the MRI findings and normalisation of the electrophysiology studies. Despite a good visual recovery, the OCT can show some residual retinal damage.

Although these finding improved the clinical management and the clinician diagnostic ability, there are still several unmet needs and challenges that need to be discussed.

a. *Identifying a marker able to quantify the recovery*:

   Despite the similar relapse severity at nadir, MOGAD have a better recovery than NMOSD-AQP4. Quantifying the presence of damage outside of the acute phase can give more information regarding the pathogenesis and can be a useful marker associated with long-term disability.

b. *Evaluating the cognitive function*:

Cognition can be affected in those patients with brain involvement, however studies systematically assessing the cognitive function in MOGAD are lacking.

c. *Understanding the pathogenesis*:

Understanding the MOGAD pathogenesis may pave the way towards new possible therapeutic target to explore. Additionally, disease marker can be used as outcome in future clinical trials.

The body of work presented in this thesis stem from these considerations and from clinical practice observations.

The main aim of this project is to fill the knowledge gaps, but most importantly to translate the research findings into clinical practice and change the management of MOGAD. Given the prominent role of the MRI in the diagnosis and monitoring of demyelinating diseases and the potential for the MRI findings to be translated into clinical practice, an MRI, together with a clinical approach, was chosen for this project.

In the next section the current literature of conventional and non-conventional MRI in MOGAD will be outlined, and a comparison with NMOSD-AQP4 and MS will be described.

Finally, before presenting the experimental chapters, the thesis main structure and main objectives will be outlined.

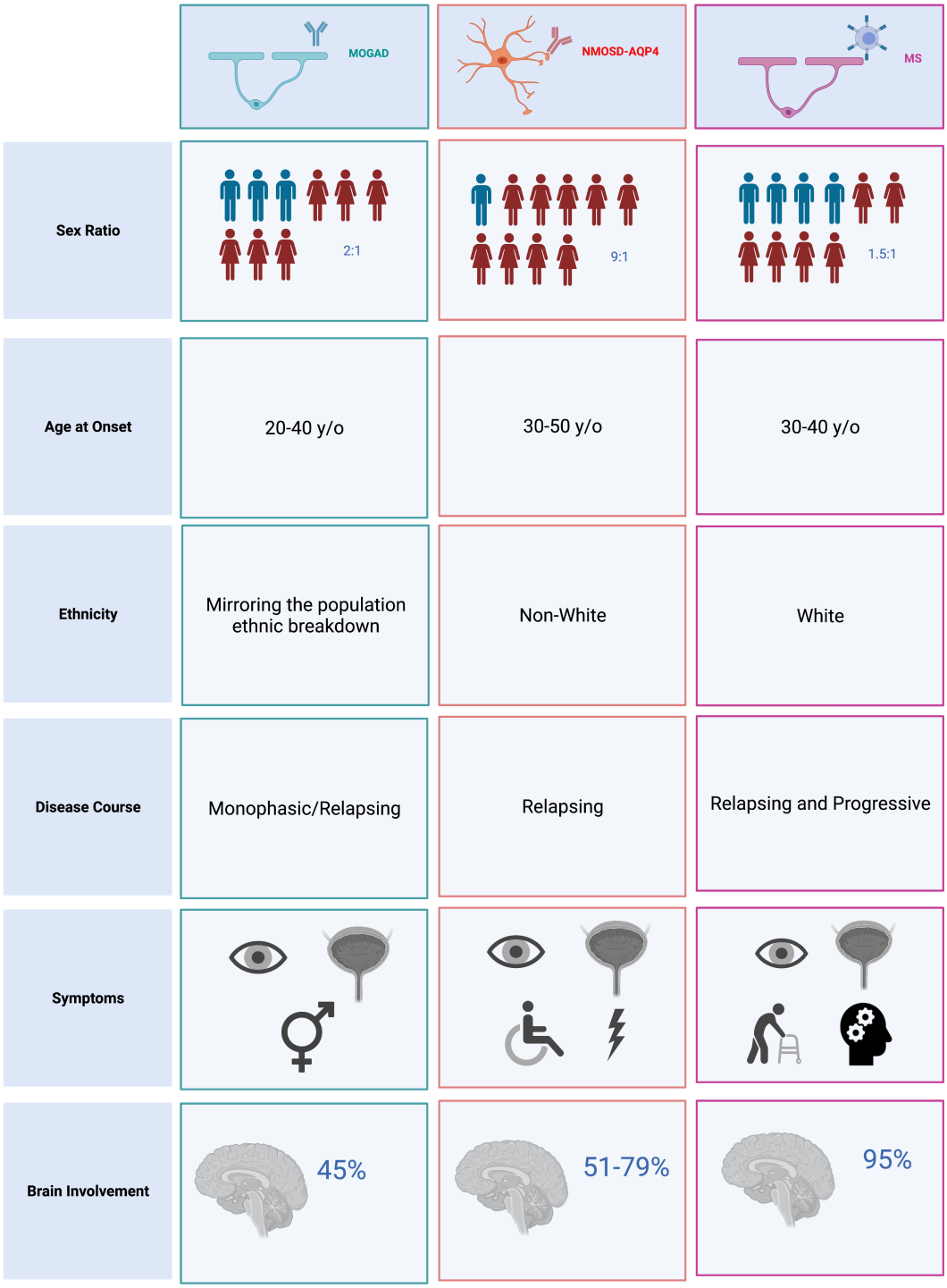


Figure 1.8 Graphical representation of the main clinical and demographic differences across MOGAD, NMOSD-AQP4 and MS. *Created with BioRender.com*

1.3 Non-conventional brain MRI in MOGAD: a comparison with NMOSD-AQP4 and MS

In this section the background of non-conventional imaging in demyelinating diseases, which prompted the set-up of this thesis, will be presented. At the time of the set-up of this study, the literature on non-conventional MRI in MOGAD was scarce. The most recent MRI studies in MOGAD, will be summarised in the discussion section of each experimental chapter and compared with the findings of every chapter.

1.3.1 *Structural MRI*

Structural MRI can be used to quantify the whole brain volume, the white/grey matter fraction and the subcortical structures (i.e., deep grey matter structures and brainstem). T1, T2 and FLAIR sequence are the core of every imaging protocol in demyelinating diseases.

Brain atrophy and deep grey matter atrophy are measures of tissue loss and can be the consequence of different pathological processes (Miller et al., 2002).

MOGAD studies using non-conventional MRI to assess white/grey matter atrophy are scarce. The most recent MRI studies, published after the set-up of this project, will be discussed and compared to the structural MRI findings in Chapter 4 (Duan et al., 2021; Schmidt et al., 2020; Zhuo et al., 2020).

Earlier NMOSD-AQP4 voxel-based morphometry studies reported conflicting results, probably due to the lack of correction for multiple comparison of the voxel-wise analysis or the use of less stringent criteria of significance (Blanc et al., 2012; Duan et al., 2012; Ota et al., 2015; Pichiecchio et al., 2012; von Glehn et al., 2014). Studies using a more conservative threshold did not find significant white or grey matter atrophy (Matthews et

al., 2015; Pache et al., 2016a). Contradictory findings are also found when volumetric measures are used. A reduced white matter volume in NMOSD-AQP4 compared to HC was described (Chanson et al., 2013), however another study did not confirm this finding (Matthews et al., 2015). Studies of the grey matter structures noted a reduced volume in NMOSD-AQP4, although less severe than in MS (Hyun et al., 2017; Liu et al., 2015a), not confirmed by studies only including AQP4-Ab positive patients (Finke et al., 2016; Matthews et al., 2015). The study of the thalamic nuclei showed an attack-related damage of the lateral geniculate nuclei, part of the thalamus, after an optic neuritis, suggesting the presence, in NMOSD-AQP4 of a selective nuclei damage rather than a diffuse thalamic damage (Papadopoulou et al., 2019). In NMOSD-AQP4, white and grey matter structural changes associated with cognitive impairment have also been explored, with some studies reporting a reduced white matter volume (Blanc *et al.*, 2012) and others deep grey matter (Liu et al., 2015b) or cortical volume atrophy (Saji et al., 2013) in cognitively impaired patients.

Several studies have shown that brain atrophy, including both deep grey matter and cortical atrophy, and cord atrophy are common findings in MS since the early stage of the disease. In particular, deep grey matter atrophy has been associated with cognitive impairment, and cord atrophy with increasing disability (Alcaide-Leon et al., 2018; Azevedo et al., 2015; Eshaghi et al., 2018; Minagar et al., 2013; Sastre-Garriga et al., 2017). The estimated extent of cerebral atrophy in MS is about 0.7-1% per year compared to 0.2-0.4% in the general population (De Stefano et al., 2010; Popescu et al., 2013; Rocca et al., 2017a). Longitudinal studies showed that deep grey matter volume loss has the fastest atrophy annual rate and is a predictor of EDSS progression (Eshaghi et al., 2018) and cognitive impairment (Eijlers et al., 2018), while the main predictor of future cognitive worsening was the cortical volume (Eijlers et al., 2018). This observation is in

line with a recent study, showing that deep grey matter atrophy is present in the early stage of the disease and in patients with mild impairment, while cortex atrophy is prevalent in patients with severe, multidomain cognitive impairment (De Meo et al., 2021).

1.3.2 *Advanced Quantitative MRI*

Structural MRI is sensitive to pathological change but not able to distinguish among different pathological process, such as demyelination, gliosis or axonal loss (Filippi et al., 2012). Advanced MRI techniques emerged in the last years, as a useful tool to differentiate and quantify pathological findings. Quantitative MRI techniques measures the physical parameters of tissue, and they are sensitive to different microstructural tissue compartments. The quantitative MRI sequences, in contrast to the conventional MRI sequences, require the acquisition of images with different timing parameters, thus resulting in a longer acquisition time. In light of this, their use in the clinical practice of demyelinating diseases is currently limited (Seiler et al., 2021).

At present, the most promising advanced MRI techniques used in NMOSD, but mostly in MS are proton MRI spectroscopy (MRS), magnetization transfer imaging (MTI), myelin water imaging (MWI), and diffusion tensor imaging (DTI) (Cortese et al., 2019; Kremer et al., 2015). To date there are no studies on MOGAD using MRS, MTI and MWI.

Tissue metabolites, measured by MRS, were not able to discriminate between NMOSD and MS in the brain (Aboul-Enein et al., 2010; de Seze et al., 2010), while in the cord low myoinositol level were found in the NMOSD cord lesions, but not in MS (Ciccarelli et al., 2013). A recent 7 T MRI study, focussing on chronic brain lesions, did not find a

significant myoinositol level difference between lesions and NAWM in NMOSD-AQP4 (Tackley et al., 2021).

MTI technique provides an indirect measure of myelin content, measuring the magnetisation transfer between free water molecule, and water molecule associated to macromolecules, i.e. myelin (Schmierer et al., 2004). The only MOGAD cord MRI study did not find any MTR difference, compared to HC, MS and NMOSD-AQP4 (Mariano et al., 2020). To date there are no studies exploring the brain MTR measures in MOGAD. Early studies, including both AQP4-Ab positive and negative patients, found MTI differences compared to HC in the grey matter and in the brain white matter in MS compared to NMOSD-AQP4 (Filippi et al., 1999; Filippi and Rocca, 2004). Recently, a 7T brain study did not found any difference in brain MTR measures in NMOSD-AQP4 compared to MS, while NAWM showed lower MTR measure when compared to HC (Chou et al., 2019).

As MTR can be influenced by non-myelin macromolecules, MWI measure, assessing the water molecules trapped in the myelin sheets, has been suggested as a more sensitive and specific myelin marker (Lee et al., 2021a). MWI has been explored in NMOSD-AQP4 and MS. Low MWI was found in NMOSD-AQP4 compared to HC, especially in the optic radiation (Jeong et al., 2017), and in both MS and NMOSD-AQP4 correlated with measures of retinal integrity (Manogaran et al., 2016). A comparison longitudinal study between MS and NMOSD-AQP4 showed, using a voxel-wise analysis, a widespread significant reduction of the MWF in MS at baseline, with no significant differences in the 1-year follow-up scan (Matthews et al., 2015).

DTI explores the diffusion of water molecules within the brain tissue and provides insight into the brain microstructure and the geometry of fibre tract orientation (Assaf et al., 2019). The diffusion of the water molecules can be represented by an ellipsoid with three

directions, the eigenvectors and the radii of the ellipsoid as the eigenvalues. The diffusion of the water molecule in the brain can be categorised in isotropic diffusion, where the water molecules diffuse equally in all the directions (i.e. CSF and grey matter) and anisotropic diffusion, where the water molecule diffuse preferentially in one direction (i.e. white matter). DTI can provide information of fibre orientation by estimating quantitative parameters such as fractional anisotropy (FA), mean diffusivity (MD), radial diffusivity (RD), and axial diffusivity (AD). FA, which can range between 0.1 and 1.0, reflects the overall directionality of the water molecule diffusion in the brain tissue, and white matter pathology can result in a reduction of FA. However, as the reduction of the FA can depend on the increase of perpendicular diffusivity or a reduction of the parallel diffusivity, to better understand the change of the abnormal tissue, other measures are necessary. MD measures the magnitude of the diffusion and is an average of the three eigenvalues. The studies of the perpendicular diffusivity (RD) and parallel diffusivity (AD) have improved the characterisation of the diffusion tensor (Alexander et al., 2007). Early histopathology studies showed that FA depends on myelin content and is reduced in demyelinated axons (Neil et al., 1998). The magnitude of diffusion, (MD) tends to reduce in early brain development, reflecting the myelination process (Suzuki et al., 2003). Mice studies showed that in absence of myelin, RD tend to increase, while AD is unchanged (Song et al., 2002). Other studies suggested that AD is more sensitive to axonal damage (Harsan et al., 2006; Sun et al., 2006).

While FA is sensitive to neurite (axon and dendrites) density and orientation dispersion, it is not able to discriminate between the cellular compartment, the CSF and the neurite compartment. Neurite orientation dispersion and density imaging (NODDI) is a novel diffusion MRI technique able to estimate Neurite Density Index (NDI) and Orientation dispersion index (ODI) (Zhang et al., 2012), providing more specific information

regarding the white and grey matter structure in the extracellular and intracellular compartments. Early NODDI-DTI studies in MS have found reduced NDI in NAWM and contrasting ODI results (Collorone et al., 2020; Granberg et al., 2017; Schneider et al., 2017).

A few studies, using different methodology (i.e., diffusion metrics and voxel-wise analysis) have looked at diffusion changes in MOGAD (Duan et al., 2021; Schmidt et al., 2020; Zhuo et al., 2020) and their findings will be discussed in Chapter 5.

Diffusion MRI studies in NMOSD-AQP4 showed differing results (Filippi and Rocca, 2004; Kremer et al., 2015; Pache et al., 2016a; Schmidt et al., 2020) probably related to whether the cohorts mix antibody positive and negative together and whether the tracts associated with lesions are accounted for (Kim et al., 2017; Matthews et al., 2015).

NMOSD diffusion studies showed reduced FA in the optic radiation and in the cortico-spinal tracts, possibly as a result of the optic neuritis and transverse myelitis Wallerian degeneration (Jeantroux et al., 2012; Matthews et al., 2015; Pache et al., 2016a), while the damage appear more widespread in MS (Matthews et al., 2015).

In a comparison study, tract-based spatial statistic (TBSS) analysis showed that in MS patients, compared to NMOSD-AQP4, the NAWM damage is focussed on the associative fibres. In particular axonal damage (higher AD) was prominent in MS patients and was not present in NMOSD-AQP4 (Kim et al., 2017). In contrast, a more widespread increased MD in associative tracts, optic tracts and corticospinal tracts was found in another TBSS study, while a more recent study using TBSS did not find any brain diffusion measures differences in NMOSD-AQP4 patients compared to HC and MOGAD (Liu et al., 2012; Schmidt et al., 2020). Diffusion grey matter studies showed increased MD in NMOSD (AQP4-Ab status unknown) compared to HC (Rocca et al., 2004) and abnormal FA in the thalamus and putamen (Zhao et al., 2012).

Compared to the other quantitative MRI techniques, diffusion MRI has been broadly studied in demyelinating diseases. Furthermore, diffusion MRI is the only advanced MRI technique which has a role in clinical practice and has changed the management of the acute stroke, suggesting that the translation into clinical practice for demyelinating disease is also technically feasible (Sims et al., 2009). Diffusion weighted imaging has also the advantage to provide information of the white and grey matter microstructure, but also of white matter pathways integrity (i.e., tract based spatial statistics). Based on these considerations, diffusion MRI has been selected as the quantitative modality of choice for this thesis.

1.3.3 *Resting State MRI*

Functional MRI (fMRI) measures the brain neural activity using the blood-oxygen-level dependent (BOLD) signal (Biswal et al., 1995). In the early years of fMRI research, behavioural manipulations (i.e., tasks) were used to detect signal fluctuations of brain activity, while the spontaneous unrelated fluctuations were removed. In 1995, Biswal et al showed that these spontaneous low-frequency fMRI fluctuations were correlated within specific brain regions and were present when the subject was at rest in the scanner, and so resting-state functional MRI (RS-fMRI) became its own entity (Biswal et al., 1995). Since then, different resting state networks have been identified, such as the default mode network (DMN), the sensorimotor network, the visual network, the auditory network, the frontoparietal network and the executive network (Smith et al., 2009).

There are only two RS-fMRI studies on MOGAD patients. In the two studies, one of them focussing on optic neuritis patients, abnormal activity of many brain regions, consistent

with visual, motor, and cognitive function, were described (Wang et al., 2017; Zhuo et al., 2020). To date there are no studies in MOGAD patients, investigating the large brain networks and the association with clinical outcome.

Resting state studies in NMOSD have led to differing results. Reduced visual cortex connectivity has been described in NMOSD, possibly as a result of Wallerian degeneration secondary to optic nerve damage (Bigaut et al., 2019; Cai et al., 2017; Wang et al., 2020). On the contrary another group showed increased primary visual network connectivity in patients with previous optic neuritis, suggesting the presence of an adaptive connectivity change when a reduced visual acuity occurs (Finke et al., 2018).

Abnormal deep GM structures connectivity (thalami, hippocampi, basal ganglia and amygdalae) (Schoonheim et al., 2014; Wu et al., 2016; Zhou et al., 2015) was described in MS, and in particular reduced connectivity in the visual area and decreased in the temporal lobes were described in clinically isolated syndrome (Liu et al., 2016). Abnormal connectivity of visual (Gallo et al., 2012), motor and cognitive resting state networks (RSNs), has been described in MS, with increased connectivity pattern in the early stage of the disease and reduced connectivity in the progressive stage (Janssen et al., 2013; Schoonheim et al., 2014).

1.4 Thesis overview

The thesis was designed to study the brain MRI findings in MOGAD, compared to NMOSD-AQP4 and MS, and a group of healthy controls (HC).

1.4.1 *The main aims of the thesis*

The main aims of this thesis are:

a. To describe the clinical characteristics and outcomes in a MOGAD cohort
b. To identify a distinct brain imaging pattern in MOGAD, compared to NMOSD-AQP4 and MS, using conventional and non-conventional MRI and to explore their relationship with disability measures i.e., EDSS and visual acuity.
c. To identify different patterns of abnormal resting state networks (RSNs) in the three CNS demyelinating diseases.
d. To describe cognitive impairment and to explore structural and functional imaging correlates in MOGAD, NMOSD-AQP4 and MS.

The objectives and the research hypothesis will be detailed in each experimental chapter.

1.4.2 *Structure of the thesis*

To address the main aims of the thesis, a clinical and MRI study were set up and the results are presented as a series of six result chapters. The MRI study overview and methods will be presented in a separate chapter. The thesis chapters as presented as follows:

Chapter 2: the clinical and demographic characteristics of the Oxford NMO service cohort are presented. The effect of steroid treatment on the risk of relapse are studied in an incident cohort. Finally, the clinical outcomes are analysed.

Chapter 3: this chapter is an overview of the MRI study. The studied cohort demographic and clinical features, including the fatigue, pain and anxiety and depression scores will be described.

Chapter 4: in this first MRI experimental chapter the results of the lesional and volumetric analysis will be presented and compared across the disease groups.

Chapter 5: in this chapter the different pattern of normal appearing white/grey matter damage in the three diseases will be described and quantified.

Chapter 6: in this clinical-MRI chapter the association between the white/grey matter measures and the disability outcomes (EDSS and visual acuity) will be explored.

Chapter 7: in this chapter the resting state MRI was used to explore the clinical relevance of the resting state networks (RSNs) as a potential marker of disability/tissue damage, independent of the disease type and to identify different patterns of abnormal RSNs across the disease groups.

Chapter 8: in this chapter the cognitive function in MOGAD was studied and compared to NMOSD-AQP4 and MS. Additionally, different patterns of cognitive impairment and their imaging correlates were explored across the three diseases.

Chapter 9: in this final chapter the considerations and challenges outlined in section 1.2.10. will be discussed, considering the thesis findings. Additionally, future projects able to translate the findings into clinical practice will be proposed.

2 Chapter 2 Clinical presentation and prognosis in MOGAD: The Oxford cohort

2.1 Introduction and background

MOGAD has been recently recognised as distinct from multiple sclerosis (MS), as typical MS patients test negative for MOG-Ab, when the conformationally intact full length MOG-Ab were used (Waters et al., 2015).

MOG-Ab were initially found in paediatric cases of acute disseminated encephalomyelitis (ADEM) and were further described in adult patients with AQP4-Ab negative NMOSD (Brilot et al., 2009; Kitley et al., 2012b).

MOGAD was considered a milder disease and less likely to relapse compared to AQP4-Ab disease (Hoftberger et al., 2015; Kitley et al., 2014a; Sato et al., 2014; van Pelt et al., 2016), however the clinical course, the risk of relapse, prognostic factors and therapy effects, were largely unknown.

Previous studies included small numbers of patients, and were biased towards predominantly relapsing cohorts, as monophasic patients could have not been identified at onset, until the recent discovery of the MOG-Ab (Jarius et al., 2016a; Jarius et al., 2016c; Kitley et al., 2014b; Pache et al., 2016b; Sepúlveda et al., 2016).

The work presented below is adapted from the publication: [*M. Jurynczyk*, S. Messina,*M. R. Woodhall*, et al. Clinical presentation and prognosis in MOG-antibody disease: a UK study, Brain. 2017 Dec 1;140(12):3128-3138. doi: 10.1093/brain/awx276 *these authors equally contributed],* where demographics, disease presentation and disease course were studied in a large cohort of UK MOGAD patients (n=252). In the

Oxford MOGAD cohort, where more detailed clinical history was available (n=75), clinical outcomes and relapse predictors were studied (Jurynczyk et al., 2017b).

The figures and results in this analysis are based on the abstract accepted as an oral communication at the Association of British Neurologist in April 2018, and published [S. *Messina, et al. Clinical outcome in mog-antibody disease: a large single site cohort. J Neurol Neurosurg Psychiatry October 2018 Vol 89 No 10]* where further 31 MOGAD patients were added to the original published analysis (n=106 Oxford Cohort).

At the time of the publication, this was the largest cohort and the first incidence cohort of MOGAD patients ever described, and the first work studying the effects of long-term steroids on the risk of further relapses. The main aims of this study were to describe the demographics, disease presentation, the disease course, and clinical outcomes, and to assess the effect of treatment on relapse risk in the Oxford MOGAD cohort.

2.1.1 *Objectives*

a) To identify the clinical characteristics of MOGAD which can prompt the clinicians to test for MOG-Ab.
b) To define the length of steroid cover after the MOGAD onset attack.
c) To describe the risk of MOGAD long-term disability.

2.1.2 *Hypothesis*

The MOGAD cohort will present a good clinical recovery and the short-term steroid cover after the onset attack will reduce the risk of further relapses.

2.2 Material and methods

2.2.1 *Ethics*

All patients signed written consent of the NMO Tissue Bank (Oxford Research Ethics Committee C Ref: 10/H0606/56).

MOG-Ab testing was performed in the Autoimmune Neurology laboratory in Oxford using a cell-based assay as described in Waters et al 2015. All patients were positive for MOG-Ab and negative for AQP4-Ab.

2.2.2 *Cohorts*

Two cohorts were selected: the 'Oxford Total cohort', the largest cohort including all the MOG-Ab positive patients present in the NMO database at the time of the data ascertainment (data collection November 2016 – April 2018), and the 'Oxford incidence cohort', including all those diagnosed at onset (where MOG-Ab was available at onset and before the first relapse).

2.2.3 *Oxford total cohort*

Data from 106 patients seen within the specialist Neuromyelitis Optica Clinic in Oxford were available and collected prospectively. These included treatment, disability outcomes, disease course and phenotype. We selected disability outcomes that were prevalent enough in the MOGAD cohort: visual acuity ≤6/36 in at least one eye, Expanded Disability Status Scale (EDSS) ≥4.0 (ambulatory without aid or rest for <500 m), neurogenic bladder dysfunction (urinary incontinence and/or urgency), neurogenic bowel dysfunction (faecal incontinence and/or constipation) and erectile dysfunction.

Outcomes were considered in the analysis if they persisted for at least 6 months and were present at last follow-up. Cognitive problems were noted when reported but were not systematically assessed and thus not analysed.

2.2.4 *Oxford incident cohort*

MOGAD has been recently recognised and thus the diagnosis was not possible before the discovery of the antibody, patients included in the prevalent cohort are likely to have been diagnosed if they present with a relapse. To avoid the bias of a mostly relapsing cohort, only patients who have been diagnosed at the first attack (MOG-Ab positive before the first relapse) were included in the Oxford incidence cohort, where the relapse risk and treatment effect were calculated. The onset date was for all the cohort, after January 2012, once the diagnostic MOG-IgG1 assay became available (see Figure 2.1)

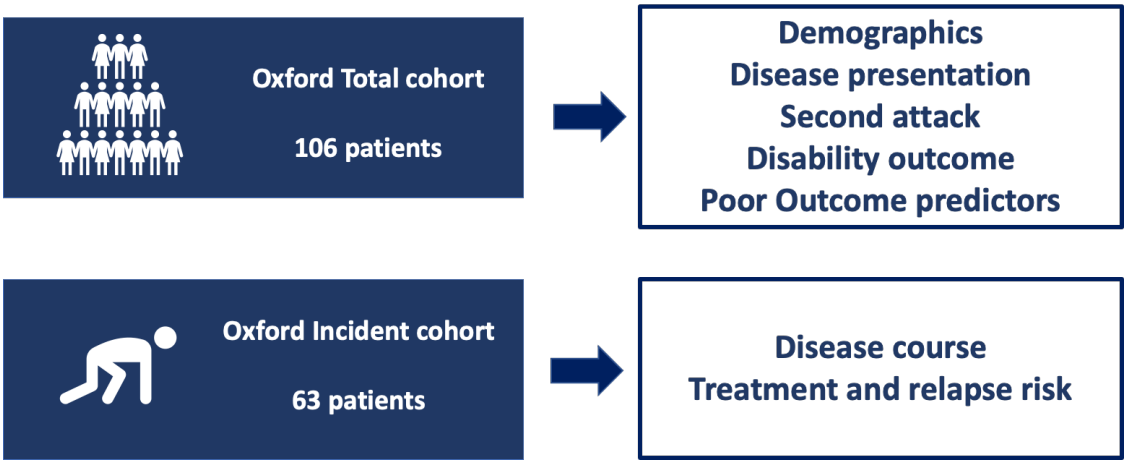


Figure 2.1 Graphical representation of the different clinical features analysed in the two cohorts

2.3 Statistical Analysis

Statistical analysis was performed with STATA 11.2 (StataCorp. 2009. Stata Statistical Software: Release 11. College Station, TX: StataCorp LP). Quantitative variables were described using means and SDs, median and range. Differences between means and differences between proportions were evaluated by t-test and $\chi 2$ test, respectively. A Shapiro-Wilk test was used to assess the normal distribution of data. In case of not normal distribution, a Wilcoxon test was performed.

ANOVA or Kruskal-Wallis tests with *post hoc* Bonferroni correction were used when comparing multiple groups. The Kaplan-Meier method was used to estimate relapse risk and disability outcomes. Univariable and multivariable logistic regression were used to identify predictors of relapses and disability. Kernel density estimate was used to identify patient sub- groups according to age of onset. Graphs were created using Rstudio (https://www.R-project.org/).

2.4 Results

2.4.1 *Demographic Data*

The demographics and clinical features of the prevalent and incident cohorts are represented in Table 2.1. There were no differences between the two cohorts, except for a lower proportion of relapsing patients and a shorter follow-up period in the incident cohort, as expected. The ethnic background, in both cohorts, was as expected in the general UK population (according to the 2011 Census, 87.2% of the UK population is White, 3% is Black/African/Caribbean/Black British, 2.3% is Asian British Indian, 1.9% is Asian British Pakistani, 2.2% is Mixed, and 3.7% is Other) (https://www.ons.gov.uk/census/2011census/2011censusdata).

In the Oxford total cohort there was a slight female preponderance of 62% and a broad onset age range of 2-69 years, with a trimodal distribution, as identified in the modelling analysis, with age cluster being <20, 20-45 years and >45 years at disease onset (see Figure 2.2).

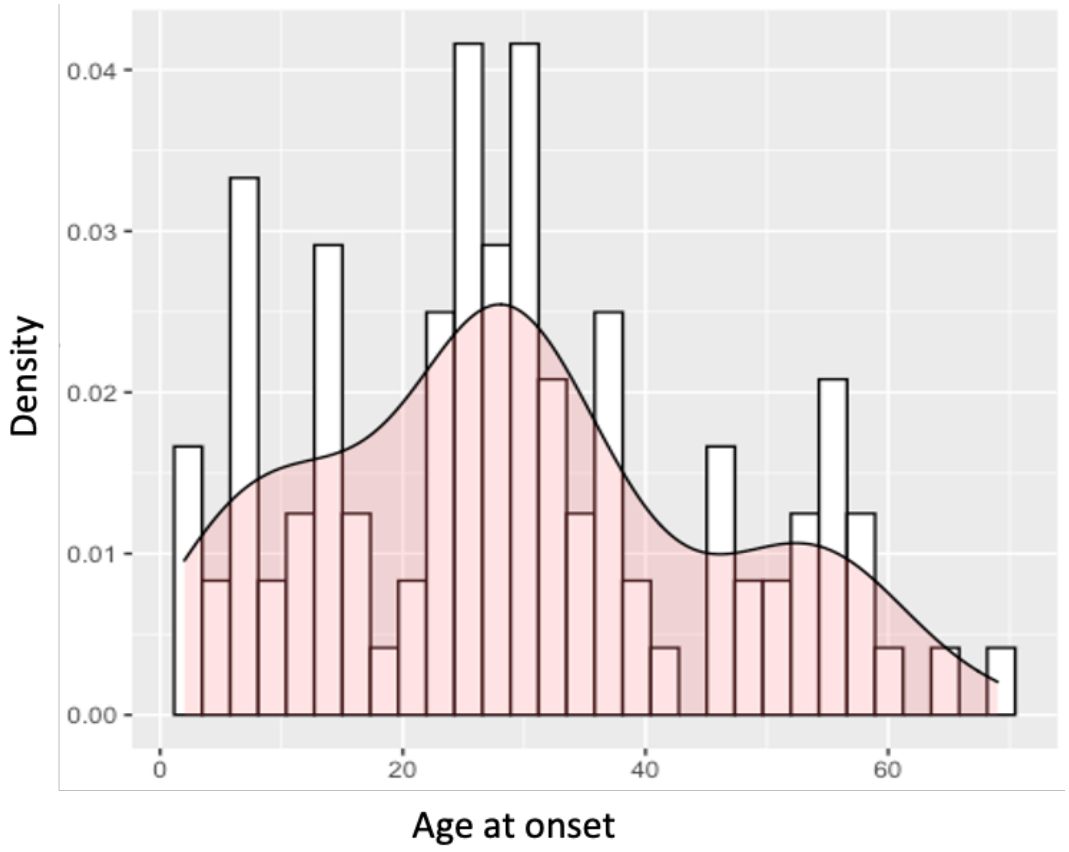


Figure 2.2 Distribution of age at onset in Oxford MOGAD patients as a histogram and density plot (in pink).

Table 2.1 Demographics and clinical features of the Oxford Prevalent and Incident Cohorts

	Oxford Prevalent Cohort	Oxford Incident Cohort
Patients, n	106	63
Mean age at onset ± SD	28.7 ± 16.6	32.8 ± 17.2
Female, % (n)	62 (66)	57.1 (36)
Ethnicity, %		
- Caucasian	76.4	79.4
- Asian	8.5	6.3
- Afro-Caribbean	2.8	4.8
- Mixed-Other	1.9	1.6
Onset attack, %		
- Unilateral ON	23.6	20.6
- Bilateral ON	30.2	33.3
- TM	17.9	19
- ADEM or ADEM-like	16	17.5
- Simultaneous ON and TM	7.5	7.9
With Short TM	0.9	0
With LETM	6.6	7.9
Disease course, %		
- Monophasic	45.3	68.3
- Relapsing	54.7	31.7
Phenotype at follow-up, %		
- ON	41.5	47.6
- TM	9.4	14.3
- ADEM/ADEM-like	22.6	23.8
- ON+TM	24.5	14.3
Paediatric onset, %	28.3	22.2
Median disease duration in months, (range)	68.2 (2-484)	19 (2-75)
Time until relapse, months*		
- 1st Quartile	7	8
- Median	36	NA
Reaching endpoints		
- VA≤6/36 in one or both eyes, %	13.2	
- Limited walking distance, EDSS≥4, %	4.7 23.6	
- Permanent bladder dysfunction, %	12.3	
- Self or in situ catheterization, %	17	
- Permanent bowel dysfunction, %	20	
- Permanent erectile dysfunction, % male		
CSF findings		
- Normal WBC (<10/ul)	29/47	
- WBC 10-50/ul	12/47	
- WBC 50-100/ul	3/47	
- WBC ≥100/ul (range)	3/47 (100-300)	
- Normal protein	27/50	
- CSF protein, 0.5-1 g/L	18/50	
- CSF protein, ≥ 1 g/L (range)	5/50 (1-2.9)	
- Elevated protein with normal WBC (protein range)	4/39 (0.6-1.7)	
- Unmatched OCB	7/57	

*Legend: *Estimated from Kaplan-Meier curves. ON = optic neuritis; TM = transverse myelitis; ADEM/ADEM-like=Acute Disseminated Encephalomyelitis; LETM=Longitudinally extensive transverse*

myelitis; VA = visual acuity; EDSS=Expanded Disability Status Scale; CSF=cerebrospinal fluid; WBC = white blood cells; OCB = oligoclonal bands.

As represented in Table 2.2, there were no differences between male and female patients, except for a preponderance of optic neuritis + transverse myelitis (the classical NMO Devic's phenotype) in male compared to female (15% vs 3%, p=0.05) (see Figure 2.3).

Table 2.2 Comparison of demographics and clinical features in female and male patients with MOGAD in the Oxford Total cohort.

	Females	**Males**
Patients, n	66	40
Mean age at onset ± SD	29.6 ± 17	27.0 ± 15.9
Ethnicity, %		
- Caucasian	72.7	82.5
- Asian	12.1	2.5
- Afro-Caribbean	3.0	2.5
- Mixed-Other	1.5	2.5
- Not available	0	1
Onset attack, %		
- Unilateral ON	25.8	20.0
- Bilateral ON	33.3	25.0
- TM	18.2	17.5
- ADEM or ADEM-like	15.1	17.5
- Simultaneous ON and TM	3.0	15
With Short TM	0	2.5
With LETM	3.0	10
- Not available	0	2.5
Disease course, %		
- Monophasic	43.9	47.5
- Relapsing	56	52.5
Median disease duration in months, (range)	37 (3-484)	26 (2-323)

Legend: SD=standard deviation; ON = optic neuritis; TM = transverse myelitis; ADEM/ADEM-like=Acute Disseminated Encephalomyelitis; LETM=Longitudinally extensive transverse myelitis.

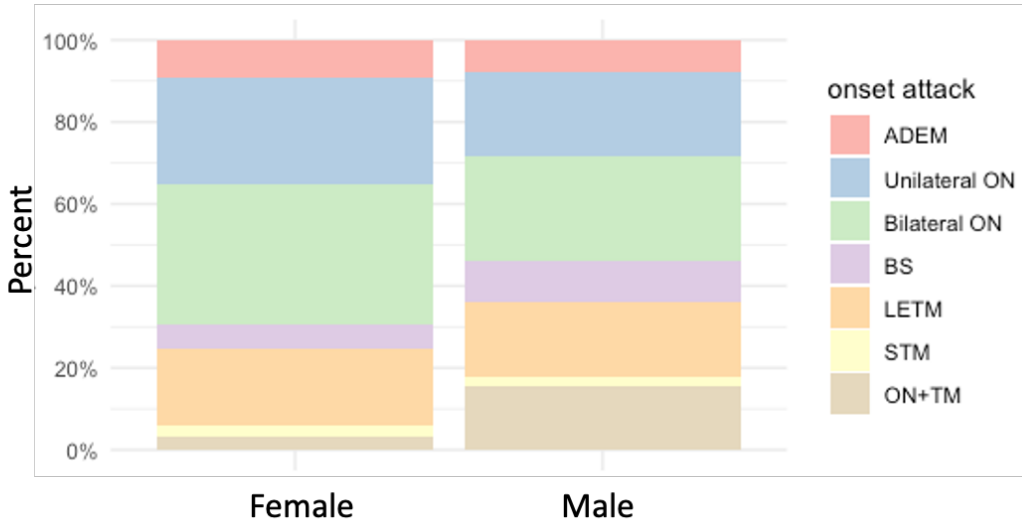


Figure 2.3 Percentage comparison of the onset attack phenotype between female and male patients with MOGAD in the Oxford Total cohort*. Legend: ADEM=acute disseminated encephalomyelitis; ON=optic neuritis; BS=brainstem; LETM=longitudinally extensive transverse myelitis; STM=short transverse myelitis; TM=transverse myelitis.*

When comparing the Caucasian and non-Caucasian patients (see Table 2.3) there was a preponderance of female in the non-Caucasians group, although the difference was not significant (78.6% vs 59.2%, p=0.2).

Table 2.3 Comparison of demographics and clinical features in Caucasians and Non-Caucasians patients with MOGAD in the Oxford Total cohort.

	Caucasians	**Non-Caucasians**
Patients, n	81	14
Mean age at onset ± SD	29.8 ± 16.9	25.9 ± 18.3
Breakdown of ethnicities		
- Asian	NA	9
- Afro-Caribbean	NA	3
- Mixed-Other	NA	2
Female, %	59.2	78.6
Onset attack, %		
- Unilateral ON	23.4	21.4
- Bilateral ON	29.6	35.7
- TM	18.5	21.4
- ADEM or ADEM-like	14.8	21.4
- Simultaneous ON and TM	9.9	0
With Short TM	1.2	0
With LETM	7.4	0
Disease course, %		
- Monophasic	43.2	42.8
- Relapsing	56.8	57.1
Median disease duration in months, (range)	32 (2-484)	41.5 (3-189)

Legend: SD=standard deviation; ON = optic neuritis; TM = transverse myelitis; ADEM/ADEM-like=Acute Disseminated Encephalomyelitis; LETM=Longitudinally extensive transverse myelitis.

2.4.2 *Disease presentation – Oxford Total cohort*

In the Oxford total cohort 53.8% of patients presented with optic neuritis (30.2% bilateral and 23.6% unilateral). About 18% of patients presented with an isolated transverse myelitis, 7.5% with transverse myelitis associated with optic neuritis and 16% with ADEM or ADEM-like. Patients with ADEM/ADEM-like were younger at onset and in patients with <20 years old represented 19% of onset phenotype (see Figure 2.4 A and B).

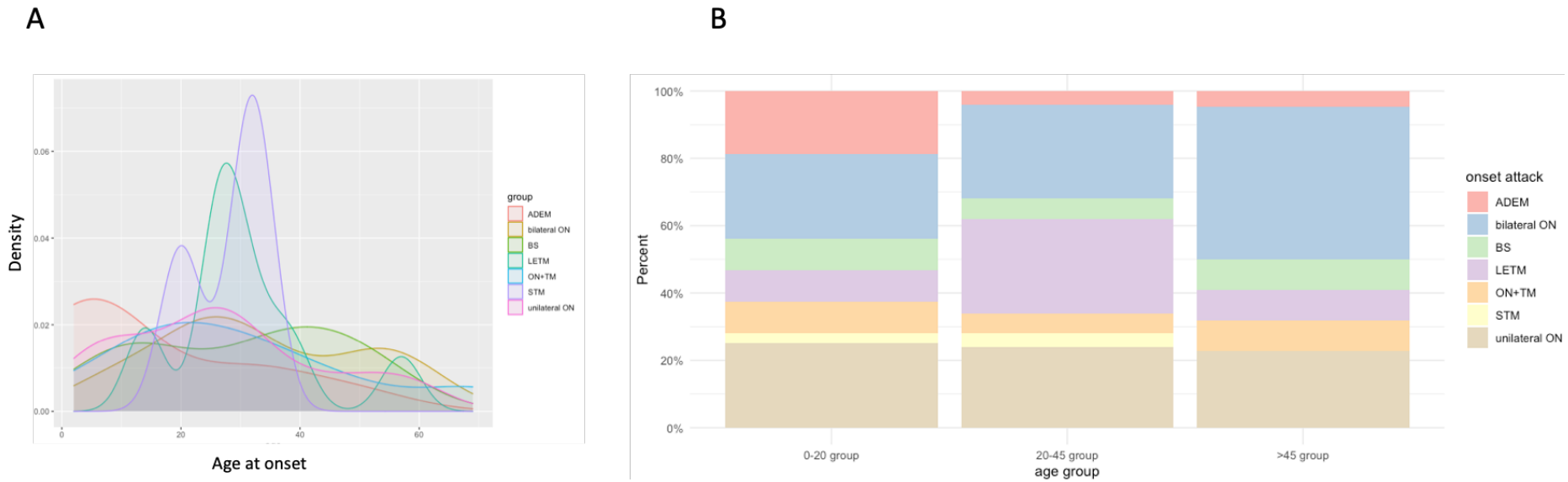


Figure 2.4 A) density plot of age at onset in distinct MOGAD phenotype. B) percentage comparison of onset phenotype between age-class. *Legend: ADEM=acute disseminated encephalomyelitis; ON=optic neuritis; BS=brainstem; LETM=longitudinally extensive transverse myelitis; TM=transverse myelitis; STM=short transverse myelitis.*

Patients with age at onset of between 20-45 years, most often presented with bilateral optic neuritis or longitudinally extensive transverse myelitis (LETM) (both 28%), while bilateral optic neuritis was the most represented phenotype in patients with >45 years. Short TM was most common among the patients 20-45 years old at onset (28%).

Area postrema syndrome (APS) symptoms (nausea, vomiting, hiccups) were present in 11 out of 106 patients (10%). Vomiting was the most frequent symptom (7 patients), followed by nausea (3 patients), hiccups (1 patient) and cough (1 patient). In 10/11 patients APS was associated with the presenting attack, and in 5/10, APS preceded the onset attack (less than one month interval between the APS and other CNS symptoms). APS preceded ADEM/ADEM-like in two patients, bilateral ON in two patients and ON+TM in one patient. APS was associated with ADEM/ADEM-like in two patients, transverse myelitis in two patients, and ON+TM in one patient at onset. In one patient APS was present at the time of the second attack (unilateral optic neuritis). Brain MRI was available for 9/11 patients at the time of symptoms. Three patients had brainstem lesion adjacent to the fourth ventricle (see Figure 2.5), one had cerebellar lesions, three had brain lesions without cerebellar or brainstem involvement, and two had a normal brain MRI.

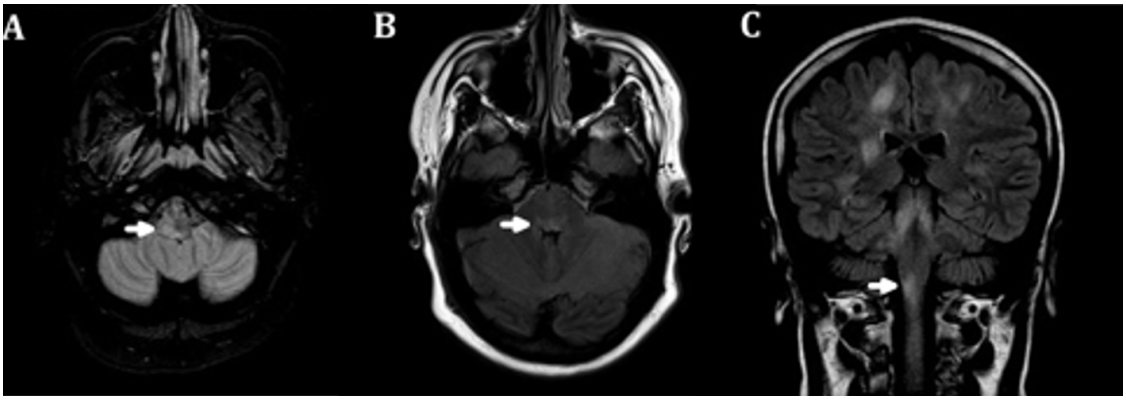


Figure 2.5 Examples of MRI brainstem lesions adjacent to 4th ventricle and involving area postrema in three different MOGAD Oxford patients with symptoms in keeping with area postrema syndrome*. Image adapted from Jurynczyk, M*, Messina, S* et al, Clinical presentation and prognosis in MOG-antibody disease: a UK study, Brain. 2017 Dec 1;140(12):3128-3138. *These authors equally contributed to the study. All rights reserved.*

2.4.3 *Disease course – Oxford Incident cohort*

The time taken until 25% of the patients had a relapse, was 7 months and was estimated from the Oxford incident cohort survival curve (see Figure 2.6 A). Thirty-eight percent experienced a relapse after 18 months (median follow up time 19 months, range 2-75 months).

When considering the 41 patients who had been followed up for at least 12 months, 29% relapse within 1 year. Of the 27 patients who had been followed up for at least 24 months, 41% relapsed within 2 years. Patients who presented with isolated optic neuritis or associated with transverse myelitis, showed a tendency to relapse more (see Figure 2.6 B)

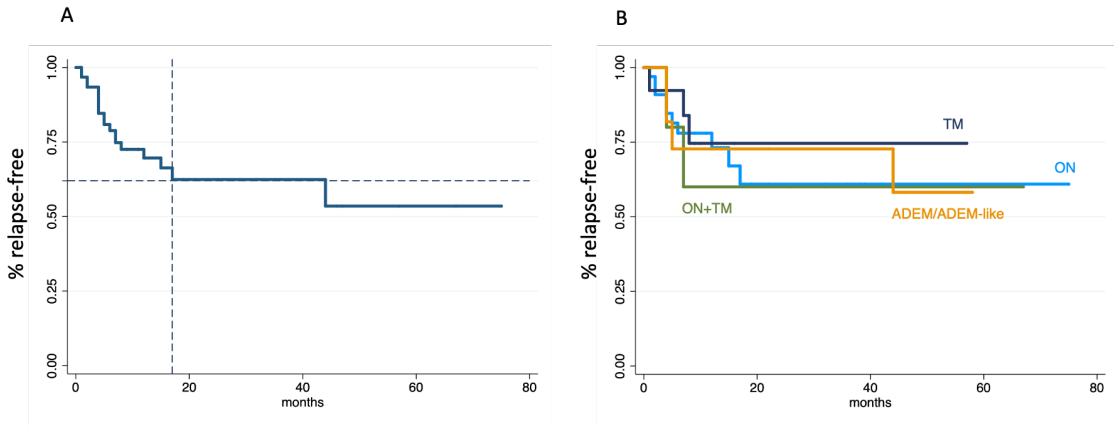


Figure 2.6 Kaplan Meier curve showing the cumulative probability over time to remain relapse free A) in the whole cohort and B) depending on the onset attack. *Legend: TM=transverse myelitis, ON=optic neuritis, ADEM/ADEM-like=acute disseminated encephalomyelitis.*

2.4.4 *Second attack – Oxford Total cohort*

The most common phenotype of the second attack was optic neuritis. 39/58 (67%) relapsing patients experienced unilateral or bilateral optic neuritis. Out of the 32 relapsing patients with optic neuritis at onset, 26 experienced a second optic neuritis (82%). Optic neuritis was the second attack phenotype in six out of 10 relapsing patients with transverse myelitis at onset (60%) and four out of 10 relapsing patients with ADEM/ADEM-like at onset (40%).

2.4.5 *Treatment and relapse risk – Oxford Incident cohort*

In the incident cohort, acute treatment data were available for 61 patients. At the time of the onset attack, four patients were not treated, 35/61 (57.4%) were treated with intra venous methylprednisolone (IVMP), 8/61 (13%) with IVMP followed by plasma exchange (PLEX), 7/61 (11.5%) with oral steroids (prednisolone or oral methylprednisolone), one with intravenous immunoglobulin (IVIG), 3/61 (4.9%) with a

combination of IVMP, IVIG and PLEX, two with IVMP and IVIG and one with other treatment and IVIG.

Out of the 63 patients in the incident cohort, 49 were started on an immunosuppressant cover after the onset attack. In particular, 41 were on oral prednisolone, one on azathioprine, six on prednisolone + azathioprine (for one patient details of the treatment were not available). Patients with shorter course of immunosuppression after the onset attack are more likely to relapse (Figure 2.7A), and this is more evident when analysing the time to relapse from the end of steroids treatment (Figure 2.7B). The risk of relapse was significantly lower in those patients treated for more than 3 months (Cox hazard ratio HR=0.14, 95% CI 0.03-0.67, p=0.013) (Figure 2.7 C).

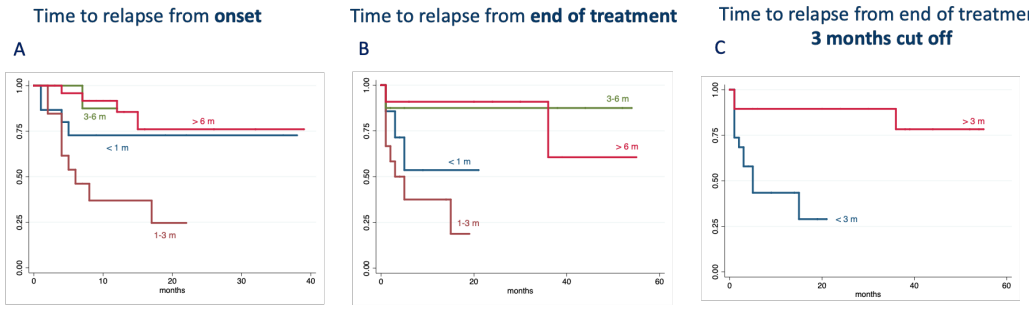


Figure 2.7 Kaplan-Meier curves showing the cumulative probability over time to remain relapse free, depending on A) how long the patients were on immunosuppression: <1 month, 1-3 months, 3-6 months and >6 months, B) the duration of the immunosuppression with baseline observation at the time of immunosuppression discontinuation, and C) using the 3 months immunosuppression duration cut-off

2.4.6 *Disability outcome – Oxford Total cohort*

In the Oxford total cohort, 43 out of 106 (40.6%) had permanent visual (visual acuity ≤6/36 in at least one eye), motor (EDSS≥4) disability, sphincter, and erectile dysfunction at the time of the last follow up. Thirty-three became disabled from the onset attack, while 11 from subsequent attacks.

Visual disability: Out of the 106 patients, two (1.8%) had visual acuity worse than 6/36 in the best eye at last follow-up. Fourteen (9 female, 5 male) out of 106 patients (13.2%) had permanent visual disability, defined as visual acuity worse than 6/36 in at least one eye and all of them had optic neuritis (± transverse myelitis or ADEM) during the onset attack. Nine out of the 69 onset optic neuritis reached the visual disability as a consequence of the onset attack. Seven of them at the time of the acute attack were treated with IVMP, one with dexamethasone and one was not treated.

Of the remaining 60 optic neuritis at onset, five became visually impaired from subsequent attacks of isolated optic neuritis. Of these five patients, three had a full recovery from the onset optic neuritis, one had a good recovery and one moderate recovery (but the visual acuity did not reach the 6/36). The remaining 55 patients with optic neurites at onset did not reach the visual disability.

Out of the five patients who became visually impaired from the subsequent attacks of optic neuritis, four were not on long-term immunosuppression, one was on a reducing dose of prednisolone and methotrexate. At the time of the acute relapse, three patients out of five received IVMP, in one patient prednisolone was increased and one patient was not treated.

The univariable logistic regression with sex, age, disease duration and onset attack, showed that younger age at onset ($p=0.02$), longer disease duration ($p<0.001$) and optic neuritis at onset (unilateral/bilateral ON $p=0.02$, more likely than other presentations) are associated with visual disability, and only disease duration ($p<0.001$) and optic neuritis at onset ($p=0.02$) retained statistical significance in the multivariable analysis. The survival analysis showed that patients with younger age and optic neuritis at onset are more likely to be visually disabled (see Figure 2.8A and B).

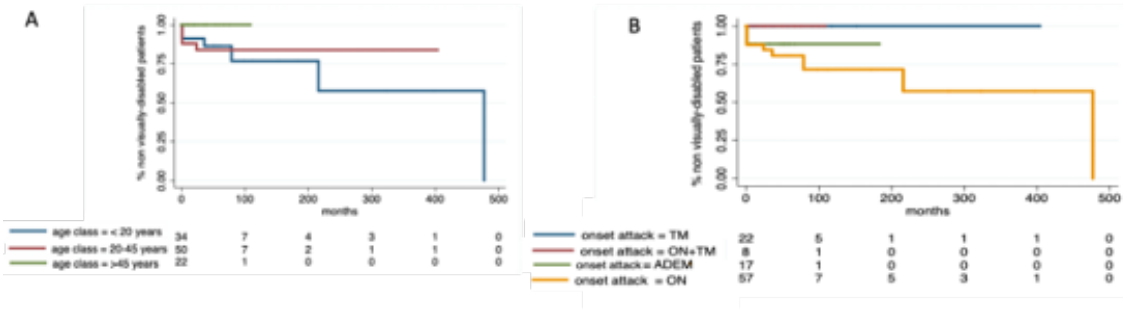


Figure 2.8 Kaplan-Meier curves showing the cumulative probability over time to remain non visually disabled, depending on A) age class: <20 years, 20-45 years and >45 years, and B) onset attack. *Legend: TM=transverse myelitis; ON=optic neuritis; ADEM=acute disseminated encephalomyelitis.*

Motor disability: five patients (two female and three men, all Caucasians) reached permanent motor disability (EDSS ≥4) at the last follow-up, and all of them had transverse myelitis (± optic neuritis or brain involvement). Out of the five patients, four had EDSS≥6 at the last follow up. Of the five patients, three reached the motor disability as a consequence of the onset attack.

Of the three patients who reached motor disability during the onset attack, two were treated at the onset attack with IVMP, plasma exchange and immunoglobulins, and one with IVMP only.

The two patients with motor disability as a consequence of subsequent attacks, presented with optic neuritis or ADEM/ADEM-like at onset, and both stopped oral corticosteroids just prior the disabling transverse myelitis attack. At the time of the transverse myelitis attack, one was treated with IVMP followed by oral prednisolone and the other had no acute treatment and was started on interferon-beta. Age at onset, disease duration, sex and attack type were not significantly associated with the motor disability outcome (see Figure 2.9 A-B).

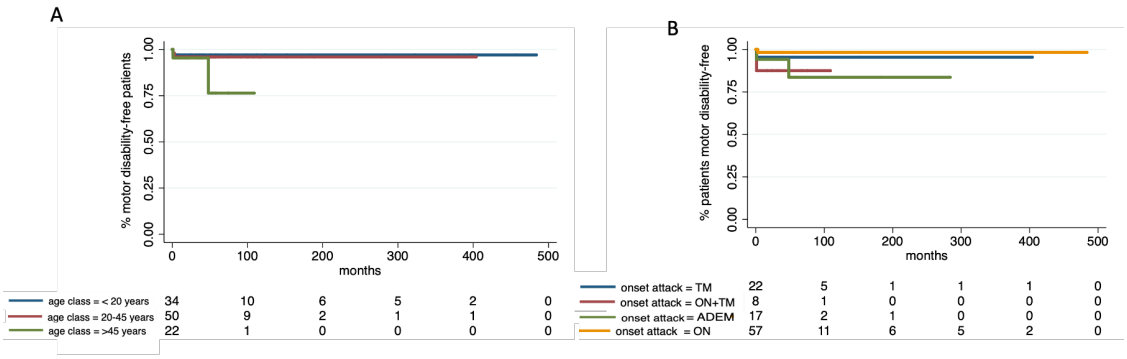


Figure 2.9 Kaplan-Meier curves showing the cumulative probability over time to remain non mobility disabled, depending on A) age class: <20 years, 20-45 years and >45 years, and B) onset attack. *Legend: TM=transverse myelitis; ON=optic neuritis; ADEM=acute disseminated encephalomyelitis.*

Bladder disability: twenty-five patients were left with bladder dysfunction at the time of last follow-up. Thirteen out of 25 patients required long-term catheterizations at the time of the last follow-up. Only two of them had associated motor disability (EDSS≥4).

In all 25 patients the bladder dysfunction was a consequence of transverse myelitis (± other features). Bladder disability was present in 12 females and 13 males, and the majority were Caucasian (20 Caucasian, two Asian and one Afro-Caribbean). Most of the patients presented with involvement of the thoracic cord and the conus and only three patients presented with cervical cord involvement only. Nineteen out of 25 patients were left disabled from the onset attack. Out of these nineteen patients, eight were treated with IVMP only, five with IVMP and plasma exchange, three with IVMP, plasma exchange and immunoglobulins and two with oral steroids (for one patient the information was missing).

Six out of 25 patients were left with bladder dysfunction from subsequent attacks (all six with transverse myelitis ± brain involvement/optic neuritis). Two of them presented with transverse myelitis, two with ADEM and two with optic neuritis at onset. Three were not on background immunosuppression, two stopped steroids within the two weeks before

the disabling attack and one was on a reducing dose of prednisolone. At the time of the disabling attack, five were treated with IVMP and one with oral methylprednisolone.

The univariable logistic regression showed that being male is associated with bladder disability at a trend level (estimate 0.14, p=0.096), while transverse myelitis (estimate=0.46, p<0.001), optic neuritis + transverse myelitis (estimate=0.46, p=0.001) and ADEM ± other features (estimate=0.44, p<0.001) at onset are significantly associated with bladder disability. Figure 2.10 B shows that patients with transverse myelitis, optic neuritis + transverse myelitis and ADEM ± other features at onset, are more likely to reach the bladder disability.

Age at onset and disease duration were not significantly associated, although the cumulative probability to reach bladder disability appear more often in the 20-45 years age group (not significant) (see Figure 2.10 A).

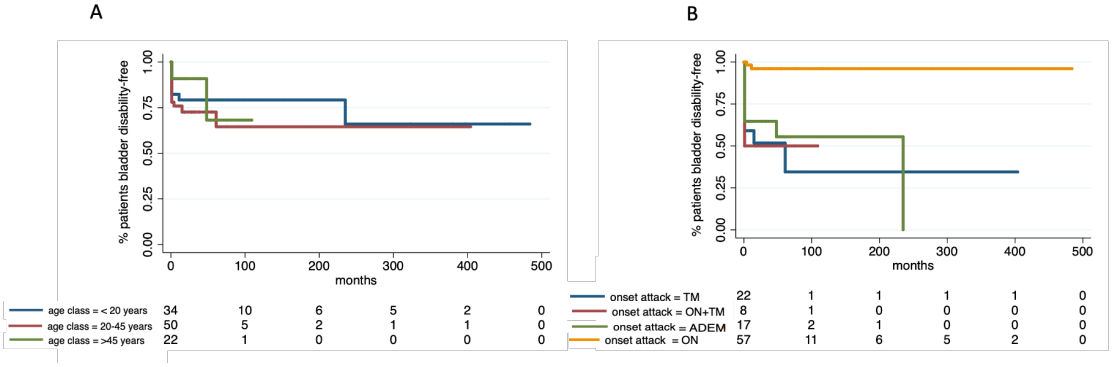


Figure 2.10 Kaplan-Meier curves showing the cumulative probability over time to remain bladder disability free, depending on A) age class: <20 years, 20-45 years and >45 years, and B) onset attack.
Legend: TM=transverse myelitis; ON=optic neuritis; ADEM=acute disseminated encephalomyelitis.

Bowels and erectile dysfunction: all patients with bowels and erectile dysfunction, were also left with bladder disability. Bowel dysfunction occurred in 18 patients (eight female and 10 men). Erectile dysfunction occurred in 21% of men and 44% of men presenting with transverse myelitis at onset.

Cognitive problems: a total of eight patients were left with cognitive problems. Seven of them presented with ADEM/ADEM-like phenotype at onset and one patient presented with optic neuritis and transverse myelitis phenotype with brain lesions (small lesions not fulfilling the ADEM definition). From the total eight patients with cognitive problems, five had a paediatric onset (16.6% of paediatric patients) and three adult-onset (3.9% of the adult patients). Of the paediatric patients, one complained of poor concentration, one presented learning difficulties, one showed psychiatric symptoms (mania, hallucination) and was also positive for NMDAR-Ab, one with memory deficit and learning difficulties, and one received a diagnosis of autism spectrum disorder. Of the three adult patients, one complained of memory impairment and low mood, one poor concentration and one somnolence. In the eight patients with cognitive problems, the brain MRI at the time of the attack which caused the cognitive disability, showed basal ganglia involvement in four, cortical/subcortical involvement in two, extensive white matter lesions in one (for one patient the MRI was not available).

2.4.7 *Poor outcome predictors - Oxford Total cohort*

In the total Oxford Cohort, 44 out of the 106 patients (44%) reached at least one disability outcome (visual, motor, sphincter, and cognitive outcome) with a median follow up time of 55.5 months (range 7-484).

Transverse myelitis (± optic neuritis) and ADEM at onset are predictors of poor outcome (transverse myelitis estimate=0.30, p=0.01, optic neuritis + transverse myelitis estimate=0.38, p=0.03, ADEM estimate=0.52, p<0.001). Older age at onset (estimate=0.006, p=0.03) was significantly associated, while disease duration showed a

trend (estimate=0.0009, p=0.06). Disease duration and onset-attack maintained significance in the multivariable model.

2.4.8 *Acute brain MRI involvement*

Among the 25 patients who had brain lesions, 17 presented with ADEM/ADEM-like at onset, three with optic neuritis, four with transverse myelitis and one with optic neuritis + transverse myelitis. Of the 25 patients four presented seizures, one had positive NMDAR-ab, one had a low positive NMDAR-Ab results followed by a negative one. Seven patients presented with brainstem and basal ganglia involvement, two with isolated basal ganglia involvement, five with isolated brainstem involvement, four with brainstem and middle cerebellar peduncles involvement, three with white matter lesions (one with extensive hemispheric lesions, one with juxtacortical lesions and one with internal capsule and middle cerebellar peduncles lesions), and three with cortical/subcortical involvement.

2.5 Discussion

This chapter describes the largest single site and the first incident MOGAD cohort. MOGAD patients present at onset more frequently with optic neuritis, which is also the most common presentation at the time of the second attack (~70%). There is a slightly preponderance of female compared to men. There is no ethnic difference, and the disease in the UK is more common among Caucasians. Most of the patients are relapsing, with the risk of a relapse depending on the length of the steroids cover after the onset attack. The prognosis is good, although a proportion of patients can be left with sphincter

dysfunction, cognitive problems (especially in those with silent/clinically significant brain involvement) or poor vision, mainly associated to the onset attack.

Optic neuritis being the most common presentation at onset, and at the time of the first relapse, regardless of the onset attack, has been confirmed in further studies. (Cobo-Calvo et al., 2018; Ramanathan et al., 2018). ADEM/ADEM-like presentation is common among younger patients, while short TM can be found in those between 20-45 years. The classic Devic's phenotype, ON+TM, is a less common presentation and is more common among men.

Early studies focusing on ON+TM MOGAD, indicated that the presence of MOG-Ab was a predictor of a monophasic phenotype (Kitley et al., 2012b; Kitley et al., 2014b). However, the clinical MOGAD phenotype is now recognised to be much broader and include a relapsing phenotype (Hoftberger et al., 2015; Sato et al., 2014).

In contrast to the present study, showing an annualised relapse rate for the total cohort of 0.2, previous studies reported a higher relapse rate and risk of relapses, which was possibly an overestimate due to the inclusion of a predominantly relapsing population, since patients with onset prior to the discovery of the MOG-Ab, are most likely to be re-assessed if they present with a further relapse. The use of the incidence cohort, including only those patients with MOGAD diagnosis at onset, and before further relapses, avoided the bias towards relapsing disease, allowing a real estimate of the relapse risk.

Furthermore, the policy of the Oxford NMO service to treat patients for at least 6 months after the onset attack, appears to reduce the relapse risk over time (<50% after 2 years) and may explain the lower relapse rate in the Oxford cohort. It is still possible that not all

monophasic patients have been referred to the service, thus this may be an estimate of a potentially lower relapse risk.

The long-term prognosis in MOGAD has been largely debated, especially before the publication of the present study, as previous studies included small numbers, or were multicentre therefore including a more heterogeneous population.

A previous study including 50 patients from different centres, found a high percentage of visually disabled patients (36%, visual disability defined as VA<0.5 in one or both eyes) and walking impaired patients (25%) (Jarius et al., 2016c). Another study including 56 MOGAD patients, found a lower percentage of visually impaired (19%, sustained visual acuity <0.2) and only 11% with EDSS>4 (Sepulveda et al., 2016), in keeping with our figures of 13.2% of visually impaired and ~4% with EDSS>4. A more recent study found a similar percentage of visual impairment (12.6% VA<=0.2) in adult MOGAD patients (Cobo-Calvo et al., 2021).

When considering EDSS>6 (patient needs unilateral support to walk), previous studies found only 4-6% of patients were impaired, in line with our figures of 3.7% (Kim et al., 2015b; Sepulveda et al., 2016).

Visual disability occurred more frequently related to the onset attack, but could also result from subsequent relapses, while motor disability was rare and resulting from both onset attack and subsequent relapses.

Sphincter, and erectile dysfunction in men, were more frequent than motor disability, in contrast with what has been observed in MS, where sphincter dysfunction and motor disability coexist (Miller et al., 1965) and are less frequent than MOGAD (Dubey et al., 2019).

Cognitive problems were reported in 16% of paediatric MOGAD and 3.9% of adult MOGAD, and when MRI was available, a prevalent involvement of the deep grey matter structures, was noted.

A recent study showed that academic difficulties, used as an indirect measure of cognitive function, can be present in up to 26% of children with MOGAD, and were associated with the presence of deep grey matter lesions (Cobo-Calvo et al., 2021). Although academic performance has been used as a surrogate of cognitive function in children, it is not as objective as a formal cognitive test, as it can be affected by different social and economic factors, therefore not reflecting the real prevalence in the paediatric population. Cognitive function has never been systematically assessed with a cognitive battery in the MOGAD population, therefore it is possible that these figures are not a correct estimate of the real burden in adult and paediatric patients with brain involvement.

MOGAD when compared to NMOSD-AQP4 is less disabling. When considering those patients with 25 months of follow up, visual disability and permanent motor disability (EDSS>6) were ~2% and ~4% in the MOGAD population, while in the UK NMOSD study was 20% and 25% respectively (as estimated from the survival curves, with a median follow up time of 25 months) (Kitley et al., 2012a). In the UK NMOSD-AQP4 study sphincter dysfunction was not assessed as a disability outcome, but anecdotal evidence suggest that is associated with motor disability, and rarely present as the only disability outcome.

Brainstem involvement, and in particular area postrema syndrome (nausea, vomiting, hiccups), typical of NMOSD-AQP4 (~40%)(Dos Passos et al., 2018), has been described in MOGAD (10%) as well.

The main limitation of the study is the retrospective data collection and the relatively short follow-up. Some of the outcomes, such as sphincter dysfunction and erectile dysfunction, cannot be captured with neurological examination and have not been systematically tested with investigations, but reported by the patients and assessed with symptoms questionnaires in clinic. However, visual acuity and motor disability which have been objectively evaluated, are more reliable as disability outcome, and support the finding of MOGAD as a less disabling disease when compared to NMOSD-AQP4.

2.6 Conclusion

MOGAD is a recently identified condition, distinct from multiple sclerosis and NMOSD-AQP4. It can present with attack involving the optic nerve, the spinal cord, then brain and the brainstem. The risk of relapse is moderate, and this study showed for the first time that the relapse risk can be higher within the first year from onset and can be reduced with an immunosuppression cover after the onset attack. The prognosis is good, although a proportion of patients can be left with visual, motor, sphincter and erectile dysfunction, and cognitive problems, especially after the onset attack.

3 Chapter 3 MRI study overview: methods, clinical assessment, and cohort

3.1 Introduction and Background

In the previous chapter the clinical characteristics and the long-term outcomes of the MOGAD cohort have been described. Two main considerations raised from the previous chapter: a) the MOGAD patients have a better recovery than NMOSD-AQP4, although comparison with previously described cohorts showed that they are similar in term of clinical manifestations and conventional MRI findings b) the actual impact of cognition on the adult population and the possible relationship with the brain involvement have not been fully elucidated. In light of these considerations, an imaging study was set up to better quantify the MRI changes behind the residual tissue damage in the remission stage and the association with disability outcomes and cognition in the MOGAD participants, compared to healthy controls (HC) and to NMOSD-AQP4 and MS.

The overview of the MRI study and the studied cohort are described in this chapter. The dataset consists of clinical and imaging data collected specifically for the purpose of this project and the results are outlined in Chapter 4-8.

Part of the methods described in this chapter has been adapted from the publication Messina et al. *Contrasting the brain imaging features of MOG-Antibody disease, with AQP4- Antibody NMOSD and Multiple Sclerosis (Messina et al., 2021b).*

3.2 Study design

This cross-sectional study was designed to compare lesion distribution, volumetric, diffusion and functional brain imaging across four group of participants: participants with MOGAD, participants with NMOSD-AQP4, participants with relapsing remitting MS and HC. The association between the MRI findings and clinical outcomes were then explored, as outlined in Figure 3.1.

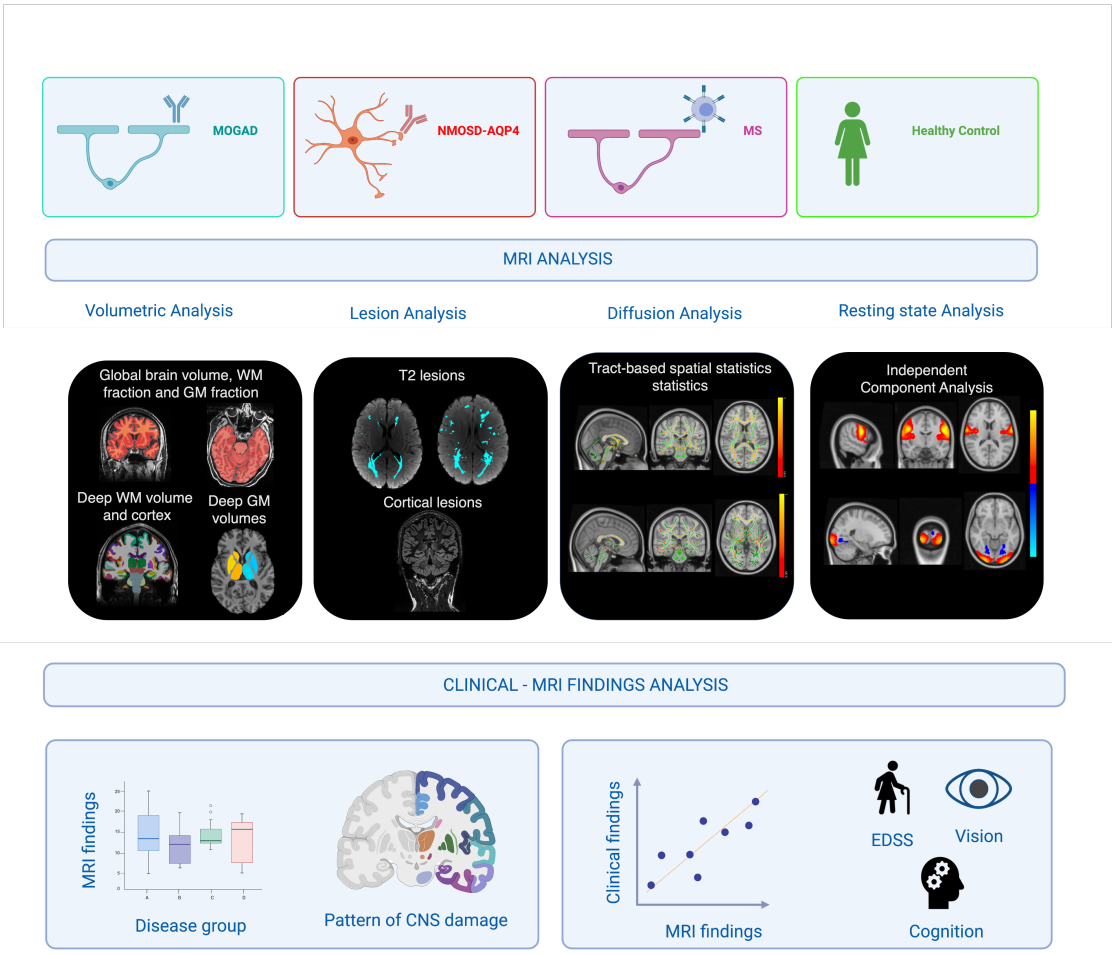


Figure 3.1 Outline of the study workflow. *In the following result chapters, the following colour-codes have been used to identify the different groups in the figures. NMOSD-AQP4=red, MOGAD=blue, MS=purple, Healthy volunteers/controls=green. Created with BioRender.com*

3.2.1 *Ethics*

In adherence to ethical regulations from the UK National Research Ethics Service, all participants were fully informed of the techniques and potential risks and signed a detailed consent form. Ethical approval was obtained with the following project code: REC 17/EE/0246 Cambridge South. Additional patients' clinical data were collected from existing NMOSD service database, MS service database, clinic letters or notes under the following ethical approval: REC 16/SC/0224 (Neuromyelitis Optica Spectrum Disorders and Multiple Sclerosis Research Tissue Bank).

3.2.2 *Consideration for powering the study*

The difficulty in calculating the power and sample size for this project was related to the difficulty to detect a true effect size for different parameters, having used a multimodal approach, as power can be different, based on the chosen modality (i.e., structural, diffusion and functional MRI). Sample size calculation can be a concern when studying rare diseases and is particularly difficult and controversial for multimodal neuroimaging studies (Suckling et al., 2014). NMOSD and MOGAD are rare diseases, with a prevalence in Oxfordshire of 1.2/100,000 and 2.0/100,000 respectively (O'Connell et al., 2020). Given the rarity of the studied conditions, recruiting in the setting of an NHS nationally commissioned service, was an advantage to increase the sample size. Using the same scanner and protocol, along with reliable diagnostic ability, will reduce 'noise' and improve the power.

Nevertheless, the study was designed to have the power to detect group differences in metrics, based on previous NMOSD and MS MRI studies (Chanson et al., 2013; Jeong et

al., 2017; Liu et al., 2014; Lopes et al., 2015; Matthews et al., 2015; Pichiecchio et al., 2012; Rocca et al., 2004).

3.2.3 *Study participants recruitment*

Patients were recruited from the Diagnostic and Advisory service for Neuromyelitis Optica and the MS service at John Radcliffe Hospital, Oxford University Hospital Foundation Trust, Oxford, UK. The NMOSD Access Database was screened to identify participants with brain or spinal cord involvement (either symptomatic or asymptomatic). Testing for the presence of AQP4-ab and MOG-Ab were performed in the Autoimmune Neurology Laboratory using a cell-based assay as described by Waters et al (Waters et al., 2015; Waters et al., 2012). All NMOSD participants had an AQP4-Ab positive assay and none of the MOGAD participants were positive for AQP4-Ab. All MOGAD participants had a MOG-Ab positive antibody assay and were negative for AQP4 antibodies. All MS participants were approached at consecutive clinic visit and they were enrolled in the study if confirmed relapsing remitting MS.

Inclusion criteria

- Confirmed diagnosis of NMOSD-AQP4 (according to Wingerchuck criteria) (Wingerchuk et al., 2015), MOGAD (positive for MOG-Ab using the most accurate cell-bases assay as outlined above) or MS (according to 2010 McDonald criteria) (Polman et al., 2011) or, if HC study participants should be in good health.
- Brain and/or cord involvement (either symptomatic or asymptomatic)
- Study visit completed at least six months after an acute attack and/or acute steroid treatment (as this can potentially be a confounder when studying the MRI findings)

- Fluency in English language to complete consent form and MRI safety questionnaire.
- Aged 18 years or above at the time of the scan
- Adult-onset disease

Exclusion criteria

- Any contraindication to the MRI scanning, including claustrophobia.
- Participant unwilling to sign consent or unable to fully understand the consent or the MRI safety questionnaire.
- Pregnancy
- A concurrent disease/disorder that, as determined by the specialist neurologist, may confound the data, or lead to undue risk to the patient. HC were screened for symptoms or conditions that may confound the findings (i.e., other neurological conditions).

3.3 Study visits and clinical data

All participants underwent the same visit protocol which consisted of the following evaluations:

- Neurological examination assessed by the Expanded Disability Status Scale (EDSS) (Kurtzke, 1983).
- Visual acuity (VA).
- The Brief Repeatable Battery of Neuropsychological Tests (BRB-N) and Stroop test (Rao, 1990; Stroop, 1935) (30-40 minutes).
- Brief pain inventory (BPI) (Cleeland and Ryan, 1994).
- Modified fatigue impact scale (MFIS) (Fisk et al., 1994a).

- Hospital Anxiety and Depressions scale (HADS) (Snaith and Zigmond, 1986).
- Brain MRI (40 minutes) (see Table 3.1 for the MRI protocol)

3.3.1 *Motor disability*

All participants were examined by raters with Level C certificate in EDSS examination (www.neurostatus.net). An EDSS score was assigned based on the neurological examination to each disease group participants. EDSS is a method to quantify disability in MS, and it has been extensively used in other demyelinating diseases (i.e., NMOSD and MOGAD). It ranges from 0.0 (normal examination) to 10.0 (death due to the demyelinating disease). Disability milestones are EDSS 4.0 (significant disability but able to walk without support), EDSS 6.0 (requiring a walking-aid) and EDSS 8.0 (patient essentially restricted in bed or chair).

3.3.2 *Visual Disability*

The visual acuity was evaluated using the Early Treatment in Diabetes Retinopathy Study charts (ETDRS) at a 1-m distance. The logarithm of the minimum angle of resolution (logMAR) was calculated. LogMAR scale range from 0.0, which corresponds to the Snellen score 6/6 (normal vision) to 1.0 which correspond to the Snellen score 6/60. In case of VA worse than 6/60, the participant vision was described as counting fingers (CF), hand movements (HM), light perception (LP) and non-light perception (NLP), and then was transformed in LogMAR according to (Bonnan et al., 2018; Holladay, 1997; Schulze-Bonsel et al., 2006).

3.3.3 *Cognitive function*

The Rao's Brief Repeatable Battery of neuropsychological test (BRB-N) was administered in a quiet room before the MRI scan, preferentially in the morning, by a researcher with previous experience with this battery (Rao et al., 1991). The BRB-N was chosen as it has been extensively used in MS and NMOSD cohorts (Messina and Patti, 2014; Oertel et al., 2019). To date there are no studies using the BRB-N to explore the cognitive function in MOGAD patients.

The BRB-N consists of five tests exploring four main cognitive domains: verbal and long-term memory, visuospatial memory, attention and concentration, and executive function (Rao, 1990). As the executive functions are not extensively represented in the BRB-N (only one test explores verbal fluency), the Stroop word-colour test was added (Amato et al., 2006).

Tests were administered according to the following fixed order:

The Selective Reminding Test (SRT) tests verbal learning and delayed recall. It consists of a list of 12 words and six consecutive learning trials and one delayed recall trial (performed after the attention and concentration tests). A word recalled in two consecutive trials, it will be considered as entering the long-term storage (LTS) memory, therefore scored as LTS in the following trials. If an LTS word is recalled in every consecutive trial, it will be scored as Consistent Long-Term Retrieval (CLTR). The SRT-LTS and SRT-CLTR scores are the total number of LTS words and CLTR words at the end of the six trials. The delayed recall (SRT-D) is the total number of words recalled after the delayed period (Buschke and Fuld, 1974).

The 10/36 Spatial Recall Test (SPART) tests visuo-spatial memory and delayed recall and it is a modified version of the 7/24 SPART (Barbizet and Cany, 1968). A checkboard with a pattern was showed to the participant for 10 seconds. Then the participant was

asked to reproduce the same pattern on an empty checkboard (printed on a paper sheet) using a pen. The scores are the total numbers of correct answers in every trial (there are three consecutive trials) (SPART) and the correct answers after the delayed period (SPART-D).

The Symbol Digit Modality Test (SDMT) is a measure of information processing speed. The participant was given a sheet with a legend on top of the page, where nine symbols are represented, paired with single digit (from 1-9). In the rest of the page there is a pseudorandomised sequence of the symbols, and the participants was asked to write the corresponding digit, using the legend. The final score is given by the total number of correct answers in 90 seconds (Smith, 2017).

The Paced Auditory Serial Addition Test (PASAT) is another test of information processing speed. The participant was asked to listen to a recorded voice, saying a list of 61 consecutive numbers. The participant was asked to add each digit to the one immediately preceding it. The final score is the number of correct answer (maximum score 60).

There are two versions of PASAT: in the PASAT3, the digits are presented at a rate of one every three seconds, while in PASAT2, every two seconds (Gronwall, 1977).

The Word List Generation (WLG) is a measure of verbal fluency (executive function) and tests the ability of the participant to say as many words as possible starting with a letter of the alphabet (phonemic stimulus). The test consists of three one-minute trials, with three different letters (F, O and J). The words were not accepted if they were proper names, numbers or a different form of a previously given word (e.g., “nip” was accepted, “nipped” was not accepted). The total score was the number of total correct words for each trial. In addition, the number of inadmissible words due to rule violation

("intrusions") and repetitions ("perseverations") were recorded to help with the scoring (Lezak, 1983).

Stroop word-colour test (ST) is a measure of attention and executive functions and tests the ability to inhibit an automatic response when performing a task based on conflicting stimuli. A 100-item version was used. First, the participant was asked to read a list of colours (printed in black and white) for 90 seconds. Then, the participant was asked to name a list of coloured squares for 90 seconds. Finally, the participant was asked to name the colour of a written word, where every word represent a colour (which does not correspond to the ink colours) for 90 seconds. The number of correct answers in the three trials, were used to calculate an age, sex and education adjusted residual score which was then transformed into a t-score (Stroop, 1935) (Golden and Freshwater, A manual for Clinical and Experimental use).

3.3.4 *Pain score*

The Brief Pain Inventory (BPI) short form consists of 10 questions which form the pain score. In the first question the participants were asked to score their pain (if they have any) based on their neurological disease, rather than on other type of non-neuropathic pain, i.e., musculoskeletal pain or joint pain. Then, they were asked to shade the area where they feel pain on a diagram representing the human body (this question is not counted in the final scoring). The pain severity score (PSS) is based on four questions (out of 40), rated between zero, no pain, to 10, the worst pain imaginable. The four questions ask about average pain, current pain, maximal pain, and minimal pain in the last 24 hours. The pain functional interference score (PIS) measures how much the pain interferes with daily activities and is based on seven questions assessing the impact of pain on general activity, mood, walking ability, work (both work outside the home and

housework), relations with other people, sleep, and enjoyment of life. Each question is rated from zero, pain does not interfere, to 10, pain completely interferes. Overall, the maximum total pain score is 110 (PSS=40, PIS=70). In addition to the PSS and PIS questions, the participants are asked to list their pain medications (if any) and to assess how much relief the pain medication have provided in the last 24 hours (in percentage from zero, no relief to 100% complete relief). These two questions are not counted in the final scoring (Cleeland and Ryan, 1994).

3.3.5 *Fatigue Score*

The modified Fatigue Impact Scale (MFIS) was used to assess fatigue in the cohort. It consists of 21 statements describing the effects of fatigue. Participants were asked to assess how often fatigue have affected them in the last four weeks. Each statement is rated from 0 (never) to four (almost always). The maximum total MFIS score is 84.

The questions can be further divided into a physical subscale (nine questions), cognitive subscale (10 questions), and psychosocial subscale (two questions). The physical score ranges from zero to 36, the cognitive score ranges from zero to 40, and the psychosocial score ranges from zero to eight (Fisk et al., 1994b). Total fatigue score higher than 38, is thought to represent clinical fatigue, as showed in previous studies (Kos et al., 2005; Larson, 2013; Téllez et al., 2008).

3.3.6 *Anxiety and Depression scores*

The Hospital Anxiety and Depression Scale (HADS) is a self-assessment scale which consists of 14 questions. Seven questions assess “depression” and seven assess “anxiety”. Each item can be scored by the participant from 0 to three, so the total score ranges from

0 to 21 for anxiety, and 0 to 21 for depression. A total score from zero to seven was regarded as being normal, from eight to 10 borderline for anxiety/depression, and 11 or higher indicates probable presence of the mood disorder (Snaith and Zigmond, 1986).

3.4 MRI hardware and acquisition protocol

3.4.1 *Brain imaging hardware*

All imaging was performed in Oxford's Functional Magnetic Resonance Imaging Centre for the Brain (FMRIB) on a 3-tesla Siemen's MAGNETOM® Verio MR scanner, using a 64-channel head and neck coil. The head coil was fitted with a mirror in order for the participant to look at a fixed cross during the resting state functional MRI acquisition and then they were offered a choice of a movie or documentary to watch during the scan. There were no software upgrades during the study period.

3.4.2 *Sequence Development*

The main consideration when developing the MRI protocol, was to obtain a comprehensive assessment of the brain, in a relatively limited amount of time, using modalities able to provide robust MRI marker, with potential to be translated into clinical practice. MOGAD, NMOSD-AQP4 and MS are part of the spectrum of the demyelinating disease, but they have different pathological features, as discussed in Chapter 1. Therefore, as the goal was to obtain imaging findings potentially relevant in discriminating across the three studied conditions, modalities able to estimate the anatomical structures (global and regional volumetric MRI), the pathological tissue (lesions), the microstructure (diffusion MRI - dMRI) and the brain function (functional MRI – RS-fMRI) were included.

Volumetric measures (global and regional) have shown an association with motor disability and cognition, and they are potentially a better marker of disability in MS, compared to lesion volume. Although lesion volume as a marker is poorly correlated with clinical outcome, it can be easily assessed with conventional MRI, and could help in diagnosis and long-term monitoring of treatment efficacy.

Diffusion weighted imaging has been preferred to other quantitative technique, as not only can provide information of the white and grey matter microstructure, but also of white matter pathways integrity (i.e., tract based spatial statistics).

Resting-state functional MRI was added to the structural protocol, as it can be relatively easy to perform, also in a clinical setting, and given the reproducibility of the large brain networks across different cohorts, it has potential as a marker of functional damage and physical/cognitive impairment.

Other considerations for the final protocol were the possibility to have a unique dataset of demyelinating disease, comparable with the previous MS/NMOSD dataset available at FMRIB from the same research group, and at the same time, to use the current state-of-the-art sequences, especially for non-conventional modalities, such as diffusion MRI and functional MRI.

The functional and diffusion MRI sequence, as well as an additional 3D-FLAIR, were taken from the UK Biobank protocol (see below for further details). The UK Biobank is currently the largest population cohort with a multimodal brain imaging dataset, with one of the most advanced sequences available and a robust analysis pipeline.

The final protocol reflected these considerations and challenges, and included the following modalities: 3D-T1, 2D-T2, 2D-PD and 2D-FLAIR (optional 3D-FLAIR), dMRI, RS-fMRI, double inversion recovery (DIR) (see below for further details).

Sequence development and piloting for the study was performed under the supervision of Prof Mark Jenkinson and with the physics group and the radiographer support.

3.4.3 *Structural MRI sequences*

The 3D-T1, 2D-T2, 2D-PD and 2D-FLAIR sequences were taken from previous studies from the same research group (Matthews et al., 2015). To reduce the scanning time, the PD/T2 sequence was piloted. Since the gain in time was one minute, the final decision was to keep the two separate sequences (T2 and PD). Since there have been significant improvements in the FLAIR sequence quality and given the sensitivity of this sequence in the detection of demyelinating lesions, a 3D-FLAIR sequence has been added to the imaging protocol and was taken from the UK Biobank. Due to the time constrains, when scans needed to be repeated, due to poor quality, the preference was given to the 2D-FLAIR sequence (as it enabled comparability with previous studies from the same research group).

3.4.4 *Diffusion Imaging sequence*

Diffusion Tensor imaging (DTI) sequence (dMRI) was taken from the UK Biobank protocol. In this diffusion sequence, for the two shells, 50 distinct diffusion-encoding directions were acquired. The dMRI sequence can also be fed into more advanced biological modelling in future studies (i.e., Neurite Orientation Dispersion and Density Imaging -NODDI).

In addition, 3 pair of b=0 images are acquired with reversed phase-encoding directions for fieldmap estimation. The fieldmap can be used for distortion correction in both the dMRI and RS-fMRI dataset, resulting in a shorter acquisition time.

3.4.5 *Resting state imaging sequence*

The resting state sequence was taken from the UK Biobank protocol. The fieldmap for distortion correction will be estimated from the dMRI dataset as outlined in the previous section.

3.4.6 *Double Inversion Recovery sequence*

TheDIR sequence was taken from previous study and was developed by Dr Yazhuo Kong. Two different slices thickness were piloted: one with a slice thickness of 1.3 mm with a saturation band, and one with a slice thickness of 1 mm without a saturation band. The 1 mm thickness without saturation band was preferred after a quality assessment of the cortical lesion in the same subject.

3.4.7 *Brain Imaging Protocol*

The multimodal imaging protocol was set up to answer to the research questions outlined in Chapter 1. In Table 3.1 the MRI sequences acquired for the brain protocol are outlined. Further details and the analysis pipeline for each modality are described in the experimental chapters.

Table 3.1 MRI imaging protocol

Sequence	*Details*	*Time*	*Analysis*
3D-T1 brain	MPRAG, flip angle=8°; PE=R>>L; voxel=1x1x1 mm; TR: 2040 ms, TE: 4.7 ms	6 min	atrophy, tissue segmentation, structural segmentation
2D-T2 axial brain	2-dimensional turbo spin echo, 48 slices, slice thickness 3 mm, voxel size 0.5x0.5 mm, FOV 220x220 mm, TR 5690 ms, TE 71 ms, 1 average	4 min	Lesion segmentation, lesion location, lesion volume
2D-PD axial brain	2-dimensional, turbo spin echo, 48 slices, slice thickness 3 mm, voxel size 0.3x0.3 mm, FOV 220x220 mm, TR 3000 ms, TE 18 ms, 1 average	3 min	Lesion segmentation, lesion location, lesion volume
2D-FLAIR axial brain	2-dimensional, turbo spin echo, 48 slices, slice thickness 3 mm, voxel size 0.4x0.4 mm, FOV 220x220 mm, TR 9000 ms, TE 73 ms	2 min	Lesion segmentation, lesion location, lesion volume
Brain Diffusion Tensor Imaging (DTI)	100 diffusion directions (50 b=1000, 50 b=2000, 8 volumes with no diffusion), voxel size 2x2 mm, TR 3600 ms, TE 92 ms, FOV 210x210 mm, 72 slices, averaging mode long term	7 min	TBSS, GM, normal appearing WM
3D-FLAIR brain	3-dimensional, SPCIR, 192 slices, slice thickness 1.05 mm, voxel size 1x1 mm, FOV 192x256X256 mm, TR 5000 ms, TE 397 ms	6 min	Lesion segmentation, lesion location, lesion volume
Resting State brain	GE-EPI with 8x multislices acceleration, flip angle 52°, voxel size 2.4x2.4 mm, TR 0.735 s, TE 39 ms, FOV 88x88 mm, 64 slices, averaging mode long term	6 min	Independent component analysis
3D Double Inversion Recovery (DIR)	T2 DIR 3-dimensional SPCIR, 128 slices, slice thickness 1.33 mm, voxel size 1.3x1.3 mm, FOV 256x256 mm, TR 7500 ms, TE 316 ms, 1 average	6 min	Cortical lesion location

3.5 Data collection

A database has been created for this study. All the clinical data, the questionnaire scores and the cognitive scores were implemented in the database after each visit. The relapses history, past and current treatment data has been collected from patients' clinical notes from the NMOSD and MS service at John Radcliffe Hospital.

3.5.1 *Data protection*

This study adhered to the General Data Protection Regulation 2016/679.

3.6 Analysis overview

MRI pre-processing and analysis were conducted using FSL (FMRIB Software Library https://fsl.fmrib.ox.ac.uk/fsl/fslwiki), FreeSurfer (https://surfer.nmr.mgh.harvard.edu/). Manual lesions segmentation was performed using the software ITK-SNAPS (http://www.itksnap.org/pmwiki/pmwiki.php).

Non-imaging data were analysed using RStudio version 1.1.447 software (https://www.rstudio.com). In this chapter a Shapiro-Wilk test was used to assess the normal distribution of data. The differences across groups were evaluated by ANOVA with Bonferroni correction for pairwise comparisons (means) and $\chi 2$ test (proportion). In case of not normal distribution a Kruskal-Wallis test and a pairwise Wilcoxon Rank Sum Test with Holms-Bonferroni correction was used. The p-value of the across groups comparisons are represented in Table 3.2, while the post-hoc comparisons are discussed in the "Study Cohort" section. Further analysis details will be given in every experimental chapter.

Table 3.2 Clinical and demographic characteristics of the studied cohort.

	MOGAD	***NMOSD-AQP4***	***MS***	***HC***	***p-value***
Number	20	19	18	18	/
Mean age (SD)	41.75 (11.03)	55.6 ± 13.2	44.11 (6.61)	38.9 ± 13.4	<0.001*
Sex, F (%)	10 (50)	(68.4)	10 (55)	(55.5)	0.695
Ethnicity (%)					
White	20 (100)	10 (53)	18 (100)	15 (83)	0.001**
African/Afro-Caribbean	/	4 (21)	/	/	/
Asian	/	3 (16)	/	2 (11)	0.999
Mixed	/	2 (10)	/	1 (6)	0.999
Phenotype (%)					
Isolated TM	1 (5)	/	/		
TM + Br/Bs	5 (25)	10 (53)	12 (67)		
ON + Br/Bs	/	3 (16)	/	/	
ON + TM	6 (30)	/	/		
Br/Bs	2 (10)	2 (10)	/		
ON + TM +Br/Bs	6 (30)	4 (21)	6 (33)		
Median disease duration, years (range)	2 (0-24)	11 (0-24)	12 (1-24)	/	0.018
Median number of relapses (range)	2 (1-11)	2 (1-11)	4 (1-13)	/	0.347
Mean education years (SD)	14.32 (2.50)	17.12 (4.04)	16.40 (4.14)	18 (3.43)	0.021
Median EDSS (range)	1.5 (0-7.0)	3 (0-7.0)	2.0 (0.0-6.0)	/	0.025
Mean LogMAR VA [average OD and OS] (SD)	-0.03 (0.6)	0.4 (0.9)	-0.08 (0.1)	/	0.022
Pain total score	11.15 (23.36)	29.42 (22.87)	13.11 (19.56)	/	0.014
Mean total fatigue score (SD)	25.05 (17.76)	32.89 (20.60)	38.50 (15.61)	6.72 (6.68)	<0.001
Mean cognitive fatigue score (SD)	12.42 (9.56)	13.94 (9.08)	17.17 (8.01)	3.39 (4.03)	<0.001
Mean physical fatigue score (SD)	12.63 (9.84)	18.18 (9.55)	18.11 (7.91)	2.67 (2.97)	<0.001
Mean Psychosocial fatigue score (SD)	2.58 (3.79)	3.06 (2.36)	3.22 (1.77)	0.67 (0.97)	<0.001
Mean HADS Anxiety score (SD)	7.28 (5.57)	6.33 (4.43)	6.75 (3.80)	4.67 (4.40)	0.304
Mean HADS Depression score (SD)	3.06 (2.92)	4.94 (3.52)	4.00 (3.81)	1.47 (1.85)	0.010

*Legend: SD=standard deviation; VA=visual acuity; *after Bonferroni comparison: NMOSD-AQP4 vs HC, p=0.002; MS vs HC, p=1.0; MOGAD vs HC, p=0.999. **comparison of White participants.*

3.7 The study cohort

The clinical and demographic characteristics of the four group are represented in Table 3.2. The cognitive battery scores will be presented and analysed in Chapter 8.

Most variables are matched across the groups, however exact matching was not possible due to the expected demographic differences between the three diseases and the rarity of the antibody diseases. The age post-hoc comparison showed a statistically significant difference between NMOSD-AQP4 and HC (p=0.002), while the remaining comparisons were not significant (MOGAD vs HC p>0.999, MS vs HC p>0.999). Age was not comparable across the groups, thus was handled by adjusting in the statistical analysis (details of the analysis will be outlined in every result chapter).

As expected, the female preponderance was more evident in the NMOSD-AQP4 group, however the percentage of female participants was not significantly different across groups. The NMOSD-AQP4 showed a more diverse ethnic background, compared to the other groups, as described in population studies (Papp et al., 2021). The disease duration was shorter in the MOGAD group, as it is a recently recognised condition.

3.7.1 *Disability and disease activity outcomes*

The number of relapses were similar across groups, however the NMOSD-AQP4 showed higher motor disability, as showed by the EDSS score. Post-hoc comparisons, showed a significant difference when compared to the MOGAD group (p=0.027), while there were no statistically significant differences in EDSS score between NMOSD-AQP4 and MS (p=0.238), and MOGAD and MS (p=0.238).

Visual acuity was worse in NMOSD-AQP4 (expressed as the average of the right and left eye visual acuity) when compared to MOGAD (p=0.015) and MS (p=0.037), while there was no difference between MOGAD and MS (p=0.492).

3.7.2 *Pain score*

The presence of pain and its severity was assessed with the BPI, as described in the "clinical assessment" section. The total pain score was different across disease. In particular, the post-hoc comparisons showed a significantly higher score in NMOSD-AQP4 participants compared to MOGAD participants (p=0.026), while there were no statistically significant differences in MS, when compared to NMOSD-AQP4 (p=0.078) and MOGAD (p=0.297).

3.7.3 *Fatigue scores*

The fatigue scores (total score, cognitive, physical, and psychosocial fatigue) were assessed with the MFIS. The total and the subscale fatigue scores were significantly different across groups. The total fatigue score was significantly higher in the three disease groups (MS group has the highest value) compared to the HC (MOGAD p=0.003, NMOSD-AQP4 p=0.007, MS p<0.001), while the remaining comparisons were not significant (MOGAD vs NMOSD-AQP4 p=0.789; MOGAD vs MS p=0.06; NMOSD-AQP4 vs MS p=0.789).

Similarly, both the cognitive and physical scores are significantly higher in the three disease groups compare to the HC (cognitive fatigue MOGAD p=0.004, NMOSD-AQP4

p=0.004, MS p<0.001; physical fatigue MOGAD p=0.001, NMOSD-AQP4 p=0.0001, MS p<0.001) with no significant differences across groups (cognitive fatigue MOGAD vs NMOSD-AQP4 p=0.780, MOGAD vs MS p=0.178, NMOSD-AQP4 vs MS p=0.780; physical fatigue MOGAD vs NMOSD-AQP4 p=0.205, MOGAD vs MS p=0.183, NMOSD-AQP4 vs MS p=0.895).

The psychosocial fatigue score was significantly different from HC in NMOSD-AQP4 (p=0.013) and MS (p=0.0002), while was not significant in MOGAD (p=0.125). The remaining comparisons were not significant (MOGAD vs NMOSD-AQP4 p=0.503, MOGAD vs MS p=0.173, NMOSD-AQP4 vs MS p=0.987).

3.7.4 *Anxiety and Depression scores*

MOGAD participants had the highest anxiety scores, however the post-hoc comparisons did not show significant differences (MOGAD vs HC p=0.490, NMOSD-AQP4 vs HC p=0.730, MS vs HC p=0.490, MOGAD vs NMOSD-AQP4 p>0.999, MOGAD vs MS p>0.999, NMOSD-AQP4 vs MS p>0.999).

Depression score was significantly higher in NMOSD-AQP4 compared to HC (p=0.014). The remaining comparisons were not significant (MOGAD vs HC p=0.318, MS vs HC p=0.067, MOGAD vs NMOSD-AQP4 p=0.318, MOGAD vs MS p=0.694, NMOSD-AQP4 vs MS p=0.694).

3.8 Limitations

The main limitation of the study is the small sample size per disease group related to the selection of four sub-groups, two of which are rare diseases. Because the brain is spared in many patients with these syndromes, the enrolment was even more challenging, as the antibody disease cohorts were enriched with patients with brain lesions. The use of four different groups however, allowed comparison of three inflammatory diseases against healthy controls and each other; one, likely T-cell driven against myelin and two auto-antibody conditions, one against myelin and one against astrocyte antigens. This approach can potentially give interesting insights into pathological differences. Although relatively small numbers, the homogeneity of a single centre study using the same scanner and protocol, along with reliable diagnostic ability is an advantage. Additionally, it was not possible to match all characteristics across the groups, i.e., NMOSD-AQP4 disease affects older patients and has a greater preponderance of females and is more severe, but this was handled in the statistical analysis by adjusting for the different characteristics.
Observations from this study can then be used to build hypotheses and design future multicentre studies.

3.9 Conclusions

In this chapter the overview of the MRI study and the characteristics of the studied cohorts have been presented.
The results of the volumetric, lesion, diffusion, and resting state analysis across the four groups, will be presented in the following result Chapters.

4 Chapter 4 Lesion distribution and volumetric changes in demyelinating disease: a structural MRI study

4.1 Introduction and Background

The previous chapter showed that MOGAD patients have a better recovery from attacks, compared to NMOSD-AQP4, despite similar severity at the time of the acute attack. The use of structural MRI in the remission stage may help to better understand the mechanism behind recovery in MOGAD, compared to NMOSD-AQP4 and MS, and the presence of damage outside of the acute phase might be a useful marker associated with long-term disability.

MRI plays a fundamental role in the diagnosis and the monitoring of inflammatory CNS diseases. Brain lesions have been reported in up to 60% of NMOSD-AQP4 patients (Pittock et al., 2006a). Lesions localise to areas rich in AQP4 water-channel (e.g. periependymal regions, area postrema) although, non-specific white matter lesions are more common (Matthews et al., 2013) and a wide range of other lesions and enhancements are described (Wingerchuk et al., 2015). MOGAD brain lesions can be difficult to distinguish from NMOSD-AQP4 (Hoftberger et al., 2015; Jurynczyk et al., 2017a). The presence of lateral and inferior temporal lobe lesions, or Dawson's fingers or U/S shaped juxtacortical lesions, may help distinguish MS from the antibody disorders (Jurynczyk et al., 2017a).

Cortical lesions have been reported in MS, while they are not present in NMOSD-AQP4 (Calabrese et al., 2010a; Calabrese et al., 2012) and, at the time of this study, had not been studied in MOGAD. Volumetric measures have been studied extensively in MS and NMOSD-AQP4. While in MS, deep grey matter atrophy is well characterised and has been associated with disability and cognitive impairment, in NMOSD-AQP4 the findings

are contradictory, with authors reporting both lower volumes and volumes that are not significantly different compared to healthy controls (Finke et al., 2016; Liu et al., 2018). At the time of this study, volumetric measures had not been investigated in MOGAD. The main aim of this study was to identify different pathological patterns across diseases in the remission stage, using structural MRI.

4.1.1 *Objectives*

a) To compare the T2 lesion distribution in MOGAD, NMOSD-AQP4 and MS, using a quantitative approach.
b) To compare cortical lesion distribution in MOGAD, NMOSD-AQP4 and MS.
c) To compare global and regional volumetric measures across diseases.

4.1.2 *Hypotheses*

MS will have a higher T2 lesion volume and a higher number of cortical lesions with lower global and regional volume, compared to MOGAD and NMOSD-AQP4.

4.1 Material and Methods

4.1.3 *Subjects*

A total of 20 MOGAD, 19 NMOSD-AQP4, and 18 MS were included in this study (see Table 4.1). Out of the 20 MOGAD, six were excluded from the T2 lesions analysis as they did not have brain lesions at the time of the research MRI, therefore the final MOGAD cohort for this project consisted of 14 participants. The DIR images for cortical

lesion analysis were available for 16 NMOSD-AQP4, 19 MOGAD and 17 MS. The total cohort of 75 participants was included in the volumetric analysis.

Table 4.1 Clinical and demographic characteristics of the studied cohort.

	MOGAD	***NMOSD-AQP4***	***MS***	***HC***
Number	20	19	18	18
Mean age (SD)	41.75 (11.03)	55.6 (13.2)	44.11 (6.61)	38.9 (13.4)
Sex, F (%)	10 (50)	13 (68.4)	10 (55)	10 (55.5)
Ethnicity (%)				
White	20 (100)	10 (53)	18 (100)	15 (83)
African/Afro-Caribbean	/	4 (21)	/	/
Asian	/	3 (16)	/	2 (11)
Mixed	/	2 (10)	/	1 (6)
Phenotype (%)				
Isolated TM	1 (5)	/	/	/
TM + Br/Bs	5 (25)	10 (53)	12 (67)	
ON + Br/Bs	/	3 (16)	/	
ON + TM	6 (30)	/	/	
Br/Bs	2 (10)	2 (10)	/	
ON + TM +Br/Bs	6 (30)	4 (21)	6 (33)	
Median disease duration, years (range)	2 (0-24)	11 (0-24)	12 (1-24)	/
Median number of relapses (range)	2 (1-11)	2 (1-11)	4 (1-13)	/
Median EDSS (range)	1.5 (0-7.0)	3 (0-7.0)	2.0 (0.0-6.0)	/
Mean LogMAR VA [average OD and OS] (SD)	-0.03 (0.6)	0.4 (0.9)	-0.08 (0.1)	/

Legend: SD=standard deviation; TM=transverse myelitis; Br/Bs=brain/brainstem; ON=optic neuritis.

4.1.4 *MRI images*

The T1, FLAIR, PD and DIR images were acquired with the following parameters – 3DT1: MPRAGE image voxels size 1 x 1 mm, slice thickness 1 mm, TR 2040 ms, TE: 4.7 ms, flip angle=8 degrees; FLAIR: 2D turbo spin echo, voxels size 0.4x0.4 mm, slice thickness 3 mm, TR 9000 ms, TE 73 ms; PD: 2D, turbo spin echo, voxel size 0.3x0.3 mm, slice thickness 3 mm, TR 3000 ms, TE 18 ms; DIR: 3 dimensional SPCIR, voxel size 1.3x1.3 mm, slice thickness 1.33 mm, TR 7500 ms, TE 316 ms.

4.1.5 *MRI Analysis*

Imaging data were analysed using the FMRIB Software Library of tools (University of Oxford, UK) (Jenkinson et al., 2012; Smith et al., 2004; Woolrich et al., 2009) and FreeSurfer (http://surfer.nmr.mgh.harvard.edu)(Dale et al., 1999; Fischl et al., 1999; Fischl et al., 2002).

T2 lesion analysis: for every subject the T2 hyperintense lesions were segmented manually by myself on the axial FLAIR, with simultaneous reference to PD and T1 images using ITK-SNAP (www.itksnap.org). FLAIR lesion masks were registered to the T1 image with a linear registration, and the T1 image was registered to the Montreal Neurological Institute (MNI) 1-mm standard space template using a non-linear transformation (Jenkinson et al., 2002). Then FLAIR lesion masks were transformed to the MNI space, by combining the previous transformations. After transformation, the lesion mask for each subject was thresholded at 50% and binarized, to avoid volume increases due to trilinear interpolation.

The number of lesions and the lesion volume for each subject were obtained from the lesion mask, in MNI space. The lesion masks for all subjects were then merged and averaged to create a lesion probability map for each disease group. Three subtraction maps were obtained for the three diseases group (NMOSD-AQP4 minus MOGAD; MS minus NMOSD-AQP4, MS minus MOGAD). A voxel-wise analysis between disease groups (NMOSD-AQP4 vs MOGAD; MS vs NMOSD-AQP4, MS vs MOGAD) was performed using the non-parametric permutation testing tool *randomise* (part of FSL) with Threshold-Free Cluster Enhancement (5000 permutations of each of the three contrasts -TFCE) (Winkler et al., 2014). The clusters with a p-value <0.05 (corrected for multiple comparisons over voxels) will be shown in the results.

Cortical lesion analysis: cortical lesions were counted visually on each double inversion recovery (DIR) image with simultaneous reference to FLAIR images and T1 images by myself and a researcher with extensive experience and expertise in the detection of cortical lesions (Prof Massimiliano Calabrese), blinded to the participant status. In case of disagreement, a final consensus was reached between the raters. After scoring had been finished, scans were unblinded.

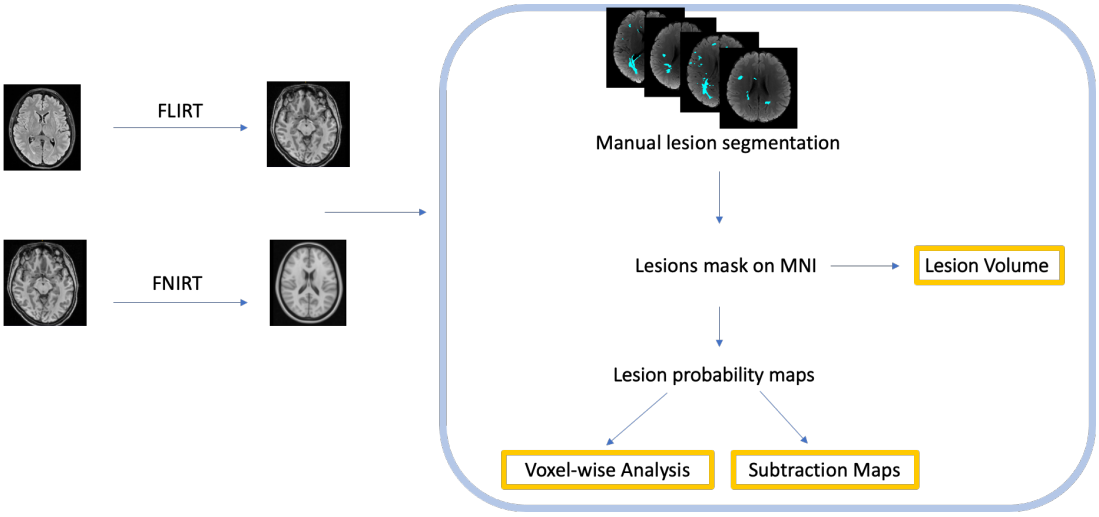


Figure 4.1 T2 lesion analysis pipeline.

Total Brain Volume, white matter and grey matter fraction: as the volumetric analysis may be affected by the presence of lesions, the T1 sequence was bias-corrected and the lesions were filled using the manually obtained FLAIR lesion mask, and using the method described in (Gelineau-Morel et al., 2012). The FLAIR sequence was bias corrected before registration.

The brain tissue volume, white matter, and grey matter, normalised for subject head size, were estimated with SIENAX, part of FSL (Smith et al., 2004). The total brain, white matter fraction and grey matter fraction volume, in mm^3, were divided by 1,000,000.

SIENAX starts by creating brain and skull images using segmentations of the single whole head input data (Smith et al., 2002). The brain image is then affine-registered to MNI152 space (Jenkinson et al., 2002) (Jenkinson and Smith, 2001) (using the skull image to determine the registration scaling); this is primarily to obtain the volumetric scaling factor, to be used as a normalisation for head size. Next, tissue-type segmentation with partial volume estimation is carried out (Zhang et al., 2001) in order to calculate the total volume of brain tissue (including separate estimates of the volumes of grey matter, white matter, peripheral grey matter and ventricular CSF).

Deep grey matter volumes: as the accurate quantification of deep grey matter structures could be affected by measurement techniques (Amiri et al., 2018), two methods were used to estimate the deep grey matter volume measures: the basal ganglia volume (thalamus, caudate, putamen, pallidum, amygdala and accumbens), the hippocampus and the brainstem volumes were calculated using the automated segmentation tool FIRST, part of FSL (Patenaude et al., 2011) as well as with FreeSurfer (Dale et al., 1999) (Fischl et al., 1999). A strong correlation was noted between the FIRST and FreeSurfer volumes for most of the deep grey matter structures and so it was decided that the FIRST volumes would be used for the volumetric analysis (see Figure 4.2).

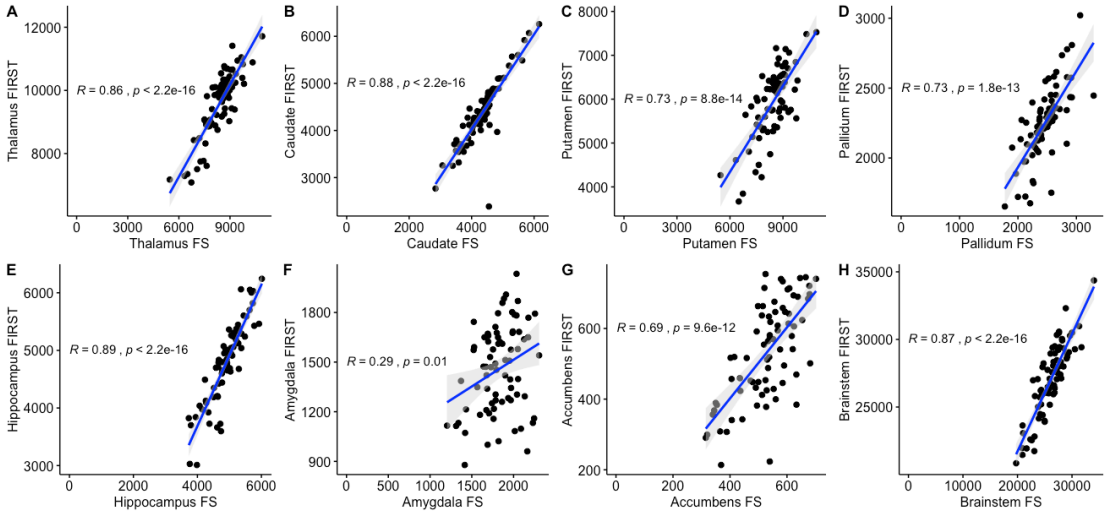


Figure 4.2 Pearson correlation between grey matter volumes obtained with FIRST and FreeSurfer (FS)*. Legend: The bold lines show the linear correlation between measures, the areas around the lines represent the 95% confidence interval.*

Cortical thickness, cortical and deep white/grey matter volumes: the Freesurfer image analysis suite (Dale et al., 1999; Fischl et al., 1999) includes both a volumetric and a surface-based stream. The volumetric stream includes the removal of non-brain tissue using a hybrid watershed/surface deformation procedure (Segonne et al., 2004), automated Talairach transformation, segmentation of the subcortical white matter and deep grey matter volumetric structures (Fischl et al., 2002; Fischl et al., 2004) and intensity normalisation (Sled et al., 1998). The output brain mask was then labelled using a Bayesian estimation method with probabilistic atlas priors. In the surface-based stream, voxels are classified as white matter or something other than white matter based on intensity and neighbour constraints. This initial surface is then refined to follow the intensity gradients between the white and grey matter (this is referred to as the white surface). The white surface is then propagated outwards to follow the intensity gradients between the grey matter and CSF (this is the pial surface). The distance between the white and the pial surfaces gives the thickness at each location of cortex (Fischl and Dale, 2000).

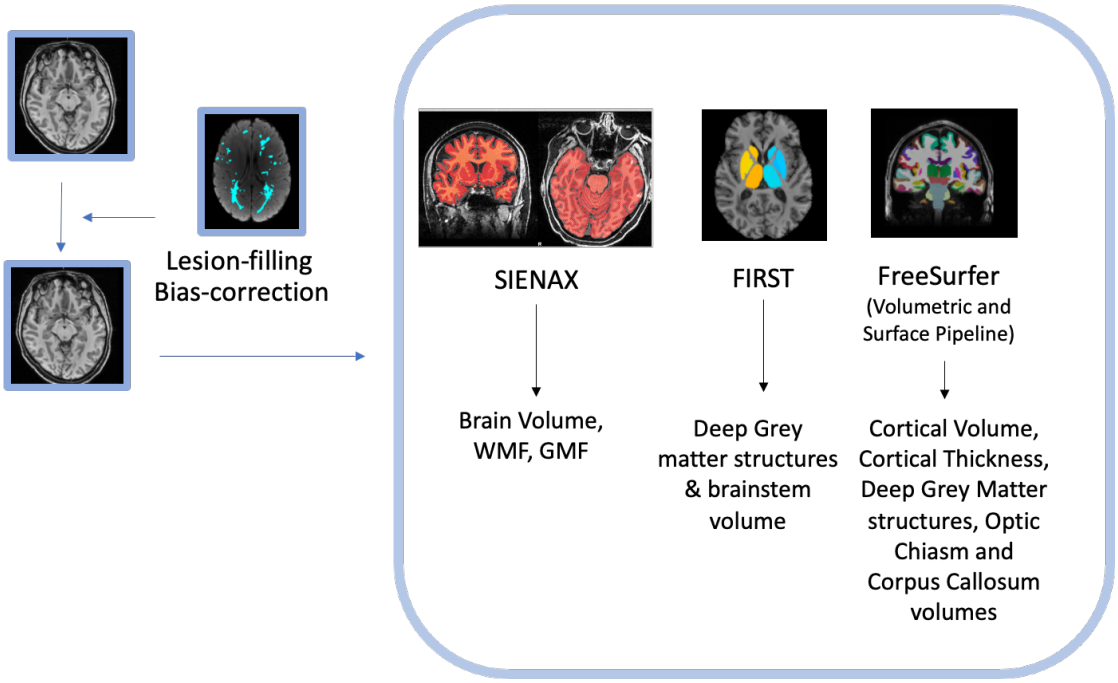


Figure 4.3 Volumetric analysis pipeline

4.1.6 *Statistical Analysis*

The statistical analysis of non-imaging data was performed using RStudio version 1.1.447 (https://www.rstudio.com/). Quantitative variables were described using mean and standard deviation (SD), median and range. A Shapiro-Wilk test was performed to assess the normality of the data distribution. Linear models with sex and age as independent variables were fit to compare the MRI findings between the three study groups. A Bartlett test was performed to assess the variance before including the variables in the linear regression model. In case of non-equal variance, the variables were transformed. The estimated marginal means were calculated based on the final model and a Bonferroni pairwise-comparison between groups was calculated. The results were expressed as estimates and standard errors. The significant *post hoc* comparisons are shown in the

results section. Pearson's correlation was used to test the relationship between MRI findings.

For the cortical lesion analysis Cohen's kappa was calculated to assess inter-rater agreement. A k<0 indicates poor agreement, 0.01–0.20 slight, 0.21– 0.40 fair, 0.41–0.60 moderate, 0.61–0.80 substantial and 0.81–1.0 almost perfect agreement.

For all analyses, $p < 0.05$ was considered statistically significant.

4.2 Results

The clinical and demographic characteristics of the groups are represented in Table 4.1. As discussed in Chapter 3, exact matching was not possible due to the expected demographic differences between the three disease groups and the rarity of the antibody diseases. Age was not directly comparable across the groups, and thus was included in the regression model, together with sex. MOGAD is a recently recognised condition, thus the disease duration was shorter than the other groups.

The comparisons between groups are shown as the difference of volume estimates between groups in mm^3, standard error [SE], and p-value; when compared to HCs a negative value indicates a lower volume in the disease group; when describing disease comparisons, the negative value indicates a lower volume in the disease group first mentioned in the comparison.

4.2.1 *Lesion number and lesion volume*

Seventeen out of 20 MOGAD patients (85%) had brain lesions acutely, of whom 14 (70%) still had lesions at the time of the research scan.

All MS and NMOSD-AQP4 had acute brain lesions with persistent lesions at the time of the research scan. Only two healthy controls had brain lesions, one had two punctiform small lesions, normal for the aging brain, and another had a few small punctiform non-specific lesions. The MS patients had a higher lesion volume when compared to NMOSD-AQP4 disease (1.326 mm^3 [0.503] p=0.034) and MOGAD patients (2.219 mm^3 [0.545] p=0.0005) (see Figure 4.4 A). Lesion volume was positively associated with disease duration in MS (R^2=0.37, p=0.008) and MOGAD (R^2=0.43, p=0.011), but not in NMOSD-AQP4 patients (Figure 4.4 B).

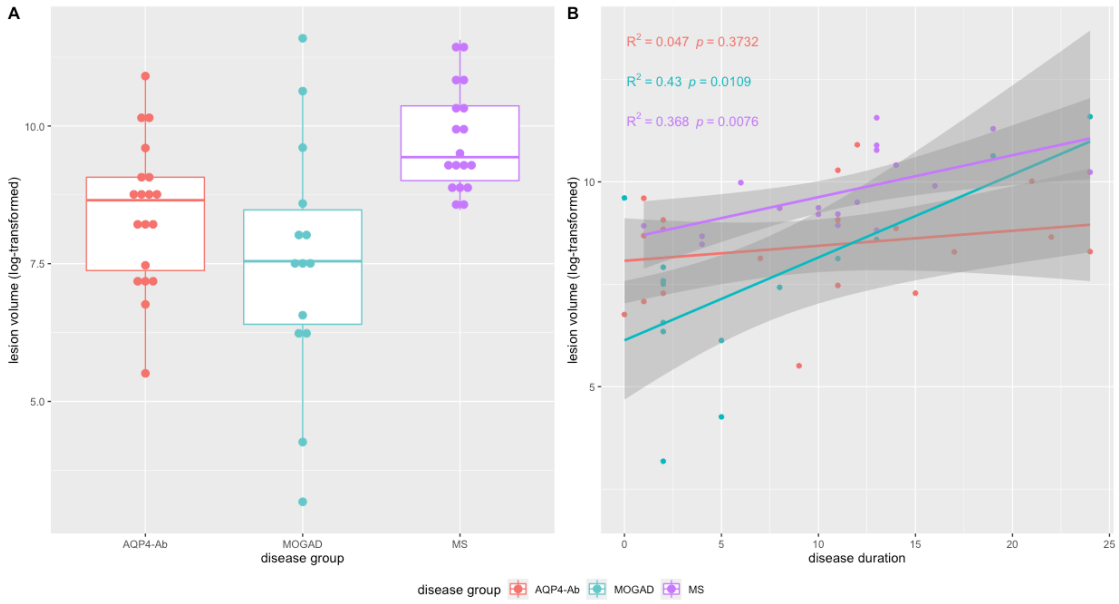


Figure 4.4 (A) Lesion volume across group and (B) association with disease duration. *The lesion volume was log transformed. Legend: AQP4-Ab=NMOSD-AQP4*

4.2.2 *Lesion probability maps*

In the NMOSD-AQP4 group the lesion map showed a widespread distribution, with the highest percentage of patients having lesions in the lateral ventricle anterior horns (31.5%), in the right lingual gyrus of the occipital lobe (42%) and in the corpus callosum (10.5%).

In the MOGAD group the lesion map showed a widespread distribution, with the highest percentage of patients having lesions in the lingual gyrus bilaterally (50% right and 57.1% left), small lesions in the anterior horns of the right and left lateral ventricles (42.8%), in the superior frontal gyrus (14.3%), and in the medial frontal gyrus (14.3%).

In the MS group the lesion map showed a more focal distribution, with the highest percentage of patients having lesions in the periventricular anterior horns area (88.8% on the right and 94.4% on the left lateral ventricles), in the brainstem (16.6%), in the cerebellum (11.1%), and in the corpus callosum (55.5%) (see Figure 4.5 A).

Subtraction maps (Figure 4.5 B) were created by subtracting the averaged NMOSD-AQP4 and MOGAD maps from the averaged MS map and the averaged NMOSD-AQP4 map from the averaged MOGAD map. Compared to the other two disease groups, the lesions in the NMOSD-AQP4 group are more likely to occur in the periependymal area of the corpus callosum. In MS, compared to both groups, lesions are more likely to occur in the periventricular and juxtacortical areas.

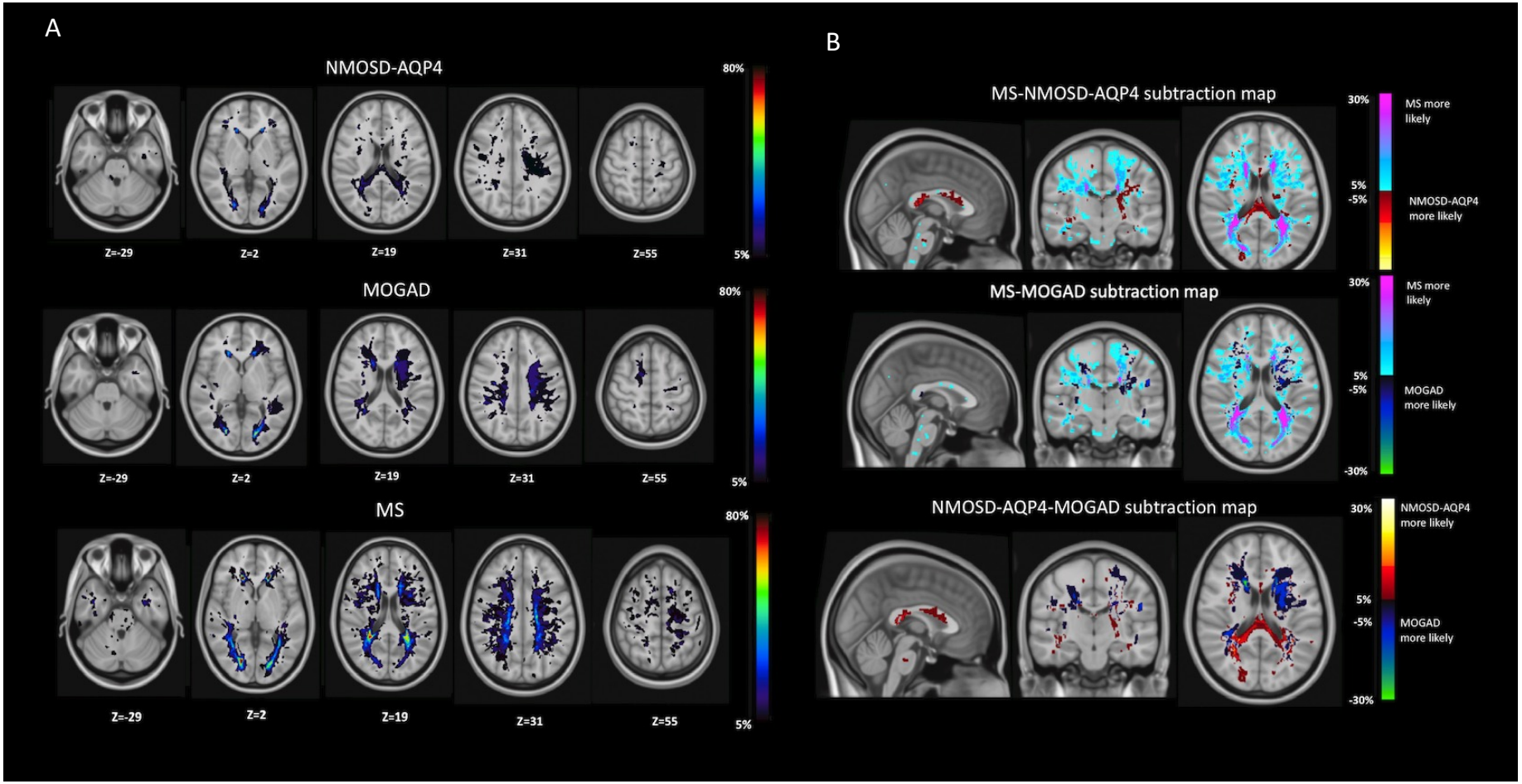


Figure 4.5 (A) Lesion probability maps in NMOSD-AQP4, MS and MOGAD; (B) Subtraction maps: MS-AQP4-Ab disease, MS-MOGAD, AQP4-Ab disease-MOGAD. *Legend: lesions identified on the lesion map with cluster tool (part of FSL) and using the Talairach Atlas. (A) The colour scale (from 5% to 80%) represents the minimum to maximum probability of a lesion occurring in a particular spatial location. Montreal Neurological Institute (MNI) standard space template Z coordinate is shown in millimetres. (B) Subtraction map where the average NMOSD-AQP4 and MOGAD lesion map have been subtracted from the average MS map to allow direct statistical comparison of the lesion distributions. The colour scale from 5% to 30% represents the minimum to maximum probability difference of a lesion occurring in a particular spatial location, while the scale from -5% to -30% represents the maximum and minimum of probability difference of a lesion occurring in a particular location.*

The voxel-wise analysis between NMOSD-AQP4 and MOGAD was not significant, while the MS analysis showed that lesions are statistically more frequent in the periventricular areas than NMOSD-AQP4 and MOGAD ($p<0.05$) (see Figure 4.6).

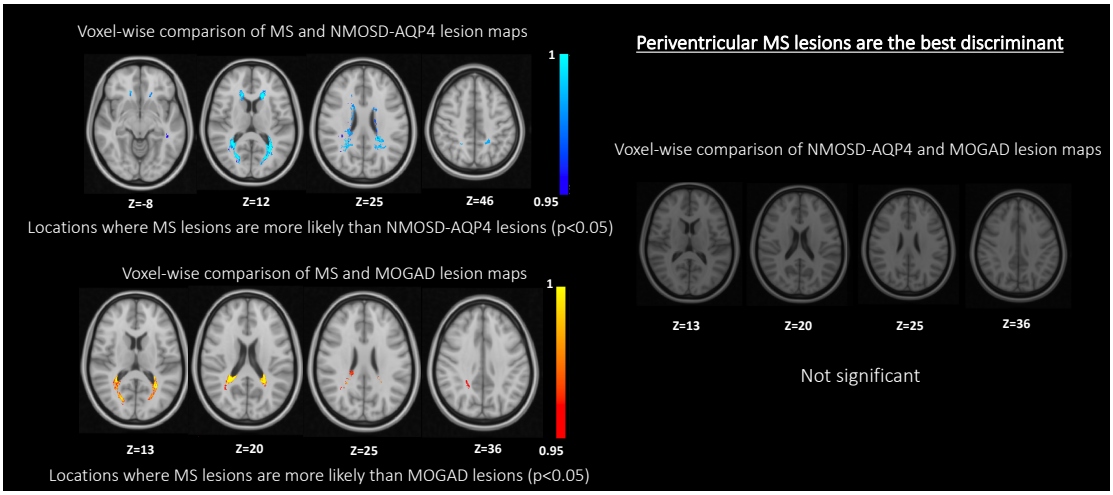


Figure 4.6 Voxel-wise comparison across groups. *Statistically significant voxel locations (values represent 1-p value, TFCE corrected) are represented in blue (MS vs NMOSD-AQP4) and red (MS vs MOGAD).*

4.2.3 *Cortical lesion analysis*

A total of 69 DIR images were available for the cortical lesion analysis (16 HC, 16 NMOSD-AQP4, 19 MOGAD and 17 MS). Cortical lesions were defined as those lesions within the cortex or extending from the cortex to the adjacent white matter and juxtacortical lesions as white matter lesions in direct contact with the cortex (Filippi et al., 2019). Three MOGAD patients (15.7%) showed cortical/juxtacortical lesions (type I; one patient with a single curvilinear lesion and one patient with a single ovoid lesion, and one patient with three curvilinear lesions), while 11 (65%) of MS patients had identifiable cortical/juxtacortical (leukocortical) lesions, with three patients presenting at least one pure cortical lesion (type II) (see Figure 4.7 A-D) and one an extensive subpial lesion (see Table 4.2 with p-value).

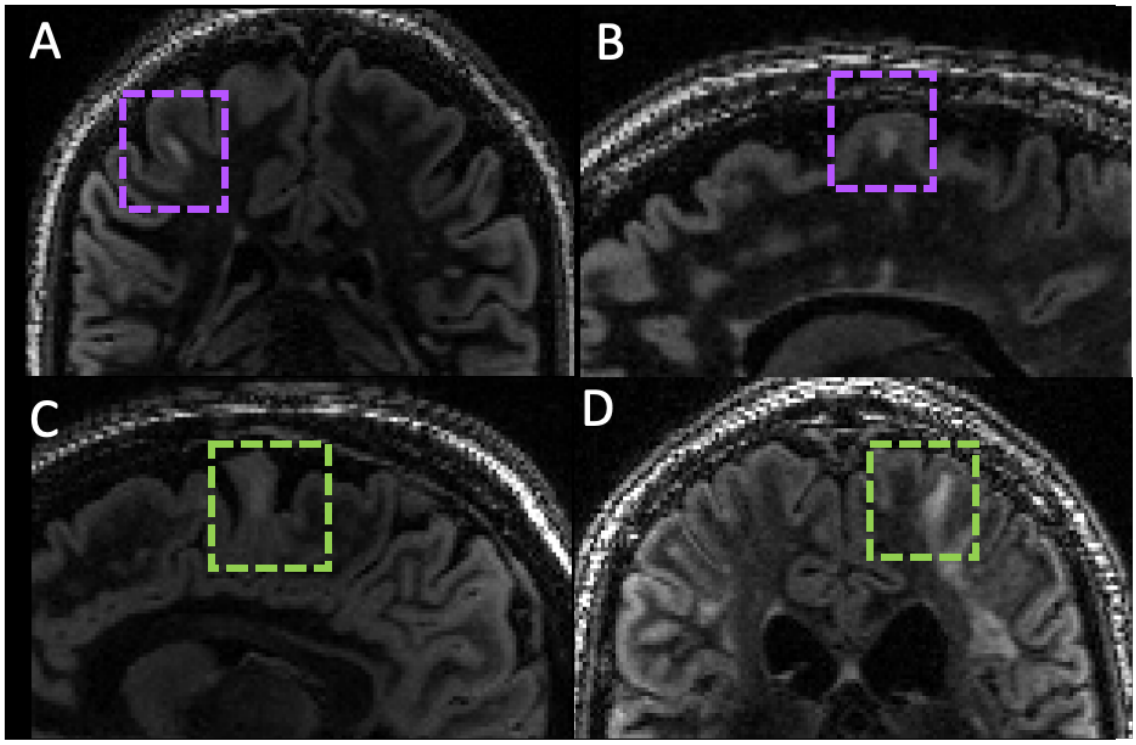


Figure 4.7 (A) ovoid cortical lesion in an MS patient; (B) an ovoid cortical/juxtacortical lesion in an MS patient; (C-D) curvilinear juxtacortical lesions in two MOGAD patients.

Table 4.2 Cortical/juxtacortical lesion number across the disease groups.

	NMOSD-AQP4	***MOGAD***	***MS***	***Chi-square p-value***
Patients, n	16	19	17	
Patients with at least 1 cortical/juxtacortical lesion, n (%)	0	3 (15.8)	11 (64.7)	**0.005**
Patients with 1 cortical/juxtacortical lesion, n (%)	0	2 (10.5)	3 (17.6)	0.650
Patients with >1 cortical/juxtacortical lesions, n (%)	0	1 (5.3)	8 (47)	**0.006**
Number of cortical/juxtacortical lesions, median (range)	0	0 (0-3)	1 (0-12)	

Legend: p<0.05 in bold

4.2.4 *Volumetric analysis*

Non-normalised volumes are shown in Appendix (Table S4.1).

Total Brain Volume, white/grey matter fraction and third/fourth ventricular volumes: no significant differences were found in brain volume, white matter fraction, grey matter fraction (see Table 4.3 and Figure 4.8), third ventricle volume and fourth ventricle volume (see Table 4.4).

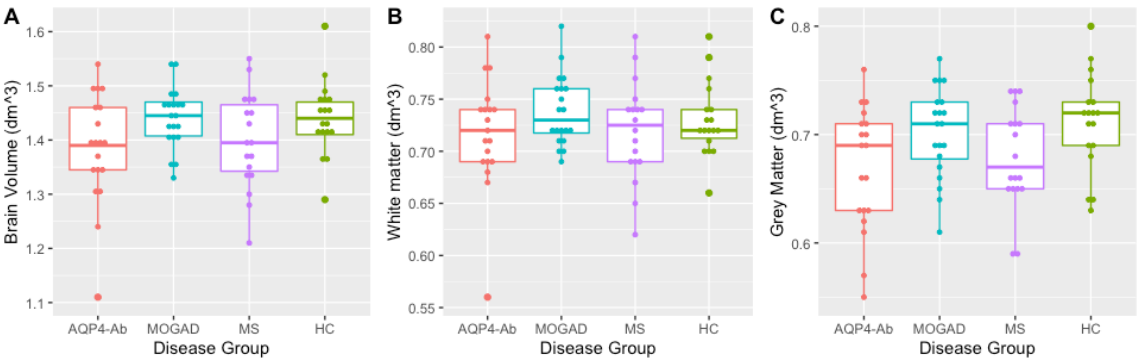


Figure 4.8 The brain volume (A), the white matter fraction (B) and grey matter fraction (C) comparison between disease groups. *The graphs represent the median and, the 25th and 75th percentile; AQP4-Ab=NMOSD-AQP4.*

Table 4.3 Brain volume, white and grey matter fraction estimates, SE and p-value across groups

	Brain Volume			***White Matter Fraction***			***Grey Matter Fraction***		
	Estimates	*SE*	*p-value*	*Estimates*	*SE*	*p-value*	*Estimates*	*SE*	*p-value*
AQP4-Ab vs HC	-0.037	0.03	0.999	-0.016	0.02	0.999	-0.022	0.01	0.807
AQP4-Ab vs MOGAD	-0.021	0.03	0.999	-0.016	0.01	0.999	-0.005	0.01	0.999
AQP4-Ab vs MS	-0.0007	0.03	0.999	-0.004	0.01	0.999	0.004	0.01	0.999
HC vs MOGAD	0.016	0.02	0.999	0.00009	0.01	0.999	0.017	0.01	0.999
HC vs MS	0.036	0.02	0.084	0.012	0.01	0.999	0.026	0.01	0.305
MOGAD vs MS	0.020	0.02	0.999	0.012	0.01	0.999	0.009	0.01	0.999

Legend: SE=standard error; AQP4-Ab=NMOSD-AQP4

Table 4.4 Third and fourth ventricle volume estimates, SE, and p-value across groups.

	Third Ventricle Volume			***Fourth Ventricle Volume***		
	Estimates	*SE*	*p-value*	*Estimates*	*SE*	*p-value*
AQP4-Ab vs HC	0.246	0.2	0.999	0.036	0.08	0.999
AQP4-Ab vs MOGAD	0.050	0.2	0.999	0.050	0.08	0.999
AQP4-Ab vs MS	-0.131	0.2	0.999	0.002	0.08	0.999
HC vs MOGAD	-0.196	0.2	0.999	0.014	0.08	0.999
HC vs MS	-0.378	0.2	0.263	-0.035	0.08	0.999
MOGAD vs MS	-0.182	0.2	0.999	-0.048	0.08	0.999

Legend: SE=standard error; AQP4-Ab=NMOSD-AQP4

Grey matter volumes: when considering the total deep GM volumes, both MOGAD and MS showed lower volumes when compared to HC (MOGAD -2609 mm^3 [880], p=0.02; MS -4092 mm^3 [891], p=0.0001; Figure 4.9 A). The putamen volume was significantly lower in MOGAD (-615.4 mm^3 [226], p=0.05) while in MS there is a more diffuse atrophy across the individual grey matter structures (see Figure 4.9 B-I). Of interest, the brainstem was smaller in NMOSD-AQP4 (-2575.8 mm^3 [933], p=0.04) when compared to HC. Compared to NMOSD-AQP4, the caudate was significantly smaller in MS (-650 mm^3 [202], p=0.01).

For the individual deep grey matter structures, compared to HC, the putamen was significantly smaller in MOGAD (-615.4 mm^3 [226], p=0.05), while the remaining structures were smaller but not significantly (thalamus -699 mm^3 [297], p=0.2; caudate -493 mm^3 [192], p=0.07; pallidus -80.39 mm^3 [64.5], p>0.999; amygdala -206.9 mm^3 [80.8], p=0.08; accumbens -83.1 mm^3 [40.9], p=0.3; hippocampus -422 mm^3 [199], p=0.2; brainstem -2092.1 mm^3 [834], p=0.09).

In NMOSD-AQP4 the deep grey matter structures were not significantly smaller (thalamus -821 mm^3 [332], p=0.09; caudate -335 mm^3 [215], p=0.7; pallidus -73.85 mm^3 [72.1], p=1.0; putamen -171.5 mm^3 [253], p>0.999; amygdala -234.3 mm^3 [90.3], p=0.07; accumbens -102.6 mm^3 [45.7], p=0.2; hippocampus -255 mm^3 [222], p>0.999).

In MS, compared to HC, the thalamus, caudate, hippocampus, accumbens, amygdala and brainstem, were all significantly smaller (thalamus -1220 mm^3 [301], p=0.0008; caudate -984 mm^3 [194], p<0.001; hippocampus -677 mm^3 [201], p=0.008; accumbens -130.1 mm3 [41.4], p=0.01; amygdala -277.5 mm3 [81.8], p=0.007; brainstem -2663.9 mm3 [845], p=0.01). The putamen and pallidus were not significantly smaller in MS when compared to HC (putamen -598.8 mm^3 [229], p=0.07; pallidus -203.5 mm^3 [85.2], p>0.999).

There were no significant differences between MOGAD and NMOSD-AQP4 (thalamus 152.5 mm^3 [317], p>0.999; caudate -158 mm^3 [205], p>0.999; pallidus -6.54 mm^3 [68.9], p>0.999; putamen -443.9 mm^3 [242], p=0.4; amygdala 27.5 mm^3 [86.3], p>0.999; accumbens 19.5 mm^3 [43.7], p>0.999; hippocampus -166 mm^3 [212], p>0.999; brainstem 483.7 mm^3 [891], p>0.999), and MOGAD and MS (thalamus 551 mm^3 [295], p=0.4; caudate 492 mm^3 [191], p=0.07; pallidus 84.6 mm^3 [64.1], p>0.999, putamen -16.5 mm^3 [225], p>0.999; amygdala 70.7 mm^3 [80.3], p>0.999; accumbens 47 mm^3 [40.6], p>0.999; hippocampus 255 mm^3 [197], p>0.999; brainstem 571.8 mm^3 [829], p>0.999). Compared to NMOSD-AQP4, the caudate was significantly smaller in MS (-650 mm^3 [202], p=0.01), while the remaining comparisons were not significant (thalamus -399 mm^3 [312], p>0.999; pallidus -91.13 mm^3 [67.9], p>0.999; putamen -427.3 mm^3 [238], p=0.5, amygdala -43.2 mm^3 [85], p>0.999; accumbens -27.5 mm^3 [43], p>0.999, hippocampus -422 mm^3 [209], p=0.3, -88.2 mm^3 [878], p>0.999).

The deep grey matter volume was not correlated with the number of relapses in the three disease groups (MOGAD R=-0.43, p=0.062, NMOSD-AQP4 R=-0.4, p=0.089, MS R=-0.19, p=0.48).

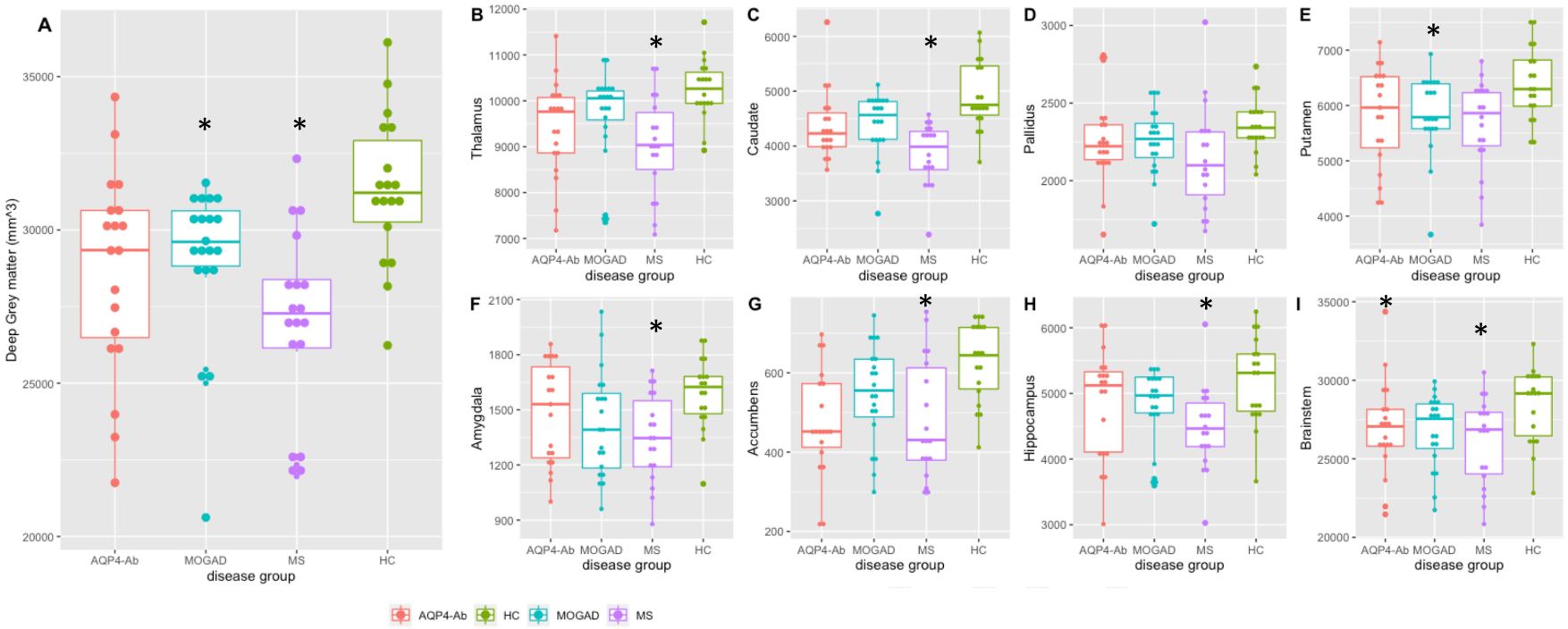


Figure 4.9 Total deep grey matter volumes (A), basal ganglia, hippocampus and brainstem volumes (B-I) between disease groups.
*The graphs represent the median and, the 25th and 75th percentile; Legend: * = p<0.05 when compared to HC, on the linear model adjusted for age, sex and volume scaling factors; AQP4-Ab=NMOSD-AQP4.*

Cortical thickness and volumes: cortical thickness and volumes were not significantly different between groups although the cortical volume was lower in the NMOSD-AQP4 group at a trend level (compared to HC -39748 [15873] mm^3, p=0.09).

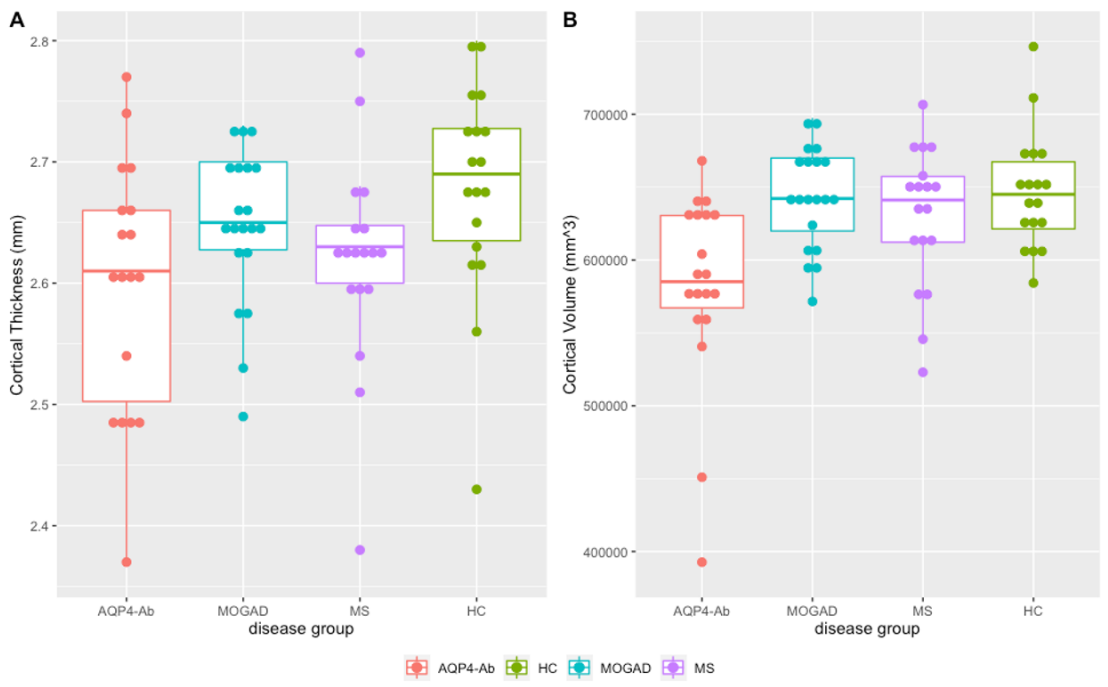


Figure 4.10 Cortex measures between groups. (A) cortical thickness (mm) and (B) cortical volume (mm^3). *The graphs represent the median and, the 25th and 75th percentile. Legend: AQP4-Ab=NMOSD-AQP4.*

White matter region of interest volumes: given that visual function is often involved in antibody-mediated diseases, and association fibres can be abnormal in MS, the optic chiasm and corpus callosum were selected as regions of interest for volume analysis. No significant difference in optic chiasm volumes were seen, but when comparing those with at least one attack of optic neuritis (ON) with those without ON (NON), NMOSD-AQP4-ON had significantly lower chiasmatic volumes when compared to the other groups (NMOSD-AQP4-NON -153.54 mm^3 [23.8], p<0.001; HC -121.43 mm^3 [23.3], p<0.001,

MOGAD-ON -80.05 mm^3 [24.8], p=0.04, MS-ON -95.51 mm^3 [28.1], p=0.02) likely reflecting the recognised posterior location of NMOSD-AQP4-ON and its severity (see Table 1). This effect was not seen in the MOGAD-ON group (see Figure 4.11 A).

There were no significant differences in the corpus callosum volumes across groups (MOGAD vs HC -73.5 mm^3 [146], p>0.999; MOGAD vs NMOSD-AQP4 -179.5 mm^3 [156], p>0.999, MOGAD vs MS 223.8 mm^3 [145], p=0.8; NMOSD-AQP4 vs HC 106 mm^3 [163], p>0.999, NMOSD-AQP4 vs MS 403.3 mm^3 [103], p=0.06, MS vs HC -297.3 mm^3 [148] p=0.3) (see Figure 4.11 B).

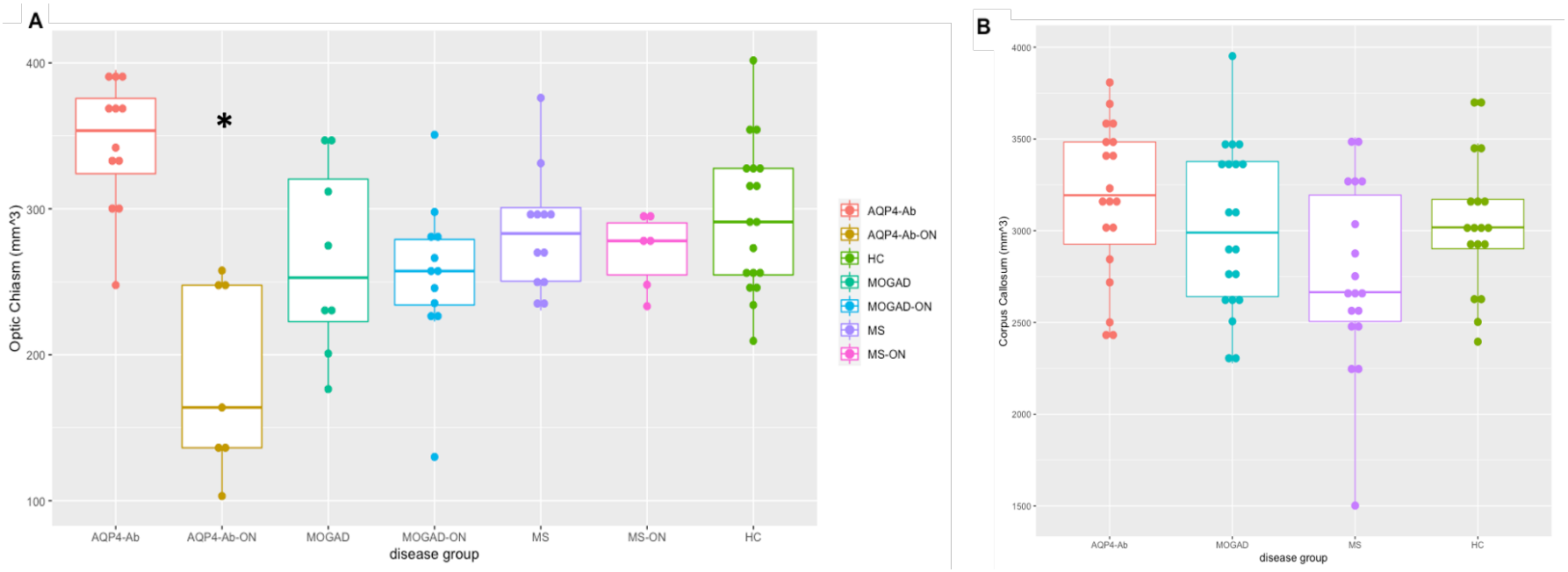


Figure 4.11 (A) Optic chiasm (mm^3) and (B) corpus callosum (mm^3) volumes between disease groups*. The graphs represent the median and, the 25th and 75th percentile. Legend: * = p<0.05 when compared to HC, MOGAD-ON and MS-ON on linear model, adjusting for age, sex, and volume scaling factor. AQP4-Ab=NMOSD-AQP4-NON; AQP4-Ab-ON=NMOSD-AQP4-ON; AQP4-Ab=NMOSD-AQP4.*

4.2.5 *Lesion volume and grey matter volumes in NMOSD-AQP4, MOGAD and MS*

Because the predominant differences in MOGAD were in grey matter structures, the relationship between lesion volume and total deep grey matter volume were explored. Significant negative correlations were found in MOGAD and MS for deep grey matter volumes (Pearson's correlation coefficients; MOGAD R=-0.93, p<0.001, MS R=-0.65, p=0.0034,) and for cortical thickness (MOGAD=-0.71, p=0.005, MS R=-0.64, p=0.0042). No significant correlations were found with cortical volume. Due to the above correlation, the correlation between deep grey matter lesion volume and deep grey matter volume was explored and no significant correlation was found, although the numbers of lesions here were low (Pearson's correlation coefficients; MOGAD R=-0.13, p=0.59, NMOSD-AQP4 R=-0.34, p=0.16, MS R=-0.15, p=0.55).

4.2.6 *Monophasic and relapsing MOGAD*

MOGAD can be monophasic or relapsing and thus may be associated with different pathological mechanisms. Deep grey matter volumes (where abnormalities were most apparent) in the monophasic group (n=6) were compared to those with relapses not affecting the brain/brainstem (n=8) to remove a dose effect of repeated brain damage. Hippocampal volumes were lower but not significant (see Figure 4.12), and caudate volumes were significantly higher in this relapsing group compared to the monophasic group (hippocampus -411 mm^3 [218], p=0.09; caudate -471 mm^3 [118] p=0.03). However, only the hippocampal volume difference seemed plausible since there was also a lower volume in the group that had relapses with brain/brainstem attacks.

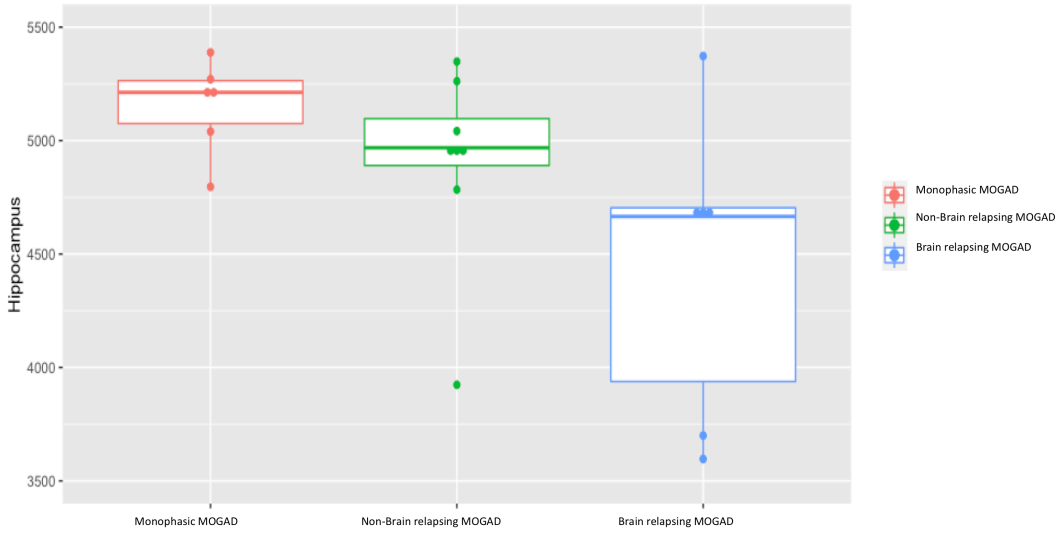


Figure 4.12 Comparison of hippocampus volumetric measures for patients with MOGAD and either a monophasic, relapsing with a brain relapse or relapsing with a non-brain relapse phenotype.
Legend: The graphs represent the median, the 25th and 75th percentile.

4.3 Discussion

This work, using structural MRI, showed that demyelinating diseases have different lesional and volumetric pathological patterns.

Significant volume loss was noted in the deep grey matter structures in MS and MOGAD but not in NMOSD-AQP4, despite the greatest disability being seen in NMOSD-AQP4 and the least in MOGAD. In the white matter, optic chiasm volume was reduced only in NMOSD-AQP4 participants with optic neuritis. Lesion volume was greatest in MS followed by MOGAD and in these two diseases the lesion volumes correlated with disease duration, cortical thickness, and deep grey matter volumes (disease duration was longer in MS, see Table 4.1). Cortical/juxtacortical (type I) fluffy, curvilinear lesions were seen in a minority of MOGAD patients, while cortical/juxtacortical and purely cortical (type II) ovoid lesions were identified in the majority of MS patients and in none of the NMOSD-AQP4 participants.

The global measures were not significantly different across groups, in line with a recent study comparing MOGAD, NMOSD-AQP4 with HC (Schmidt et al., 2020). The findings of this chapter confirmed that deep grey matter structures are most sensitive to atrophy in MS (Messina and Patti, 2014; Zhang et al., 2020) and, for the first time, this was identified as the only region of atrophy in the MOGAD group. Of note is the fact that deep grey matter volume was lower, but not significantly reduced, in NMOSD-AQP4, despite poorer outcomes. It appears that this measure is less sensitive in NMOSD-AQP4, in line with previous studies (Duan et al., 2012; Eshaghi et al., 2016; Matthews et al., 2015).

It is intriguing to note that grey matter volume changes occurred in the two conditions thought to primarily target myelin – a predominant white matter component. Wider pathological CNS involvement in MS is well recognised while, the expression of MOG throughout the CNS needs to be studied. This study supports the growing evidence of grey matter involvement in MOGAD: grey matter lesions have been described in ADEM and over half of children with ADEM have MOG-antibodies (Hacohen et al., 2017; Salama et al., 2019b), and grey matter atrophy was also recently found in the spinal cord in MOGAD (Mariano et al., 2020). Additionally, recent studies confirmed the findings of this chapter, with MOGAD showing reduced cortex and deep grey matter volume (Duan et al., 2021; Zhuo et al., 2020). The white matter lesions in MS and MOGAD, but not in NMOSD-AQP4, correlated negatively with deep grey matter volume suggesting current persistent lesions could be driving the atrophy by disruption of the white matter bundles projecting into the deep grey matter structures, similarly to what has been described in MS (Geurts and Barkhof, 2008).

Cortical lesions were, as expected, identified in the majority of MS patients and none were found in NMOSD-AQP4. Of note, three MOGAD patients had cortical/juxtacortical lesions. This finding, again is intriguing, considering MS and MOGAD may have similar predominantly white matter targets (i.e., myelin). Cortical involvement is well known in MS (Calabrese et al., 2010a) and cortical signal changes associated with seizure have been reported as a rarer isolated phenotype in MOGAD (Ogawa et al., 2017). Additionally, cortical/juxtacortical lesions have been described in clinical MRI (Salama et al., 2019a). A recent study confirmed the presence of cortical lesions in the MOGAD group, however they did not use DIR images, which are deemed among the most sensitive scan to detect cortical lesions, but FLAIR images (Duan et al., 2021). Cortical lesions in the two conditions may be different and further studies are needed. Most of the MOGAD cortical lesions were curvilinear and fluffy, involving adjacent juxtacortical regions (type I) whereas in MS they were mainly ovoid, and some were purely cortical (type II). Cortical/juxtacortical lesions have been described as absent in NMOSD (Calabrese et al., 2012) or have been identified in only a minority of NMOSD-AQP4 patients during the acute phase (Kim et al., 2016). Although cortex is rich in AQP4 water-channels, no lesions were found, but cortical volume was lower, although not significant. It is possible that the disruption of water homeostasis, due to the presence of antibodies directed against the cortex water-channel, is the key pathological mechanism in NMOSD-AQP4 in the cortex, and may explain the reduction of volume in NMOSD-AQP4 patients, in the absence of disruptive lesion damage (Popescu et al., 2010).

The lesion probability subtraction maps showed that lesions are more likely to be present in the periependymal area of the corpus callosum in NMOSD-AQP4, where AQP4 is highly expressed. MS showed a high number of lesions in the periventricular area, in line

with previous findings when compared to NMOSD-AQP4 (Matthews et al., 2013), and when compared to MOGAD. A specific lesion pattern distribution in MOGAD was not found, and this is partly in line with previous findings where a disperse lesion distribution was identified. Although infratentorial lesions are common in the acute phase, they were not present in this MOGAD cohort, in contrast to previous retrospective studies (Yang et al., 2020), as only patients in the remission phase were included. The location of lesions outside of the acute phase, i.e., persistent lesions, is likely to be more useful in associating them with long-term pathological effects on disability.

The white matter region of interest volumetric analysis focused on the optic chiasm and corpus callosum, being the predominant brain areas involved in NMOSD and MS, respectively. A significant reduction in optic chiasm volumes, in NMOSD-AQP4 patients who have had at least one optic neuritis attack, was noted and is in keeping with the clinical residual severity of optic neuritis associated with AQP4 antibodies. The lack of abnormality in the optic chiasm in MS and MOGAD participants having optic neuritis reflects their better recovery and the lack of posterior involvement typically seen with NMOSD-AQP4 (Khanna et al., 2012).

MOGAD can present with a monophasic or relapsing phenotype. Relapses can occur in up to 50% (Cobo-Calvo et al., 2018; Jurynczyk et al., 2017b) of patients and the risk is higher within the first year after the onset attack. Those who become antibody negative are less likely to relapse (Jurynczyk et al., 2017b; Mariotto et al., 2017). This study showed that relapsing patients have lower brain volumetric measures. Additionally, when removing those with relapses that involved either the brain or brainstem, relapsing disease still associated with lower hippocampal volumes though it was not significant, possibly due to the small numbers within these subgroups. Longitudinal studies may determine if

hippocampal atrophy after a single attack is a predictor of relapsing disease and may help identify who should be immunosuppressed from onset.

The main limitation of this study is the small sample size per disease group, as has been discussed in Chapter 3. The use of four different groups, however, allowed comparison of three inflammatory diseases against healthy controls and each other. Although relatively small numbers, the homogeneity of a single centre study using the same scanner and protocol, along with reliable diagnostic ability (using the same expert clinicians and highly accurate assays) is an advantage and will reduce 'noise' and improve power. Additionally, NMOSD-AQP4 disease affects older patients and has a greater preponderance of females while also being more severe, but this was accounted for by adjusting for age and sex in the analyses. Observations from this study can then be used to build hypotheses and design future multi-centre studies.

4.4 Conclusions

MOGAD disease is clinically less severe than NMOSD-AQP4, often with patients recovering completely, and with conventional MRI showing resolution of the brain and spinal cord lesions. This study shows that in MOGAD, deep grey matter atrophy can occur and is associated with persistent lesions. It also highlights the relative sparing of deep grey matter in NMOSD-AQP4 disease, despite being associated with greater disability.

Larger imaging studies in MOGAD and NMOSD-AQP4 patients may identify differences across the different clinical phenotype subgroups and identify new markers of damage that would be useful in clinical trials.

5 Chapter 5 Lesional and non-lesional tissue integrity in demyelinating diseases: a diffusion MRI study

5.1 Introduction and Background

In the previous chapter, structural MRI showed a different pattern of lesion distribution and atrophy across demyelinating diseases. Despite the potential as a valuable tool in a clinical setting, structural MRI still lacks specificity for the pathological mechanisms behind lesional tissue and atrophy (Inglese and Bester, 2010).

In the last years, quantitative and non-conventional brain imaging has emerged as a tool able to provide information on tissue integrity in the abnormal tissue (i.e., lesions) and outside of lesions (i.e., normal appearing tissue).

Among all different quantitative modalities, diffusion MRI (dMRI) was chosen as it provides an indirect measure of cell structure and fibre orientation *in vivo* and is also able to provide a three-dimensional reconstruction of the white matter pathways (i.e. tractography) (Cercignani and Gandini Wheeler-Kingshott, 2019).

Furthermore, diffusion parameters (which have been described in detail in Chapter 1), such as fractional anisotropy (FA) and mean diffusivity (MD) have shown a strong correlation with myelin content, thus representing good candidates as markers of demyelination, which is a primary pathology in MS and MOGAD, and secondary to astrocyte damage in NMOSD-AQP4 (Schmierer et al., 2007). Additionally, axial diffusivity (AD) and radial diffusivity (RD) have been used as more specific markers of axonal and myelin integrity, respectively (Fink et al., 2010; Song et al., 2002).

The presence of occult white and grey matter damage in MS, detected using non-conventional MRI, is well known, while opinion varies as to whether NMOSD-AQP4 causes normal appearing white (NAWM) and grey matter abnormalities (Kremer et al.,

2015; Pache et al., 2016a; Rocca et al., 2004; Schmidt et al., 2020) whether the cohorts mix antibody positive and negative together and whether the tracts associated with lesions are accounted for (Kim et al., 2017; Matthews et al., 2015). A few studies using different methodologies (i.e. diffusion metrics and voxel-wise analysis) have looked at diffusion changes in MOGAD either showing evidence of abnormal NAWM (Schmidt et al., 2020; Zhuo et al., 2020) or no difference compared to HC (Duan et al., 2021).

In this chapter, these considerations are addressed. First, a voxel-wise analysis, excluding persistent lesions, was performed to investigate the main white matter tracts involved. Then, a region of interest (ROI) analysis of the white matter lesions, and NAWM and grey matter were performed (deep grey matter and cortex). Due to the absence of an anisotropic organisation in the grey matter, only the MD was calculated in this compartment (Ceccarelli et al., 2007).

Finally, as optic neuritis is frequent across the three demyelinating diseases and is the hallmark of the Ab-mediated diseases, the optic radiation FA, obtained with tractography, was studied, and compared across diseases.

5.1.1 *Objectives*

The main aims of this chapter are a) to identify different patterns of normal appearing white/grey matter damage in the three diseases and b) to quantify the damage during the remission stage (at least six months after the onset of the most recent attack).

These aims relate to the following, more detailed, objectives:

a) To evaluate the presence of occult white matter damage in the three diseases group against HC and across diseases, using a voxel-wise analysis (i.e., tract-based spatial statistics - TBSS).
b) To perform ROI analysis:

- To assess lesional and non-lesional tissue integrity using FA, MD, RD, and AD.
- To assess grey matter tissue integrity using MD (deep grey matter and cortex)
- To assess the optic radiation tract (obtained with tractography) damage using FA.

5.1.2 *Hypothesis*

The main hypotheses are:

a) The voxel-wise analysis will be able to identify tissue damage in NMOSD-AQP4 and MOGAD, in particular in the optic radiation and corticospinal tracts, with more diffuse damage in MS.
b) NAWM will be abnormal in MS and able to discriminate between MS and Ab-mediated diseases.
c) There will be increased MD in the deep grey matter and cortex in the demyelinating diseases compared to the HC.
d) Optic radiation FA will be abnormal in the three demyelinating diseases.

The work presented in this chapter has been adapted from the publication Messina et al. *Contrasting the brain imaging features of MOG-Antibody disease, with AQP4- Antibody NMOSD and Multiple Sclerosis* (Messina et al., 2021b).

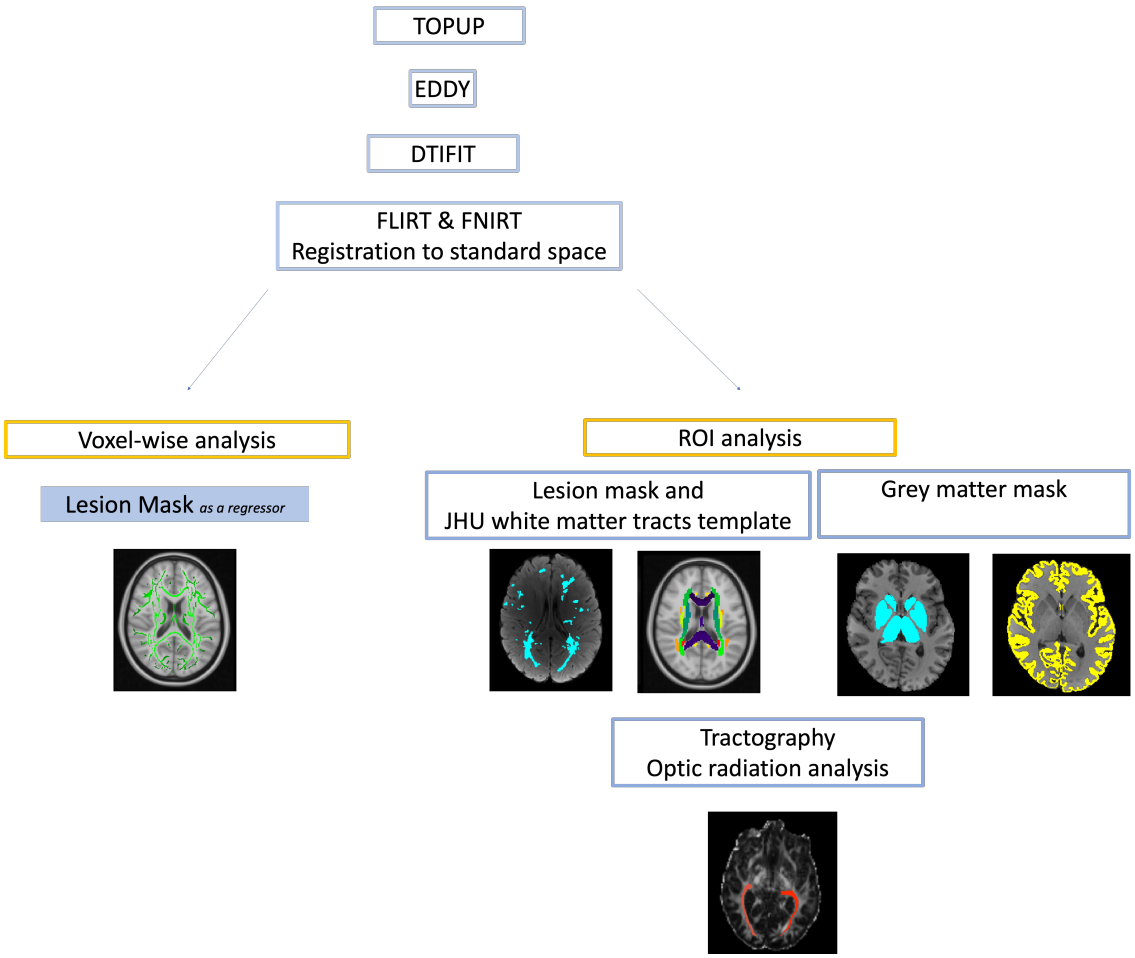


Figure 5.1 Study flow-chart and diffusion pipeline. *Legend: TBSS=tract based spatial statistics, ROI=region of interest, JHU=John Hopkins University.*

5.2 Methods

5.2.1 *Subjects*

The clinical and demographic characteristics of the studied cohort are represented in Table 5.1. Diffusion MRI was not available for one MOGAD, two NMOSD-AQP4, one MS and one HC participant. An additional diffusion MRI for an MS participant was discarded due to poor quality.

Table 5.1 Clinical and demographic characteristics of the studied cohort.

	MOGAD	***NMOSD-AQP4***	***MS***	***HC***
Number	19	17	16	17
Mean age (SD)	42.63 (10.58)	56.47 (13.41)	44.38 (6.51)	39.06 (13.81)
Sex, F (%)	10 (50)	13 (77)	9 (56)	9 (53)
Ethnicity (%)				
Caucasian	19 (100)	9 (53)	16 (100)	14 (82)
African/Afro-	/	3 (18)	/	/
Caribbean	/	3 (18)	/	2 (12)
Asian	/	2 (11)	/	1 (6)
Mixed				
Phenotype (%)				/
Isolated TM	1 (5)	/	/	
TM + Br/Bs	5 (26)	9 (53)	11 (69)	
ON + Br/Bs	/	3 (18)	/	
ON + TM	6 (32)	/	/	
Br/Bs	1 (5)	2 (11)	/	
ON + TM +Br/Bs	6 (32)	3 (18)	5 (31)	
Median disease duration, years (range)	2 (0-24)	9 (0-24)	11 (1-19)	/
Median number of relapses (range)	2 (1-11)	2 (1-11)	3 (1-6)	/
Median EDSS (range)	2.0 (0-7.0)	3.0 (0.0-7.0)	2.0 (0.0-6.0)	/
Mean LogMAR VA (mean OD and OS) (SD)	0.01 (0.57)	0.33 (0.61)	-0.10 (0.12)	/

Legend: SD=standard deviation; TM=transverse myelitis; Br/Bs=brain/brainstem; ON=optic neuritis.

5.2.2 *Statistical Analysis*

The statistical analysis of non-imaging data was performed using RStudio version 1.1.447. Quantitative variables were described using means and SDs, median and range. Distribution of data was assessed using Shapiro-Wilk test. In case the distribution was not normal, a Wilcoxon test was performed. Linear models with sex and age as independent variables were fit to compare the MRI findings between the four study groups. A Bartlett test was performed to assess the variance before including the variables in the linear regression model. In the case of non-equal variance, the variables were transformed. The estimated marginal means were calculated based on the final model and

a Bonferroni pairwise comparison between groups was calculated. The results were expressed as estimates, standard errors, and p-value.

For all analyses, $p < 0.05$ was considered statistically significant, while results between $p>0.05$ and $p<0.1$ were defined as a trend of significance.

5.3 MRI Imaging protocol

The diffusion-weighted sequences were acquired using echo-planar imaging with 50 distinct diffusion-encoding directions for the two diffusion-weighted shells (50 x b=1000 and 50 x b=2000) and 5 x b=0 (with additional 3 x b=0 images with a reversed phase-encoding direction).

5.3.1 *Image Analysis*

Imaging data were analysed using the FMRIB Software Library of tools (FSL; University of Oxford, UK) (Jenkinson et al., 2012; Smith et al., 2004; Woolrich et al., 2009).

Pre-processing of the diffusion imaging: The diffusion images were pre-processed to correct for eddy-current-induced distortions and subject movements, using the eddy tool (Andersson and Sotiropoulos, 2016), part of FSL. Three b=0 images were collected with reversed phase-encode blips, resulting in pairs of images with distortions going in opposite directions. From these pairs the susceptibility induced off-resonance field was estimated using a method similar to that described in (Andersson et al., 2003) as implemented in FSL.

Fractional anisotropy (FA), mean diffusivity (MD), axial diffusivity (AD) and radial diffusivity (RD) maps were created from FMRIB's Diffusion Toolbox (FDT) output. The

RD map was calculated using the following formula, where L2 and L3 are the second and third eigenvalues of the diffusion tensor:

$$\frac{L2 + L3}{2}$$

Tract Based Spatial Statistics: voxel-wise statistical analysis of the FA data was carried out using TBSS (Tract-Based Spatial Statistics) (Smith et al., 2006), part of FSL (Smith et al., 2004). All subjects' FA data were aligned into a common space using the non-linear registration tool FNIRT (J.L.R. Andersson, 2007). Next, the mean FA image was created and thinned to create a mean FA skeleton that represents the centres of all tracts common to the group. Each subject's aligned FA data was then projected onto this skeleton and the resulting data was fed into voxel-wise cross-subject statistics. Data were compared according to groups, using non-parametric permutation testing implemented by *randomise* (part of FSL) with Threshold-Free Cluster Enhancement. Lesion masks (obtained as described in Chapter 4) were entered as a voxel-wise nuisance regressor in the final model so that lesioned voxels would be disregarded, on a per subject basis, in the statistical comparison between groups.

T2 lesions and normal white matter diffusion measures: the distortion-corrected b=0 diffusion image was registered to the T1 structural image. The transformation matrix was then used to the transform the FA, MD, RD, and AD diffusion images to T1 structural image space. FLAIR lesion masks, obtained as described in Chapter 4, were transformed to the T1 image space, using a non-linear transformation. White matter tracts, obtained from the JHU atlas, were also transformed to the T1 space using a non-linear transformation. The diffusion-derived measures were evaluated in the main white matter tracts and not in the whole NAWM, to focus on the tracts that are more consistent across participants and to compensate for possible registration errors that may occur in the rest

of the white matter (Zamboni et al., 2019). The white matter tracts were thresholded and binarized to obtain masks.

Lesion masks were inverted and multiplied with the T1 transformed white matter tracts to obtain non-lesioned white matter tracts for each subject. FA, MD, RD, and AD values were then calculated within regions of interest (ROIs) defined by the lesion mask and non-lesioned white matter tracts.

Cortical and deep grey matter MD: the cortical mask was created from the right and left cortex labels, output by FreeSurfer. First, the cortical segmentation was binarized, then transformed to the same space as the FSL structural (T1) image results. Finally, the cortical segmentation was binarized again, after transformation and interpolation. The deep grey matter volumes obtained with FSL were binarized to obtain a deep grey matter mask. MD was calculated within the cortex and deep grey matter ROIs.

Tractography: the preprocessed diffusion MRI data were also fed into a tractography-based analysis to obtain the optic radiation tracts. The analysis begins with a within-voxel modelling of multifibre tract orientation structure via the Bayesian Estimation of Diffusion Parameters Obtained using Sampling Techniques tool (BEDPOSTx) from FSL. The BEDPOSTx outputs are then used to run the probabilistic tractography (with crossing fibre modelling) using PROBTRACKx (Behrens et al., 2003; Behrens et al., 2007; Jbabdi et al., 2012). Automated mapping of the optic radiation tracts was performed in the standard space of each participants using start/stop region of interest masks, implemented using the AutoPtx plugin for FSL (de Groot et al., 2013), to obtain tract-averaged FA measures of the tracts of interest. The optic radiation tracts were transformed to the T1 space using a non-linear transformation, via the B0 image, then they were thresholded and binarized to create a mask. Lesion masks were inverted and multiplied with the T1 transformed optic radiation tracts to obtain non-lesioned optic radiation tracts. FA was

then calculated in the transformed non lesioned optic radiation tracts. The right and left optic radiation tracts were then averaged and compared across groups.

5.4 Results

See Appendix, Table S5.1 for average diffusion measures across groups.

5.4.1 *Tract-based spatial statistics of NAWM FA*

TBSS voxel-wise analysis of FA NAWM showed a significant reduction in NMOSD-AQP4 when compared with HC in the external capsule, corona radiata, the anterior limb of the internal capsule, posterior limb of the internal capsule (including fibres of the optic radiation), retrolenticular internal capsule, corpus callosum, posterior thalamic radiation (including the optic radiation), and in the brainstem, the cerebral peduncle, the middle cerebellar peduncles, medial lemniscus, the pontine crossing tracts (corticospinal tracts) and the inferior cerebellar peduncles (see figure 5.2A).

MS compared to HC, showed a significant reduction of the FA in the corpus callosum, corona radiata, and posterior thalamic radiation (see figure 5.2B), and a trend for a reduction in the posterior part of the corpus callosum when compared to MOGAD ($p=0.07$, figure not shown).

The TBSS voxel-wise analysis in MOGAD did not show any significant difference when compared with HC (figure 5.2D).

FA NAWM in NMOSD-AQP4 when compared to MOGAD, showed a more widespread significant reduction (figure 5.2C).

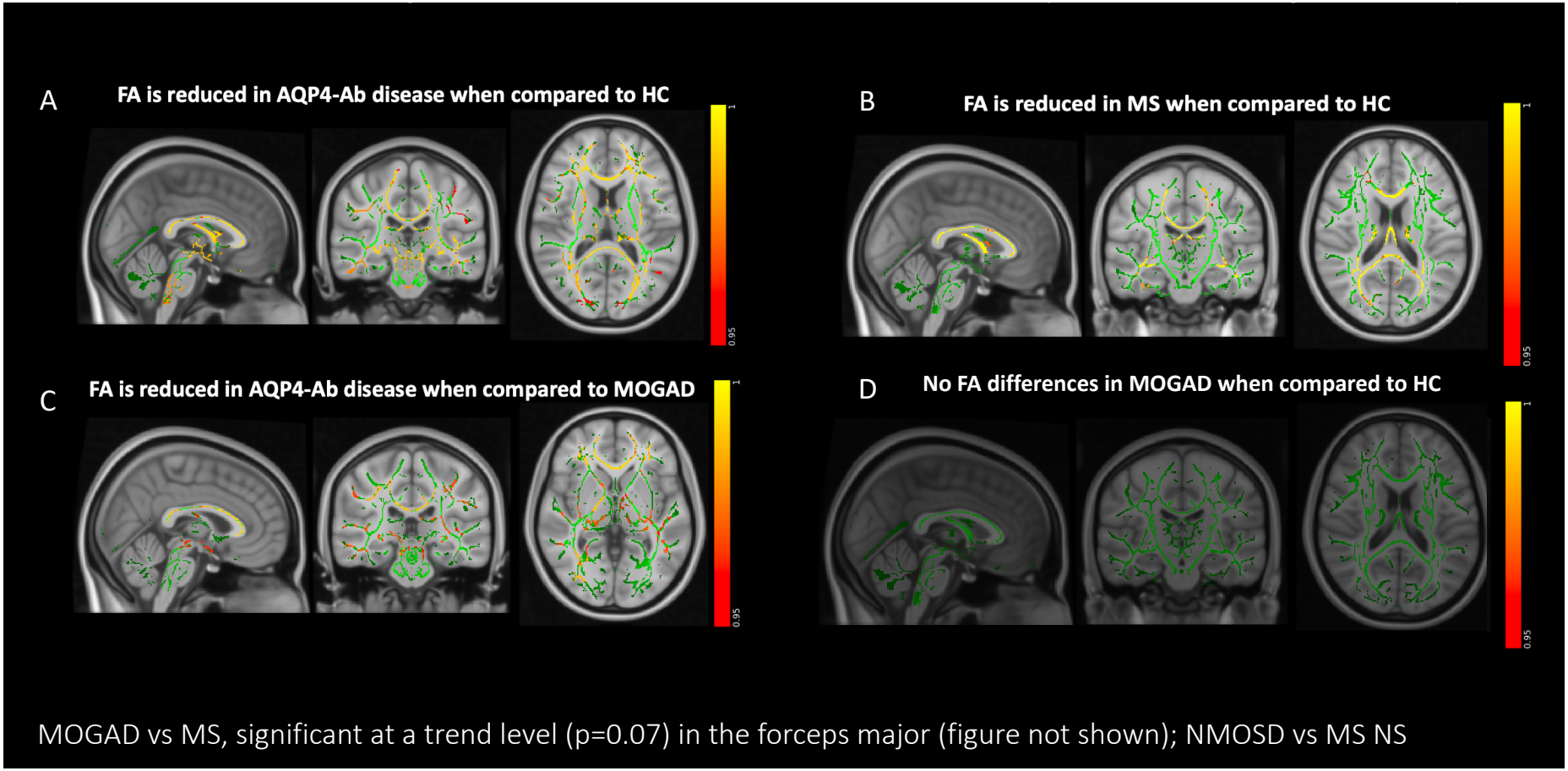


Figure 5.2 tract based spatial statistics FA in NMOSD-AQP4 vs HC A), MS vs HC B), NMOSD-AQP4 vs MOGAD C), and MOGAD vs HC D). *Legend: The FA skeleton is shown in green with a threshold of 0.2, tracts with lower FA are shown in red-yellow (values represent 1-p value, TFCE corrected). AQP4-Ab=NMOSD-AQP4.*

5.4.2 *ROI analysis*

All group comparisons used linear regression with Bonferroni correction and were adjusted for age and sex (results are shown as the difference of diffusion measure estimates between groups, standard error [SE], p-value).

White matter diffusion metrics: fractional anisotropy (FA) and mean diffusivity (MD in 10^{-3} mm^2 s^{-1}), axial diffusivity (AD in 10^{-3} mm^2 s^{-1}) and radial diffusivity (RD in 10^{-3} mm^2 s^{-1}) were calculated within the lesion voxels (lesion-FA, lesion-MD, lesion-RD, lesion-AD) using the lesion masks, and in the normal-appearing white matter (NAWM).

Lesion-FA was lower, and lesion-MD and RD were higher when compared to the NAWM within all the three diseases (see Figure 5.3 A-D), and also compared to HC (lesion-FA NMOSD-AQP4 -0.16 [0.02], MOGAD -0.16 [0.02], MS -0.15 [0.02], $p<0.001$ in each group; lesion-MD NMOSD-AQP4 0.11 [0.03], $p=0.002$, MOGAD 0.13 [0.03], MS 0.17 [0.03] $p<0.001$ in MOGAD and MS; lesion-RD NMOSD-AQP4 0.16 [0.03], MOGAD 0.15 [0.02], MS 0.17 [0.02], $p<0.001$ in each group), but no differences were found in AD values. NAWM-FA in MOGAD and NMOSD-AQP4 was similar to HC and only in MS was it lower compared to both HC and MOGAD (-0.03 [0.01], $p=0.01$, -0.03 [0.01], $p=0.03$) (see Figure 5.3 A-D).

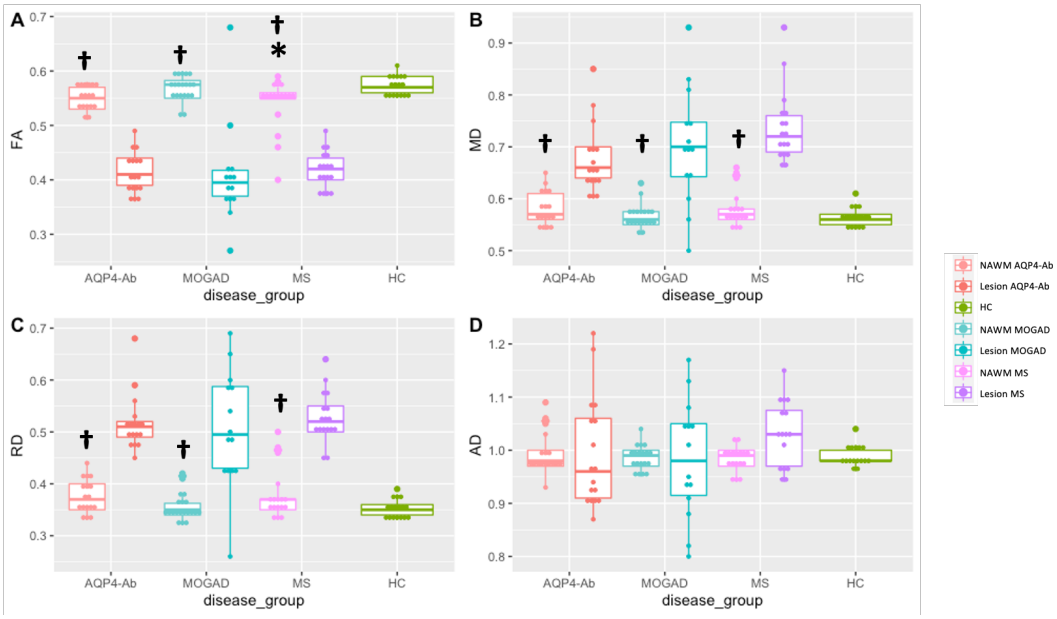


Figure 5.3 FA, MD RD, and AD T2 lesion and NAWM comparison in the four groups (A-D)*; The graphs represent the median, the 25th and 75th percentile. Legend: (A-D) †= p<0.05 when compared to NAWM and HC; * = p<0.05 when compared to HC and MOGAD NAWM, on the linear model adjusted for age and sex. NAWM boxplots are on the left of lesion boxplots in the pair for each disease group. FA=fractional anisotropy, MD=mean diffusivity, RD=radial diffusivity, AD=axial diffusivity, NAWM=normal appearing white matter, AQP4=NMOSD-AQP4.*

Grey matter diffusion metrics: MD values were analysed in the cortical and deep grey matter structures. There were no differences in the cortex MD values across groups (MOGAD vs HC -0.002 [0.01], p>0.999; NMOSD-AQP4 vs HC 0.005 [0.01], p>0.999; MS vs HC 0.02 [0.01], p=0.7; NMOSD-AQP4 vs MOGAD 0.008 [0.01], p>0.999; MS vs MOGAD 0.02 [0.01], p=0.4; MS vs NMOSD-AQP4 0.01 [0.01], p>0.999). Although three multiple sclerosis patients showed higher values in the deep grey matter (all three had EDSS>4), there were no differences across groups (MOGAD vs HC -0.003 [0.01], p>0.999; NMOSD-AQP4 vs HC -0.002 [0.01], p>0.999; MS vs HC 0.01 [0.01], p>0.999; NMOSD-AQP4 vs MOGAD 0.001 [0.01], p>0.999; MS vs MOGAD 0.02 [0.01], p=0.5; MS vs NMOSD-AQP4 0.01 [0.01], p=0.9) (see Figure 5.4).

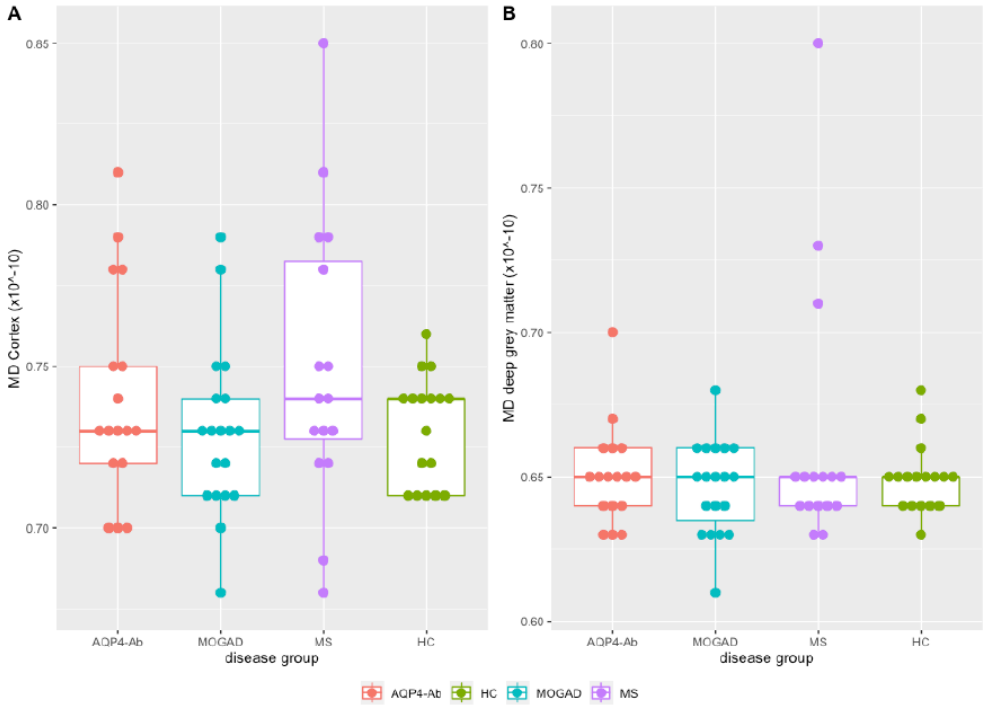


Figure 5.4 MD in the cortex (A) and in the deep grey matter structures (B) between groups. *The graphs represent the median, the 25th and 75th percentile. Legend: AQP4-Ab=NMOSD-AQP4, MD=mean diffusivity.*

Optic radiation: FA was calculated in the optic radiation mask obtained with tractography. The comparisons across groups showed a significantly lower FA value in MS compared to HC (-0.029 [0.009], p=0.008) and a trend for a lower FA in NMOSD-AQP4 compared to HC (-0.0245 [0.010], p=0.094). The remaining comparisons were not significant (NMOSD-AQP4 vs MOGAD -0.013 [0.009], p=0.960, NMOSD-AQP4 vs MS 0.005 [0.009], p>0.999, HC vs MOGAD 0.011 [0.008], p>0.999, MOGAD vs MS 0.018 [0.008], p=0.210).

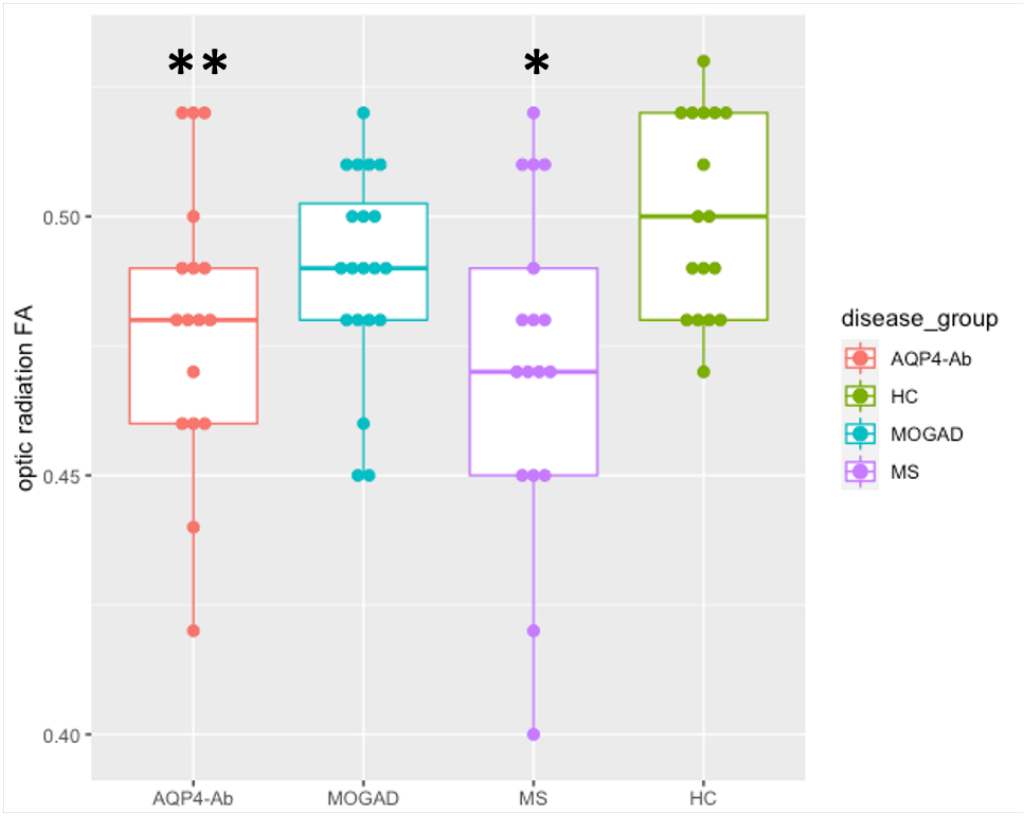


Figure 5.5 FA in the optic radiation tract (left and right sides averaged) between groups. The graphs represent the median, the 25th and 75th percentile*. Legend: * = p<0.05 when compared to HC, on the linear model adjusted for age and sex, ** trend level of significance (p<0.1), when compared to HC, on the linear model adjusted for age and sex. AQP4-Ab=NMOSD-AQP4, FA=fractional anisotropy.*

5.5 Discussion

The white and grey matter microstructural changes in demyelinating diseases showed that diffusion measures were abnormal in lesions of all disease group participants, but, overall, non-lesional FA was only reduced in MS. However, focal reductions were noted in NMOSD-AQP4 patients, reflecting mainly optic nerve and corticospinal tract pathways. The ROI analysis of the optic radiation showed abnormal FA in MS and NMOSD-AQP4 (although at a trend level in the latter), while no significant difference in MOGAD compared to HC. Diffusion measures (i.e., MD) could not discriminate and explain the grey matter pathology across diseases in this cohort, although a higher cortical MD was found in some MS patients.

Table 5.2 Summary of the key-findings.

	NMOSD-AQP4	*MOGAD*	*MS*
White matter measures			
Lesion FA	↓↓	↓↓	↓↓
Lesion MD	↑↑	↑↑	↑↑
Lesion RD	↑↑	↑↑	↑↑
Lesion AD	↔	↔	↔
Normal appearing white matter FA	↓	↔	↓↓
Normal appearing white matter MD	↑	↔	↑
Normal appearing white matter RD	↑	↔	↑
Normal appearing white matter AD	↔	↔	↔
Optic Radiation FA	↓↓†	↔	↓↓
Grey matter measures			
Cortex MD	↔	↔	↑
Basal ganglia MD	↔	↔	↔

Legend: compared to HC ↔ no difference, ↓ lower but not significant; ↓↓† non-significantly lower (trend level), ↓↓ significantly lower; ↑ higher but not significant; ↑↑ significantly higher.

Of interest is that the lesions across all diseases, appeared similarly affected on diffusion metrics and were abnormal when compared to the NAWM measures, suggesting that the damage from permanent lesions, as detected using DTI, was similar. All diffusion measures, except for AD, were able to discriminate between lesional and non lesional tissue, possibly demonstrating a predominantly myelin, rather than axonal, lesional damage.

In MOGAD, no abnormal diffusion measures were found in the NAWM, although 14 out of 20 participants presented with white matter lesions, and 8 out of 20 participants had large acute lesions at the time of the onset attack. This finding, together with the structural finding of the previous chapter (i.e., low deep grey matter), suggests a distinct pathological pattern in MOGAD, compared to the other two demyelinating conditions,

where grey matter is more sensitive to damage than non-lesional white matter in the remission stage.

This finding is of particular interest, as MOGAD patients present with severe attacks at nadir, similarly to that in NMOSD-AQP4; however, most of them have a good/full recovery (Jurynczyk et al., 2017b; Mariano et al., 2019). The lack of abnormal white matter outside of the persistent lesion area in the recovery phase, also in participants who presented with large brain lesions in the acute stage, is consistent with the overall good clinical recovery in MOGAD.

One hypothesis is that lesions with different pathology may co-exist in MOGAD in the acute stage: the persistent lesions are likely associated with demyelination, and abnormal FA, similarly to MS and NMOSD-AQP4, while the "resolved" lesions may recover pathologically better, and the current diffusion measures are not able to capture the pathology changes, or may be associated with a reversible process, such as oedema.

The hypothesis of an "efficient" and rapid remyelination process has been hypothesised in a recent pathology study (Höftberger et al., 2020). The authors suggested that, as MOG is mainly expressed on mature oligodendrocytes, but not on the progenitor cells, remyelination may occur in the early stage via recruitment of the progenitor oligodendrocytes cells.

Additionally, in contrast to early pathology studies in MOGAD, which showed complement activation similarly to the "MS lesion type II" described in MS (Lucchinetti et al., 2000; Spadaro et al., 2015b), a recent study did not confirm this finding, showing perivascular demyelination and oligodendrocyte preservation (Takai et al., 2020).

Three diffusion MRI studies in MOGAD, using different methodologies (i.e. diffusion metric comparisons and voxel-wise analysis) showed differing results, with two studies describing abnormal NAWM (Schmidt et al., 2020; Zhuo et al., 2020) and the other no

difference, compared to HC (Duan et al., 2021). The contrasting results might be related to the inclusion of patients that are possibly still within the acute stage (4 weeks after the attack), thus possibly still presenting with acute lesions or the presence of persistent lesions, not accounted for in the voxel-wise analysis.

In this experimental chapter, the participants were enrolled at least six months after the acute attack, thus avoiding the possibility of including patients still in the acute stage. Furthermore, the effect of the lesioned voxels was removed from the voxel-wise analysis by using subject-wise spatial regressors, thus focussing the analysis on the non-lesional tissue.

In NMOSD-AQP4 the lesions are more destructive and are characterised by astrocytes and only then subsequent oligodendrocyte loss with complement activation and more generalised tissue destruction. The tract-based analysis did identify damage in NMOSD-AQP4 but predominantly affecting the visual and pyramidal pathways, supporting the presence of remote damage secondary to inflammation of the optic nerve and spinal cord, areas commonly affected in this disease. The predominance of visual and pyramidal pathway tract remote involvement is supported by other studies (Kim et al., 2017; Matthews et al., 2015). Additionally, the abnormal corpus callosum FA mirroring the periependimal lesion distribution described in the previous chapter suggests that the abnormal diffusion measure may also be a consequence of the local damage caused by the NMOSD-AQP4 lesions.

In light of this, one may postulate that the NMOSD-AQP4 lesions present a different pathology than MOGAD lesions, despite the similar diffusion measures. the lack of resolution of lesions is consistent with poor recovery (Jurynczyk et al., 2017b).

This hypothesis is also confirmed by the ROI analysis of the optic radiation and is in line with the optic chiasm volumetric analysis described in the previous chapter. Even though the severity of the optic neuritis is similar, there is a good/full recovery in MOGAD, while only a poor recovery in NMOSD-AQP4, as reflected by the abnormal optic radiation FA in the NMOSD-AQP4 group, but normal in MOGAD, and the low chiasmatic volume as shown in the previous chapter.

It is well known that NAWM in MS is significantly abnormal when using FA, a sensitive measure of demyelination. The abnormal NAWM FA could represent widespread lesion-related damage (related to remote lesions or 'resolved' lesions) and/or non-lesional pathology in the white matter. The tract based spatial statistics showed that damage was prevalent in the corpus callosum and the associative tracts, such as the corona radiata. The overall FA in the NAWM was significantly lower in MS than HC and MOGAD, and this is evident also in the ROI of the optic radiation. Visual symptoms are usually milder in MS than NMOSD-AQP4 and MOGAD, suggesting that possibly the optic radiation damage is due to the diffuse NAWM damage rather than the Wallerian degeneration secondary to optic neuritis (You et al., 2020).

The general limitations of this study, mostly related to the small sample size, have been discussed in Chapter 3. However, there are also limitations more specific to this chapter that need to be considered.

The presence of cortical grey matter lesions has not been accounted for in the diffusion analysis. In addition, the current imaging methods cannot detect all the cortical lesions. Hence, it is possible that the lesions could have affected the diffusion measures, especially

in MS. In MOGAD, there were very few lesions in the grey matter, therefore it is plausible that they had a limited effect on the diffusion results.

In MOGAD, the role of the different phenotypes was not explored, due to the limited number for each phenotype group. Most participants had brain lesions in the acute stage, to maintain the cohort as homogenous as possible. Future studies should focus on the diffusion measures across different phenotypes.

No changes in the NAWM were found in MOGAD; however, given the limited sample size, it is possible that a larger study may capture subtle or milder pathology changes.

5.6 Conclusions

In this diffusion study, different patterns of microstructural damage across the three demyelinating diseases have been described. FA, MD, and RD, but not AD, were able to differentiate between lesional and non-lesional tissue in the three conditions. The microstructural lesion damage across the three diseases is similar, while the NAWM is preserved in MOGAD and is overall abnormal in MS and focussed on tracts related to ON and TM in NMOSD-AQP4.

Widespread lower FA values were found in MS, while in NMOSD-AQP4 there were abnormal FA values focussed on the optic radiation and corticospinal tracts. Despite the mild visual symptoms in MS compared to NMOSD-AQP4, the optic radiation is abnormal in both MS and NMOSD-AQP4, supporting the presence of subclinical damage in MS.

Larger studies and longitudinal studies are needed to better clarify the microstructural damage in MOGAD, and to compare the NAWM integrity across different phenotypes. Understanding the differences between groups may give more pathological information.

In addition, the presence of damage outside of the acute phase can be a useful marker associated with long-term disability.

The association of the structural and diffusion MRI findings with the clinical disability scores will be explored in the next chapter.

6 Chapter 6 Clinical outcomes and their association with structural and diffusion imaging findings in demyelinating diseases

6.1 Introduction and Background

In the previous chapters, the lesional, volumetric and diffusion measures were described and compared across the disease groups.

Although the MRI measures are sensitive to pathological changes, they cannot provide information of the different pathological mechanisms behind each disease, where demyelination is a primary pathological event, i.e., MOGAD and MS, or a secondary event, i.e., NMOSD-AQP4. A multimodal approach can give the advantage of exploring different aspects of the tissue damage, thus providing a signature possibly able to discriminate across inflammatory demyelinating CNS diseases. As shown in previous chapters, grey matter atrophy is the main non-lesional pathological change in MOGAD, while MS presented both abnormal non-lesional white and grey matter changes, and NMOSD-AQP4 abnormal non-lesional white matter changes. In this chapter, the clinical relevance of different MRI measures will be explored.

The association of the MRI metrics with EDSS has been extensively explored in MS, and has shown, that at the time of the first clinical event, and in both the remission and progressive stage, the non-lesional abnormality, rather than the lesional areas, are strongly correlated with disability (Brownlee et al., 2019; Filippi et al., 2013; Rocca et al., 2017b). In particular, grey matter atrophy has been described as particularly relevant, and recently has been used as an outcome metric of disability in clinical trials (Gaetano et al., 2018). Visual function was associated with myelin content measures in patients with at least one episode of optic neuritis (Caverzasi et al., 2020).

In NMOSD-AQP4, abnormal white matter FA has been associated with worse EDSS (Duan et al., 2021), while visual pathway volumetric structures, such as the optic chiasm and lateral geniculate nucleus (part of the thalamus) have been associated with optic neuritis and worse visual outcome (Juenger et al., 2020; Papadopoulou et al., 2019).

In MOGAD, in a recent study, worse EDSS associated with deep grey matter structure volume, and, in another study, with hippocampus/parahippocampus measures (Duan et al., 2021; Zhuo et al., 2020).

This chapter aims to explore the relationship with disability measures, i.e., EDSS and visual acuity, using measures representing the white matter and grey matter compartment, in the whole disease group (MOGAD, NMOSD-AQP4 and MS), and then in each group disease group separately.

Understanding which compartment is mainly associated with disability may help to better understand the pathological process in each disease and may provide possible target for therapeutic intervention.

Part of this chapter has been adapted from the publication: "Contrasting the brain imaging features of MOG-antibody disease, with AQP4-antibody NMOSD and multiple sclerosis" (Messina et al., 2021b).

6.1.1 *Objective*

a) To study the relationship between EDSS and the MRI findings in the whole disease group (MOGAD, NMOSD-AQP4 and MS) and in each disease group separately.
b) To study the relationship between visual acuity (VA) and MRI findings in the disease groups (MOGAD, NMOSD-AQP4 and MS) and in each disease group separately.

6.1.2 *Hypothesis*

a) MRI metrics will show an association with disability in each disease group.

b) Visual pathway measures will be associated with visual acuity in each disease group.

6.2 Methods

6.2.1 *Subjects and clinical measures*

The 75 participants of the cohorts described in Chapter 4 and 5 were included in the analysis. The details of the demographics and clinical outcomes of the studied cohort have been given in Chapter 3 and Table 3.1. The following clinical measures were considered as clinical outcomes in this chapter:

- EDSS: a measure of physical disability (as described in Chapter 3)
- Visual acuity (in LogMAR and averaged between the two eyes, as described in Chapter 3)

6.2.2 *MRI measures*

To avoid collinearity due to the large number of variables explored in the previous analysis, only those variables significantly different across groups, along with age and sex, were include in this analysis. The following MRI variables were used as independent variables in the EDSS model:

- Deep grey matter volume
- Brainstem volume

- Average normal-appearing white matter (NAWM) FA in the white matter mask (as described in Chapter 5)
- Lesion volume

For visual acuity disability, because in these diseases it will be predominantly due to ON, we focussed on the anterior visual pathway measures, along with age and sex:

- Thalamic volume (containing the lateral geniculate nucleus)
- optic chiasm volume

6.2.3 *Statistical Analysis*

RStudio version 1.1.447 for non-imaging data was used. Differences were evaluated by ANOVA (to test means) and $\chi 2$ (to test proportion). Non-parametric tests were performed when not normally distributed.

A multivariable linear regression model with a stepwise variable selection based on the Akaike information criterion (AIC) was fitted in the whole disease group (MOGAD, NMOSD-AQP4 and MS) and every disease group separately, using age and sex, disease group, and MRI measures (selected as described above) as independent variables, and EDSS as the dependent variable.

For visual acuity (mean LogMAR), the same demographic variables (age and sex), disease group, and only two *a priori* MRI measures as independent variables (optic chiasm and thalamus volume due to their connection to the anterior visual pathways) were used in the multivariable linear regression model. For all analyses, $p < 0.05$ was considered statistically significant.

6.3 Results

6.3.1 *Disability – EDSS*

As shown in Chapter 3, EDSS is higher in NMOSD-AQP4 than the other disease groups, reflecting the higher severity of this condition.

The association of MRI findings with EDSS was explored across all diseases (MOGAD, NMOSD-AQP4 and MS), using a stepwise multivariable regression model which showed that the lower NAWM FA was the only MRI variable associated with worse EDSS (R-squared=0.28; slope=-19.98, p=0.004).

Table 6.1 Final model after multivariate linear regression across the disease groups (MOGAD, NMOSD-AQP4, MS); *EDSS: dependent variable. CI=95% confidence intervals*

	EDSS		
Predictors	*Estimates*	*CI*	*p*
(Intercept)	12.754	5.170 – 20.338	0.001
Female sex	0.625	-0.235 – 1.484	0.151
FA NAWM	-19.976	-33.119 – -6.833	**0.004**
NMOSD-AQP4	0.890	-0.146 – 1.926	0.091
MS	0.030	-1.052 – 1.113	0.955
R^2 / R^2 adjusted	0.281 / 0.225		

The association of MRI findings with EDSS, was then explored within each disease group, using a stepwise multivariable regression model. This analysis showed that lower NAWM FA in NMOSD-AQP4 (R-squared=0.49; slope=-61.67, p<0.001), lower deep grey matter volumes and female sex in MS (R-squared=0.47; deep grey matter volume slope=-0.0002, p=0.05; beta value for sex=2.09, p=0.005) and lower brainstem volume

in MOGAD (R-squared=0.23; slope=-0.0003, p=0.03) were associated with worse EDSS (see Table 6.2-6.4).

Table 6.2 Final model after multivariate linear regression in the NMOSD-AQP4 group; *EDSS: dependent variable. CI=95% confidence intervals*

	EDSS		
Predictors	*Estimates*	*CI*	*P*
(Intercept)	37.067	19.172 – 54.962	<0.001
FA NAWM	-61.667	-94.087 – -29.246	**0.001**
R^2 / R^2 adjusted	0.486 / 0.456		

Table 6.3 Final model after multivariate linear regression in the MOGAD group; *EDSS: dependent variable. CI=95% confidence intervals*

	EDSS		
Predictors	*Estimates*	*CI*	*P*
(Intercept)	10.421	2.548 – 18.293	0.012
Brainstem volume	-0.0003	-0.0006 – -0.00003	**0.031**
R^2 / R^2 adjusted	0.233 / 0.190		

Table 6.4 Final model after multivariate linear regression in the MOGAD group; *EDSS: dependent variable. CI=95% confidence intervals*

	EDSS		
Predictors	*Estimates*	*CI*	*p*
(Intercept)	7.448	1.264 – 13.631	0.021
Female sex	2.090	0.726 – 3.455	**0.005**
Deep grey matter volume	-0.0002	-0.0005 – -0.00000	**0.049**
R^2 / R^2 adjusted	0.467 / 0.395		

6.3.2 *Disability - Visual acuity*

The association between the MRI findings and visual acuity across the disease groups (MOGAD, NMOSD-AQP4 and MS) showed that the presence of AQP4-Ab, lower optic chiasm volume and lower thalamus volume are associated with worse visual acuity (see Table 6.5).

Lower optic chiasm in NMOSD-AQP4 (R-squared=0.63; slope=-0.007, p<0.001), and lower thalamic volume and female sex in MOGAD (R-squared=0.42; slope=-0.0004, p=0.006; beta value for sex=0.48, p=0.04) were associated with worse visual outcome. No significant predictors were found in the MS group (see Table 6.6-6.8).

Table 6.5 Final model after multivariate linear regression in the whole disease group (MOGAD, NMOSD-AQP4 and MS); *Visual Acuity: dependent variable. CI=95% confidence intervals*

	Average Visual Acuity		
Predictors	*Estimates*	*CI*	*p*
(Intercept)	3.161	1.587 – 4.735	<0.001
Optic Chiasm Volume	-0.004	-0.007 – -0.002	**<0.001**
Thalamus Volume	-0.000	-0.000 – -0.000	**0.006**
NMOSD-AQP4-Ab	0.484	0.140 – 0.828	**0.007**
MS	-0.112	-0.475 – 0.250	0.536
R^2 / R^2 adjusted	0.422 / 0.375		

***Table 6.6 Final model after multivariate linear regression in the NMOSD-AQP4 group**; Visual Acuity: dependent variable. CI=95% confidence intervals*

	Visual Acuity		
Predictors	*Estimates*	*CI*	*P*
(Intercept)	4.843	1.879 – 7.808	**0.003**
Optic Chiasm volume	-0.007	-0.010 – -0.004	**<0.001**
Thalamus volume	-0.0003	-0.0006 – 0.00004	0.081
R^2 / R^2 adjusted	0.630 / 0.581		

***Table 6.7 Final model after multivariate linear regression in the MOGAD group;** Visual Acuity: dependent variable. CI=95% confidence intervals*

	Visual Acuity		
Predictors	*Estimates*	*CI*	*P*
(Intercept)	3.34660	0.93524 – 5.75795	**0.009**
Female sex	0.47857	0.02814 – 0.92901	**0.039**
Thalamus volume	-0.00037	-0.00062 – -0.00012	**0.006**
R^2 / R^2 adjusted	0.422 / 0.354		

***Table 6.8 Final model after multivariate linear regression in the MS group;** Visual Acuity: dependent variable. CI=95% confidence intervals*

	Visual Acuity		
Predictors	*Estimates*	*CI*	*P*
(Intercept)	-0.115	-0.809 – 0.579	0.726
Age	0.008	-0.003– 0.019	0.151
Optic Chiasm volume	-0.001	-0.003 – 0.0007	0.198
R^2 / R^2 adjusted	0.230 / 0.111		

6.4 Discussion

This chapter showed that abnormal NAWM was associated with higher disability in NMOSD-AQP4, while the deep grey matter was the main driver of disability associated with female sex in MS. In MOGAD, brainstem volume was associated with a worse motor disability.

The selected anterior visual pathway structures, i.e., optic chiasm and thalamus, are associated with the visual function in the antibody-mediated disease. In particular, the optic chiasm showed a strong association in NMOSD-AQP4, and the thalamus with MOGAD. No visual pathway structures associated with visual disability in MS.

Different MRI predictors of disability within the individual disease groups could suggest different pathological mechanisms contribute to the tissue damage across these diseases. It is not surprising that NAWM FA was associated with EDSS in NMOSD-AQP4 disease because the regional changes we identified were in those tracts mainly associated with the optic nerve and corticospinal tract and might relate to remote damage from attacks of ON and transverse myelitis or local damage left by acute lesions. This finding is in line with previous studies, where lower white matter FA was found as the main MRI finding associated with disability (Duan et al., 2021). NAWM FA was the only MRI finding associated with worse EDSS, independent of disease type, suggesting that this measure can potentially be considered a marker of disability in CNS disease.

Lower deep grey-matter volume and female sex, associated with worse EDSS in MS, possibly reflecting the widespread atrophy of the deep grey matter structures noted in MS, and is in line with previous findings (Filippi et al., 2013). A longitudinal study showed that deep grey matter volume has the fastest atrophy annual rate and is a predictor of EDSS progression (Eshaghi et al., 2018).

Brainstem volume was the only MRI measure associated with EDSS in MOGAD, and this may reflect its eloquent site for ambulatory disability and is in line with observations that the presence of brainstem lesions is associated with a worse recovery from transverse myelitis attacks (Mariano et al., 2019).

In the NMOSD-AQP4 group lower optic chiasm volumes could explain reduced visual acuity, in line with previous observations of preferential involvement of the chiasm, which is rich in astrocytes, in NMOSD-AQP4 (Harvey et al., 2021; Khanna et al., 2012), reflecting the recognised lack of chiasmatic involvement in MOGAD (Kupfer et al., 1967).

Interestingly, only lower thalamic volume was associated with MOGAD. Although only 42% of the visual disability may be explained by the model (including the female sex), this intriguing finding may suggest a possible involvement of axons from the lateral retina, which remain ipsilateral and do not cross the chiasm (Kupfer et al 1967).

Both optic chiasm and thalamus volume, together with the presence of AQP4-Ab, are associated with worse visual outcomes, when analysed across all diseases, possibly reflecting the severity of optic neuritis in NMOSD-AQP4.

In this chapter the association with white and grey matter compartment measures has been explored. Besides the more general limitations already discussed in the previous chapters and due to the small sample size, there are some limitations specific to this chapter that need to be discussed. First, the selection of different variables may have affected the final model, as it cannot be excluded that other variables may contribute to overall disability. The variables were selected based on the significant results of the previous analysis showed in Chapter 4 and 5, and it was necessary to avoid multicollinearity and over-fitting of the model, given the limited number of subjects.

Finally, these results need to be replicated in larger multicentre study, where a larger number of variables can be studied, and machine learning or deep learning model can be applied.

6.5 Conclusions

Using a multimodal approach, different pattern of tissue damage and disability have been demonstrated in this chapter. White tissue damage is associated with a worse outcome in NMOSD-AQP4, while the grey matter is predominantly associated with disability in MS. In MOGAD, despite the overall low disability, the brainstem damage is associated with worse outcome. Optic chiasm atrophy associates with poor visual acuity in NMOSD-AQP4, while in MOGAD, the association with the thalamus may play a role.

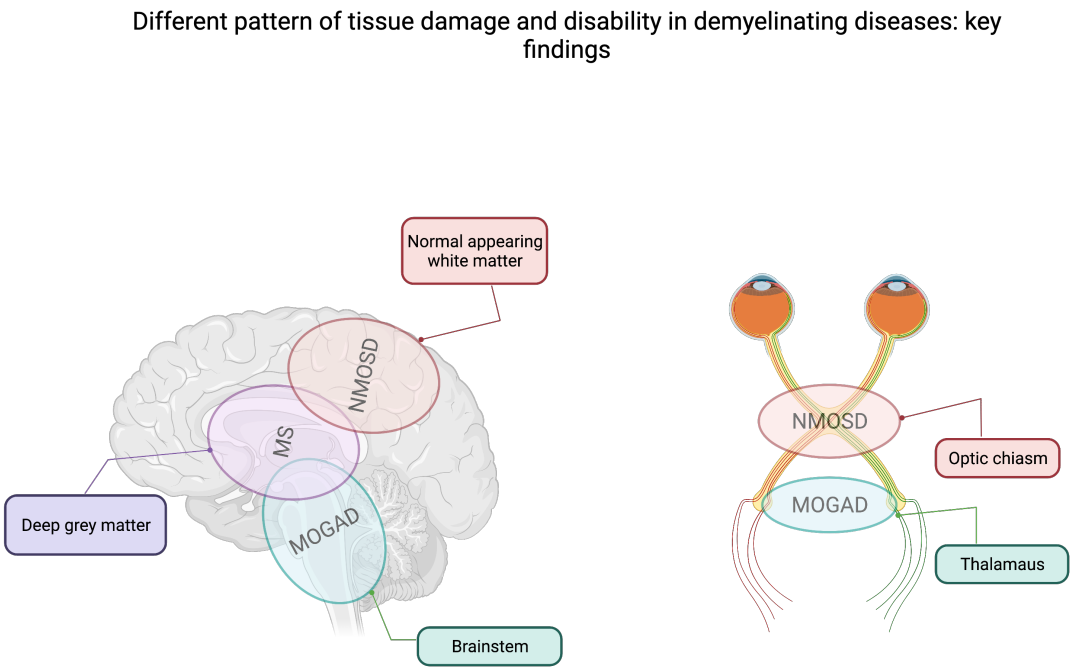


Figure 6.1 graphical representation of the key findings. *Legend: NMOSD=NMOSD-AQP4. Created with BioRender.com.*

7 Functional connectivity analysis in the spectrum of demyelinating diseases: the sensory and motor networks

7.1 Introduction and Background

The previous chapters have shown, using structural and quantitative MRI, that MOGAD has a different pattern of CNS damage, compared to NMOSD-AQP4 and MS. It was found that the grey matter is mainly affected in the two primary demyelinating diseases, MOGAD and MS, while it is relatively spared in NMOSD-AQP4, despite the higher disability. In Chapter 4 it was shown that in MOGAD the grey matter atrophy is associated with lesion volume, however little is known regarding the clinical consequences of grey matter atrophy in this antibody-mediated disease, where disability is relapse-related and there is not a progressive stage (Akaishi et al., 2021). As it has been shown in MS, different MRI markers have a limited clinical value, (i.e. the clinical-radiological paradox), possibly due to the fact that there is not a single parameter able to capture all the pathological changes of MS, and due to the relative eloquence of the anatomical location affected (Barkhof, 2002).

In light of this, the study of large brain networks may give more insight into the intrinsic organization of brain function and the correlation with clinical impairment (Sbardella et al., 2015).

The presence of brain and spinal cord lesions, or occult white/grey matter damage can modify the functional brain activity and connectivity, which can be investigated using functional MRI (fMRI). fMRI studies the brain neural activity using the blood-oxygen-level dependent (BOLD) signal (Biswal et al., 1995). Capturing similar BOLD signals in different brain areas suggests connectivity between those areas. BOLD signals can be

investigated when the subject is not required to perform any specific task (resting state – RS-fMRI), which is an advantage when studying patients with clinical disability (Sbardella et al., 2015).

The brain functional connectivity can be studied with different approaches, i.e., voxel-based and node-based. Among the voxel-based approaches, independent component analysis (ICA), a data-driven exploratory approach, was chosen for this chapter. ICA has the advantage of estimating the full structure of the networks of interest and differentiating the networks of interest from noise (Cole et al., 2010; Smith et al., 2009). Furthermore, ICA is able to describe multiple networks, rather than being limited to the pattern of the selected seed region of interest (Bijsterbosch et al., 2017).

Abnormal connectivity of visual (Gallo et al., 2012), motor and cognitive resting-state networks (RSNs), has been described in MS, with increased connectivity in the early stage of the disease and reduced connectivity in patients with progressive MS (Janssen et al., 2013; Schoonheim et al., 2014). The study of NMOSD-AQP4 using fMRI has been mainly focused on the study of the visual networks, as the optic nerve is one of the preferential targets of the AQP4-Ab (Backner et al., 2020; Finke et al., 2018; Wang et al., 2020).

Cognitive networks have also been studied in NMOSD-AQP4, and a visual-cognitive disconnection has been proposed to explain the cognitive deficit in NMOSD-AQP4 (Chavarro et al., 2020).

In the only two RS-fMRI studies of MOGAD, one of them focused on optic neuritis patients, abnormal activity in many brain regions, consistent with visual, motor, and cognitive function were found (Wang et al., 2017; Zhuo et al., 2020). To date there are

no studies in MOGAD patients investigating the large brain networks, and the association with clinical outcome, using an ICA approach.

In this chapter the ICA approach was used to identify the RSNs of interest (sensory/motor RNSs).

As the RSNs can be easily recognised and reproduced in a different cohort, the potential as a discriminatory marker across diseases was investigated. The average of the connectivity within the networks of interest was calculated (the networks included were statistically significant in the voxel-wise analysis for disease vs HC) and then compared across the four groups, adjusting for age and sex.

The association with clinical/MRI findings was then investigated, in the whole disease groups (MOGAD, NMOSD-AQP4 and MS as a whole group), and then in each disease individually.

7.1.1 *Objectives*

a) To identify the main sensory/motor, sub-cortical and associative RSNs.
b) To compare the RSNs between diseases and HC (MOGAD vs HC, NMOSD-AQP4 vs HC and MS vs HC), and between disease groups (MOGAD vs NMOSD-AQP4, MOGAD vs MS, NMOSD-AQP4 vs MS)
c) To calculate the average within-network connectivity (WNC) in those sensory/motor RSNs of interest, which were statistically significant in the comparison between disease and HC.
d) To compare the WNC of the sensory/motor RSNs of interest across the four groups and to investigate the associations between the WNC of the RSNs of interest and MRI findings/clinical outcomes across all disease groups and in each disease group individually (when clinically plausible).

7.1.2 *Hypothesis*

a) There will be different abnormal networks in the three diseases.
b) There will be an association between visual networks and visual functions, motor networks and motor disability in the three conditions.

7.2 Methods

7.2.1 *Subjects*

The resting state sequence was available for 71 participants. One MS patient's resting state data was not analysed, as the diffusion-weighted data (from which the gradient field was calculated) were discarded due to poor quality. Four participants did not have the RS-fMRI acquired due to time constrains. To avoid exceeding the scanning time (as per ethics regulations), when scans needed to be repeated due to poor quality, the preference was given to the structural sequences. The clinical and demographic characteristics of the 71 participants are represented in Table 7.1.

Table 7.1 Clinical and demographic characteristics of the RS-fMRI cohort

	MOGAD	***NMOSD-AQP4***	***MS***	***HC***
Number	20	17	17	17
Mean age (SD)	41.75 (11.03)	56.47 (13.41)	44.65 (6.40)	39.06 (13.81)
Sex, F (%)	10 (50)	13 (77)	9 (53)	9 (53)
Ethnicity (%)				
Caucasian	20 (100)	9 (53)	17 (100)	14 (82)
African/Afro-	/	3 (18)	/	/
Caribbean	/	3 (18)	/	2 (12)
Asian	/	2 (11)	/	1 (6)
Mixed				
Phenotype (%)				/
Isolated TM	1 (5)	/	/	
TM + Br/Bs	5 (25)	9 (53)	12 (71)	
ON + Br/Bs	/	3 (18)	/	
ON + TM	6 (30)	/	/	
Br/Bs	2 (10)	2 (11)	/	
ON + TM +Br/Bs	6 (30)	3 (18)	5 (29)	
Median disease duration, years (range)	2 (0-24)	9 (0-24)	11 (1-24)	/
Median number of relapses (range)	2 (1-11)	2 (1-11)	3 (1-6)	/
Median EDSS (range)	1.5 (0-7.0)	3.0 (0.0-7.0)	2.0 (0.0-6.0)	/
Mean LogMAR VA (Mean OD and OS) (SD)	-0.03 (0.6)	0.33 (0.61)	-0.09 (0.13)	/
Mean BPI total score (SD)	11.15 (23.36)	29.42 (22.87)	15.39 (20.81)	0

Legend: SD= standard deviation; F=female; TM=transverse myelitis; Br=brain; Bs=brainstem; ON=optic neuritis; EDSS=expanded disability status scale; LogMAR=logarithm of the minimum angle of resolution; VA=visual acuity; OD=oculus dexter (right eye); OS=oculus sinister (left eye); BPI=brief pain inventory.

7.2.2 *MRI RS-sequence*

The RS-MRI sequence was acquired with the following parameters: GE-EPI with x8 multislice acceleration, no iPAT, flip angle 52, fat saturation, 64 slices per volume, 480 volumes in 6 minutes, eyes open with cross fixation. Voxel size 2.4 x 2.4 x 2.4 mm, slice thickness 2.40 mm, TR: 735 ms, TE: 39 ms; a separate "single-band reference scan" was also acquired. This has the same geometry (including EPI distortion) as the timeseries

data, but has higher between-tissue contrast to noise, and was used as the reference scan in head motion correction (Miller et al., 2016).

7.2.3 *MRI preprocessing*

The analysis of resting state fMRI data was performed using the FSL software package (Jenkinson et al., 2012). A modified BioBank pipeline was used for the analysis. The B0 fieldmap was estimated from the B=0 d-MRI images with opposite phase-encoding directions (AP=anterior-posterior and PA=posterior anterior) using topup, part of FSL (Andersson et al., 2003). The magnitude output from topup was then registered to the T1 structural space with a linear method (epi_reg). Then the fieldmap obtained from topup was transformed to the T1 space by combining the previous registration, masked using the T1 brain mask and transformed in radians (multiplying by 2*π). The pipeline uses the B0 fieldmap transformed to the T1 space to do the registration and distortion correction of the functional images from their native space to T1 space. The T1 bias-corrected images were brain extracted and used as anatomical reference for the RS-MRI data. The preprocessing steps included image motion correction with MCFLIRT, brain extraction, distortion correction using the fieldmap data, 100s FWHM High-pass temporal filtering. Single subject independent component analysis (ICA) was performed with MELODIC tool (Beckmann and Smith, 2004) with automated dimensionality estimation used for ICA-based artefact removal. The independent components (ICs) obtained with ICA were classified into signal and noise using FIX (Griffanti et al., 2014; Salimi-Khorshidi et al., 2014), and then the noise components were regressed from the data. As the RS-MRI sequence parameters used in this study matched the UK BioBank (UKBB) RS-fMRI sequence parameters, the UKBB trained-weighted files were used as a training dataset for FIX. To check the performance of the FIX IC classification, the output was compared to

the IC manual classification of one of the HC participants (Griffanti et al., 2017). The cleaned ICA single subject data were then spatial smoothed using a Gaussian kernel of sigma 1.8 mm and transformed to standard space with applywarp, part of FSL, using the transformations/warps generated by non-linear registration (with the FNIRT tool) when running the single-subject preprocessing with MELODIC.

7.2.4 *RSNs analysis*

Voxel-wise analysis*:* The template of ICs for this study was obtained from all 71 participants (17 HC and 54 disease group participants) using a group-ICA with dimensionality d=40, to enable the identification of the basal ganglia as a separate component, as described by (Griffanti et al., 2016). The set of spatial maps from the group-average analysis was used to generate subject-specific versions of the spatial maps, and associated timeseries, using dual regression (Nickerson et al., 2017). First, for each subject, the group-average set of spatial maps is regressed (as spatial regressors in a multiple regression) into the subject's 4D space-time dataset. This results in a set of subject-specific timeseries, one per group-level spatial map. Next, those timeseries are regressed (as temporal regressors, again in a multiple regression) into the same 4D dataset, resulting in a set of subject-specific spatial maps, one per group-level spatial map. Finally, the difference between the HC group and each disease group (MOGAD, NMOSD-AQP4 and MS) and between diseases, was tested using FSL's *randomise* permutation-testing tool. Results were considered significant for $p< 0.05$ after correction for multiple comparisons using the threshold-free cluster enhancement (TFCE) approach. See Figure 7.1 for the resting-state pipeline.

Within network connectivity (WNC) analysis: The subject-specific spatial maps, one per group-level spatial map, were used to calculate the average connectivity in the whole sensory/motor RSNs that showed a significant difference in the comparison between disease groups and healthy controls. To do this, the whole RSN of interest was extracted from the MELODIC ICA output, thresholded (threshold=4) and binarized to obtain a mask of the RSN, and within this the WNC (based on the z-transformed correlation values from dual regression) was calculated. This strategy was used as whole RSNs are easily reproducible in different cohorts, therefore they are potentially more useful as marker than a single significant cluster. The RSN WNC values were initially compared across the four groups. The association with clinical and MRI findings was investigated in the whole disease groups (including MOGAD, NMOSD-AQP4 and MS). Finally, to identify different patterns of abnormal RSNs in the three diseases, the disease groups were analysed individually.

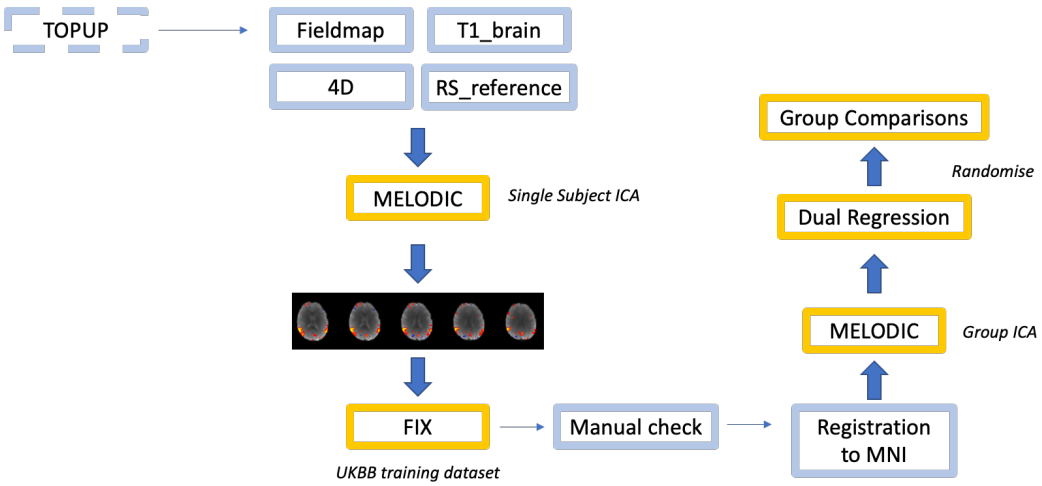


Figure 7.1 Resting-state analysis pipeline *Legend: UKBB=UK brain biobank; RS=resting state; ICA=independent component analysis; MNI=Montreal Neurological Institute.*

7.2.5 *Statistical analysis*

The statistical analysis of non-imaging data was performed using Rstudio version 1.1.447 (http://www.rstudio.com). Data cleaning was performed before the data analysis. Quantitative variables were described using means and SDs, median and range. A Shapiro-Wilk test was performed to assess the normal distribution of data.

Linear models with RSN WNC as dependent variables, were fit to compare the RSN WNC findings across the four study groups. Age in NMOSD-AQP4 was significantly different from HC (as described in Chapter 3), thus was included in the group comparison regression models, together with sex as independent variables. The assumptions were checked regarding linearity, normal distribution of the residuals and equal variance of the variables. The estimated marginal means were calculated based on the linear model and a Bonferroni pairwise-comparison between groups was calculated. Results are shown as WNC post-hoc comparison estimated marginal means (EMM) and *p*-values.

Finally, to explore the association between the RSN WNC values, and the clinical/MRI findings, multiple linear regression models were fitted in all disease groups, and in each disease group. These used the WNC values as the dependent variables while clinical/MRI findings, and age and sex were the independent variables.

Given the exploratory nature of the study, the WNC values were also analysed without adjusting for age and sex (the results, not age and sex adjusted, are presented when significant). For all analyses, $p < 0.05$, after correction for multiple comparisons, was considered statistically significant.

7.3 Results

7.3.1 *Identifying the main RSNs*

Out of the 40 RSNs obtained as described above, 32 RSNs of interest have been identified (see Table 7.2) and 15 of them are shown in Figure 7.2. The RSNs of interest have been identified through reference to previous literature (Smith et al., 2009) and to the Harvard-Oxford Cortical Structural Atlas.

The following sensory/motor networks will be compared across groups, while the associative and subcortical RSNs will be analysed in the next chapter together with the cognitive scores.

Medial, Lateral and Occipital Pole visual network: the medial visual network comprises the primary visual cortex area located in the calcarine sulcus, associated with visual processing and colour identification. The lateral visual network is located in the occipital pole extending laterally towards the temporal-occipital junction and has been associated with motion processing and visual attention (Rosa et al., 2009; Tootell et al., 1998). The occipital pole visual network is located in the posterior-most part of the occipital lobe and is associated with foveal vision (central vision)(Wong and Sharpe, 1999).

As the visual cortex receives visual information from the optic nerves, through the chiasm, the thalamus and the optic radiations, the association between visual networks and visual system structures was explored (i.e., chiasm volume, thalamus, and FA optic radiation). As in MOGAD and NMOSD-AQP4, optic neuritis (ON) is common and potentially very severe, in contrast to MS, ON effect and time from last ON event, were studied in the visual networks of the two antibody-mediated diseases.

Sensorimotor network: it is located in the pre- and post-central gyri and comprises the supplementary motor areas, sensorimotor cortex and secondary somatosensory cortex

(Kim et al., 1993; Porro et al., 1996). The relationship with the EDSS (an outcome of physical disability) was investigated.

Salience network: the salience network is comprised of the anterior insula and the cingulate cortex, and it is involved in several mechanisms of behavioural response, including pain processing (Hegarty et al., 2020). In light of this, and although the salience network is classically considered an associative network, the association with pain scores, was investigated in this chapter.

Auditory network: it is located in in the superior temporal gyrus, Heschl's gyrus, posterior insula and is involved in speech, language and auditory process (Hackett, 2011). As AQP4-Ab is also expressed in the vestibular and cochlear nuclei regions in the brainstem (Pittock et al., 2006b), the association with the brainstem volume was investigated.

Table 7.2 RSNs obtained from group-ICA.

Resting state network	***Volume number***
*Lateral Visual network**	Volume 0
*Anterior Default Mode network**	Volume 1
Occipital Pole Visual network	Volume 2
*Medial Visual Network**	Volume 3
Left Frontotemporal Network	Volume 4
*Right Frontotemporal Network**	Volume 5
Salience Network	Volume 6
*Left Frontotemporal Network II**	Volume 7
*Posterior Default Motor Network**	Volume 8
Medial Visual Network II	Volume 10
Precuneus network	Volume 11
Right Frontotemporal II	Volume 12
*Sensorimotor network**	Volume 13
Posterior Default Mode Network II	Volume 14
Left Frontotemporal Network III	Volume 15
Posterior Default Mode Network III	Volume 16
*Executive Function Network**	Volume 17
Salience Network II	Volume 18
*Cerebellum Network**	Volume 19
Executive Function Network II	Volume 20
Sensorimotor Network II	Volume 21
*Salience Network III**	Volume 22
Sensorimotor Network III	Volume 23
Sensorimotor Network IV	Volume 24
*Occipital Pole visual Network**	Volume 25
*Auditory Network**	Volume 26
Precuneus Network II	Volume 27
Cerebellum Network II	Volume 28
Right Frontemporal Network III	Volume 29
Temporal Pole Network	Volume 34
*Basal Ganglia Network**	Volume 37
*Frontostriatal Network**	Volume 39

*Legend: RSN=resting state network; *RSNs shown in Figure 7.2.*

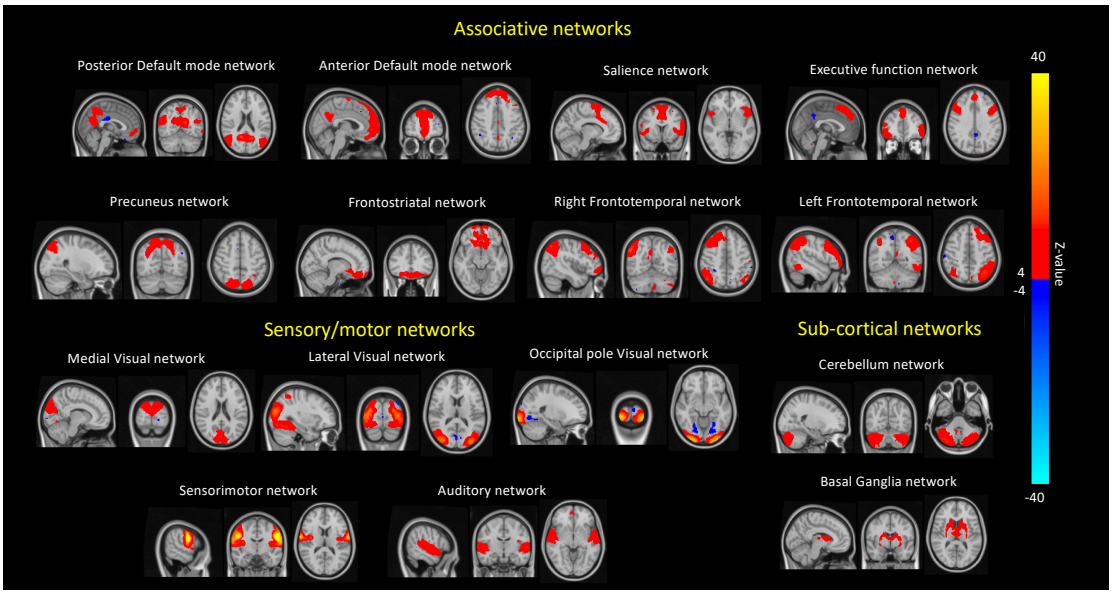


Figure 7.2 Resting state networks (RSNs). RSNs obtained via group ICA of the MRI data of all 71 participants. RSNs are represented in red- yellow and blue-light blue (z-score). *Legend: ICA=independent component analysis.*

7.3.2 *Comparing the RSNs across the groups using voxel-wise analysis*

See Table 7.3 for a summary of the significant networks, their coordinates and cluster size. Given the exploratory nature of this study, no minimum cluster size cut-off was used, and all the significant results are represented and discussed.

7.3.2.1 MOGAD vs HC analysis

The occipital pole visual network (volume 25) was the only network with an area of significant difference between MOGAD and HC (see Figure 7.3), with MOGAD showing lower connectivity.

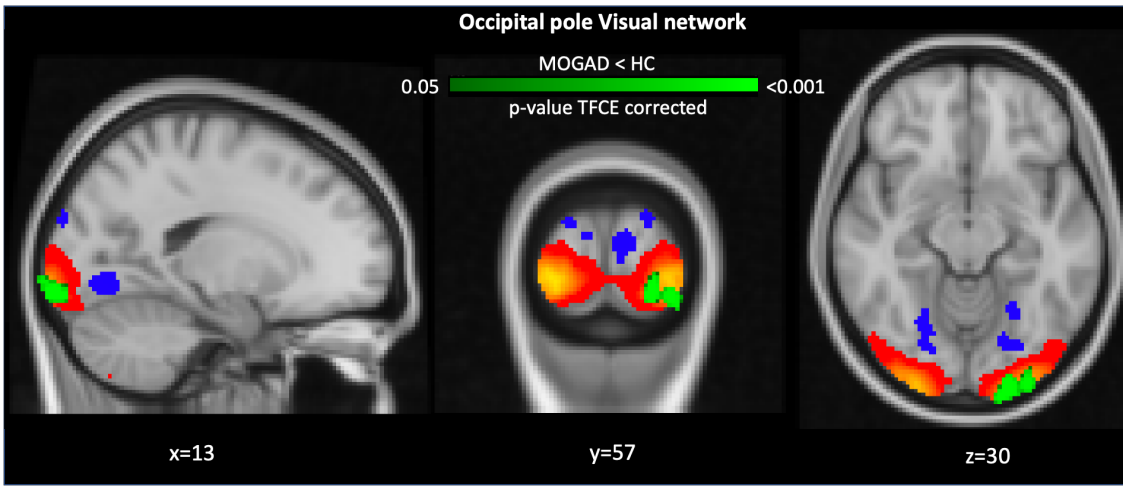


Figure 7.3 Voxel-wise between-group difference (MOGAD<HC) in the occipital pole visual network (represented in red-yellow). The green voxels represent the area of significant difference, corrected for multiple comparisons using the TFCE approach. No significant difference was found using the opposite contrast (MOGAD>HC)*. Legend: TFCE=threshold-free cluster enhancement.*

7.3.2.2 NMOSD-AQP4 vs HC analysis

The comparison between NMOSD-AQP4 and HC, showed lower connectivity in the lateral (volume 0) and medial visual network (volume 3), in the auditory network (volume 26), the anterior and posterior DMN (volume 1 and 16), in the salience network (volume 18), the sensorimotor network (volume 23 and 24), and the associative networks, such as left frontotemporal network II (volume 15), executive function network (volume 20) (see Figure 7.4).

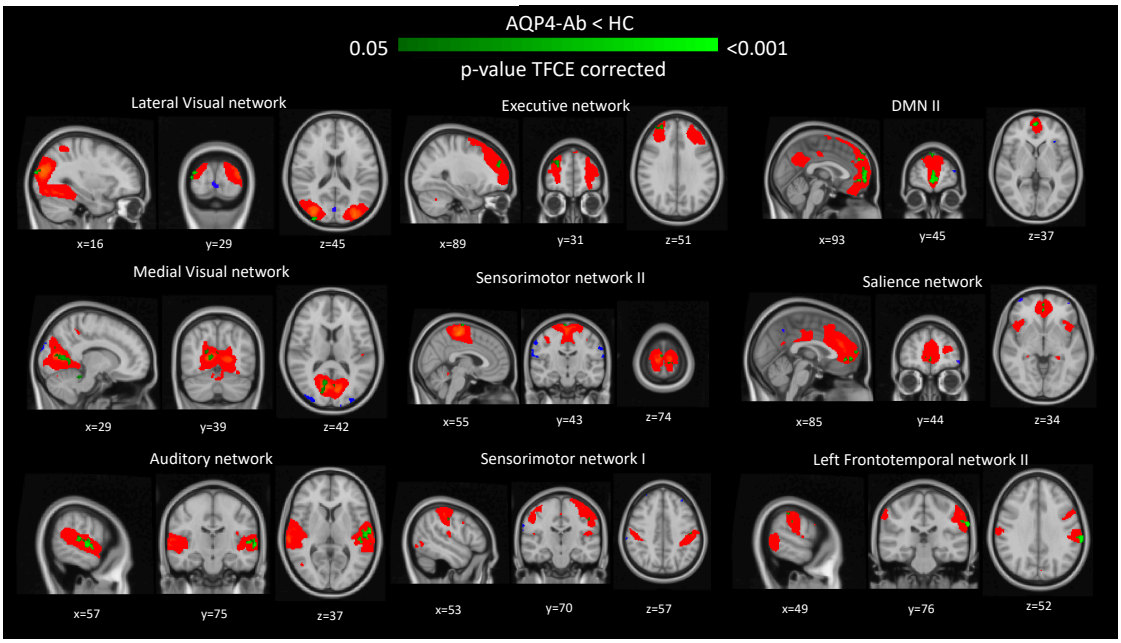


Figure 7.4 Voxel-wise between-group differences (AQP4-Ab<HC) in various networks (represented in red-yellow). The green voxels represent the area of significant difference, corrected for multiple comparisons using the TFCE approach. No significant difference was found using the opposite contrast (AQP4-Ab>HC) in the depicted networks. *Legend: TFCE=threshold-free cluster enhancement.*

7.3.2.3 MS vs HC analysis

The comparison showed that the lateral visual network (volume 0) and the basal ganglia network (volume 37) have lower connectivity in MS (see Figure 7.5).

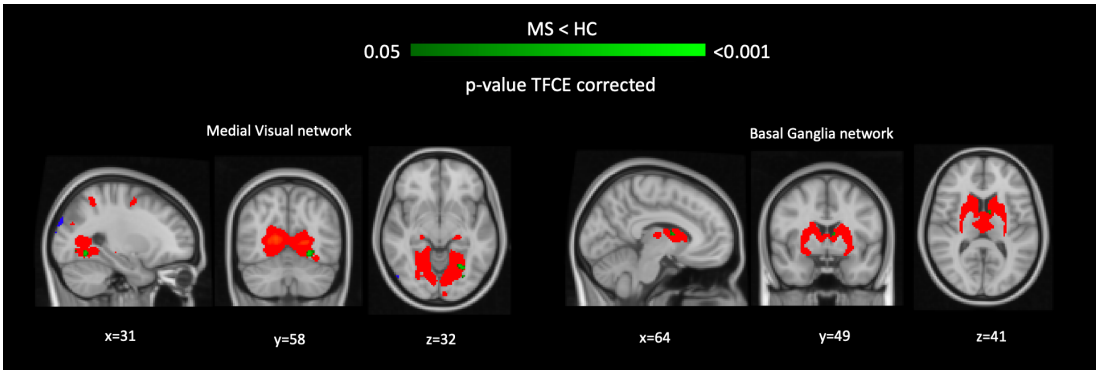


Figure 7.5 Voxel-wise between-group difference (MS<HC) in the medial visual and basal ganglia networks (represented in red-yellow). The green voxels represent the area of significant difference, corrected for multiple comparisons using the TFCE approach. *No significant difference was found using the opposite contrast (MS>HC) in the depicted networks. Legend: TFCE=threshold-free cluster enhancement.*

7.3.2.4 NMOSD-AQP4 vs MOGAD analysis

The NMOSD-AQP4 group showed a reduction of the executive function (volume 20), salience (volume 22 and 18) and sensorimotor (volume 23) networks when compared to MOGAD (see Figure 7.6).

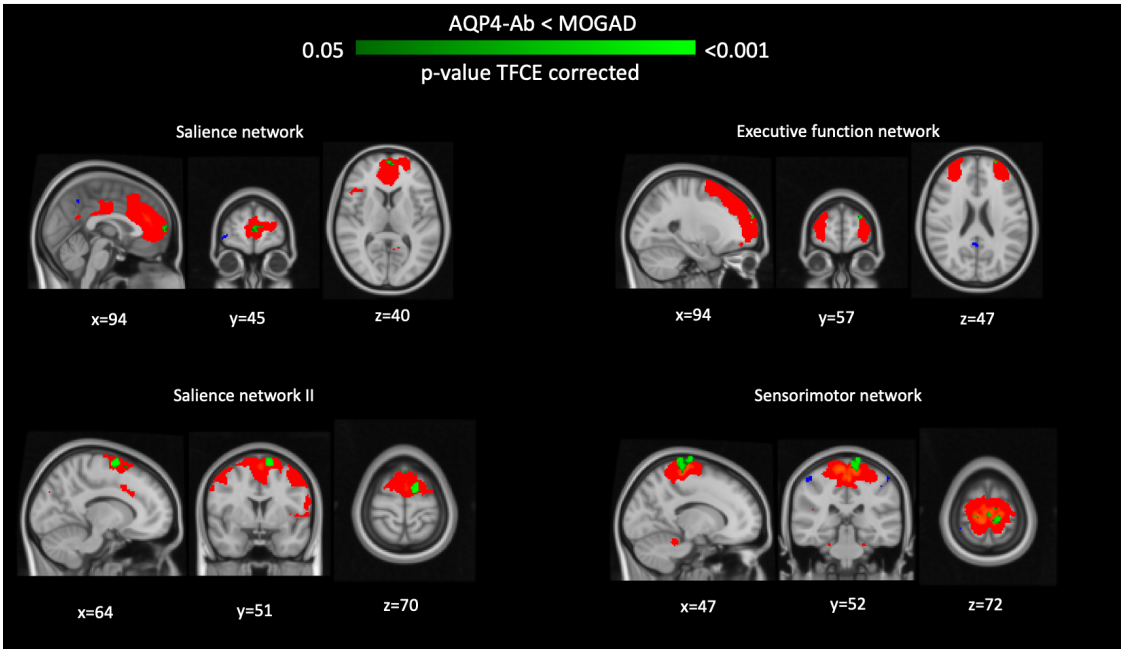


Figure 7.6 Voxel-wise between-group difference (AQP4-Ab<MOGAD) in the salience, executive function and sensorimotor networks (represented in red-yellow). In green the area of significant difference, corrected for multiple comparisons using the TFCE approach. *No significant difference was found using the opposite contrast (AQP4-Ab>MOGAD) in the depicted networks. Legend: TFCE=threshold-free cluster enhancement*

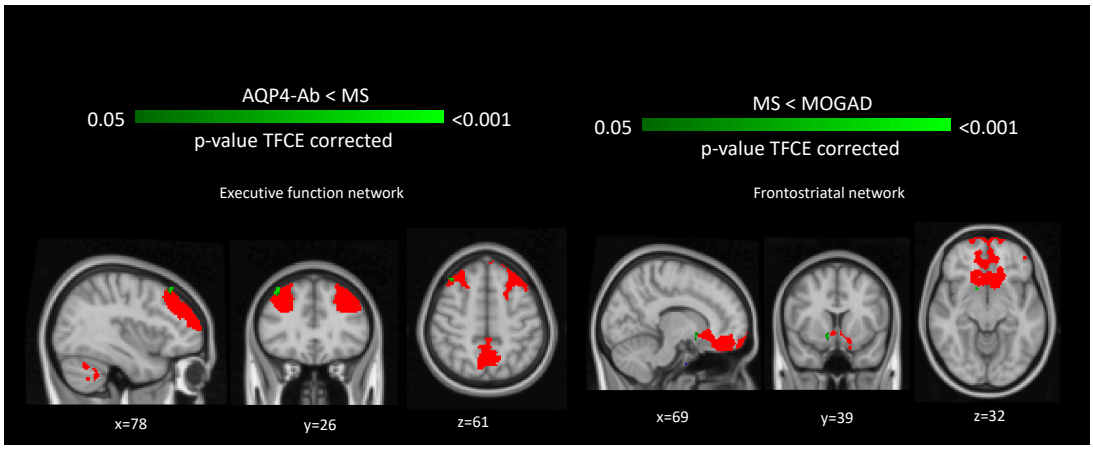


Figure 7.7 Voxel-wise between-group difference in the executive function (AQP4-Ab<MS) and frontostriatal networks (MS<MOGAD) (represented in red-yellow). In green the area of significant difference, corrected for multiple comparisons using the TFCE approach. *No significant difference was found using the opposite contrast (AQP4-Ab>MS and MS>MOGAD) in the depicted networks. Legend: TFCE=threshold-free cluster enhancement.*

7.3.2.5 NMOSD-AQP4 vs MS analysis

The NMOSD-AQP4 showed a reduction of the executive function network (volume 20) when compared to MS (see Figure 7.7).

7.3.2.6 MS vs MOGAD analysis

The MS group showed a reduced FC in the frontostriatal network (volume 39) when compared to the MOGAD group (see Figure 7.7).

Table 7.3 Statistical peaks of significant resting state networks (RSNs) across groups (TFCE corrected p-values), organized by contrast (voxel-wise analysis)*. Coordinates are reported in mm in Montreal Neurological Institute (MNI) space. When more clusters were significant, the largest was represented in the table*

			MNI coordinates (mm)			***Cluster size (voxels)***
Contrast	*RSN*	*Volume number*	*x*	*y*	*z*	
MOGAD<HC	Occipital Visual	25	55	14	29	339
AQP4<HC	Lateral Visual	0	28	15	45	75
AQP4<HC	Medial Visual	3	40	30	41	191
AQP4<HC	Auditory	26	77	55	37	316
AQP4<HC	Executive	20	32	87	49	61
AQP4<HC	Sensorimotor III	23	36	51	78	43
AQP4<HC	Sensorimotor IV	24	59	14	45	15
AQP4<HC	DMN II	1	44	93	33	315
AQP4<HC	Salience	18	45	90	35	17
AQP4<HC	L frontotemporal II	15	79	48	51	97
MS<HC	Medial Visual	3	57	32	31	55
MS<HC	Basal ganglia	37	49	64	41	10
AQP4<MOGAD	Salience	18	45	94	40	72
AQP4<MOGAD	Salience II	22	51	62	69	110
AQP4<MOGAD	Executive	20	34	98	39	41
AQP4<MOGAD	Sensorimotor I	23	52	53	78	550
AQP4<MS	Executive	20	26	78	62	21
MS<MOGAD	Frontostriatal	39	39	68	31	12

Legend: MNI= Montreal Neurological Institute; RSN=resting state network; AQP4=NMOSD-AQP4.

7.3.3 *WNC analysis of the sensory/motor RSNs of interest*

The within network connectivity (WNC) was calculated in those networks that showed a significant difference in the voxel-wise comparison between disease groups and healthy controls, as shown in the previous section.

The WNC was analysed in the medial, lateral, and occipital pole visual cortex, sensorimotor, salience and auditory network. The associative networks will be analysed in the next chapter, together with the cognitive function.

7.3.3.1 Visual networks

WNC comparison across groups

The three disease groups had low WNC compared to the HC in the medial visual RSN (see Figure 7.8A). In the lateral visual RSN, NMOSD-AQP4 participants had the lowest score (Figure 7.8B), while MOGAD participants presented the lowest score in the occipital visual RSN (Figure 7.8C), in line with what was observed in the voxel-wise analysis. In the linear model adjusting for age and sex, the comparisons across groups, did not show significant results in the three visual networks (see group comparisons in Table 7.4).

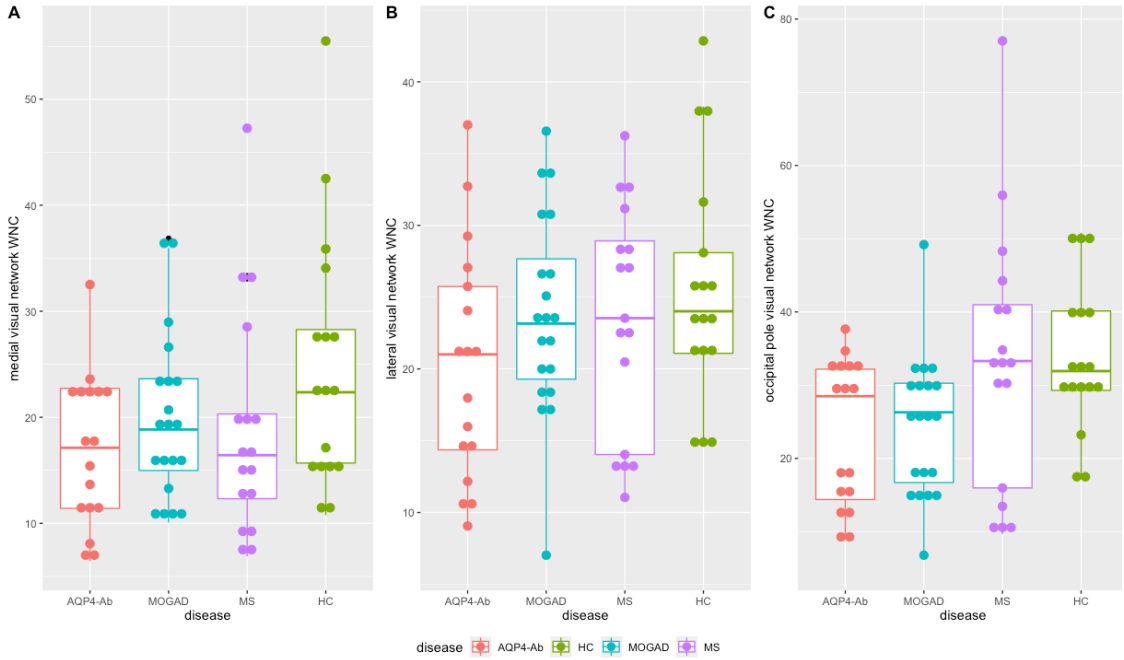


Figure 7.8 Medial (A), lateral (B) and occipital pole (C) visual cortex network WNC between disease groups. *The graphs represent the median and, the 25th and the 75th percentile. Legend: AQP4-Ab=NMOSD-AQP4.*

Table 7.4 Age and sex adjusted comparisons of within network connectivity (WNC) values, Bonferroni corrected, across groups.

	Medial Visual Cortex			***Lateral Visual Cortex***			***Occipital Pole visual Cortex***		
	Estimates	*SE*	*p-value*	*Estimates*	*SE*	*p-value*	*Estimates*	*SE*	*p-value*
AQP4-Ab vs HC	-3.335	3.62	0.999	-1.464	2.96	0.999	-4.965	4.61	0.999
AQP4-Ab vs MOGAD	0.984	3.40	0.999	-0.201	2.79	0.999	3.808	4.34	0.999
AQP4-Ab vs MS	1.123	3.40	0.999	-0.395	2.79	0.999	-5.458	4.33	0.999
HC vs MOGAD	4.319	3.05	0.973	1.263	2.50	0.999	8.773	3.89	0.165
HC vs MS	4.458	3.21	0.999	1.069	2.63	0.999	-0.493	4.09	0.999
MOGAD vs MS	0.140	3.06	0.999	-0.193	2.50	0.999	-9.266	3.89	0.121

Legend: AQP4-Ab=NMOSD-AQP4; SE=standard error

WNC comparison between "good" and "impaired" vision (in at least one eye)

Disease groups: the WNC was compared between participants with normal visual acuity (VA) and participant with impaired VA in the three visual RSNs (see Figure 7.9). Impaired VA was defined as a VA LogMAR >0.0 in at least one eye (higher LogMAR equates to worse vision). In all three networks, participants with impaired VA showed lower WNC. In the lateral visual network, the comparison not adjusted for age and sex, showed a trend towards significance (impaired VA vs normal VA -4.35 [2.47], p=0.08). The remaining comparisons, age and sex adjusted, were not significant (impaired vs normal VA: medial visual network -2.88 [2.86], p=0.31; lateral visual network -3.07 [2.46], p=0.218; occipital visual network -2.16 [4.37], p=0.623).

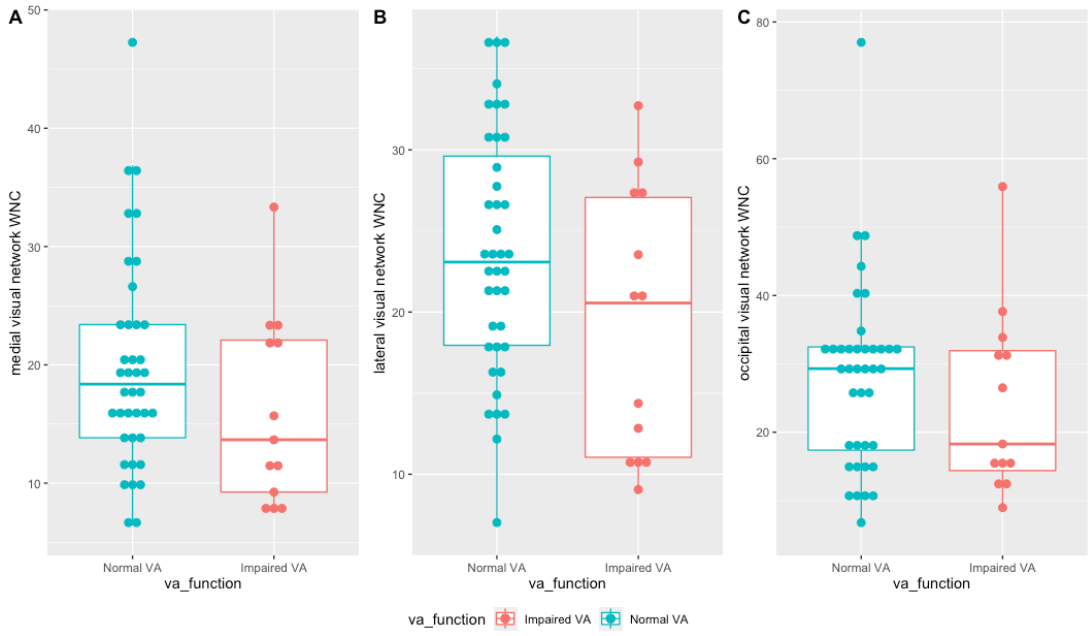


Figure 7.9 Medial (A), lateral (B) and occipital pole (C) visual cortex WNC between participants with normal and impaired VA. *The graphs represent the median and, the 25th and the 75th percentile; Legend: VA=visual acuity*

MOGAD, NMOSD-AQP4 and MS: The WNC within the three visual networks were compared between normal and impaired VA in every disease group. In the NMOSD-AQP4 and MS group, participants with impaired vision showed low WNC in all the three visual networks, although the difference was not significant (impaired vs normal vision NMOSD-AQP4 medial visual network -5.17 [3.34], p=0.14; lateral visual network -2.69, [4.25], p=0.53; occipital visual network -4.15 [5.28], p=0.45; MS medial visual network -5.17 [3.34], p=0.15, lateral visual network -2.69 [4.25], p=0.54; occipital visual network -4.15 [5.28], p=0.45). Among MOGAD participants, only one had impaired VA, therefore the comparisons were not calculated (see Figure 7.8).

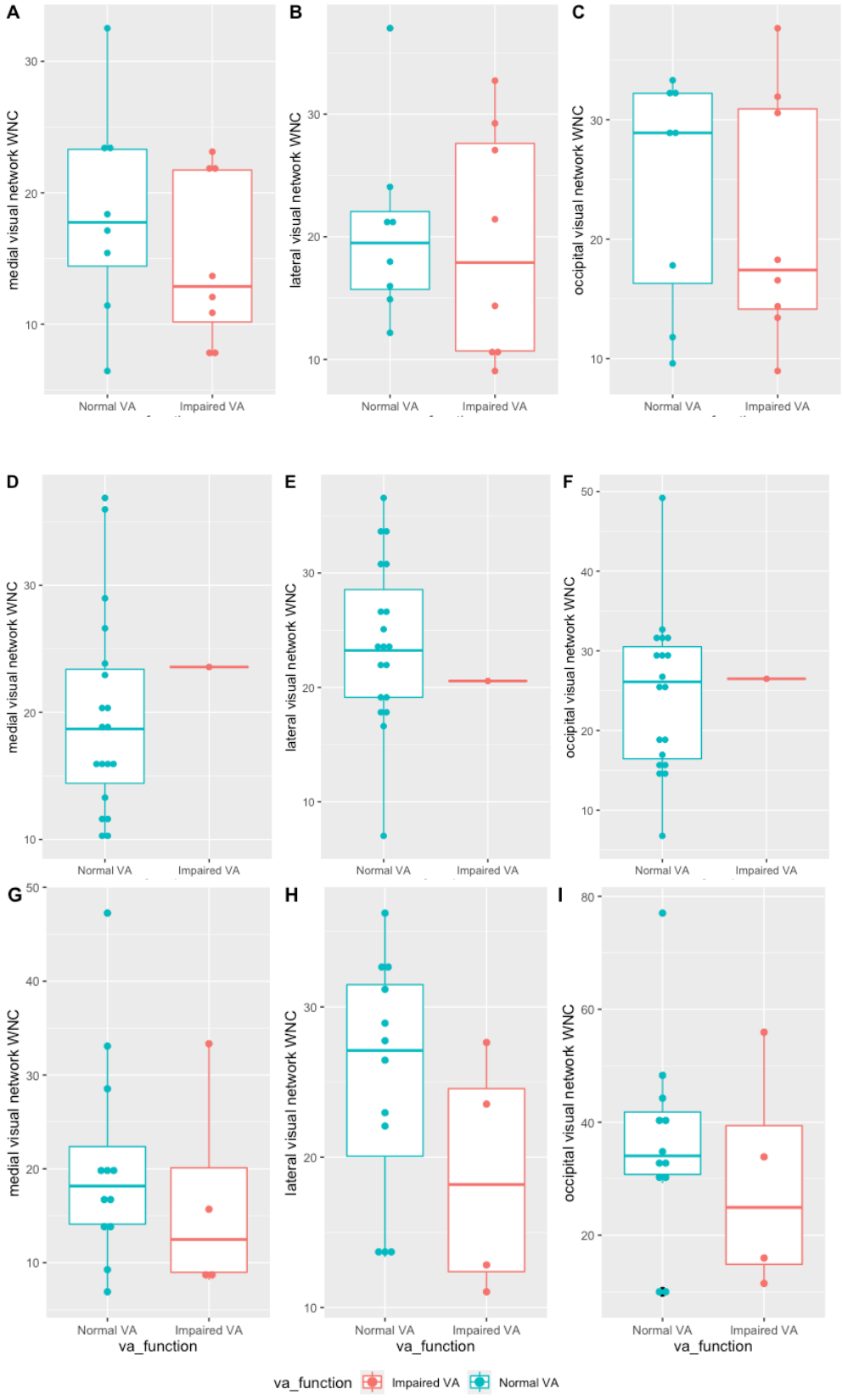


Figure 7.10 visual cortex network WNC between participants with normal and impaired VA in the three disease groups. NMOSD-AQP4 (A-C), MOGAD (D-F) and MS (G-I) WNC in the medial, lateral, and occipital visual networks. *The graphs represent the median and, the 25th and the 75th percentile.*

Association between WNC and MRI findings

Disease groups: in Chapter 6 it was shown that lower chiasm volumes and lower thalamic volumes were associated with worse visual outcomes. The associations between the volumetric findings, together with the optic radiation FA, and the resting-state visual networks were explored in a multivariable linear model.

No significant associations were found (optic chiasm and medial [slope 0.012, p=0.510], lateral [slope=0.008, p=0.605] and occipital [slope 0.019, p=0.510] visual networks; thalamus volume and medial [slope -1.299, p=0.272], lateral [slope 0.319, p=0.765] and occipital [slope -1.937, p=0.29] visual networks; optic radiation and medial [slope -0.768, p=0.535], lateral [slope -1.281, p=0.248] and occipital [slope -2.821, p=0.137] visual networks).

MOGAD, NMOSD-AQP4 and MS: in the univariable analysis the only significant associations between the MRI findings and the visual networks were found in the MOGAD groups: the optic chiasm volume was significantly associated with the medial (0.0658 [0.0283], p=0.032) and occipital visual networks (0.0744 [0.0354], p=0.049), and the FA optic radiation was associated with the medial visual network (-187.44 [82.06], p=0.0347). In the multivariable linear model adjusting for age and sex, the association between medial visual network and FA optic radiation was the only significant result (see Table 7.7). The remaining associations were not significant (see Table 7.5 and 7.6).

Table 7.5: multiple linear regression model for WNC, age and sex adjusted, between optic chiasm and the visual networks in the three disease groups

	Medial visual network – NMOSD-AQP4			**Medial visual network - MOGAD**			**Medial visual network – MS**		
Predictors	*Estimates*	*CI*	*p*	*Estimates*	*CI*	*p*	*Estimates*	*CI*	*p*
(Intercept)	28.318	8.411 – 48.226	0.009	2.105	-14.904 – 19.114	0.796	44.095	-7.365 – 95.555	0.087
Optic Chiasm Volume	0.015	-0.031 – 0.060	0.495	0.080	-0.004 – 0.164	0.062	-0.072	-0.224 – 0.079	0.321
Age	-0.265	-0.539 – 0.010	0.058	-0.029	-0.436 – 0.379	0.884	-0.205	-1.079 – 0.670	0.622
Sex	-2.548	-11.435 – 6.339	0.546	-3.376	-10.756 – 4.004	0.347	9.632	-1.003 – 20.266	0.072
Observations	17			20			17		
R^2 / R^2 adjusted	0.273 / 0.105			0.274 / 0.137			0.290 / 0.126		

Legend: WNC=within network connectivity

Table 7.6: multiple linear regression model for WNC, age and sex adjusted, between thalamus volume and the visual networks in the three disease groups

	Medial visual network – NMOSD-AQP4			**Medial visual network - MOGAD**			**Medial visual network – MS**		
Predictors	*Estimates*	*CI*	*p*	*Estimates*	*CI*	*p*	*Estimates*	*CI*	*p*
(Intercept)	38.707	1.072 – 76.342	0.045	43.376	1.558 – 85.195	0.043	30.418	-33.032 – 93.868	0.319
Thalamus Volume	-0.001	-0.004 – 0.003	0.684	-0.003	-0.007 – 0.001	0.105	-0.000	-0.006 – 0.005	0.916
Age	-0.264	-0.542 – 0.014	0.061	0.217	-0.111 – 0.545	0.180	-0.297	-1.184 – 0.589	0.482
Sex	-1.727	-10.257 – 6.803	0.669	-2.010	-9.216 – 5.195	0.562	9.220	-2.014 – 20.454	0.100
Observations	17			20			17		
R^2 / R^2 adjusted	0.256 / 0.084			0.233 / 0.089			0.232 / 0.055		

Legend: WNC=within network connectivity

Table 7.7: multiple linear regression model for WNC, age and sex adjusted, between optic radiation FA and the visual networks in the three disease groups

	Medial visual network – NMOSD-AQP4			**Medial visual network - MOGAD**			**Medial visual network – MS**		
Predictors	*Estimates*	*CI*	*p*	*Estimates*	*CI*	*p*	*Estimates*	*CI*	*p*
(Intercept)	41.839	-25.408 – 109.086	0.202	106.936	22.200 – 191.672	0.017	-17.105	-96.738 – 62.529	0.650
FA optic radiation	-20.757	-160.683 – 119.168	0.754	-195.935	-367.688 – -24.183	**0.028**	115.297	-63.989 – 294.584	0.188
Age	-0.257	-0.536 – 0.023	0.069	0.230	-0.076 – 0.536	0.130	-0.515	-1.409 – 0.379	0.236
Sex	-1.344	-10.071 – 7.383	0.745	-1.409	-7.995 – 5.176	0.656	10.048	-0.316 – 20.412	0.056
Observations	17			20			17		
R^2 / R^2 adjusted	0.252 / 0.079			0.334 / 0.209			0.331 / 0.176		

Legend: WNC=within network connectivity

The effect of optic neuritis on MOGAD and NMOSD-AQP4 visual network WNC values

When subdividing the MOGAD and NMOSD-AQP4 populations, based on the occurrence of at least one episode of optic neuritis (ON), the NMOSD-AQP4-ON patients showed the lowest WNC values in the medial and lateral visual networks, however the comparisons were not significant. The WNC for the MOGAD-ON occipital pole network were significantly lower than those for HCs in the comparison without adjusting for age and sex, (11.02 [3.72], p=0.047) and showed a trend towards significance in the age and sex adjusted model (see Figure 7.11, and Table 7.8 for estimates and p-value).

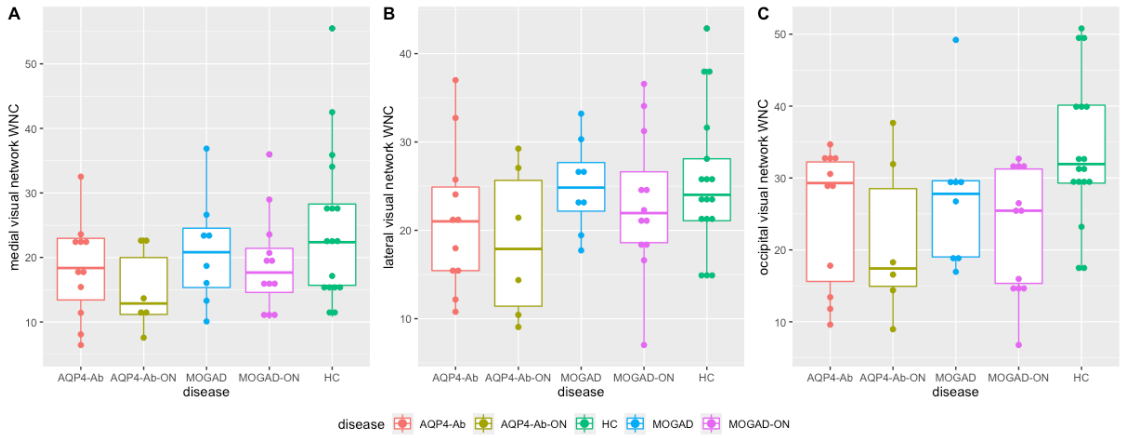


Figure 7.11 WNC in the medial visual network (A), lateral visual network (B) and occipital pole visual network (C) between participants with or without at least one episode of ON in the NMOSD-AQP4 and MOGAD group. *The graphs represent the median and, the 25th and the 75th percentile.*

Table 7.8 Age and sex adjusted comparisons of WNC, Bonferroni corrected, in the NMOSD-AQP4 and MOGAD, based on the occurrence of at least one episode of ON, and HC.

	Medial Visual cortex			***Lateral Visual cortex***			***Occipital Pole Visual cortex***		
	Estimates	*SE*	*p-value*	*Estimates*	*SE*	*p-value*	*Estimates*	*SE*	*P-value*
AQP4-Ab vs AQP4-Ab-ON	3.830	4.58	0.999	3.324	3.86	0.999	3.82	5.01	0.999
AQP4-Ab vs HC	-2.455	3.95	0.999	-0.841	3.33	0.999	-5.70	4.31	0.999
AQP4-Ab vs MOGAD	0.416	4.54	0.999	-1.544	3.83	0.999	0.39	4.96	0.999
AQP4-Ab vs MOGAD-ON	2.668	4.12	0.999	1.615	3.47	0.999	4.89	4.50	0.999
AQP4-Ab-ON vs HC	-6.285	4.59	0.999	-4.165	3.87	0.999	-9.52	5.02	0.639
AQP4-Ab-ON vs MOGAD	-3.415	5.19	0.999	-4.868	4.37	0.999	-3.43	5.66	0.999
AQP4-Ab-ON vs MOGAD-ON	-1.162	4.73	0.999	-1.708	3.98	0.999	1.06	5.16	0.999
HC vs MOGAD	2.870	3.96	0.999	-0.703	3.34	0.999	6.09	4.33	0.999
HC vs MOGAD-ON	5.123	3.41	0.999	2.457	2.87	0.999	10.58	3.73	0.066*
MOGAD vs MOGAD-ON	2.253	4.28	0.999	3.160	3.60	0.999	4.50	4.67	0.999

*Legend: *trend towards significance. Significant in the model not adjusted for age and sex. AQP4-Ab=NMOSD-AQP4; ON=optic neuritis*

To explore the effect that the time from the last ON had on the pattern of changes in the visual network, the seven NMOSD-AQP4-ON and 12 MOGAD-ON were divided into participants who experienced the last ON less than 36 months and more than 36 months before the MRI. The 36 months cut-off was used to have two groups with similar number of subjects.

The participants (including both MOGAD-ON and NMOSD-AQP4-ON) with the last ON <36 months before the MRI showed a lower WNC when compared to those with an ON >36 months before the MRI (see Figure 7.12), however the comparison was not significant (medial visual network -4.75 [3.66], p=0.216; lateral visual network -3.88 [4.34], p=0.386; occipital pole visual network -4.48 [4.88], p=0.374). The analysis of the two disease groups separately showed that this difference is more evident in the NMOSD-AQP4-ON group (given the small sample size a statistical comparison was not calculated; see Figure 7.13).

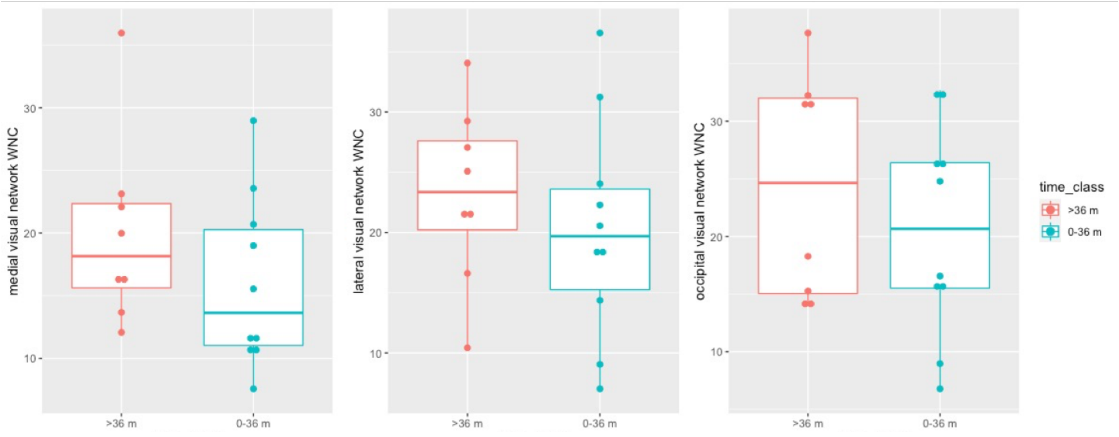


Figure 7.12 WNC in the medial visual network (A), lateral visual network (B) and occipital pole visual network (C) between the NMOSD-AQP4-ON and MOGAD-ON participants, based on the time from the last episode of ON. *The graphs represent the median and, the 25th and the 75th percentile. Legend: AQP4-Ab=NMOSD-AQP4; ON=optic neuritis*

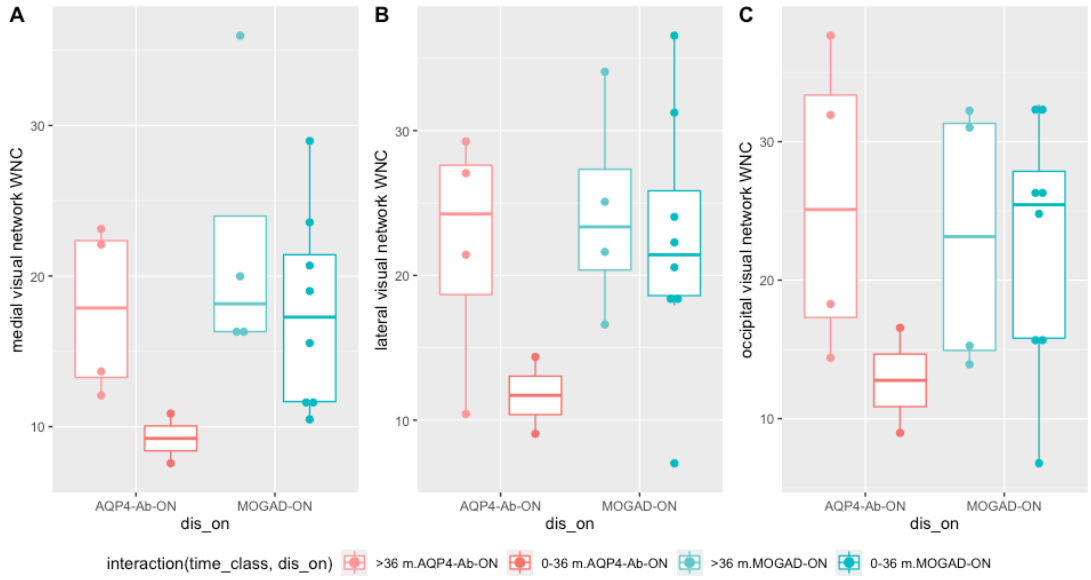


Figure 7.13 : WNC in the medial visual network (A), lateral visual network (B) and occipital pole visual network (C) between the NMOSD-AQP4-ON and MOGAD-ON participants, based on the time from the last episode of ON. *The graphs represent the median and, the 25th and the 75th percentile. Legend: AQP4-Ab=NMOSD-AQP4; ON=optic neuritis*

7.3.3.2 Salience network

WNC comparisons across groups

The comparison across groups (MOGAD, NMOSD-AQP4, MS, and HC), showed that NMOSD-AQP4 participants had lower WNC compared to MOGAD (-4.165 [1.44], p=0.03) and HC (-3.951 [1.50], p=0.06), however these differences were not significant when adjusting for age and sex. The remaining comparisons were not significant (see Figure 7.14 and Table 7.9).

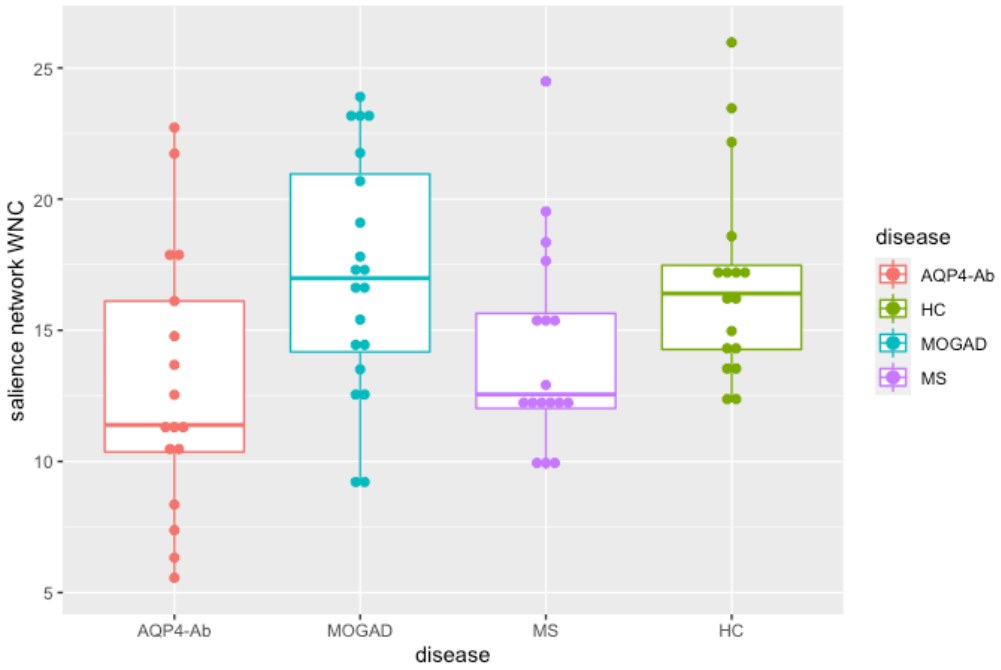


Figure 7.14 Salience network WNC between disease groups. *The graphs represent the median and, the 25th and the 75th percentile. AQP4-Ab=NMOSD=AQP4.*

Table 7.9 : Age and sex adjusted comparisons of WNC, Bonferroni corrected, in the four groups.

	Salience network		
	Estimates	*SE*	*p-value*
AQP4-Ab vs HC	-2.112	1.65	0.999
AQP4-Ab vs MOGAD	-2.475	1.56	0.698
AQP4-Ab vs MS	0.088	1.55	0.999
HC vs MOGAD	-0.364	1.40	0.999
HC vs MS	2.199	1.47	0.830
MOGAD vs MS	2.564	1.40	0.425

Legend: AQP4-Ab=NMOSD-AQP4; WNC=within network connectivity

WNC comparison between "pain" and "no pain" participants

Disease groups: the association with pain scores was investigated in the disease groups (MOGAD, NMOSD-AQP4 and MS). The comparison between participants with a pain score >0 ("pain") and participants with pain score 0 ("no pain"), did not show significant differences (no pain vs pain -0.416 [1.28], p=0.909) (see Figure 7.15)

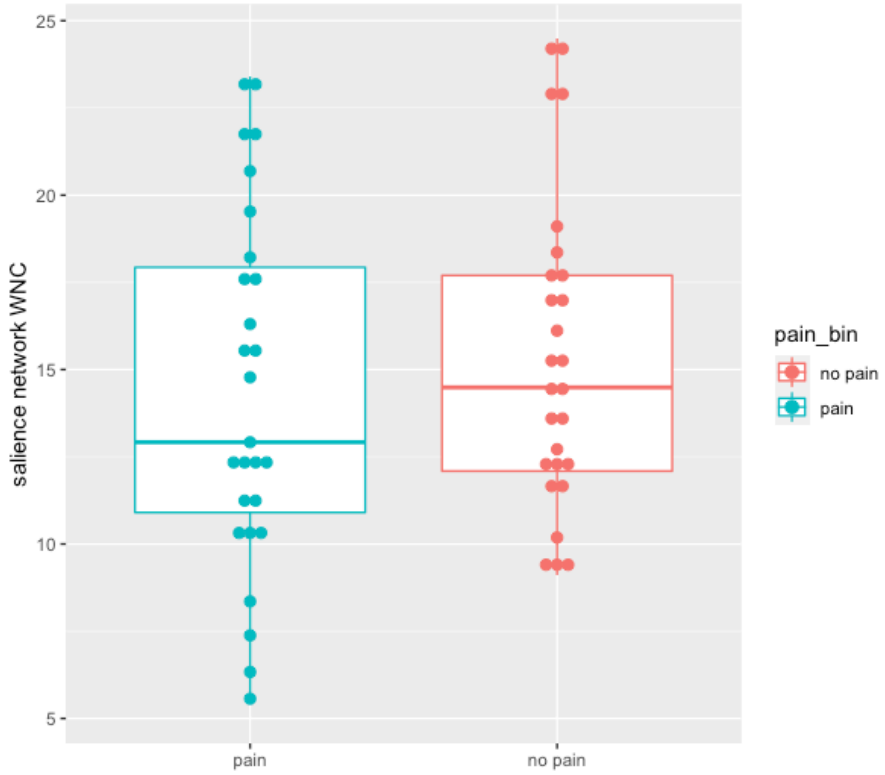


Figure 7.15 Salience network WNC between "pain" and "no pain" groups. *The graphs represent the median and, the 25th and the 75th percentile*

MOGAD, NMOSD-AQP4 and MS: The WNC of the salience network were compared between "pain" and "no pain" participants in each disease group (see Figure 7.16). The NMOSD-AQP4 participants with pain, showed lower WNC in the salience network compared to the no-pain group, however this was not significant (-3.4 [2.49], p=0.19). Interestingly, in the MOGAD group, the pain group showed a significantly higher

salience network WNC compared to the no-pain group (3.49 [1.68], p=0.05) while MS participants did not show any difference (-0.426 [2.12], p=0.84) (see Figure 7.16).

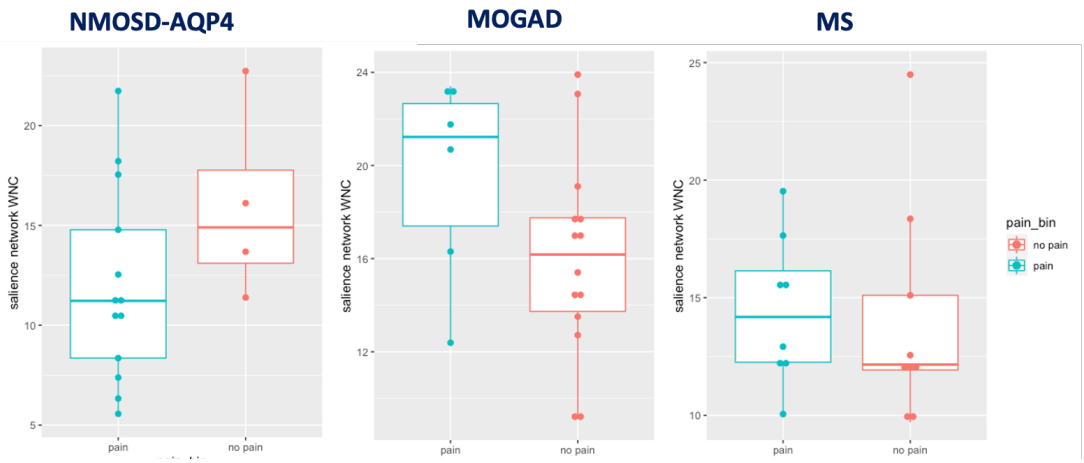


Figure 7.16 Salience network WNC between "pain' and "no pain" participants in the three disease groups. *The graphs represent the median and, the 25th and the 75th percentile.*

Given the different pattern of salience network activation between pain and no pain participants in the three disease groups, the association between the pain score and the salience network WNC was explored in every disease group, adjusting for age and sex. The pain score and age were significantly associated with the salience network, explaining 56% of the variability, in the NMOSD-AQP4 group. In the MOGAD group, only male sex was significantly associated with the salience network WNC, while there were no significant associations in the MS group (see Table 7.10).

Table 7.10 Multiple linear regression model, age and sex adjusted, between pain score the WNC in and the salience network in the three disease groups.

	Salience network – NMOSD-AQP4			**Salience network - MOGAD**			**Salience network – MS**		
Predictors	*Estimates*	*CI*	*p*	*Estimates*	*CI*	*p*	*Estimates*	*CI*	*p*
(Intercept)	29.498	20.842 – 38.154	<0.001	11.190	3.718 – 18.663	0.006	21.023	4.502 – 37.545	0.017
Total Pain score	-0.717	-1.164 – -0.269	**0.004**	0.156	-0.290 – 0.602	0.468	0.229	-0.436 – 0.895	0.470
Age	-0.231	-0.367 – -0.095	**0.003**	0.071	-0.098 – 0.240	0.386	-0.154	-0.532 – 0.223	0.393
Sex	2.070	-2.059 – 6.199	0.298	5.230	1.606 – 8.855	**0.007**	-1.029	-5.436 – 3.378	0.622
Observations	17			20			17		
R^2 / R^2 adjusted	0.643 / 0.560			0.409 / 0.298			0.094 / -0.115		

Legend: CI=confidence interval.

7.3.3.3 Sensorimotor network

Comparisons across groups

The NMOSD-AQP4 and MS participants had the lowest WNC, however the comparisons across groups were not significant (see Figure 7.17 and Table 7.11 for group comparisons).

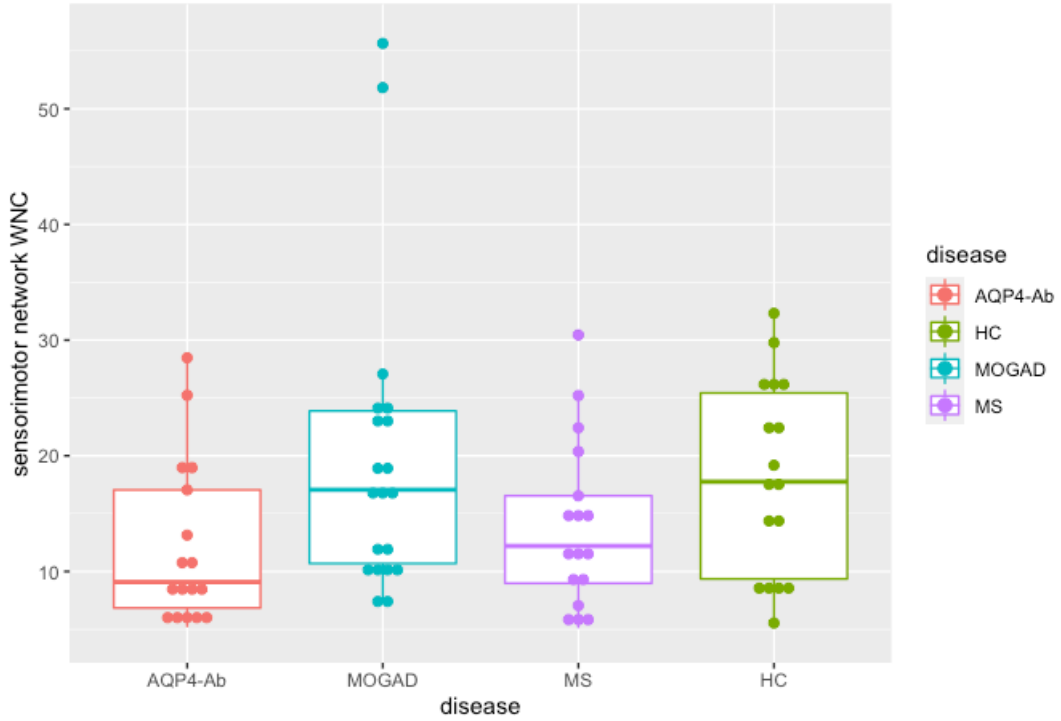


Figure 7.17 Sensorimotor network average WNC between disease groups. *The graphs represent the median and, the 25th and the 75th percentile. Legend: AQP4-Ab= NMOSD-AQP4*

Table 7.11 Age and sex adjusted comparisons of WNC, Bonferroni corrected, in the four groups.

	Sensorimotor network		
	Estimates	*SE*	*p-value*
AQP4-Ab vs HC	3.907	3.64	0.999
AQP4-Ab vs MOGAD	-5.601	3.42	0.640
AQP4-Ab vs MS	-0.009	3.42	0.999
HC vs MOGAD	-1.694	3.07	0.999
HC vs MS	3.897	3.23	0.999
MOGAD vs MS	5.591	3.07	0.440

Legend: AQP4-Ab=NMOSD-AQP4; WNC= within network connectivity, SE=standard error

WNC comparison between higher and lower disability levels

Disease groups*:* the relationship between the WNC in the sensorimotor network and the EDSS score (as a marker of disability) was explored in the disease groups. An EDSS score of 4 was chosen as a cut-off of disability, due to the rarity of higher disability levels in the MOGAD group, as shown in Chapter 2. The comparison between all disease participants (MOGAD, NMOSD-AQP4 and MS) with an EDSS score <4 and participants with an EDSS score≥4 showed that participants with higher EDSS scores had lower sensorimotor network WNC (see Figure 7.18), however the difference was not significant (3.59 [4.31], p=0.41).

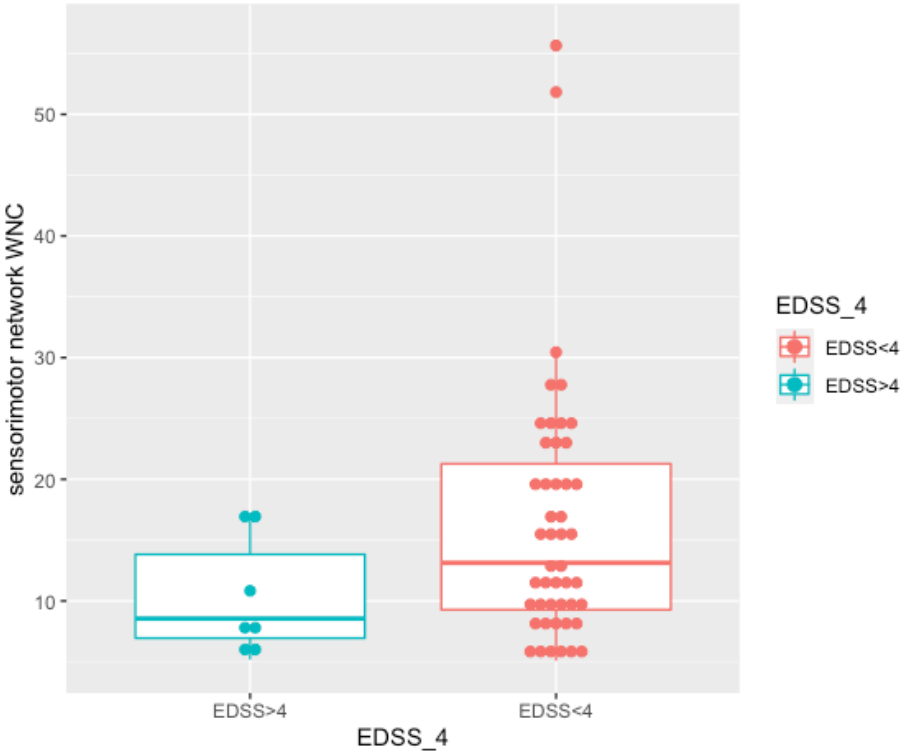


Figure 7.18 Sensorimotor network WNC between the high disability (EDSS≥4) and the low disability (EDSS<4 groups). *The graphs represent the median and, the 25th and the 75th percentile.*

MOGAD, NMOSD-AQP4 and MS: the WNC of the sensorimotor network were compared between the EDSS <4 and EDSS score≥4 participants in each disease group (see Figure 7.19). The NMOSD-AQP4 participants with EDSS ≥ 4 showed lower WNC in the sensorimotor network compared to the EDSS<4 group, however this was not significant (-3.7 [4.06], p=0.376).

Only one participant in the MOGAD group and two in the MS had an EDSS≥4, therefore the comparison was not calculated.

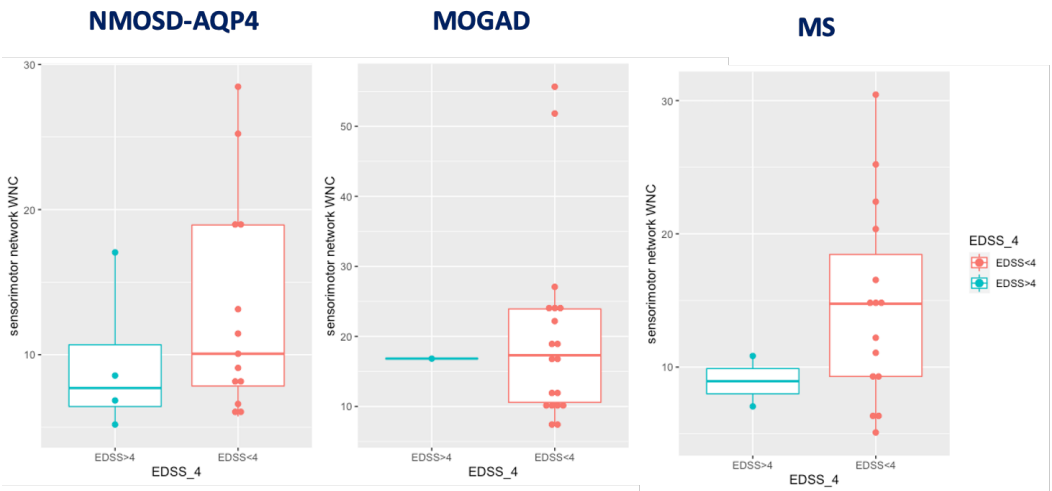


Figure 7.19 Sensorimotor network WNC between the high disability subgroup (EDSS≥4) and the low disability subgroup (EDSS<4) across disease groups. *The graphs represent the median and, the 25th and the 75th percentile*

Finally, the association between the EDSS score and the sensorimotor network WNC was explored in each disease group, adjusting for age and sex using multiple linear regression. In the NMOSD-AQP4 group, age was the only variable associated with the sensorimotor network WNC, while there were no significant associations in the MOGAD and MS groups (see Table 7.12).

Table 7.12 Multiple linear regression model of WNC, age and sex adjusted, between pain score and the sensorimotor network in the three disease groups.

	Sensorimotor network – NMOSD-AQP4			**Sensorimotor network - MOGAD**			**Sensorimotor network – MS**		
Predictors	*Estimates*	*CI*	*p*	*Estimates*	*CI*	*p*	*Estimates*	*CI*	*p*
(Intercept)	29.265	15.947 – 42.582	<0.001	4.073	-23.788 – 31.934	0.761	22.317	-8.299 – 52.933	0.139
Total Pain score	-0.677	-2.329 – 0.975	0.392	-0.675	-4.908 – 3.559	0.740	-0.040	-2.878 – 2.798	0.976
Age	-0.285	-0.517 – -0.053	**0.020**	0.371	-0.227 – 0.969	0.207	-0.222	-0.859 – 0.415	0.465
Sex	4.650	-2.578 – 11.877	0.188	2.805	-9.894 – 15.503	0.646	3.442	-6.250 – 13.134	0.457
Observations	17			20			17		
R^2 / R^2 adjusted	0.491 / 0.374			0.130 / -0.033			0.105 / -0.102		

Legend: CI=confidence interval; WNC=within network connectivity.

7.3.3.4 Auditory network

Comparison across groups

In this section the auditory network WNC was investigated across all groups. The NMOSD-AQP4 and MS participants had the lowest WNC, with the NMOSD-AQP4 showing a significant difference, when compared to the HC (-6.38 [2.12], p=0.02), however this was not significant when adjusting for age and sex (see Figure 7.20). The remaining comparisons were not significant (see Table 7.13 for group comparisons).

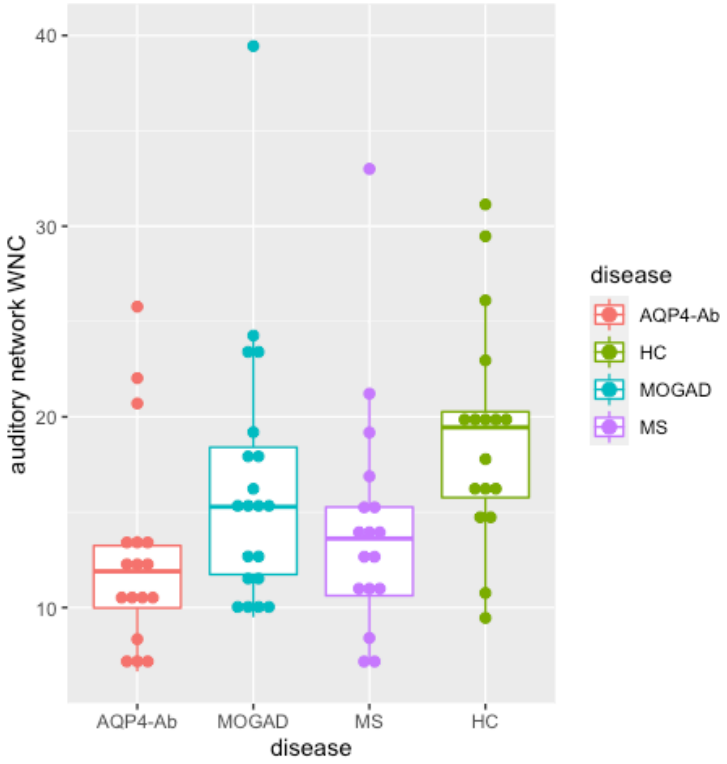


Figure 7.20 Auditory network WNC between disease groups. *The graphs represent the median and, the 25th and the 75th percentile.*

Table 7.13 Age and sex adjusted comparisons of WNC, Bonferroni corrected, in the four groups.

	Sensorimotor network		
	Estimates	*SE*	*p-value*
AQP4-Ab vs HC	-4.195	2.39	0.507
AQP4-Ab vs MOGAD	-1.803	2.25	0.999
AQP4-Ab vs MS	0.078	2.25	0.999
HC vs MOGAD	2.391	2.02	0.999
HC vs MS	4.273	2.12	0.291
MOGAD vs MS	1.881	2.02	0.999

Legend: AQP4-Ab=NMOSD-AQP4; WNC=within network connectivity; SE=standard error

Association between WNC and MRI findings

Disease groups: the association between the auditory network WNC and the brainstem volume was explored in the whole disease group, adjusting for age and sex. Age was the only variable significantly associated with the auditory network WNC [slope -0.17, p=0.02].

MOGAD, NMOSD-AQP4 and MS: the association between the auditory network WNC and the brainstem volume was explored in every disease group, adjusting for age and sex. In the NMOSD-AQP4 group, age was the only variable associated with the auditory network WNC, while there were no significant associations in the MOGAD and MS groups (see Table 7.14).

Table 7.14 Multiple linear regression model of WNC, age and sex adjusted, between pain score and the auditory network in the three disease groups

	Auditory network – NMOSD-AQP4			**Auditory network - MOGAD**			**Auditory network – MS**		
Predictors	*Estimates*	*CI*	*p*	*Estimates*	*CI*	*p*	*Estimates*	*CI*	*p*
(Intercept)	34.185	14.298 – 54.073	0.003	-4.977	-49.672 – 39.717	0.816	27.336	24.342 – 79.015	0.274
Total Brainstem	-0.000	-0.001 – 0.001	0.523	0.001	-0.001 – 0.003	0.403	0.000	-0.001 – 0.002	0.934
Age	-0.278	-0.442 – -0.113	**0.003**	0.055	-0.293 – 0.402	0.743	-0.329	-0.880 – 0.221	0.218
Sex	1.356	-3.549 – 6.261	0.561	-0.552	-8.225 – 7.121	0.881	0.322	-7.297 – 7.941	0.929
Observations	17			20			17		
R^2 / R^2 adjusted	0.562 / 0.461			0.069 / -0.106			0.121 / -0.082		

Legend: CI=confidence interval; WNC=within network connectivity

7.4 Discussion

This chapter investigated RSNs across demyelinating diseases. The voxel-wise analysis found that the visual networks were abnormal in all the three conditions when compared to healthy controls. In NMOSD-AQP4 the sensory/motor networks (sensorimotor and auditory) and the associative networks (executive, DMN, salience and frontotemporal networks) were also abnormal, while the subcortical basal ganglia network was the only abnormal network in MS.

When comparing the two Ab-mediated diseases, the NMOSD-AQP4 voxel-wise analysis showed abnormal salience, sensorimotor and, to a lesser extent, executive function network. When comparing MS to the Ab-mediated diseases, the executive function network was different from NMOSD-AQP4, while the frontostriatal network was the only different network when comparing MS to MOGAD.

The RSNs are the result of the coactivation of different brain structures and the networks have been shown to be easily reproducible in different cohorts. In this chapter the subject-specific spatial maps, containing z-transformed correlation values, have been used to quantify a "within network connectivity" (WNC) for each RSNs of interest, to explore possible differences and abnormalities across groups. One interpretation of the observed differences is that a lower WNC could be associated with structural damage (both local damage or secondary to Wallerian degeneration), while a higher WNC may be related to reorganisation of the cortex, secondary to structural damage (both local or due to secondary Wallerian degeneration).

In line with this interpretation, low WNC was more evident in the visual cortex of subjects with abnormal vision, independent of the disease group (although the comparison was not significant). When investigating each disease individually, a negative association

between the medial visual network and optic radiation tissue integrity was only found in MOGAD, with a higher WNC when the FA optic radiation is lower, possibly suggesting a reparative mechanism in the primary visual cortex in this group, in line with the overall good vision recovery. The occurrence of at least one episode of optic neuritis appeared to affect the medial and lateral visual network in NMOSD-AQP4 (although the comparisons did not reach statistical significance, possibly watered down by the effect of both eyes on cortex) and the occipital visual network in MOGAD. The optic neuritis effect was more pronounced in the NMOSD-AQP4 group and when the optic neuritis occurred more than 36 months before (although not statistically significant).

The salience network showed lower WNC in the NMOSD-AQP4 group (not significant) and was significantly associated with higher pain scores. No statistically significant differences were found in the MS group, while interestingly in the MOGAD group there was a significantly increased WNC in the participants with pain.

A reduced WNC was found in the sensorimotor and auditory network in the NMOSD-AQP4 and MS participants, but no association was found with either disability (EDSS in the sensorimotor) or tissue damage (brainstem atrophy in the auditory network) (see Table 7.15 for a summary of the significant key-findings).

It is not surprising that the voxel-wise analysis showed that visual networks are abnormal in all the three disease groups, as optic neuritis is a hallmark of the three diseases and it can be particularly severe in the two Ab-mediated conditions (Filippatou et al., 2020). Overall, the NMOSD-AQP4 group has the worse visual ability, and showed abnormality of both the medial visual network, where the primary visual cortex is located, and the lateral, where the supplementary visual cortex is anchored. The MOGAD participants, despite the good visual acuity (only one had impaired vision) showed a significantly

lower WNC of the occipital pole in the voxel-wise analysis, but not in the medial and lateral visual function. This is particularly intriguing when considering previous studies describing the representation of central vision in the occipital pole (Wong and Sharpe, 1999). Recent findings have shown that despite visual acuity being worse in NMOSD-AQP4 compared to MOGAD, the foveal thickness and macula (obtained with OCT, an imaging tool to investigate the retinal structure, where the central vision is located) are similar (Sotirchos et al., 2020). One hypothesis is that in MOGAD the occipital pole, where the central vision is located, is more sensitive to the optic neuritis damage and this is possibly reflected by the foveal thinning. In NMOSD-AQP4, where the visual impairment is more severe, it is possible that the medial and lateral visual cortex, where the primary visual cortex and higher order visual processing is located, are more sensitive to damage, leading to a more severe impairment. In addition, in NMOSD-AQP4 there may be other retinal damage which can explain the worse visual outcome (Roca-Fernández et al., 2021). A possible adaptative mechanism in MOGAD may be supported by the association found between WNC and the optic radiation FA. As damage in the optic radiation (low FA) is correlated to a higher medial visual network WNC, this suggests the possibility that in MOGAD there is an association between post-chiasmatic visual system damage and visual cortex reorganization.

The presented findings, showing abnormal visual RSN in NMOSD/MS, are mostly in line with previous studies (Bigaut et al., 2019; Cai et al., 2017; Wang et al., 2020). Task-based fMRI studies in MS patients have shown decreased activation of the visual cortex in patients with optic neuritis (Gareau et al., 1999; Rombouts et al., 1998). In contrast with the finding of this chapter, one study investigating the effects of optic neuritis on the visual cortex in NMOSD, found an increase in the connectivity within the visual networks, which is associated with retinal damage (Finke et al., 2018). One possible

explanation for the different direction of the changes in visual network WNC in the current study is the presence of brain lesions in the presented cohort, while in Finke at al study the presence of brain lesions is not specified. As showed in Chapter 5, in the NMOSD-AQP4 cohort there is white matter damage, especially in the corticospinal and optic tract, possibly caused by lesions, and this can lead to cortical reorganization. Another possible difference is the older age of the described NMOSD-AQP4 cohort compared to HC. However, as shown in the analysis of WNC, adjusting for age reduces, but does not remove the effect. In addition, in contrast with Finke et al, a study-specific group-based RSN template was used, using both the healthy controls and disease participants, as specified in (Griffanti et al., 2016). This approach can guarantee that the template is representative of the whole cohort, while maintaining the biologically meaningful variance of the disease groups.

Functional connectivity is a dynamic process, and several factors can affect the intrinsic structure of the brain networks, especially in inflammatory relapsing conditions. Networks may have a different susceptibility to the inflammatory damage, which cannot be captured by a cross sectional study, as it has been already shown in MS (Toosy et al., 2005). Longitudinal studies may be better placed to disentangle the cortical plasticity in response to optic neuritis and the recovery from inflammation.

In the second section of this chapter the salience network and the association with pain was explored. The voxel-wise analysis showed that salience network was abnormal in NMOSD-AQP4 and the WNC analysis showed that higher pain scores in NMOSD-AQP4 were significantly associated with lower WNC in the salience network. RS-fMRI has been used to aid in understanding the mechanisms behind chronic pain. Different large-scale brain networks have been described, such as the somatomotor, frontoparietal and

dorsal attention networks (Lee et al., 2021b). Recently a meta-analytic approach has identified the main structures behind chronic pain development in the anterior insula and the midcingulate cortex, which have been described as nodes of the salience network (Ferraro S, 2021). The salience network plays a role in the regulation of behaviour in response to internal and extra personal stimuli and has been described as associated with pain (Cauda et al., 2009; Hemington et al., 2016; Wu et al., 2013). Chronic neuropathic pain is one of the most common symptoms in NMOSD-AQP4 after a transverse myelitis (prevalence ranging from 44-74%) and can be very disabling (Li et al., 2020a; Tackley et al., 2017). The abnormal salience network, as shown in the voxel-wise analysis, and the association with pain severity in NMOSD-AQP4, could result from a maladaptive reorganization of anterior insula and cingulate cortex, leading to chronic pain in NMOSD participants. Despite this, MOGAD patients can experience very severe transverse myelitis, but they less frequently experience severe pain. This is particularly interesting as in MOGAD the WNC in the salience network is significantly higher in participants with pain compared to those with no pain, suggesting a possible adaptative mechanism. This study shows, for the first time, a different pattern of salience network activation and its association with pain in NMOSD and MOGAD, suggesting possible new lines of research into chronic neuropathic pain in these inflammatory conditions.

The sensorimotor network was abnormal in NMOSD-AQP4 compared to HC in the voxel-wise analysis, but no association with the EDSS score was found in the WNC analysis. This is not surprising, as NMOSD-AQP4 patients have a higher disability compared to the other groups, due to the severity of the transverse myelitis. However, the EDSS, as marker of disability, is mostly affected by walking difficulties, thus showing a better association with spinal cord measures (Mariano et al., 2020).

Finally, the auditory network was abnormal in NMOSD-AQP4 and did not show a significant correlation with brainstem volume (where the nucleus of the vestibulocochlear nerve is located). The auditory function is rarely explored in demyelinating disease, although the common brainstem involvement (Banks et al., 2020) and cases with retro-cochlear type of hearing loss have been described in NMOSD-AQP4 patients (Bonnan and Cabre, 2017; Castillo-Torres et al., 2020; Gratton et al., 2014; Jarius et al., 2013). A recent case report showed a cochlear-type of hearing loss in a NMOSD-AQP4 patient, suggesting that the involvement of the cochlear structure, which is rich in AQP4 water channels, can be more frequent (Shaw et al., 2021). In this chapter measures of auditory performance were not available and the EDSS is not able to capture it in the total score. The finding from this chapter could be replicated in larger study to better understand if subclinical hearing loss is present, and often undetected, in this disease. However, given the significance of the age in the multiple regression, the effect of age in the reduction of the auditory performance, and consequent reorganization of the auditory network, cannot be fully ruled out.

This chapter showed several important key findings (see Table 7.15) and proved again that, despite clinical and conventional MRI similarities, NMOSD-AQP4 and MOGAD are distinct conditions and different in terms of clinical outcome and pathogenesis. However, there are some limitations specific to this chapter that need to be discussed.
The effect of lesions was not considered in this study. As brain lesions can be particularly destructive in NMOSD-AQP4, and they are pathologically different from MS and MOGAD lesions (Takai et al., 2020; Takai et al., 2021), future studies should focus on understanding their effect on large brain networks in NMOSD and MOGAD, particularly

because lesions tend to be fewer than in MS, where there are multiple lesions and NAWM damage. The association between retinal damage and visual networks was not explored, as the study of visual function was not the primary aim of this study. OCT measures may be helpful to understand the novel finding of "good vision-abnormal visual network paradox" in MOGAD described in this chapter. In addition, spinal cord measures were not explored, especially in association with the sensorimotor network or the salience network. Spinal cord measures and the presence of cord lesions may affect the cortical organization of the sensorimotor cortex and can offer a better understanding of the relationship between pain and the salience network.

As the within network connectivity was calculated as an average over the whole network, most of the significant differences observed in the voxel-wise analysis were washed out. Although more research is needed to better interpret the difference of WNC across group, it is interesting to note that most of the differences observed were clinically plausible.

Table 7.15 Summary of the key-findings. Voxel-wise analysis results of disease group vs HC.

	MOGAD	*NMOSD-AQP4*	*MS*
Visual networks	Abnormal occipital pole visual network (voxel-wise analysis) * Association with optic radiation damage (WNC analysis) Abnormal after ON (WNC analysis)	Abnormal medial and lateral visual networks (voxel-wise analysis) *	Abnormal medial visual network (voxel-wise analysis) *
Salience network	Higher WNC with higher pain score (WNC analysis)	Lower WNC is associated with higher pain score (WNC analysis)	No significant findings
Sensorimotor Network	No significant findings	Abnormal sensorimotor network (voxel-wise analysis) *	No significant findings
Auditory Network	No significant findings	Abnormal auditory network (voxel-wise analysis) *	No significant findings

*Legend: FC=functional connectivity; ON=optic neuritis. WNC=within network connectivity. *Compared to HC.*

7.5 Conclusions

Overall, the NMOSD-AQP4 cohort differed more in term of its brain resting-state connectivity levels, compared to the other groups, possibly due to the higher level of disability in this disease group. In MS, findings are in line with previous studies, showing a preferential involvement of the deep grey matter structures (Janssen et al., 2013). The findings in this chapter showed for the first time that in MOGAD, despite the good visual recovery and the absence of structural damage and microstructural tissue damage, the connectivity of the visual cortex is abnormal. This may open new avenues to further studies, to better understand if repetitive optic neuritis damage can, in the long-term, lead

to change of the visual cortex and to visual impairment in people with MOGAD. Understanding the longitudinal changes in functional connectivity in response to repetitive optic neuritis may potentially help to identify those patients that may be more prone to long term visual disability. In the MOGAD cohort an abnormal salience network was found, with WNC changing in the opposite direction compared to NMOSD-AQP4, where an association with chronic pain was also detected. The identification of the salience network as a marker of pain may help to better understand, in a longitudinal setting, the mechanism behind chronic pain and can be potentially useful to test pain medication or rehabilitation strategy. Finally, the abnormal auditory network supports the recent findings of involvement of auditory function in NMOSD-AQP4 and points towards benefits in further assessment of this, often neglected, clinical outcome.

RS-fMRI has potential as a marker to distinguish between diseases and to explore the biological mechanisms underpinning clinical recovery in MOGAD, although further studies are needed to confirm these findings.

In the next chapter the association with “invisible” symptoms, such as cognition and fatigue, will be explored, combing RS findings with structural GM measures.

8 Chapter 8 The “invisible” symptoms in CNS demyelinating disorders: cognition and fatigue, and their imaging correlates

8.1 Introduction

In the previous chapters it was shown that ‘visible disability’ (i.e., motor, and visual impairment) is associated with different pattern of tissue damage in the three CNS demyelinating disorders, as measured by quantitative and functional MRI.

“Invisible symptoms”, such as cognitive impairment and fatigue, can impact patients’ quality of life, but are often neglected. Recognition of these deficits is important since they are amenable to therapeutic interventions (Lakin et al 2021).

Cognitive function and fatigue cannot be captured by EDSS (the main disability score used for demyelinating conditions) and their evaluation can often be affected by other factors, such as anxiety, depression, education and social environment (Lakin et al., 2021)

Approximately 80% of people with MS experience fatigue and up to 70% have cognitive impairment (Benedict et al., 2020; Giovannoni, 2006). Cognitive impairment varies across the life span in MS and is an important feature in progressive MS (Ontaneda et al., 2017) with cognitive processing speed and episodic memory being the most frequently affected domains (Benedict et al., 2020).

Fatigue has been reported by NMOSD-AQP4 and MOGAD patients and is thought to be explained by factors such as disability, age, and pain (Yeo et al., 2020).

The prevalence of cognitive impairment in NMOSD-AQP4 ranges from 30 to 70%, however, it is still not clear whether cognitive abnormalities are a general feature of all patients or are limited to those with brain disease (Oertel et al., 2019). Cognitive function has been explored in MOGAD paediatric cohorts but adult studies, using standardized

cognitive batteries for demyelinating disease, are lacking (Armangue et al., 2020; Bruijstens et al., 2020a; Deiva et al., 2020).

Whether patients with antibody mediated CNS demyelination have a similar pattern of cognitive dysfunction as MS is unknown.

The pathological mechanism underlying cognitive dysfunction is not clear in MS, however growing evidence suggest that a dysregulation of the dopaminergic circuit between the frontal lobe and the basal ganglia could be involved (Cercignani et al., 2021; Dobryakova et al., 2015).

Brain MRI studies have tried to elucidate the mechanisms behind cognitive impairment in demyelinating diseases, especially in MS. In this disease group, deep grey matter and cortical damage are most reliably associated with cognitive decline than white matter lesion volume (Daams et al., 2016; De Meo et al., 2021; Eijlers et al., 2018; Rocca et al., 2015). In recent years a more comprehensive MRI approach, including both structural and functional measures, has tried to disentangle the complex mechanisms behind cognitive dysfunction in MS (Petracca et al., 2021). Resting state studies hypothesised that there is compensatory functional reorganization in the brain in the early stage of the disease but then, as tissue damage accumulates over time, there is a reduction of functional connectivity and the development of cognitive impairment (Schoonheim et al., 2015).

In NMOSD-AQP4, there is some evidence that white and grey matter structural changes and functional network disruption may associate to cognitive impairment, (Blanc et al., 2012; Liang et al., 2011; Liu et al., 2015b; Saji et al., 2013).

In MOGAD, there is only one study on adult population investigating the correlation between cognitive score and MRI findings, however using uncorrected scores and a battery that is not standardized for demyelinating diseases.

This chapter aims to fill in some of these literature gaps and identifying the different patterns of cognitive impairment and their imaging correlates that may prove useful in differentiating MS, NMOSD-AQP4 and MOGAD.
Given that in previous chapter, grey matter damage emerged as a potential discriminant between MOGAD and NMOSD-AQP4, its association with cognition was explored.

8.1.1 *Objectives*

The main objectives of this chapter are:

a) To compare the cognitive test scores across groups (MOGAD, NMOSD-AQP4, MS and HC) and to identify the cognitively impaired patients in each disease group.
b) To explore the association between the cognitive performance and RSNs/structural measures within each disease group.
c) To compare the fatigue scores across groups.
d) To describe the association between fatigue and cognition, and the association with MRI findings.

8.1.2 *Hypothesis*

a) Cognitive impairment will be present in the three disease and there will be no difference across disease groups.

b) The cognitive performance will associate with evidence of structural and/or functional brain changes in the three CNS demyelinating disorders.

c) Fatigue will affect the cognitive performance in the three diseases.

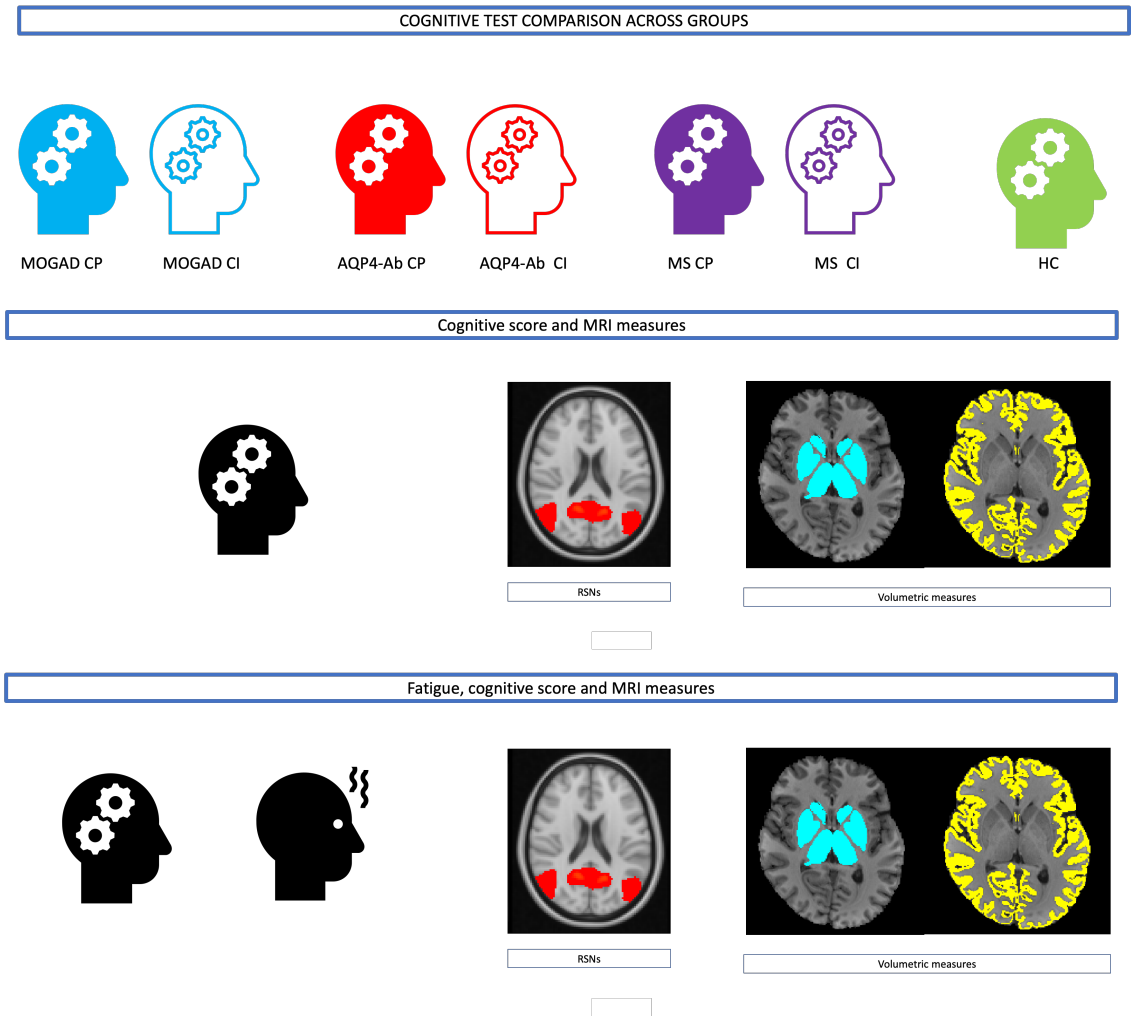


Figure 8.1 Outline of this chapter workflow. *Legend: CI=cognitively impaired, CP=cognitively preserved, AQP4-Ab=NMOSD-AQP4*

8.2 Methods

8.2.1 *Subjects*

The cognitive assessment was available for 71 subjects. For four subjects the cognitive assessment was not performed due to time constrains. In this case the preference was

given to the MRI scans. One participant only performed the SDMT, therefore the global cognitive score was not calculated. Fatigue, anxiety, and depression were also evaluated in this study as they can influence cognition. The details of the fatigue, anxiety and depression questionnaires have been described in Chapter 3.

8.2.2 *Cognitive Assessment*

The Rao's Brief Repeatable Battery of neuropsychological test (BRB-N) was administered in a quiet room before the MRI scan, preferentially in the morning, by myself, a researcher with previous experience with the administration of this battery (Rao et al., 1991). The BRB-N was chosen as it has been extensively used in MS and NMOSD cohorts.

It consists of five tests exploring four main cognitive domains: verbal and long-term memory, visuospatial memory, attention and concentration, and executive function (Rao, 1990). As the executive functions are not extensively represented in the BRB-N (only one test explores verbal fluency), the Stroop word-colour test was added (Amato et al., 2006). Tests were administered according to the following fixed order.

The Selective Reminding Test (SRT), the 10/36 Spatial Recall Test (SPART), the Symbol Digit Modality Test (SDMT), the Paced Auditory Serial Addition Test (PASAT), The SRT delayed recall (SRT-D), the SPART delayed recall (SPART-D), the Word List Generation (WLG), the Stroop word-colour test (ST). The cognitive tests have been described in detail in Chapter 3.

8.2.3 *MRI measures*

The following MRI measures were used in the analysis. The MRI pre-processing and analysis of the structural and functional measures have already been described in Chapter 4 and 7 respectively.

Structural grey matter measures: deep grey matter volume, cortical volume, and thickness (calculated as described in Chapter 4).

Functional measures: the following RSNs were selected as they were significantly different from HC in the voxel-wise analysis, and the within-network connectivity (WNC) was calculated for each RSN of interest (as described in Chapter 7).

Anterior and posterior Default Mode Network (DMN): the DMN is the most studied brain network in resting state analysis and is deactivated in task-based RS-fMRI studies. The DMN is strongly anti-correlated with cognitive functions. It can be divided in two subnetworks, the anterior DMN which comprises the medial prefrontal cortex and the posterior DMN which comprises the precuneus/posterior cingulate cortex (Buckner et al., 2008; Knyazev, 2012; Smith et al., 2009).

The left frontoparietal RSN: together with the right frontoparietal RSN, are the only two lateralised networks and they mirror each other. While the right RSN is associated with perception/somesthesis/pain, the left RSN is associated with language function (consistent with the Broca's and Wernicke's areas) (Smith et al., 2009).

The executive function RSN: it comprises the anterior cingulate and paracingulate cortex, bilateral frontal gyri, and angular gyri. It is associated with executive function, decision-making, and action inhibition (Smith et al., 2009; Zhang and Li, 2012).

The basal ganglia RSN: this RSN comprises the pallidum, putamen, subthalamic nucleus, substantia nigra and sometimes the thalamus was also described together with the basal

ganglia RSN (Robinson et al., 2009). The basal ganglia have been associated with motor control and executive/cognitive control functions (Di Martino et al., 2008).

8.2.4 *Statistical Analysis*

The statistical analysis of non-imaging data was performed using Rstudio version 1.1.447 (http://www.rstudio.com). Data were double entered into the database and data cleaning was also performed before the data analysis. Quantitative variables were described using means and SDs, median and range. A Shapiro-Wilk test was performed to assess the normal distribution of data. Linear models were fit to assess the effect of age, sex, and years of educations on cognitive test performance. The assumptions were checked with linearity, normal distribution of residuals and equal variance of variables.

Each participant residual score was calculated using the regression *beta* and applying the following equation:

$$corrected\ score = raw\ score - \beta age \cdot (Age - mean\ age) - \beta education \cdot (Education - mean\ education) - \beta sex$$

where mean age is the average age and mean education the average years of education in the total cohort (Abbott et al., 2019; Amato et al., 2006). The scores were then standardized as z-scores (z score=[x-mean]/SD).

Linear models of each cognitive tests were fit to compare the score across groups (MOGAD, NMOSD-AQP4, MS and HC). The estimated marginal means were calculated based on the linear model and a Bonferroni pairwise-comparison between groups was calculated. The results were expressed as estimates marginal means, standard errors, and significant post hoc comparisons.

Based on the z-score performance on each test, participants were considered as cognitively impaired (CI) if they failed in at least two tests assessing two different cognitive domains (the delayed recall test for SRT and SPART were considered as different domain, as representing verbal and visuospatial long-term memory) The remaining participants were defined as cognitively preserved (CP).

The test performance was considered as impaired if the z-score was <-1.5.

The global cognitive performance (BRB-N global cognitive index) was calculated averaging the z-score for each test. The SRT-LTS, SRT-CLTR and SRT-D z-score were averaged to calculate the *learning and verbal memory* performance. The SPART and SPART-D z-score were averaged to calculate the *visual memory* performance. The SDMT, PASAT3 and PASAT2 were averaged to calculate the *attention and concentration* performance. WLG and ST were averaged to calculate the *executive function* performance.

When patients did not complete all the cognitive tests, the cognitive function subscores were calculated if the score of at least one test representing that function was available.

To explore the association between the RSNs, and the clinical/MRI findings, multiple linear regression models were fitted in each disease group, using the global cognitive index/cognitive domain scores as independent variable and the clinical/MRI findings as the dependent variables.

Finally, linear models with anxiety and depression, age, and sex as independent variables, were fit to compare the fatigue scores between the four study groups. The estimated marginal means were calculated based on the linear model and a Bonferroni pairwise-comparison between groups was calculated. The results were expressed as estimates marginal means, standard errors, and significant post hoc comparisons.

For all analyses, $p < 0.05$ was considered statistically significant.

8.2.5 *Analysis of imaging data*

A voxel-wise correlation analysis between the cognitive scores and the RSNs, was tested using FSL's *randomise* permutation-testing tool, in each disease group (MOGAD, NMOSD-AQP4 and MS)(Winkler et al., 2014). Results were considered significant for $p < 0.05$ after correction for multiple comparisons using the threshold-free cluster enhancement (TFCE) approach.

8.3 Results

The clinical and demographic characteristics of the studied cohort are represented in Table 8.1.

Table 8.1 Clinical and demographic characteristics of the studied cohort.

	MOGAD	*NMOSD-AQP4*	*MS*	*HC*
Number	20	17	18	17
Mean age (SD)	41.75 (11.03)	56.47 (13.41)	44.11 (6.61)	38.06 (13.27)
Sex, F (%)	10 (50)	13 (77)	10 (55)	9 (53)
Ethnicity (%)				
White	20 (100)	9 (53)	18 (100)	15 (88)
African/Afro-Caribbean	/	3 (18)	/	/
Asian	/	3 (18)	/	2 (12)
Mixed	/	2 (11)	/	/
Phenotype (%)				
Isolated TM	1 (5)	/	/	
TM + Br/Bs	5 (25)	9 (53)	12 (67)	
ON + Br/Bs	/	3 (18)	/	/
ON + TM	6 (30)	/	/	
Br/Bs	2 (10)	2 (11)	/	
ON + TM +Br/Bs	6 (30)	3 (18)	6 (33)	
Median disease duration, years (range)	2 (0-24)	9 (0-24)	12 (1-24)	/
Median number of relapses (range)	2 (1-11)	2 (1-11)	4 (1-13)	/
Median EDSS (range)	1.5 (0-7.0)	3.0 (0.0-7.0)	2.0 (0.0-6.0)	/
Mean education years (SD)	14.32 (2.50)	17.12 (4.04)	16.40 (4.14)	18.00 (3.43)
Mean total fatigue score (SD)	27.85 (19.88)	38.41 (18.31)	38.50 (15.61)	7.12 (6.67)
Mean cognitive fatigue score (SD)	12.42 (9.56)	14.81 (8.61)	17.17 (8.01)	3.59 (4.06)
Mean physical fatigue score (SD)	12.63 (9.84)	19.31 (8.60)	18.11 (7.91)	2.82 (2.98)
Mean Psychosocial fatigue score (SD)	2.58 (3.79)	3.25 (2.29)	3.22 (1.77)	0.71 (0.99)
Mean HADS Anxiety score (SD)	7.28 (5.57)	6.53 (4.49)	6.22 (3.89)	4.67 (4.40)
Mean HADS Depression score (SD)	3.06 (2.92)	4.82 (3.59)	3.89 (3.61)	1.47 (1.85)

Legend: SD=standard deviation, F=female, TM=transverse myelitis, BR/BS=brain/brainstem, ON=optic neuritis, EDSS=expanded disability status scale, HADS=Hospital Anxiety and Depression Scale. HADS score in the MOGAD group calculated in 18 participants.

8.3.1 *Cognitive function*

A total of 71 participants performed the cognitive battery. One patient only completed the SDMT. Eight participants did not complete PASAT-3 and 17 did not complete PASAT-2 as they were considered stressful by the participants. One participant did not complete the word-colour Stroop test because he is colour-blind. The cognitive scores are first presented as raw data (see Table 8.2). There were no significant differences in the group comparisons.

As age, sex and education can affect the score results, and importantly the NMOSD-AQP4 group were older these variables were included in the linear model comparisons across groups (see Figure 8.2).

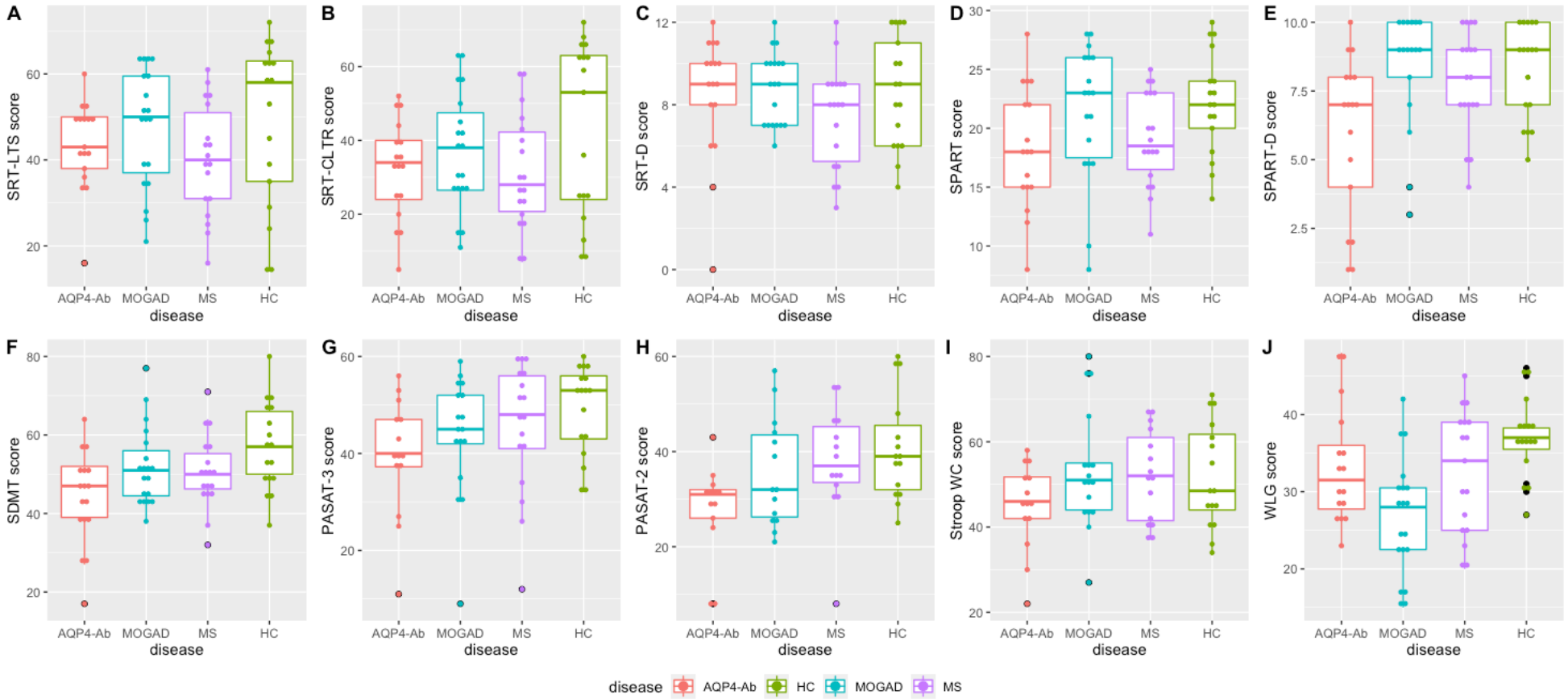


Figure 8.2 Cognitive test score between disease groups (A-J). *The graphs represent the median and, the 25th and the 75th percentile.*

Table 8.2 Raw scores of the cognitive assessment in the studied cohorts.

	MOGAD	***NMOSD-AQP4***	***MS***	***HC***
Number	20	17	18	17
Mean SRT-LTS (SD)	47.37 (13.76)	43.41 (10.24)	40.17 (12.99)	48.88 (19.28)
Mean SRT-CLTR (SD)	37.05 (15.91)	32.35 (13.36)	31.33 (15.43)	43.06 (23.62)
Mean SRT-D (SD)	8.79 (1.75)	8.47 (3.02)	7.44 (2.48)	8.65 (2.67)
Mean SPART (SD)	21.33 (5.79)	18.29 (5.19)	19.11 (3.98)	22.18 (4.35)
Mean SPART-D (SD)	8.35 (2.15)	5.94 (2.93)	7.83 (1.86)	8.24 (1.71)
Mean SDMT (SD)	51.89 (10.06)	44.00 (11.89)	50.67 (9.31)	57.12 (11.22)
Mean PASAT-3 (SD)	43.88 (12.30)	39.57 (12.09)	45.47 (13.48)	49.12 (9.16)
Mean PASAT-2 (SD)	35.50 (11.43)	27.69 (9.84)	37.86 (11.52)	40.73 (11.09)
Mean WLG (SD)	26.74 (7.63)	33.25 (7.56)	32.59 (7.99)	36.88 (4.99)
Mean Stroop WC (SD)	53.41 (14.02)	44.93 (10.15)	51.93 (10.72)	51.94 (12.22)

Legend: SRT-LTS=Selective reminding test long term storage, SRT-CLTR=Selective reminding test consistent long-term storage, SRT-D=Selective reminding test delayed recall, SPART=Spatial recall test, SPART-D=Spatial recall test delayed, SDMT= Symbol digit modality test, PASAT-3 and PASAT-2=Paced Auditory Serial Addition Test at 3 and 2 seconds, WLG=Word list generation, Stroop WC=Stroop word-colour test score

In the group comparison, adjusted for age, sex, and education, the MOGAD participants showed a significant lower WLG score compared to HC (9.50 [2.60], p=0.003). In the SRT-D the MS participants showed a lower score when compared to NMOSD-AQP4, at trend level of significance (2.33 [0.87], p=0.055). The remaining comparisons were not significant (see Table 8.3).

Table 8.3 Age, sex and education adjusted comparisons of the cognitive scores, Bonferroni corrected, across groups.

	SRT-LTS	***SRT-CLTR***	***SRT-D***	***SPART***	***SPART-D***	***SDMT***	***PASAT-3***	***PASAT-2***	***WLG***	***Stroop WC***
	Estimates (SE) *p-value*									
AQP4-Ab vs HC	5.16 (4.98) p>0.999	2.34 (6.14) p>0.999	1.76 (0.91) p=0.352	-1.93 (1.99) p>0.999	-1.19 (0.87) p>0.999	-7.36 (4.14) p=0.483	-7.11 (5.23) p>0.999	-7.11 (5.23) p>0.999	-1.91 (2.99) p>0.999	-3.91 (5.12) p>0.999
AQP4-Ab vs MOGAD	1.10 (5.23) p>0.999	2.05 (6.45) p>0.999	1.00 (0.96) p>0.999	-1.31 (2.12) p>0.999	-1.61 (0.93) p=0.524	-2.86 (4.34) p>0.999	-2.50 (5.76) p>0.999	-2.50 (5.76) p>0.999	7.59 (3.17) p=0.119	-2.91 (5.58) p>0.999
AQP4-Ab vs MS	10.79 (4.71) p=0.152	9.25 (5.80) p=0.697	2.33 (0.87) p=0.055*	1.11 (1.88) p>0.999	-0.96 (0.82) p>0.999	-1.47 (3.93) p>0.999	-3.52 (5.12) p>0.999	-3.52 (5.12) p>0.999	1.69 (2.85) p>0.999	-3.82 (4.89) p>0.999
HC vs MOGAD	-4.06 (4.44) p>0.999	-0.30 (5.47) p>0.999	-0.76 (0.82) p>0.999	0.623 (1.8) p>0.999	-0.43 (0.80) p>0.999	4.51 (3.74) p>0.999	4.61 (4.43) p>0.999	4.61 (4.43) p>0.999	9.50 (2.60) **p=0.003**	1.00 (4.44) p>0.999
HC vs MS	5.63 (4.36) p>0.999	6.90 (5.37) p>0.999	0.56 (0.80) p>0.999	3.04 (1.74) p=0.515	0.23 (0.76) p>0.999	5.90 (3.65) p=0.667	3.59 (4.32) p>0.999	3.59 (4.32) p>0.999	3.60 (2.60) p>0.999	0.09 (4.30) p>0.999
MOGAD vs MS	9.69 (4.41) p=0.190	7.20 (5.43) p>0.999	1.33 (0.81) p=0.640	2.42 (1.79) p>0.999	0.65 (0.79) p>0.999	1.39 (3.69) p>0.999	-1.02 (4.44) p>0.999	-1.02 (4.44) p>0.999	-5.90 (2.59) p=0.159	-0.91 (4.47) p>0.999

*Legend: SRT-LTS=Selective reminding test long term storage, SRT-CLTR=Selective reminding test consistent long-term storage, SRT-D=Selective reminding test delayed recall, SPART=Spatial recall test, SPART-D=Spatial recall test delayed, SDMT= Symbol digit modality test, PASAT-3 and PASAT-2=Paced Auditory Serial Addition Test at 3 and 2 seconds, WLG=Word list generation, Stroop WC=Stroop word-colour test score. *Trend towards significance. In bold, significant result.*

Out of the total cohort (71 participants), five NMOSD-AQP4, four MOGAD and three MS were classified as cognitively impaired (CI) (participants were considered as CI if they failed in at least two tests assessing two different cognitive domains, using the corrected z-score).

In NMOSD-AQP4 the most affected domain was visual memory. Of the five NMOSD-AQP4 participants classified as CI, one was the oldest in the group (female, 81-year-old) and the presence of associated dementia was considered likely (sadly, the participant died one year after being enrolled in this study). One participant presented with very large symptomatic frontal and thalami lesions at the time of a relapse (female, 40-year-old). One presented with a lesion in the splenium of the corpus callosum (rarely described in NMOSD), which caused a disconnection syndrome (female, 58-year-old). This participant also had clinically significant anxiety, as defined by the HADS-A score. The final two participants (male, 61-year-old and female, 53-year-old) presented with non-specific brain lesions. The female, 53-year-old participant had clinically significant depression defined by the HADS-D score. Overall, four of five presented with fatigue (all female), and all of them presented with clinically significant pain.

In MOGAD, the most affected domains were visual memory and executive functions. Of the four MOGAD participants defined as CI, one (male, 41-year-old) presented at onset with a bilateral ON and thalami lesions. He has been recently investigated for nocturnal seizures and is currently on antiepileptic drugs (not yet started at the time of the cognitive assessment). One participant (male, 41-year-old) presented with recurrent brain lesions. One (female, 40-year-old), presented at onset with large, confluent brain lesions. Finally, one (male, 48-year-old), presented with large brain lesions, had epileptic seizures and the

clinical longitudinal brain MRI showed a degree of brain atrophy. Two of the five had clinically significant anxiety and one both anxiety and depression. Three of the four had significant fatigue and pain, as defined by the MFIS and BPI scores respectively.

In MS, the most affected domain in the cognitively impaired MS was verbal memory. Of the three MS participants defined as CI, two female participants with cognitive impairment were among the oldest in the group (51-year-old and 55-year-old), while the male participant (49-year-old) had the longest disease duration (24 years) (see Figure 8.3). None of them had clinically significant anxiety and/or depression and they all had clinically significant fatigue. One had significant pain.

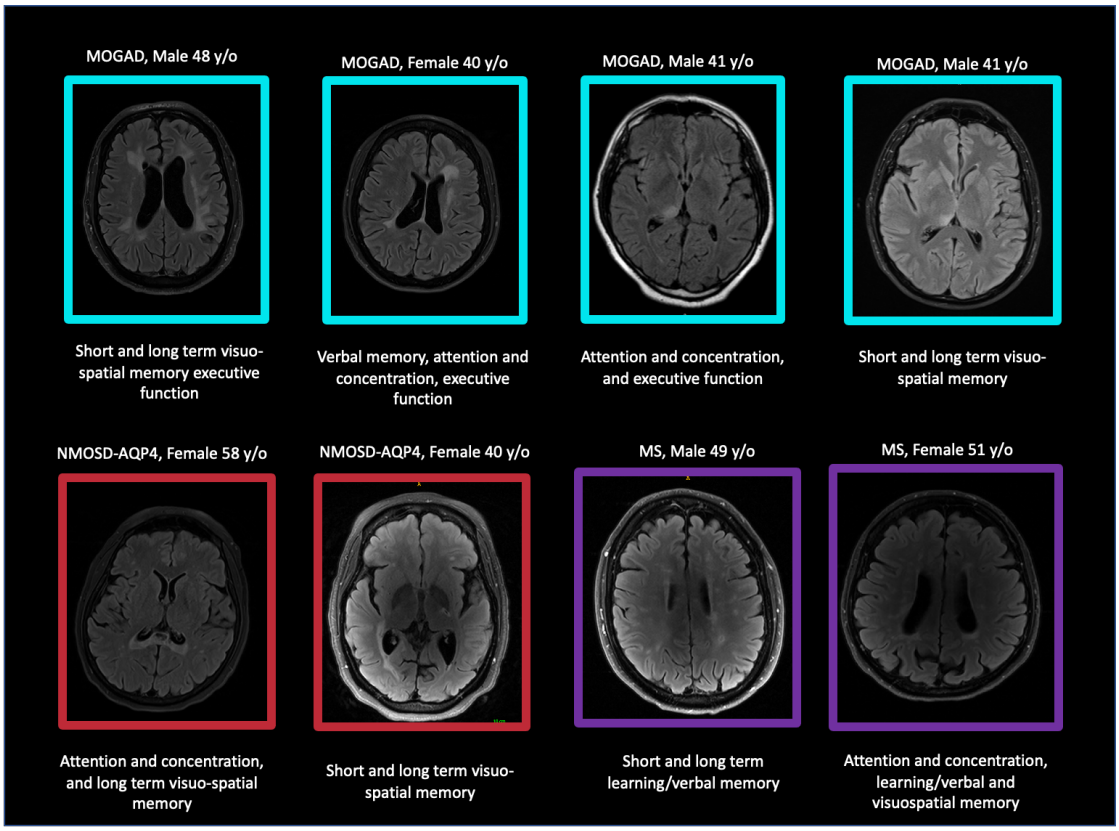


Figure 8.3 Brain MRI of the participants classified as cognitively impaired (four MOGAD, two NMOSD-AQP4 and two MS, as an example). *For two of the MOGAD patients, the clinical MRIs at the time of the attack are represented, as the remission MRI were normal (NHS MRI, patients consented under Tissue Bank Ref: 10/H0606/56).*

8.3.2 *Cognition: the role of the grey matter*

Functional Connectivity measures

The following RSNs were selected for the analysis as they were significantly different from HC in the voxel-wise analysis (as described in Chapter 7): the anterior DMN (volume 16), the posterior DMN (volume 1), the left frontoparietal RSN (volume 15), the executive function RSN (volume 20), and the basal ganglia RSN (volume 37).

A voxel-wise correlation of the RSNs of interest with global cognitive index, and the cognitive domains, *learning and verbal memory*, *visual memory*, *attention and concentration, executive function* (calculated as described in the statistical analysis section) was investigated in each disease group separately. The voxel-wise analysis did not show significant associations.

Structural MRI measures

The associations between DGM volume, cortical volume and cortical thickness, and the (global cognitive index were explored in each disease group separately. Additionally, the association between the grey matter structures measures and the cognitive domains were studied in each disease group.

MOGAD group: the DGM volume showed a significant association with the global cognitive index (R^2=0.248, p=0.026), with the visual memory score (R^2=0.336, p=0.009) and the executive function score (R^2=0.309, p=0.014). There was no significant association with the attention and concentration score (R^2=0.051, p=0.339). No significant associations were found with cortical volume and cortical thickness (except

for a trend towards significance between visual memory and cortical thickness, R^2=0.16, p=0.090).

NMOSD-AQP4 group: the global cognitive index score was significantly associated with the cortical volume (R^2=0.261, p=0.036). There was a significant association between the visual memory score and the cortical volume (R^2=0.473, p=0.0023) and the DGM volume (R^2=0.269, p=0.033). The DGM volume was also associated with the executive function score (R^2=0.244, p=0.052). The remaining associations were not significant.

MS group: the global cognitive index and the executive function score are significantly associated with the DGM volume (global cognitive score R^2=0.221, p=0.049; executive function R^2=0.346, p=0.01).

There is a trend towards significance between the visual memory score and both the DGM volume (R^2=0.162, p=0.098), and the cortical volume (R^2=0.161, p=0.098). Cortical thickness is significantly associated with visual memory (R^2=0.245, p=0.037). There is a significant association between executive function and cortical volume (R^2=0.247, p=0.036) and a trend with cortical thickness (R^2=0.177, p=0.082) (see Figure 8.4)

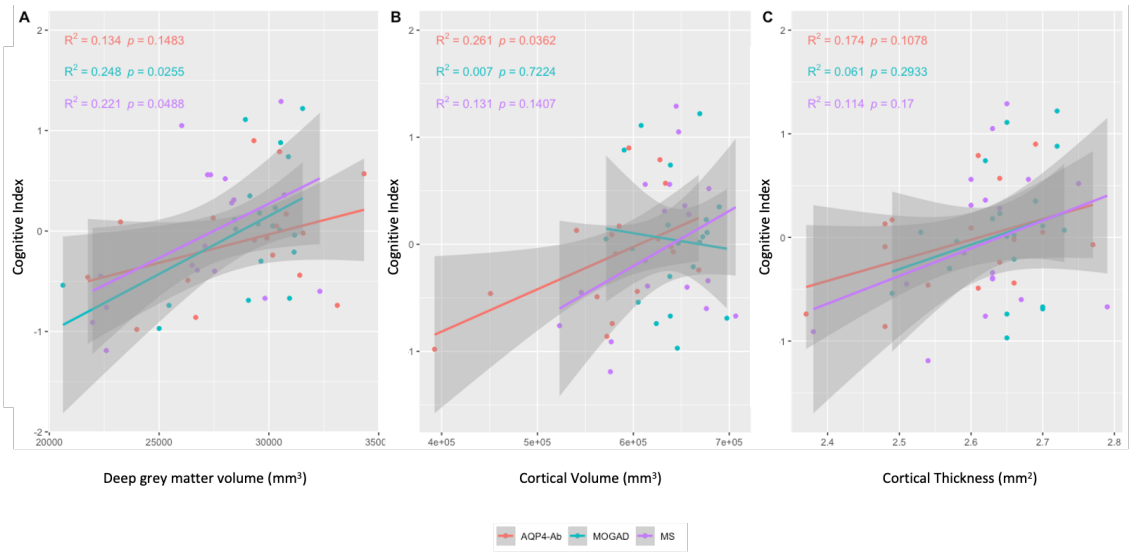


Figure 8.4 The association between cognitive index and the grey matter structure measures in the three disease groups. *The graph represents the regression line in the three disease groups, in grey the standard error.*

	MOGAD	NMOSD-AQP4	MS
Cognitive Index			
Verbal Memory	NS	NS	NS
Visual Memory			
Attention and Concentration	NS	NS	NS
Executive functions			

Figure 8.5 representation of the significant association between the cognitive index/cognitive domain scores and the grey matter structure measures in the three disease groups*. Legend: Blue=deep grey matter structures, yellow=cortical volume/thickness.*

8.3.3 *Fatigue*

The scores are represented as estimated marginal mean (EMM) and standard error (SE), The comparisons are represented as estimate [standard error] and p-value.

As both anxiety and depression are associated with fatigue total score, in a univariable linear model (anxiety estimate 1.37 [0.51], p=0.009, depression estimate 4.13 [0.56], p<0.001) they were both included in the fatigue linear model, together with age and sex.

The comparison of the fatigue total score across disease, showed that among disease group, MOGAD has the lowest score (30.2 [3.18]), while MS had the highest score (MS 36.7 [3.10]; NMOSD-AQP4 30.4 [3.74], HC 15.3 [3.37]).

The comparison across groups showed a significant higher score in MOGAD and MS, compared to HC, and a trend towards significance in NMOSD-AQP4 compared to HC (see Table 8.24).

Table 8.4 Fatigue score comparisons, Bonferroni corrected, across groups.

Total Fatigue score			
	Estimates	*SE*	*p-value*
AQP4-Ab vs HC	15.13	5.67	0.059*
AQP4-Ab vs MOGAD	0.272	5.18	0.999
AQP4-Ab vs MS	-6.27	4.84	0.999
HC vs MOGAD	-14.86	4.71	**0.015**
HC vs MS	-21.40	4.81	**0.0002**
MOGAD vs MS	-6.54	4.45	0.883

*Legend: AQP4-Ab=NMOSD-AQP4, SE=standard error. *a trend towards significance, in bold significant results.*

The cognitive fatigue score was significantly different in MS when compared to HC (MS 16.40 [1.58], MOGAD 12.91 [1.60], NMOSD-AQP4 11.66 [1.93], HC 7.48 [1.85]).

See Table 8.5 for across group comparisons.

Table 8.5 Cognitive fatigue score comparisons, Bonferroni corrected, across groups

	Cognitive Fatigue score		
	Estimates	*SE*	*p-value*
AQP4-Ab vs HC	4.18	2.88	0.915
AQP4-Ab vs MOGAD	-1.26	2.63	0.999
AQP4-Ab vs MS	-4.74	2.49	0.371
HC vs MOGAD	-5.43	2.38	0.158
HC vs MS	-8.92	2.44	**0.003**
MOGAD vs MS	-3.48	2.26	0.767

Legend: AQP4-Ab=NMOSD-AQP4, SE=standard error. In bold significant results.

The fatigue physical score was higher in MS (MS 17.00 [1.62], NMOSD-AQP4 16.3 [1.99], MOGAD 13.9 [1.65], HC 5.9 [1.90] and was significantly different in the three disease groups when compared to the HC (see Table 8.6).

Table 8.6 Physical fatigue score comparisons, Bonferroni corrected, across groups

	Physical Fatigue score		
	Estimates	*SE*	*p-value*
AQP4-Ab vs HC	10.373	2.97	**0.005**
AQP4-Ab vs MOGAD	2.336	2.71	0.999
AQP4-Ab vs MS	-0.722	2.56	0.999
HC vs MOGAD	-8.038	2.45	**0.011**
HC vs MS	-11.096	2.51	**0.0003**
MOGAD vs MS	-3.058	2.33	0.999

Legend: AQP4-Ab=NMOSD-AQP4, SE=standard error. In bold significant results.

The psychosocial fatigue score was higher in MOGAD (MOGAD 2.96 [0.49], NMOSD-AQP4 2.49 [0.59], MS 2.77 [0.48], HC 1.57 [0.565] but was not significantly different across groups (see Table 8.7).

Table 8.7 Psychosocial fatigue score comparisons, Bonferroni corrected, across groups

	Psychosocial Fatigue score		
	Estimates	*SE*	*p-value*
AQP4-Ab vs HC	0.918	0.88	0.999
AQP4-Ab vs MOGAD	-0.473	0.81	0.999
AQP4-Ab vs MS	-0.279	0.76	0.999
HC vs MOGAD	-1.391	0.73	0.368
HC vs MS	-1.197	0.75	0.683
MOGAD vs MS	0.194	0.70	0.999

Legend: AQP4-Ab=NMOSD-AQP4, SE=standard error.

8.3.4 *Fatigue: the role of grey matter*

Given the association of cognition with structural grey matter volume and the influence of fatigue on cognition in MOGAD and MS, the role of grey matter measures and fatigue was explored.

Functional connectivity measures

A voxel-wise correlation of every RSN of interest with the total fatigue score, the cognitive fatigue score, and the physical fatigue score, was tested in each disease group (the psychosocial fatigue score was not investigated as was not significantly different across groups, as shown in the previous section).

The voxel-wise correlation analysis of each RSN with fatigue score (total fatigue, cognitive fatigue, physical fatigue) did not show significant clusters.

Structural MRI measures

The association between fatigue scores and grey matter structures was explored in each disease group separately.

MOGAD group: there is a negative significant association between the DGM volumes and total fatigue score (R^2=0.276, p=0.017), which is driven by the cognitive fatigue score (R^2=0.503, p<0.001). The physical fatigue score and psychosocial fatigue scores are not significantly associated (R^2=0.110, p=0.165 and R^2=0.058, p=0.319 respectively).

There are no associations between fatigue scores and cortical volume (total fatigue R^2=0.125, p=0.127; cognitive fatigue R^2=0.137, p=0.119, physical fatigue R^2=0.131, p=0.128; psychosocial fatigue R^2=0.004, p=0.797), and fatigue scores and cortical thickness (total fatigue R^2=0.032, p=0.452; cognitive fatigue R^2=0.148, p=0.103, physical fatigue R^2=0.007, p=0.742; psychosocial fatigue R^2=0.012, p=0.655).

NMOSD-AQP4 group: there were no significant associations between fatigue scores and DGM volumes (total fatigue R^2=0.036, p=0.464; cognitive fatigue R^2=0.077, p=0.297,

physical fatigue R^2=0.019, p=0.616; psychosocial fatigue R^2=0.177, p=0.105), fatigue scores and cortical volume (total fatigue R^2=0.000, p=0.933; cognitive fatigue R^2=0.001, p=0.909, physical fatigue R^2=0.002, p=0.885; psychosocial fatigue R^2=0.048, p=0.417), fatigue scores and cortical thickness (total fatigue R^2=0.003, p=0.852; cognitive fatigue R^2=0.002, p=0.874, physical fatigue R^2=0.005, p=0.809; psychosocial fatigue R^2=0.011, p=0.711).

MS group: there were no significant associations between fatigue scores and DGM volumes (total fatigue R^2=0.039, p=0.433; cognitive fatigue R^2=0.016, p=0.6152, physical fatigue R^2=0.046, p=0.390; psychosocial fatigue R^2=0.041, p=0.422), fatigue scores and cortical volume (total fatigue R^2=0.035, p=0.455; cognitive fatigue R^2=0.035, p=0.460, physical fatigue R^2=0.017, p=0.601; psychosocial fatigue R^2=0.051, p=0.368), fatigue scores and cortical thickness (total fatigue R^2=0.002, p=0.877; cognitive fatigue R^2=0.000, p=0.961, physical fatigue R^2=0.003, p=0.834; psychosocial fatigue R^2=0.003, p=0.835) (see Figure 8.6).

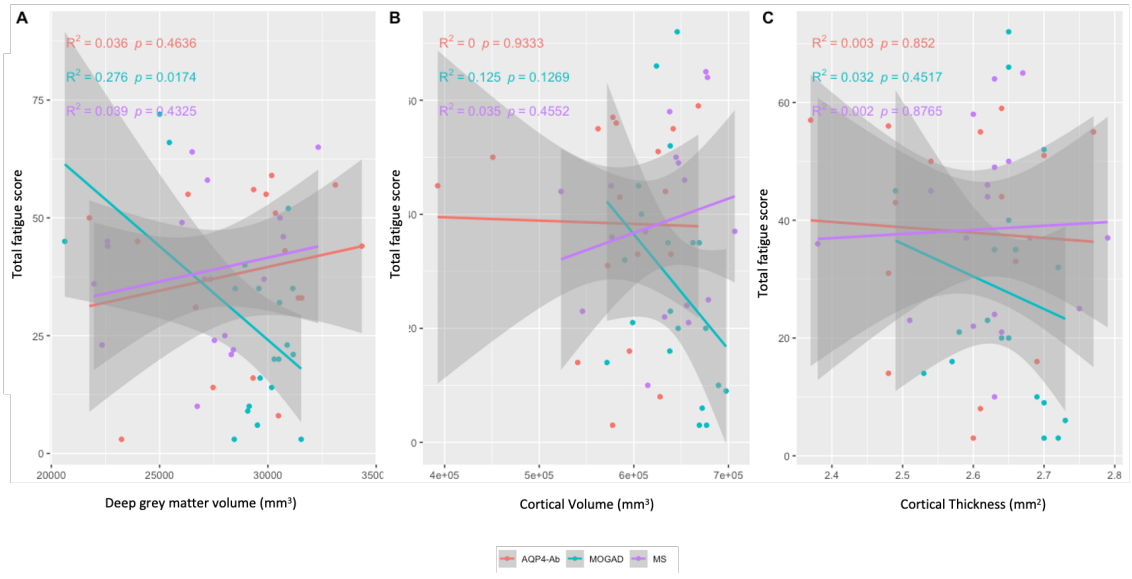


Figure 8.6 The association between fatigue score and grey matter volume measures. *The graph represents the regression line in the three disease groups, in grey the standard error.*

8.3.5 *The influence of fatigue, depression, and anxiety on cognition*

Given the presence of fatigue and mood disturbances in MOGAD and NMOSD-AQP4 participants, the influence of fatigue, anxiety and depression on cognition was investigated.

The total fatigue score was associated with global cognitive index score in MOGAD (R^2=0.226, p=0.0342) and NMOSD-AQP4 (R^2=0.247, p=0.0425), but not in MS (R^2=0.005, p=0.7889) (see Figure 8.7A). In particular, the cognitive fatigue score associated with cognition in both NMOSD-AQP4 and MOGAD (see Figure 8.7B), while physical fatigue score was not significantly associated (MOGAD R^2=0.135, p=0.1211; NMOSD-AQP4 R^2=0.131, p=0.1688; MS R^2=0.00, p=0.9569). There was a trend towards significance of psychosocial fatigue and the global cognitive index score in the MOGAD participants (R^2=0.195, p=0.0582) and no significant association in NMOSD-AQP4 and MS (R^2=0.133, p=0.1654, MS R^2=0.151, p=0.1108).

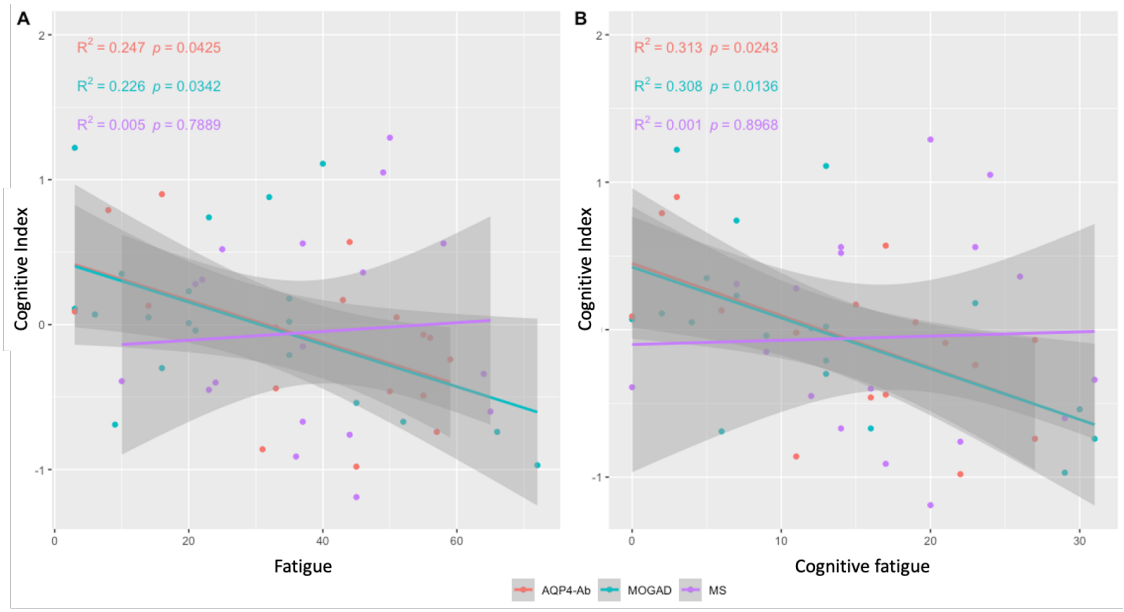


Figure 8.7 The association between cognitive index and fatigue score (A total fatigue B cognitive fatigue). *The graph represents the regression line in the three disease groups, in grey the standard error.*

No associations were found between anxiety and the global cognitive index in any of the three diseases (MOGAD R^2=0.072, p=0.2812, NMOSD-AQP4 R^2=0.163, p=0.1082, MS R^2=0.011, p=0.6819), while depression was associated with the cognitive index in the MOGAD group (R^2=0.262, p=0.03), and at a trend level, in the NMOSD-AQP4 group (R^2=0.203, p=0.0696). No association was found in the MS group (R^2=0.117, p=0.1648).

8.4 Discussion

In this chapter the presence of cognitive impairment and fatigue, and the role of grey matter in each, were investigated in MOGAD, NMOSD-AQP4, and MS participants. Additionally, the influence of anxiety and depression were also considered.

The study of the cognitive function showed that MOGAD and NMOSD-AQP4 participants with cognitive impairment, had a preferential brain involvement, and most of them had associated fatigue as well as clinically significant anxiety/depression. Overall, the cognitively impaired MS participants had lower cognitive index compared to the other groups, and none of them presented with clinically significant anxiety/depression, but all of them presented with fatigue.

The most affected cognitive domain in the cognitively impaired participants was visual memory in both MOGAD and NMOSD-AQP4 and learning and verbal memory in MS. In addition, MOGAD participants also presented impairment of the executive function, mainly driven by a significantly low WLG score.

Interestingly, cognitive fatigue and depression scores were associated with cognition in MOGAD and NMOSD-AQP4, but not in MS.

Finally, RSNs were not able to discriminate among cognitively impaired and preserved in the three disease groups, and the voxel-wise analysis did not show a significant association with the cognitive domain scores.

In the MOGAD group deep grey matter showed a significant association with global cognitive index, visual memory, and executive function (the cognitive domains mostly affected in MOGAD). In NMOSD-AQP4 cognitive function and visual memory are mostly associated with cortical volume, while in MS the global cognitive score is associated with deep grey matter (similarly to MOGAD) (see Table 8.8).

Table 8.8 Summary of the key-findings

	MOGAD	***NMOSD-AQP4***	***MS***
Cognitive Index	Brain involvement common in all the four participants (thalami lesions described in the acute phase or in remission).	Brain involvement (two participants with non-specific lesions).	Lowest global cognitive index, compared to other diseases.
Cognitive domain affected	Executive function and visual memory	Visual memory	Verbal memory
MRI findings	Global cognitive index associated with deep grey matter volume	Global cognitive index associated with cortex volume	Global cognitive index associated with deep grey matter volume
Fatigue and mood outcomes	Higher physical fatigue score Cognitive fatigue and depression are associated with cognitive function and deep grey matter structure	Higher physical fatigue score Cognitive fatigue and depression are associated with cognitive function	Higher fatigue score, especially cognitive fatigue. No association with cognitive function

The total fatigue score is higher in MS, as expected, and is mainly driven by the cognitive fatigue component, while in MOGAD and NMOSD-AQP4, physical fatigue component is the main discriminant, compared to HC.

Resting state connectivity measures were not able to discriminate between fatigued and non-fatigued participants across groups, while the deep grey matter volume was associated with total fatigue score in both the primary demyelinating disease, i.e.,

MOGAD and MS. In particular, in MOGAD an association with cognitive fatigue was also found. No associations were found in the NMOSD-AQP4 group.

Chapter 2 study showed that about half of the ADEM/ADEM-like patients were left with cognitive symptoms and most of them presented with lesions in the deep grey matter acutely.

This observation led to the hypothesis that cognition was affected in MOGAD patients with brain involvement, although studies systematically assessing cognition were lacking. This study showed for the first time, using a cognitive battery standardized for demyelinating disease (MS), that MOGAD participants with brain involvement, can be left with cognitive impairment and fatigue, and that cognitive fatigue can influence the cognitive performance. The association of both cognition and fatigue with deep grey matter structure is of particular interest, as in the previous chapters it was shown that lower deep grey matter was the only abnormal pathological change in MOGAD and was not associated with physical disability (i.e., EDSS).

A recent MRI study, using Montreal Cognitive Assessment (MoCA), SDMT and California verbal learning test (CVLT) showed an association in MOGAD with left superior temporal gyrus/insula and left hippocampus/parahippocampal gyrus and cognitive score. Although their conclusions are mostly in line with the findings presented in this chapter, the use of a battery not standardised for demyelinating disease and the use of uncorrected scores limits the robustness of these results (Zhuo et al., 2020). MoCA is a battery mainly assessing the cortical function and has been deemed as not sensitive nor specific to detect cognitive impairment in MS (McNicholas et al., 2018). As MOGAD is a primary demyelinating disease, it is plausible that the cognitive impairment pattern is

more subcortical than cortical (as it happens in MS), therefore MoCA may not be able to capture the full cognitive performance.

Therefore, a comprehensive battery able to capture all subcortical domains, such as BRB-N is recommended. Cognitive impairment has been described in paediatric MOGAD cohorts, ranging from 10 to 50% of cases, and mostly associated with ADEM/ADEM-like phenotype (Armangue et al., 2020; Bruijstens et al., 2020a; Hacohen et al., 2018a; Hacohen et al., 2018b).

A recent study, investigating the academic performance as a proxy of cognitive impairment in a cohort of paediatric MOGAD, showed that cognitive impairment was present in MOGAD children with ADEM phenotype and associated with radiological deep grey matter involvement (putamen and thalami) (Deiva et al., 2020), in line with the findings presented in this chapter in an adult population. A case report of adult MOGAD patient with brain involvement has shown that cognition can be present in an adult patient with MOGAD and can be progressive and associated with a vasculitis-like pattern, suggesting a possible pathological mechanism (Baba et al., 2019).

It is not surprising that executive function is the most affected domain, especially when assessing the verbal fluency. It has been shown that verbal fluency, is anchored to the connection between the basal ganglia and the prefrontal cortex (Fu et al., 2002). One hypothesis is that in MOGAD there is atrophy of the basal ganglia which can cause secondary disconnection of the fronto-striatal pathway.

This study shows that in AQP4-Ab positive participants with brain involvement cognitive impairment may be present and that the global cognitive index is associated with cortical volume rather than the deep grey matter structure, as seen in MS and MOGAD. As was demonstrated in the volumetric chapter, deep grey matter structures were not significantly

lower in NMOSD-AQP4, but the cortical volume was lower, at a trend level, compared to HC.

Two possible mechanisms may coexist and explain the cortical involvement. First, the presence of white matter lesions can cause a secondary disconnection at the level of the cortex, with consequent axonal loss, similar to what has been described in MS (Geurts and Barkhof, 2008). Secondly, as the cortex is one of the areas of the brain richest in AQP4 water channels, it is possible that the disruption of water homeostasis, due to the presence of antibodies directed against the cortex water-channel, is the key pathological mechanism and may explain the reduction of volume and the consequent correlation with cognitive impairment (Popescu et al., 2010). The relationship between cognitive function and involvement of the cortex was previously demonstrated in a study describing the prevalence of cognitive impairment and the associated pathological findings in NMOSD-AQP4 participants. This study showed that cognitive impairment was present and the cortex showed loss of AQP4-Ab immunoreactivity and cortical neuronal loss, without demyelination (Saji et al., 2013), suggesting that the involvement of the cortex may underlie the reduced cognitive performance seen in NMOSD-AQP4.

This association was also supported by mice studies, where the link between AQP4-Ab and cognition has been explored. They demonstrated that AQP4-Ab can inhibit neural plasticity, thus affecting spatial memory consolidation which interestingly is the most affected domain in the NMOSD-AQP4 cohort describe in this chapter (Scharfman and Binder, 2013; Skucas et al., 2011).

MS participants in our cohort showed a preferential impairment of the verbal memory and the global cognitive index score was associated with deep grey matter volume loss. Cognitive impairment in MS is well known and described and is present in 65-70% of patients (Messina and Patti, 2014). Cognitive dysfunction in MS is a dynamic process and

it is determined by a temporal sequence of impairment of cognitive domain, where memory and executive function impairment are prevalent in the later stage (Wojcik et al., 2021). A longitudinal study showed that in MS at baseline the main MRI correlate of cognition was the deep grey matter, while the main predictor of future worsening was the cortical volume (Eijlers et al., 2018). This is also in line with a recent study, showing that deep grey matter is involved in the early stage and in patient with mild impairment, while the involvement of the cortex is prevalent in patients with severe, multidomain cognitive impairment (De Meo et al., 2021). It can be postulated that as this cohort is relatively young and with low disability, the deep grey matter atrophy is associated with the global cognitive score, while when focussing on memory and executive function, which are usually impaired in the later stages, the association with cortex measures emerged.

Surprisingly, impairment of the information processing speed, which is thought generally to be the most affected domain in the early stage of MS, was not affected in this cohort. As information processing speed can be influenced by cognitive reserve and education, one possible explanation could be the relatively high education level of the studied cohort (Benedict et al., 2010). However, another recent study also found no abnormality in information processing speed in a group of patients with minimal impairment, challenging the postulate that impaired information processing speed precedes memory impairment (De Meo et al., 2021).

Interestingly, in this cohort, MOGAD and NMOSD-AQP4 cognitively impaired participants also showed clinically significant measures of depression and cognitive fatigue, in contrast with MS participants, where this association is lacking. This finding suggests, again, that cognition in MS is a different process related to specific pathological changes, while in NMOSD and MOGAD cognitive impairment may co-exist and be

influenced by other factors, possibly related to the higher disability (in NMOSD-AQP4) and mood disturbances (in MOGAD).

RS-fMRI has been largely studied in cognition and demyelinating diseases, with different methods and differing results (Han et al., 2020; Janssen et al., 2013; Rocca et al., 2012; Rocca et al., 2018; Savoldi et al., 2020; Tahedl et al., 2018; Wang et al., 2017). Surprisingly RS WNC and behavioural scores-network correlation were not significant in this cohort. These networks were selected because they were found to be impaired when compared to HC in the dual regression analysis in NMOSD-AQP4 and MS.

One possible explanation for the lack of association in NMOSD-AQP4 and MS could be the low statistical power, and the choice of a dual regression with high dimensionality (40 ICA), as this may have led to a parcellation of different hubs of the RSNs across many components, reducing the strength of the studied networks. However, as already demonstrated by the structural analysis, the role of the deep grey matter structure is central in cognition, and as demonstrated by previous studies, the choice of the high dimensionality was needed to identify the basal ganglia network (Griffanti et al., 2016). No associative networks were impaired in MOGAD, as shown in the previous chapter, and so it was expected that no associations would be found in this group.

In addition to the RS analysis limitation, there are other limitations in this study that need to be discussed further.

The effect of cognitive reserve and the influence on cognitive performance were not assessed. Cognitive reserve comprises premorbid intelligence, level of education and cognitively enriching leisure activities (e.g. reading, music) and, as it has been shown in MS, may influence the cognitive performance and slow the cognitive decline (Sumowski, 2015). In this study, the scores were corrected for years of education, however future

studies should include at least a pre-morbid intelligent quotient, to better estimate the frequency of cognitive impairment in NMOSD-AQP4 and MOGAD patients.

As this study was not designed to assess the frequency of cognitive impairment in the NMOSD-AQP4, MOGAD and MS population, it cannot address the real burden of cognition. Only population studies and a more diverse cohort (also including patients without brain or little brain involvement) can give a real estimate of cognition (Patti et al., 2015), however this study represents a possible paradigm of cognitive assessment in demyelinating conditions, which can be replicated in larger cohorts and generates hypotheses using a well-defined clinical cohort on which future studies can be built.

Finally, the lack of standardized normative value in a large healthy population, may affect the individual stratification of participants in cognitively impaired and preserved. However, in this cohort cognitive z-score were calculated using the age/sex/education years regression coefficients from the whole cohort, including both disease participants and healthy controls, thus reducing the age effect (as NMOSD-AQP4 are older than HC) and maintaining the variance of sex and education effect of the study groups.

8.5 Conclusion

In this chapter, for the first time, cognition was studied in MOGAD using a standardized cognitive battery for demyelinating disease, compared to NMOSD-AQP4 and MS, and correlated with functional and structural MRI measures. Cognitive performance is influenced by fatigue and depression in MOGAD and NMOSD-AQP4, not in MS.

The primary domains affected were executive function and visual memory in MOGAD, visual memory in NMOSD-AQP4, and verbal memory in MS. Cognition is associated with deep grey matter volume loss in MOGAD and MS, while is mainly driven by cortical

volume loss in NMOSD-AQP4. Resting state measures were not able to capture the pathological mechanism behind cognitive performance in the studied cohorts.

Longitudinal studies in NMOSD and MOGAD are needed to better elucidate if cognitive impairment is relapse-related or has a progressive component, as in MS.

These findings are useful for clinicians, as they suggest that cognition can be affected in MOGAD patients and so should be assessed by clinicians even when not reported by patients.

In the next chapter the clinical and MRI findings of this thesis will be discussed and their potential translation into clinical practice explored.

Acknowledgment

A special thanks to Prof Rao for kindly providing the "Manual for the Brief, Repeatable Battery of Neuropsychological Tests in Multiple Sclerosis" and the SRT forms.

9 Chapter 9 Discussion

9.1 Introduction

The findings of this thesis contribute to broadening our understanding of MOGAD, using a combined clinical and multimodal MRI approach. They also provide additional insights into the MRI pattern of NMOSD-AQP4 and MS.

In this final chapter the findings of the clinical and MRI study will be outlined in response to the main aims of the thesis outlined in Chapter 1.

9.2 Aims and key findings of the thesis

The aims of thesis are outlined in this section *(in italic)* and the main key findings are outlined below each aim.

a. *To describe the clinical characteristics and outcome in the MOGAD cohort*

   MOGAD patients have a good recovery from visual and physical disability compared to NMOSD-AQP4, although some of them can be left with sphincter, erectile dysfunction, and cognitive impairment, especially after the onset attack. The risk of relapse, assessed in an incident population, was moderate and higher within the first year from the onset attack, and can be reduced with short-term immunosuppression.

b. *To identify a distinct MRI pattern in MOGAD, compared to NMOSD-AQP4 and MS, using conventional and non-conventional MRI and to explore their relationship with disability measures i.e., EDSS and visual acuity.*

In MOGAD participants, deep grey matter atrophy was present and associated with persistent T2 lesions. In contrast, NMOSD-AQP4 patients showed a relative sparing of deep grey matter volumes, despite greater residual disability as compared with MOGAD patients. NMOSD-AQP4, but not MOGAD patients showed reduced FA in non-lesional tissue. MS participants showed both non lesional white and grey matter damage, and cortical lesions. Disability (EDSS) in NMOSD-AQP4 is associated with NAWM FA alone, with deep grey matter atrophy and female sex in MS, and with brainstem volume in MOGAD. Visual acuity was associated with optic chiasm volume reduction in NMOSD-AQP4 disease and with thalamic volume and female sex in MOGAD.

c. *To identify different patterns of abnormal resting state networks (RSNs) in the three CNS demyelinating diseases.*

In MOGAD, despite the good visual recovery, and the absence of structural and microstructural tissue damage, there is a reduced functional connectivity in the primary visual cortex. In NMOSD-AQP4 there is a broader involvement of the large brain networks (visual, salience, sensorimotor, DMN), possibly related to the higher level of disability (and tissue damage), while in MS, a preferential involvement of subcortical network was found (i.e., basal ganglia).

d. *To describe cognitive impairment and to explore structural and functional imaging correlates in MOGAD, NMOSD-AQP4 and MS.*

Cognitive performance is influenced by fatigue and depression in MOGAD and NMOSD-AQP4 but not in MS. A low cognitive score is associated with low deep grey matter volume in MOGAD and MS, while is mainly driven by low cortical volume in NMOSD-AQP4.

Table 9.1 : Summary of the key MRI findings.

	NMOSD-AQP4	MOGAD	MS
Global volume measures			
Brain Volume	↓	↔	↓
White Matter Volume	↓	↔	↓
Grey matter Volume	↓	↔	↓
3rd Ventricle Volume	↑	↑	↑
4th Ventricle Volume	↔	↔	↔
Grey matter measures			
Deep grey matter Volume	↓	↓↓	↓↓
Brainstem Volume	↓↓	↓↓†	↓↓
Cortex Volumes	↓↓†	↔	↔
Cortex Thickness	↓	↔	↓
Cortical lesions*	↔	↑	↑↑
Cortex MD	↔	↔	↑
Basal ganglia MD	↔	↔	↔
White matter measures			
Optic Chiasm Volume in ON	↓↓	↔	↔
Corpus Callosum Volume	↔	↔	↓
Lesion Volume*	↑	↑	↑↑
Lesion FA	↓↓	↓↓	↓↓
Lesion MD	↑↑	↑↑	↑↑
Lesion RD	↑↑	↑↑	↑↑
Lesion AD	↔	↔	↔
Normal appearing white matter FA	↓	↔	↓↓
Normal appearing white matter MD	↑	↔	↑

Normal appearing white matter RD	↑	↔	↑
Normal appearing white matter AD	↔	↔	↔
Functional RSN measures**			
Visual RSN	↓↓	↓↓	↓↓
Salience RSN	↓↓	↔	↔
Sensorimotor RSN	↓↓	↔	↔
Auditory RSN	↓↓	↔	↔
Basal Ganglia RSN	↔	↔	↓↓

*Legend: compared to HC ↔ no difference, ↓ lower but not significant; ↓↓† non-significantly lower, ↓↓ significantly lower; ↑ higher but not significant; ↑↑ significantly higher; *comparison across disease groups. **voxel-wise analysis comparisons.*

9.3 Towards a better understanding of MOGAD: filling the gaps

As outlined in Chapter 1, MOGAD has been recently recognised as a distinct condition and data are still limited. The body of work presented in this thesis has contributed to an improved clinical understanding of this condition, and to better defining disease-specific MRI patterns that differ when compared to NMOSD-AQP4 and MS, predominantly characterised by deep grey matter atrophy.

The main challenges and unmet needs described in Chapter 1, will be discussed in light of the thesis main findings. Although the thesis was not designed to specifically address these unmet needs, these new findings have the potential to prompt further studies:

a. Identifying a marker able to quantify the recovery

MOGAD patients tend to have a good recovery after relapse, despite the severity of the neurological symptoms is similar to NMOSD-AQP4. Understanding the difference may be of interest, as it can potentially help to better understand the mechanism behind it.

We found that in the remission stage, most of the MOGAD lesions tend to resolve, and that no NAWM damage is left. Persistent lesions are associated with deep grey matter atrophy.

One of the main debates is the utility of using short term immunosuppression in patients after a single attack. The use of an MRI outcome able to quantify the residual damage after the onset attack, may change the therapeutic approach. Being able to individually stratify the risk of further disabling relapses in each patient, based on the residual lesion load, may help to identify those patients that may benefit from a more aggressive immunosuppression after the onset attack.

b. Evaluating cognitive function

In this study for the first time the cognitive function has been explored in MOGAD, using a standardised cognitive battery, validated for demyelinating disease and it shows that cognitive impairment is present in patients with brain involvement, mainly driven by reduced executive dysfunction.

The basal ganglia atrophy, which is interestingly the only non-lesional tissue damage identified in MOGAD, is associated with cognitive impairment. This is similar to MS, where deep grey matter atrophy is also associated with cognitive impairment. However, in MS, verbal fluency is more affected and in MOGAD, fatigue also seems to play an important role in the performance of cognitive tasks.

c. Understanding the pathogenesis

Comparing and contrasting MOGAD to NMOSD-AQP4 and MS, can provide clues of the pathological mechanism underlying this condition. The MRI findings presented in this thesis are not sufficient to elucidate the pathology of MOGAD, but they certainly represent a stepping-stone to encourage future larger studies.

In this thesis it was demonstrated, for the first time, and confirmed by other studies published in the same period, that deep grey matter atrophy is present in MOGAD, despite the good clinical outcome and the low disability in the cohort and that it is associated with cognitive impairment. This has since been confirmed in studies focussing on spinal cord MRI, suggesting that grey matter pathology is central in MOGAD (Duan et al., 2021; Mariano et al., 2020; Zhuo et al., 2020). One hypothesis is that grey matter atrophy is dependent on the persistent lesions load, causing a disconnection and a secondary atrophy

of the grey matter. Recently, a MOGAD-associated vasculitis-like case has been described which was associated with progressive cognitive impairment. It may be that the basal ganglia are particularly sensitive to inflammatory damage, because of their proximity to vessels, and to the ventricles, where possibly the inflammatory markers accumulate. Future longitudinal studies may clarify if the cognitive impairment is relapse related, and thus dependent on the number of lesions, or if there is a progressive component.

9.4 Future steps: translating the findings into clinical practice

As discussed in Chapter 1, the thesis was set up to improve the understanding of MOGAD, but mostly to translate the observation into clinical practice. Some of these findings, have greater potential to be translated into clinical practice, while some, especially the non-conventional MRI findings, are still restricted to the research environment and require further studies. Nevertheless, novel hypotheses can be derived by these studies, and their translational potential can be discussed.

Chapter 2, together with other published clinical studies, has shown for the first time that the risk of further relapses can be reduced with at least 6 months of corticosteroid cover. This observation has now been implemented into the management of MOGAD in the specialised NMO clinical service. Additionally, being able to estimate the risk of further relapses has helped clinicians make more evidence-based management decisions and help patients understand their future and the rational for their treatment more clearly.

The clinical outcomes described in Chapter 2, have highlighted, for the first time, the presence of sphincter and erectile dysfunction in men, despite a good physical recovery,

prompting further studies to investigate this outcome (Li et al., 2020b; Mariano et al., 2019) and encourages more aggressive treatment of the acute attack.

The structural MRI study showed, using conventional MRI, that periventricular lesions can distinguish between Ab-mediated disease and MS, while cortical lesions have been described in both MS and MOGAD, and they are not present in NMOSD-AQP4. In light of these findings, the use of both T2 lesions and cortical lesions, can potentially help in distinguishing NMOSD-AQP4 and MOGAD.

2D FLAIR MRI, which are routinely used in clinical practice, associated with DIR sequence, can potentially distinguish between demyelinating diseases. The lack of periventricular lesions, and the presence of cortical/juxtacortical lesions, if confirmed in further larger studies, can point towards the diagnosis of MOGAD, and can be proposed as an MRI criterion, as diagnostic criteria are currently lacking.

The use of advanced MRI analysis showed that grey matter atrophy is present in MOGAD and MS, but not in NMOSD-AQP4. Similar to MS, the deep grey matter damage can be proposed as a possible outcome in future clinical trials (Gaetano et al., 2018). To date, no specific treatment for MOGAD is available and clinical trials are needed. Although the volumetric measures are not routinely used in clinical practice, in future the use of tools able to estimate the volumetric measures of the deep grey matter, can be implemented, and the volumetric information integrated in the radiology report, guiding the long-term management.

As discussed in Chapter 1, the quantitative and functional modalities require longer scanning times, and they currently do not have a role in clinical practice, except for diffusion imaging in stroke management. However, important considerations can be obtained by these findings.

The lack of NAWM damage found in MOGAD, is possibly associated to the good clinical outcome and the low disability of this population. As described in Chapter 4, one hypothesis is the presence of two type of lesions in MOGAD during the acute phase: a) the "non-demyelinating lesions" are the lesions that tend to resolve in the remission phase, possibly associated with oedema, b) the "demyelinating lesions" are the persistent lesions, which are possibly responsible for retrograde degeneration and the atrophy of the deep grey matter. Although the MRI findings need further validation and pathological correlation, this observation already represents a valid hypothesis for future MRI studies in larger cohorts, using more sophisticated diffusion measures, i.e., NODDI.

Similar to quantitative MRI, the functional MRI modality needs further research before being translated into clinical practice.

As RSNs have shown reproducibility in different cohorts, their use has been proposed as a possible marker of visual and physical disability. In Chapter 7 it was shown, for the first time that in MOGAD that, despite the good visual recovery there is abnormal cortical reorganization in the visual system. Studying the longitudinal changes in functional connectivity in response to repetitive optic neuritis, may improve the understanding of the good visual recovery in most of MOGAD patients, despite the severity of the visual loss during the acute attack. In the MOGAD cohort, higher "within network connectivity" in the salience network of patients with pain was found, and an adaptive reorganization of the salience network has been hypothesised, in contrast with NMOSD-AQP4, where the within salience network connectivity is lower in patients with pain and an association with chronic pain, was found. The salience network can be proposed as a marker to test pain medication or rehabilitation strategy in a clinical trial setting. Finally, the abnormal auditory network supports the recent findings of involvement of the auditory function in

NMOSD-AQP4 which is often neglected as a clinical outcome but should be studied further.

Evaluation of cognitive function in CNS demyelinating disease showed for the first time different pattern of grey matter volumetric correlates. Cognitive performance is influenced by fatigue and depression in MOGAD and NMOSD-AQP4, but not in MS. Executive function in MOGAD, visual memory in NMOSD-AQP4 and verbal memory in MS are the most affected domains. Cognition is associated with deep grey matter volume reduction in MOGAD and MS and is associated with cortical volume reduction in NMOSD-AQP4. These findings, although requiring further confirmation in larger cohorts, highlight the importance of testing the cognitive function routinely in MOGAD patients with brain involvement.

Recognising and managing sub-clinical cognitive impairment in this group of young patients should be better studied as it could potentially have positive effects on their overall quality of life.

9.4.1 *Integrating clinical management and research*

The Diagnostic and Advisory service for Neuromyelitis Optica in Oxford is a NHS nationally commissioned service, offering clinical care for people with Neuromyelitis optica and MOGAD.

This is a unique environment where clinical practice and research integrate, to improve the management of this rare condition, not only in a tertiary centre, but also locally.

Currently, all patients referred to the Neuromyelitis service are offered the opportunity to consent for a Research Tissue Bank study, where all the clinical, clinical MRI, serology and other clinically acquired data or specimens are stored.

This comprehensive dataset represents a unique opportunity to study a rare disease, as patients from all the UK are referred to the service.

The homogeneity of a single centre study using the same scanner and protocol, along with reliable diagnostic ability was an advantage for the set-up of the MRI studies presented in this thesis. However, to test the reproducibility of the observations of this thesis, a larger number of patients and prospective longitudinal studies are needed.

The Oxford NMO service already provides high quality medical care locally, through the outreach clinics and in collaboration with the referring neurologist ("satellite" services) in all the south of the UK.

In the future, the set-up of a research MRI dataset integrated with the Research Tissue Bank, involving the "satellite" centres, could represent an opportunity to offer patients clinical care and research locally.

9.5 Conclusions

The clinical and MRI studies from this thesis, represent some of the earliest studies directed at better understanding the pathological MRI changes behind MOGAD. The comprehensive clinical and MRI approach, investigating not only physical disability, but also the often-neglected cognitive function, added novelty to this body of work and builds hypotheses for future studies.

The findings from this thesis support the set-up of a MOGAD MRI data bank to validate these findings on a larger cohort. The collaboration of the "satellite" centres could represent an opportunity to offer patients innovative research in a local setting. Furthermore, this model can be applied to the international setting in order to establish a global, standardized MRI acquisition protocol across sites. Multi-centre collaborations

would lead to larger study cohorts where more sophisticated statistical analysis, i.e., machine learning, can be applied.

10 Bibliography

Abbott, R.A., et al., 2019. Normative data from linear and nonlinear quantile regression in CANTAB: Cognition in mid-to-late life in an epidemiological sample. Alzheimers Dement (Amst). 11**,** 36-44.

Aboul-Enein, F., et al., 2010. Diffuse white matter damage is absent in neuromyelitis optica. AJNR Am J Neuroradiol. 31**,** 76-9.

Akaishi, T., et al., 2016. MRI and retinal abnormalities in isolated optic neuritis with myelin oligodendrocyte glycoprotein and aquaporin-4 antibodies: a comparative study. J Neurol Neurosurg Psychiatry. 87**,** 446-8.

Akaishi, T., et al., 2021. Progression pattern of neurological disability with respect to clinical attacks in anti-MOG antibody-associated disorders. J Neuroimmunol. 351**,** 577467.

Alcaide-Leon, P., et al., 2018. Quantitative spinal cord MRI in radiologically isolated syndrome. Neurol Neuroimmunol Neuroinflamm. 5**,** e436.

Alexander, A.L., et al., 2007. Diffusion tensor imaging of the brain. Neurotherapeutics. 4**,** 316-29.

Amato, M.P., et al., 2006. The Rao's Brief Repeatable Battery and Stroop Test: normative values with age, education and gender corrections in an Italian population. Mult Scler. 12**,** 787-93.

Amiri, H., et al., 2018. Urgent challenges in quantification and interpretation of brain grey matter atrophy in individual MS patients using MRI. Neuroimage Clin. 19**,** 466-475.

Amiry-Moghaddam, M., Ottersen, O.P., 2003. The molecular basis of water transport in the brain. Nat Rev Neurosci. 4**,** 991-1001.

Andersson, J.L., Skare, S., Ashburner, J., 2003. How to correct susceptibility distortions in spin-echo echo-planar images: application to diffusion tensor imaging. Neuroimage. 20**,** 870-88.

Andersson, J.L.R., Sotiropoulos, S.N., 2016. An integrated approach to correction for off-resonance effects and subject movement in diffusion MR imaging. Neuroimage. 125**,** 1063-1078.

Armangue, T., et al., 2020. Associations of paediatric demyelinating and encephalitic syndromes with myelin oligodendrocyte glycoprotein antibodies: a multicentre observational study. Lancet Neurol. 19**,** 234-246.

Asgari, N., et al., 2011. A population-based study of neuromyelitis optica in Caucasians. Neurology. 76**,** 1589-95.

Assaf, Y., Johansen-Berg, H., Thiebaut de Schotten, M., 2019. The role of diffusion MRI in neuroscience. NMR Biomed. 32**,** e3762.

Asseyer, S., et al., 2020. Prodromal headache in MOG-antibody positive optic neuritis. Mult Scler Relat Disord. 40**,** 101965.

Azevedo, C.J., et al., 2015. Early CNS neurodegeneration in radiologically isolated syndrome. Neurol Neuroimmunol Neuroinflamm. 2**,** e102.

Baba, T., et al., 2019. MOG antibody disease manifesting as progressive cognitive deterioration and behavioral changes with primary central nervous system vasculitis. Mult Scler Relat Disord. 30**,** 48-50.

Backner, Y., et al., 2020. Cortical topological network changes following optic neuritis. Neurol Neuroimmunol Neuroinflamm. 7.

Banks, S.A., et al., 2020. Brainstem and cerebellar involvement in MOG-IgG-associated disorder versus aquaporin-4-IgG and MS. J Neurol Neurosurg Psychiatry.

Barbizet, J., Cany, E., 1968. Clinical and psychometrical study of a patient with memory disturbances. Int J Neurol. 7**,** 44-54.
Barkhof, F., et al., 1997. Comparison of MRI criteria at first presentation to predict conversion to clinically definite multiple sclerosis. Brain. 120 (Pt 11)**,** 2059-69.
Barkhof, F., 2002. The clinico-radiological paradox in multiple sclerosis revisited. Curr Opin Neurol. 15**,** 239-45.
Baumann, M., et al., 2018. MRI of the first event in pediatric acquired demyelinating syndromes with antibodies to myelin oligodendrocyte glycoprotein. J Neurol. 265**,** 845-855.
Baumann, M., et al., 2020. E.U. paediatric MOG consortium consensus: Part 2 - Neuroimaging features of paediatric myelin oligodendrocyte glycoprotein antibody-associated disorders. Eur J Paediatr Neurol. 29**,** 14-21.
Beckmann, C.F., Smith, S.M., 2004. Probabilistic independent component analysis for functional magnetic resonance imaging. IEEE Trans Med Imaging. 23**,** 137-52.
Behrens, T.E., et al., 2003. Characterization and propagation of uncertainty in diffusion-weighted MR imaging. Magn Reson Med. 50**,** 1077-88.
Behrens, T.E., et al., 2007. Probabilistic diffusion tractography with multiple fibre orientations: What can we gain? Neuroimage. 34**,** 144-55.
Benedict, R.H., et al., 2010. Cognitive reserve moderates decline in information processing speed in multiple sclerosis patients. J Int Neuropsychol Soc. 16**,** 829-35.
Benedict, R.H.B., et al., 2020. Cognitive impairment in multiple sclerosis: clinical management, MRI, and therapeutic avenues. Lancet Neurol. 19**,** 860-871.
Bennett, J.L., et al., 2009. Intrathecal pathogenic anti-aquaporin-4 antibodies in early neuromyelitis optica. Ann Neurol. 66**,** 617-29.
Bennett, J.L., et al., 2015. Neuromyelitis optica and multiple sclerosis: Seeing differences through optical coherence tomography. Mult Scler. 21**,** 678-88.
Berger, T., et al., 2003. Antimyelin antibodies as a predictor of clinically definite multiple sclerosis after a first demyelinating event. N Engl J Med. 349**,** 139-45.
Bigaut, K., et al., 2019. Resting-state functional MRI demonstrates brain network reorganization in neuromyelitis optica spectrum disorder (NMOSD). PLoS One. 14**,** e0211465.
Bijsterbosch, J., Smith, S., Beckmann, C., 2017. Introduction to Resting State fMRI Functional Connectivity, Vol.
Biotti, D., et al., 2017. Optic neuritis in patients with anti-MOG antibodies spectrum disorder: MRI and clinical features from a large multicentric cohort in France. J Neurol. 264**,** 2173-2175.
Biswal, B., et al., 1995. Functional connectivity in the motor cortex of resting human brain using echo-planar MRI. Magn Reson Med. 34**,** 537-41.
Blanc, F., et al., 2012. White matter atrophy and cognitive dysfunctions in neuromyelitis optica. PLoS One. 7**,** e33878.
Bonnan, M., Cabre, P., 2017. Meningeal and vestibulocochlear nerve enhancement in neuromyelitis optica. Eur J Neurol. 24**,** e89-e90.
Bonnan, M., et al., 2018. Short delay to initiate plasma exchange is the strongest predictor of outcome in severe attacks of NMO spectrum disorders. J Neurol Neurosurg Psychiatry. 89**,** 346-351.
Bot, J.C., et al., 2004. Spinal cord abnormalities in recently diagnosed MS patients: added value of spinal MRI examination. Neurology. 62**,** 226-33.

Boyle, L.H., et al., 2007. Splice variation in the cytoplasmic domains of myelin oligodendrocyte glycoprotein affects its cellular localisation and transport. J Neurochem. 102**,** 1853-1862.
Brilot, F., et al., 2009. Antibodies to native myelin oligodendrocyte glycoprotein in children with inflammatory demyelinating central nervous system disease. Ann Neurol. 66**,** 833-42.
Brownlee, W.J., et al., 2019. Early imaging predictors of long-term outcomes in relapse-onset multiple sclerosis. Brain. 142**,** 2276-2287.
Bruijstens, A.L., et al., 2020a. E.U. paediatric MOG consortium consensus: Part 4 - Outcome of paediatric myelin oligodendrocyte glycoprotein antibody-associated disorders. Eur J Paediatr Neurol. 29**,** 32-40.
Bruijstens, A.L., et al., 2020b. HLA association in MOG-IgG- and AQP4-IgG-related disorders of the CNS in the Dutch population. Neurol Neuroimmunol Neuroinflamm. 7.
Brunner, C., et al., 1989. Differential ultrastructural localization of myelin basic protein, myelin/oligodendroglial glycoprotein, and 2',3'-cyclic nucleotide 3'-phosphodiesterase in the CNS of adult rats. J Neurochem. 52**,** 296-304.
Buckner, R.L., Andrews-Hanna, J.R., Schacter, D.L., 2008. The brain's default network: anatomy, function, and relevance to disease. Ann N Y Acad Sci. 1124**,** 1-38.
Buschke, H., Fuld, P.A., 1974. Evaluating storage, retention, and retrieval in disordered memory and learning. Neurology. 24**,** 1019-25.
Cacciaguerra, L., et al., 2019. Brain and cord imaging features in neuromyelitis optica spectrum disorders. Ann Neurol. 85**,** 371-384.
Cai, H., et al., 2017. Subregional structural and connectivity damage in the visual cortex in neuromyelitis optica. Sci Rep. 7**,** 41914.
Calabrese, M., et al., 2010a. Imaging distribution and frequency of cortical lesions in patients with multiple sclerosis. Neurology. 75**,** 1234-40.
Calabrese, M., Filippi, M., Gallo, P., 2010b. Cortical lesions in multiple sclerosis. Nat Rev Neurol. 6**,** 438-44.
Calabrese, M., et al., 2012. No MRI evidence of cortical lesions in neuromyelitis optica. Neurology. 79**,** 1671-6.
Castillo-Torres, S.A., et al., 2020. Case of neuromyelitis optica: bilateral sensorineural hearing loss and transverse myelopathy following intrathecal chemotherapy. BMJ Case Rep. 13.
Cauda, F., et al., 2009. Altered resting state in diabetic neuropathic pain. PLoS One. 4**,** e4542.
Caverzasi, E., et al., 2020. Imaging correlates of visual function in multiple sclerosis. PLoS One. 15**,** e0235615.
Ceccarelli, A., et al., 2007. Normal-appearing white and grey matter damage in MS. A volumetric and diffusion tensor MRI study at 3.0 Tesla. J Neurol. 254**,** 513-8.
Cercignani, M., Gandini Wheeler-Kingshott, C., 2019. From micro- to macro-structures in multiple sclerosis: what is the added value of diffusion imaging. NMR Biomed. 32**,** e3888.
Cercignani, M., et al., 2021. Cognitive fatigue in multiple sclerosis is associated with alterations in the functional connectivity of monoamine circuits. Brain Commun. 3**,** fcab023.
Cerqueira, J.J., et al., 2018. Time matters in multiple sclerosis: can early treatment and long-term follow-up ensure everyone benefits from the latest advances in multiple sclerosis? J Neurol Neurosurg Psychiatry. 89**,** 844-850.

Chanson, J.B., et al., 2013. White matter volume is decreased in the brain of patients with neuromyelitis optica. Eur J Neurol. 20**,** 361-7.
Charcot, Oliver, T., 1876. Sclerosis in Scattered Patches. Edinb Med J. 22**,** 414-421.
Chavarro, V.S., et al., 2020. Visual system damage and network maladaptation are associated with cognitive performance in neuromyelitis optica spectrum disorders. Mult Scler Relat Disord. 45**,** 102406.
Chou, I.J., et al., 2019. Reduced Myelin Signal in Normal-appearing White Matter in Neuromyelitis Optica Measured by 7T Magnetic Resonance Imaging. Sci Rep. 9**,** 14378.
Ciccarelli, O., et al., 2013. Low myo-inositol indicating astrocytic damage in a case series of neuromyelitis optica. Ann Neurol. 74**,** 301-5.
Cleeland, C.S., Ryan, K.M., 1994. Pain assessment: global use of the Brief Pain Inventory. Ann Acad Med Singap. 23**,** 129-38.
Cobo-Calvo, A., et al., 2018. Clinical spectrum and prognostic value of CNS MOG autoimmunity in adults: The MOGADOR study. Neurology. 90**,** e1858-e1869.
Cobo-Calvo, A., et al., 2019. Evaluation of treatment response in adults with relapsing MOG-Ab-associated disease. J Neuroinflammation. 16**,** 134.
Cobo-Calvo, A., et al., 2021. Clinical Features and Risk of Relapse in Children and Adults with Myelin Oligodendrocyte Glycoprotein Antibody-Associated Disease. Ann Neurol. 89**,** 30-41.
Cole, D.M., Smith, S.M., Beckmann, C.F., 2010. Advances and pitfalls in the analysis and interpretation of resting-state FMRI data. Front Syst Neurosci. 4**,** 8.
Collorone, S., et al., 2020. Reduced neurite density in the brain and cervical spinal cord in relapsing-remitting multiple sclerosis: A NODDI study. Mult Scler. 26**,** 1647-1657.
Compston, A., Coles, A., 2008. Multiple sclerosis. Lancet. 372**,** 1502-17.
Correale, J., Fiol, M., 2004. Activation of humoral immunity and eosinophils in neuromyelitis optica. Neurology. 63**,** 2363-70.
Cortese, R., et al., 2019. Advances in brain imaging in multiple sclerosis. Ther Adv Neurol Disord. 12**,** 1756286419859722.
Cree, B.A.C., et al., 2019. Inebilizumab for the treatment of neuromyelitis optica spectrum disorder (N-MOmentum): a double-blind, randomised placebo-controlled phase 2/3 trial. Lancet. 394**,** 1352-1363.
Daams, M., et al., 2016. Multi-parametric structural magnetic resonance imaging in relation to cognitive dysfunction in long-standing multiple sclerosis. Mult Scler. 22**,** 608-19.
Dale, A.M., Fischl, B., Sereno, M.I., 1999. Cortical surface-based analysis. I. Segmentation and surface reconstruction. Neuroimage. 9**,** 179-94.
de Groot, M., et al., 2013. Improving alignment in Tract-based spatial statistics: evaluation and optimization of image registration. Neuroimage. 76**,** 400-11.
De Meo, E., et al., 2021. Identifying the Distinct Cognitive Phenotypes in Multiple Sclerosis. JAMA Neurol. 78**,** 414-425.
de Mol, C.L., et al., 2020. The clinical spectrum and incidence of anti-MOG-associated acquired demyelinating syndromes in children and adults. Mult Scler. 26**,** 806-814.
de Seze, J., et al., 2010. Magnetic resonance spectroscopy evaluation in patients with neuromyelitis optica. J Neurol Neurosurg Psychiatry. 81**,** 409-11.
De Stefano, N., et al., 2010. Assessing brain atrophy rates in a large population of untreated multiple sclerosis subtypes. Neurology. 74**,** 1868-76.

Deiva, K., et al., 2020. Risk factors for academic difficulties in children with myelin oligodendrocyte glycoprotein antibody-associated acute demyelinating syndromes. Dev Med Child Neurol.
DeLuca, G.C., et al., 2015. Cognitive impairment in multiple sclerosis: clinical, radiologic and pathologic insights. Brain Pathol. 25**,** 79-98.
Dendrou, C.A., Fugger, L., Friese, M.A., 2015. Immunopathology of multiple sclerosis. Nat Rev Immunol. 15**,** 545-58.
Devic, E., 1894. Myelite subaigue compliquee de neurite optique. Bull Med 8**,** 1033-1034.
Di Martino, A., et al., 2008. Functional connectivity of human striatum: a resting state FMRI study. Cereb Cortex. 18**,** 2735-47.
Dobryakova, E., et al., 2015. The dopamine imbalance hypothesis of fatigue in multiple sclerosis and other neurological disorders. Front Neurol. 6**,** 52.
Dos Passos, G.R., et al., 2018. MOG-IgG-Associated Optic Neuritis, Encephalitis, and Myelitis: Lessons Learned From Neuromyelitis Optica Spectrum Disorder. Front Neurol. 9**,** 217.
Duan, Y., et al., 2012. Comparison of grey matter atrophy between patients with neuromyelitis optica and multiple sclerosis: a voxel-based morphometry study. Eur J Radiol. 81**,** e110-4.
Duan, Y., et al., 2021. Brain structural alterations in MOG antibody diseases: a comparative study with AQP4 seropositive NMOSD and MS. J Neurol Neurosurg Psychiatry.
Dubey, D., et al., 2019. Clinical, Radiologic, and Prognostic Features of Myelitis Associated With Myelin Oligodendrocyte Glycoprotein Autoantibody. JAMA Neurol. 76**,** 301-309.
Dutra, B.G., et al., 2018. Neuromyelitis Optica Spectrum Disorders: Spectrum of MR Imaging Findings and Their Differential Diagnosis. Radiographics. 38**,** 169-193.
Eijlers, A.J.C., et al., 2018. Predicting cognitive decline in multiple sclerosis: a 5-year follow-up study. Brain. 141**,** 2605-2618.
Eshaghi, A., et al., 2016. Gray matter MRI differentiates neuromyelitis optica from multiple sclerosis using random forest. Neurology. 87**,** 2463-2470.
Eshaghi, A., et al., 2018. Deep gray matter volume loss drives disability worsening in multiple sclerosis. Ann Neurol. 83**,** 210-222.
Eskandarieh, S., et al., 2018. Environmental risk factors in neuromyelitis optica spectrum disorder: a case-control study. Acta Neurol Belg. 118**,** 277-287.
Estrada, K., et al., 2018. A whole-genome sequence study identifies genetic risk factors for neuromyelitis optica. Nat Commun. 9**,** 1929.
Ferraro S, K.-B.B., Tench CR, Yao S, Nigri A, Demichelis G, Bruzzone MG, Becker B, 2021. Dysregulated anterior insula reactivity as robust functional biomarker for chronic pain – convergent evidence from neuroimaging meta-analysis.
Filippatou, A.G., et al., 2020. AQP4-IgG and MOG-IgG Related Optic Neuritis-Prevalence, Optical Coherence Tomography Findings, and Visual Outcomes: A Systematic Review and Meta-Analysis. Front Neurol. 11**,** 540156.
Filippi, M., et al., 1999. MRI and magnetization transfer imaging changes in the brain and cervical cord of patients with Devic's neuromyelitis optica. Neurology. 53**,** 1705-10.
Filippi, M., Rocca, M.A., 2004. MR imaging of Devic's neuromyelitis optica. Neurol Sci. 25 Suppl 4**,** S371-3.
Filippi, M., et al., 2012. Association between pathological and MRI findings in multiple sclerosis. Lancet Neurol. 11**,** 349-60.

Filippi, M., et al., 2013. Gray matter damage predicts the accumulation of disability 13 years later in MS. Neurology. 81, 1759-67.
Filippi, M., et al., 2018. Multiple sclerosis. Nat Rev Dis Primers. 4, 43.
Filippi, M., et al., 2019. Assessment of lesions on magnetic resonance imaging in multiple sclerosis: practical guidelines. Brain. 142, 1858-1875.
Fink, F., et al., 2010. Comparison of diffusion tensor-based tractography and quantified brain atrophy for analyzing demyelination and axonal loss in MS. J Neuroimaging. 20, 334-44.
Finke, C., et al., 2016. Normal volumes and microstructural integrity of deep gray matter structures in AQP4+ NMOSD. Neurol Neuroimmunol Neuroinflamm. 3, e229.
Finke, C., et al., 2018. Association of Visual Impairment in Neuromyelitis Optica Spectrum Disorder With Visual Network Reorganization. JAMA Neurol. 75, 296-303.
Fischl, B., Sereno, M.I., Dale, A.M., 1999. Cortical surface-based analysis. II: Inflation, flattening, and a surface-based coordinate system. Neuroimage. 9, 195-207.
Fischl, B., Dale, A.M., 2000. Measuring the thickness of the human cerebral cortex from magnetic resonance images. Proc Natl Acad Sci U S A. 97, 11050-5.
Fischl, B., et al., 2002. Whole brain segmentation: automated labeling of neuroanatomical structures in the human brain. Neuron. 33, 341-55.
Fischl, B., et al., 2004. Automatically parcellating the human cerebral cortex. Cereb Cortex. 14, 11-22.
Fisk, J.D., et al., 1994a. The impact of fatigue on patients with multiple sclerosis. Can J Neurol Sci. 21, 9-14.
Fisk, J.D., et al., 1994b. Measuring the functional impact of fatigue: initial validation of the fatigue impact scale. Clin Infect Dis. 18 Suppl 1, S79-83.
Frohman, E.M., Racke, M.K., Raine, C.S., 2006. Multiple sclerosis--the plaque and its pathogenesis. N Engl J Med. 354, 942-55.
Fu, C.H., et al., 2002. A functional magnetic resonance imaging study of overt letter verbal fluency using a clustered acquisition sequence: greater anterior cingulate activation with increased task demand. Neuroimage. 17, 871-9.
Gaetano, L., et al., 2018. Fingolimod effect on gray matter, thalamus, and white matter in patients with multiple sclerosis. Neurology. 90, e1324-e1332.
Gallo, A., et al., 2012. Visual resting-state network in relapsing-remitting MS with and without previous optic neuritis. Neurology. 79, 1458-65.
Gao, M., et al., 2019. Low levels of vitamin D and the relationship between vitamin D and Th2 axis-related cytokines in neuromyelitis optica spectrum disorders. J Clin Neurosci. 61, 22-27.
Gareau, P.J., et al., 1999. Reduced visual evoked responses in multiple sclerosis patients with optic neuritis: comparison of functional magnetic resonance imaging and visual evoked potentials. Mult Scler. 5, 161-4.
Gasperini, C., et al., 2019. Unraveling treatment response in multiple sclerosis: A clinical and MRI challenge. Neurology. 92, 180-192.
Gelineau-Morel, R., et al., 2012. The effect of hypointense white matter lesions on automated gray matter segmentation in multiple sclerosis. Hum Brain Mapp. 33, 2802-14.
Geurts, J.J., Barkhof, F., 2008. Grey matter pathology in multiple sclerosis. Lancet Neurol. 7, 841-51.
Giovannoni, G., 2006. Multiple sclerosis related fatigue. J Neurol Neurosurg Psychiatry. 77, 2-3.

Granberg, T., et al., 2017. In vivo characterization of cortical and white matter neuroaxonal pathology in early multiple sclerosis. Brain. 140**,** 2912-2926.
Grant-Peters, M., et al., 2021. No strong HLA association with MOG antibody disease in the UK population. Ann Clin Transl Neurol. 8**,** 1502-1507.
Gratton, S., et al., 2014. Bilateral hearing loss as a manifestation of neuromyelitis optica. Neurology. 82**,** 2145-6.
Graves, J., et al., 2014. Protective environmental factors for neuromyelitis optica. Neurology. 83**,** 1923-9.
Griffanti, L., et al., 2014. ICA-based artefact removal and accelerated fMRI acquisition for improved resting state network imaging. Neuroimage. 95**,** 232-47.
Griffanti, L., et al., 2016. Challenges in the reproducibility of clinical studies with resting state fMRI: An example in early Parkinson's disease. Neuroimage. 124**,** 704-713.
Griffanti, L., et al., 2017. Hand classification of fMRI ICA noise components. Neuroimage. 154**,** 188-205.
Gronwall, D.M., 1977. Paced auditory serial-addition task: a measure of recovery from concussion. Percept Mot Skills. 44**,** 367-73.
Haase, C.G., et al., 2001. The fine specificity of the myelin oligodendrocyte glycoprotein autoantibody response in patients with multiple sclerosis and normal healthy controls. J Neuroimmunol. 114**,** 220-5.
Hackett, T.A., 2011. Information flow in the auditory cortical network. Hear Res. 271**,** 133-46.
Hacohen, Y., et al., 2017. Diagnostic algorithm for relapsing acquired demyelinating syndromes in children. Neurology. 89**,** 269-278.
Hacohen, Y., et al., 2018a. 'Leukodystrophy-like' phenotype in children with myelin oligodendrocyte glycoprotein antibody-associated disease. Dev Med Child Neurol. 60**,** 417-423.
Hacohen, Y., et al., 2018b. Disease Course and Treatment Responses in Children With Relapsing Myelin Oligodendrocyte Glycoprotein Antibody-Associated Disease. JAMA Neurol. 75**,** 478-487.
Han, Y., et al., 2020. Functional Connectivity Alterations in Neuromyelitis Optica Spectrum Disorder : Correlation with Disease Duration and Cognitive Impairment. Clin Neuroradiol. 30**,** 559-568.
Hardy, T.A., et al., 2016. Atypical inflammatory demyelinating syndromes of the CNS. Lancet Neurol. 15**,** 967-981.
Harsan, L.A., et al., 2006. Brain dysmyelination and recovery assessment by noninvasive in vivo diffusion tensor magnetic resonance imaging. J Neurosci Res. 83**,** 392-402.
Harvey, J.P., et al., 2021. Absence of Decussation in Optic Pathway Inflammation in Neuromyelitis Optica and Its Implications for Astrocyte Localization. J Neuroophthalmol. 41**,** e202-e204.
Hauser, S.L., et al., 2017. Ocrelizumab versus Interferon Beta-1a in Relapsing Multiple Sclerosis. N Engl J Med. 376**,** 221-234.
Hegarty, A.K., et al., 2020. Salience network functional connectivity is spatially heterogeneous across sensorimotor cortex in healthy humans. Neuroimage. 221**,** 117177.
Hemington, K.S., et al., 2016. Abnormal cross-network functional connectivity in chronic pain and its association with clinical symptoms. Brain Struct Funct. 221**,** 4203-4219.

Hemmer, B., Kerschensteiner, M., Korn, T., 2015. Role of the innate and adaptive immune responses in the course of multiple sclerosis. Lancet Neurol. 14, 406-19.
Hennes, E.M., et al., 2017. Prognostic relevance of MOG antibodies in children with an acquired demyelinating syndrome. Neurology. 89, 900-908.
Hinson, S.R., et al., 2012. Molecular outcomes of neuromyelitis optica (NMO)-IgG binding to aquaporin-4 in astrocytes. Proc Natl Acad Sci U S A. 109, 1245-50.
Hoftberger, R., et al., 2015. Antibodies to MOG and AQP4 in adults with neuromyelitis optica and suspected limited forms of the disease. Mult Scler. 21, 866-874.
Höftberger, R., et al., 2020. The pathology of central nervous system inflammatory demyelinating disease accompanying myelin oligodendrocyte glycoprotein autoantibody. Acta Neuropathol. 139, 875-892.
Holladay, J.T., 1997. Proper method for calculating average visual acuity. J Refract Surg. 13, 388-91.
Hor, J.Y., et al., 2020. Epidemiology of Neuromyelitis Optica Spectrum Disorder and Its Prevalence and Incidence Worldwide. Front Neurol. 11, 501.
Hyun, J.W., et al., 2017. Deep gray matter atrophy in neuromyelitis optica spectrum disorder and multiple sclerosis. Eur J Neurol. 24, 437-445.
Iglesias, A., et al., 2001. T- and B-cell responses to myelin oligodendrocyte glycoprotein in experimental autoimmune encephalomyelitis and multiple sclerosis. Glia. 36, 220-34.
Ikeda, T., et al., 2018. The pathological features of MOG antibody-positive cerebral cortical encephalitis as a new spectrum associated with MOG antibodies: A case report. J Neurol Sci. 392, 113-115.
Inglese, M., Bester, M., 2010. Diffusion imaging in multiple sclerosis: research and clinical implications. NMR Biomed. 23, 865-72.
J.L.R. Andersson, M.J.a.S.S., 2007. Non-linear registration, aka Spatial normalisation FMRIB technical report TR07JA2. www.fmrib.ox.ac.uk/analysis/techrep.
Jain, K., et al., 2021. "FLAMES: A novel burning entity in MOG IgG associated disease". Mult Scler Relat Disord. 49, 102759.
Janssen, A.L., et al., 2013. Resting-state functional connectivity in multiple sclerosis: an examination of group differences and individual differences. Neuropsychologia. 51, 2918-29.
Jarius, S., et al., 2008. Antibody to aquaporin-4 in the long-term course of neuromyelitis optica. Brain. 131, 3072-80.
Jarius, S., et al., 2011. Cerebrospinal fluid findings in aquaporin-4 antibody positive neuromyelitis optica: results from 211 lumbar punctures. J Neurol Sci. 306, 82-90.
Jarius, S., et al., 2012. Contrasting disease patterns in seropositive and seronegative neuromyelitis optica: A multicentre study of 175 patients. J Neuroinflammation. 9, 14.
Jarius, S., et al., 2013. Steroid-responsive hearing impairment in NMO-IgG/aquaporin-4-antibody-positive neuromyelitis optica. J Neurol. 260, 663-4.
Jarius, S., Wildemann, B., 2013. The history of neuromyelitis optica. J Neuroinflammation. 10, 8.
Jarius, S., et al., 2016a. MOG-IgG in NMO and related disorders: a multicenter study of 50 patients. Part 3: Brainstem involvement - frequency, presentation and outcome. J Neuroinflammation. 13, 281.

Jarius, S., et al., 2016b. Screening for MOG-IgG and 27 other anti-glial and anti-neuronal autoantibodies in 'pattern II multiple sclerosis' and brain biopsy findings in a MOG-IgG-positive case. Mult Scler. 22, 1541-1549.
Jarius, S., et al., 2016c. MOG-IgG in NMO and related disorders: a multicenter study of 50 patients. Part 2: Epidemiology, clinical presentation, radiological and laboratory features, treatment responses, and long-term outcome. J Neuroinflammation. 13, 280.
Jarius, S., et al., 2020a. Neuromyelitis optica. Nat Rev Dis Primers. 6, 85.
Jarius, S., et al., 2020b. Cerebrospinal fluid findings in patients with myelin oligodendrocyte glycoprotein (MOG) antibodies. Part 1: Results from 163 lumbar punctures in 100 adult patients. J Neuroinflammation. 17, 261.
Jbabdi, S., et al., 2012. Model-based analysis of multishell diffusion MR data for tractography: how to get over fitting problems. Magn Reson Med. 68, 1846-55.
Jeantroux, J., et al., 2012. Diffusion tensor imaging of normal-appearing white matter in neuromyelitis optica. J Neuroradiol. 39, 295-300.
Jenkinson, M., Smith, S., 2001. A global optimisation method for robust affine registration of brain images. Med Image Anal. 5, 143-56.
Jenkinson, M., et al., 2002. Improved optimization for the robust and accurate linear registration and motion correction of brain images. Neuroimage. 17, 825-41.
Jenkinson, M., et al., 2012. Fsl. Neuroimage. 62, 782-90.
Jeong, I.H., et al., 2017. Normal-appearing white matter demyelination in neuromyelitis optica spectrum disorder. Eur J Neurol. 24, 652-658.
Juenger, V., et al., 2020. Optic chiasm measurements may be useful markers of anterior optic pathway degeneration in neuromyelitis optica spectrum disorders. Eur Radiol.
Jurynczyk, M., et al., 2016. Status of diagnostic approaches to AQP4-IgG seronegative NMO and NMO/MS overlap syndromes. J Neurol. 263, 140-9.
Jurynczyk, M., et al., 2017a. Distinct brain imaging characteristics of autoantibody-mediated CNS conditions and multiple sclerosis. Brain. 140, 617-627.
Jurynczyk, M., et al., 2017b. Clinical presentation and prognosis in MOG-antibody disease: a UK study. Brain. 140, 3128-3138.
Jurynczyk, M., et al., 2017c. Brain lesion distribution criteria distinguish MS from AQP4-antibody NMOSD and MOG-antibody disease. J Neurol Neurosurg Psychiatry. 88, 132-136.
Jurynczyk, M., et al., 2019. Myelin oligodendrocyte glycoprotein (MOG) antibody-associated disease: practical considerations. Pract Neurol. 19, 187-195.
Juryńczyk, M., et al., 2021. Elucidating distinct clinico-radiologic signatures in the borderland between neuromyelitis optica and multiple sclerosis. J Neurol.
Kang, H.J., et al., 2011. Spatio-temporal transcriptome of the human brain. Nature. 478, 483-9.
Khanna, S., et al., 2012. Magnetic resonance imaging of optic neuritis in patients with neuromyelitis optica versus multiple sclerosis. J Neuroophthalmol. 32, 216-20.
Kim, H.J., et al., 2015a. MRI characteristics of neuromyelitis optica spectrum disorder: an international update. Neurology. 84, 1165-73.
Kim, S.G., et al., 1993. Functional magnetic resonance imaging of motor cortex: hemispheric asymmetry and handedness. Science. 261, 615-7.
Kim, S.H., et al., 2017. Diffusion tensor imaging of normal-appearing white matter in patients with neuromyelitis optica spectrum disorder and multiple sclerosis. Eur J Neurol. 24, 966-973.

Kim, S.M., et al., 2015b. Antibodies to MOG in adults with inflammatory demyelinating disease of the CNS. Neurol Neuroimmunol Neuroinflamm. 2**,** e163.
Kim, W., et al., 2016. Cerebral Cortex Involvement in Neuromyelitis Optica Spectrum Disorder. J Clin Neurol. 12**,** 188-93.
Kira, J.I., 2017. Unexpected exacerbations following initiation of disease-modifying drugs in neuromyelitis optica spectrum disorder: Which factor is responsible, anti-aquaporin 4 antibodies, B cells, Th1 cells, Th2 cells, Th17 cells, or others? Mult Scler. 23**,** 1300-1302.
Kitley, J., et al., 2012a. Prognostic factors and disease course in aquaporin-4 antibody-positive patients with neuromyelitis optica spectrum disorder from the United Kingdom and Japan. Brain. 135**,** 1834-49.
Kitley, J., et al., 2012b. Myelin-oligodendrocyte glycoprotein antibodies in adults with a neuromyelitis optica phenotype. Neurology. 79**,** 1273-7.
Kitley, J., et al., 2014a. Features of neuromyelitis optica spectrum disorders and aquaporin-4 with myelin-oligodendrocyte glycoprotein antibodies-reply. JAMA Neurol. 71**,** 924.
Kitley, J., et al., 2014b. Neuromyelitis optica spectrum disorders with aquaporin-4 and myelin-oligodendrocyte glycoprotein antibodies: a comparative study. JAMA Neurol. 71**,** 276-83.
Klawiter, E.C., et al., 2010. Elevated intrathecal myelin oligodendrocyte glycoprotein antibodies in multiple sclerosis. Arch Neurol. 67**,** 1102-8.
Kleiter, I., et al., 2016. Neuromyelitis optica: Evaluation of 871 attacks and 1,153 treatment courses. Ann Neurol. 79**,** 206-16.
Knyazev, G.G., 2012. Extraversion and anterior vs. posterior DMN activity during self-referential thoughts. Front Hum Neurosci. 6**,** 348.
Komatsu, T., et al., 2019. Perivascular enhancement in anti-MOG antibody demyelinating disease of the CNS. J Neurol Neurosurg Psychiatry. 90**,** 111-112.
Konuskan, B., et al., 2018. Retrospective analysis of children with myelin oligodendrocyte glycoprotein antibody-related disorders. Mult Scler Relat Disord. 26**,** 1-7.
Körtvélyessy, P., et al., 2017. ADEM-like presentation, anti-MOG antibodies, and MS pathology: TWO case reports. Neurol Neuroimmunol Neuroinflamm. 4**,** e335.
Kos, D., et al., 2005. Evaluation of the Modified Fatigue Impact Scale in four different European countries. Mult Scler. 11**,** 76-80.
Kremer, S., et al., 2015. Use of Advanced Magnetic Resonance Imaging Techniques in Neuromyelitis Optica Spectrum Disorder. JAMA Neurol. 72**,** 815-22.
Kupfer, C., Chumbley, L., Downer, J.C., 1967. Quantitative histology of optic nerve, optic tract and lateral geniculate nucleus of man. J Anat. 101**,** 393-401.
Kurtzke, J.F., 1983. Rating neurologic impairment in multiple sclerosis: an expanded disability status scale (EDSS). Neurology. 33**,** 1444-52.
Lakin, L., et al., 2021. Comprehensive Approach to Management of Multiple Sclerosis: Addressing Invisible Symptoms-A Narrative Review. Neurol Ther.
Lalive, P.H., et al., 2006. Antibodies to native myelin oligodendrocyte glycoprotein are serologic markers of early inflammation in multiple sclerosis. Proc Natl Acad Sci U S A. 103**,** 2280-5.
Lampasona, V., et al., 2004. Similar low frequency of anti-MOG IgG and IgM in MS patients and healthy subjects. Neurology. 62**,** 2092-4.
Larson, R.D., 2013. Psychometric properties of the modified fatigue impact scale. Int J MS Care. 15**,** 15-20.

Lassmann, H., 2018. Pathogenic Mechanisms Associated With Different Clinical Courses of Multiple Sclerosis. Front Immunol. 9**,** 3116.
Laurent Kremer, N.A., Maureen Mealy, Kerry Mutch, Michael Lewy, Anu Jacob, Nicolas Collongues, Jerome De Seze, 2015. Tobacco smoking and severity of neuromyelitis optica Neurology. 84 (14 Supplement)
Lee, J., et al., 2021a. So You Want to Image Myelin Using MRI: An Overview and Practical Guide for Myelin Water Imaging. J Magn Reson Imaging. 53**,** 360-373.
Lee, J.J., et al., 2021b. A neuroimaging biomarker for sustained experimental and clinical pain. Nat Med. 27**,** 174-182.
Lennon, V.A., et al., 2004. A serum autoantibody marker of neuromyelitis optica: distinction from multiple sclerosis. Lancet. 364**,** 2106-12.
Lennon, V.A., et al., 2005. IgG marker of optic-spinal multiple sclerosis binds to the aquaporin-4 water channel. J Exp Med. 202**,** 473-7.
Lezak, M.D., 1983. Neuropsychological assessment, Vol., Oxford University Press, New York.
Li, Q.Y., et al., 2020a. Painful tonic spasm in Chinese patients with neuromyelitis optica spectrum disorder: Prevalence, subtype, and features. Mult Scler Relat Disord. 45**,** 102408.
Li, V., et al., 2020b. A clinico-neurophysiological study of urogenital dysfunction in MOG-antibody transverse myelitis. Neurology. 95**,** e2924-e2934.
Liang, P., et al., 2011. Regional homogeneity changes in patients with neuromyelitis optica revealed by resting-state functional MRI. Clin Neurophysiol. 122**,** 121-7.
Lindert, R.B., et al., 1999. Multiple sclerosis: B- and T-cell responses to the extracellular domain of the myelin oligodendrocyte glycoprotein. Brain. 122 (Pt 11)**,** 2089-100.
Linington, C., et al., 1988. Augmentation of demyelination in rat acute allergic encephalomyelitis by circulating mouse monoclonal antibodies directed against a myelin/oligodendrocyte glycoprotein. Am J Pathol. 130**,** 443-54.
Liu, Y., et al., 2012. A tract-based diffusion study of cerebral white matter in neuromyelitis optica reveals widespread pathological alterations. Mult Scler. 18**,** 1013-21.
Liu, Y., et al., 2014. Cortical thinning correlates with cognitive change in multiple sclerosis but not in neuromyelitis optica. Eur Radiol. 24**,** 2334-43.
Liu, Y., et al., 2015a. Multimodal Quantitative MR Imaging of the Thalamus in Multiple Sclerosis and Neuromyelitis Optica. Radiology. 277**,** 784-92.
Liu, Y., et al., 2015b. Structural MRI substrates of cognitive impairment in neuromyelitis optica. Neurology. 85**,** 1491-9.
Liu, Y., et al., 2016. Whole brain functional connectivity in clinically isolated syndrome without conventional brain MRI lesions. Eur Radiol. 26**,** 2982-91.
Liu, Y., et al., 2018. Multimodal characterization of gray matter alterations in neuromyelitis optica. Mult Scler. 24**,** 1308-1316.
Lopes, F.C., et al., 2015. Optic Neuritis and the Visual Pathway: Evaluation of Neuromyelitis Optica Spectrum by Resting-State fMRI and Diffusion Tensor MRI. J Neuroimaging. 25**,** 807-12.
Lucchinetti, C., et al., 2000. Heterogeneity of multiple sclerosis lesions: implications for the pathogenesis of demyelination. Ann Neurol. 47**,** 707-17.
Lucchinetti, C.F., et al., 2002. A role for humoral mechanisms in the pathogenesis of Devic's neuromyelitis optica. Brain. 125**,** 1450-61.

Mandler, R.N., et al., 1993. Devic's neuromyelitis optica: a clinicopathological study of 8 patients. Ann Neurol. 34**,** 162-8.
Manogaran, P., et al., 2016. Quantifying visual pathway axonal and myelin loss in multiple sclerosis and neuromyelitis optica. Neuroimage Clin. 11**,** 743-750.
Mariano, R., et al., 2019. Comparison of Clinical Outcomes of Transverse Myelitis Among Adults With Myelin Oligodendrocyte Glycoprotein Antibody vs Aquaporin-4 Antibody Disease. JAMA Netw Open. 2**,** e1912732.
Mariano, R., et al., 2020. Quantitative spinal cord MRI in MOG-antibody disease, neuromyelitis optica and multiple sclerosis. Brain.
Mariotto, S., et al., 2017. Clinical spectrum and IgG subclass analysis of anti-myelin oligodendrocyte glycoprotein antibody-associated syndromes: a multicenter study. J Neurol. 264**,** 2420-2430.
Marrie, R.A., 2011. Demographic, genetic, and environmental factors that modify disease course. Neurol Clin. 29**,** 323-41.
Matsumoto, Y., et al., 2021. Distinctive lesions of brain MRI between MOG-antibody-associated and AQP4-antibody-associated diseases. Journal of Neurology Neurosurgery and Psychiatry. 92**,** 682-684.
Matthews, L., et al., 2013. Distinction of seropositive NMO spectrum disorder and MS brain lesion distribution. Neurology. 80**,** 1330-7.
Matthews, L., et al., 2015. Imaging Surrogates of Disease Activity in Neuromyelitis Optica Allow Distinction from Multiple Sclerosis. PLoS One. 10**,** e0137715.
McKeon, A., et al., 2008. CNS aquaporin-4 autoimmunity in children. Neurology. 71**,** 93-100.
McNicholas, N., et al., 2018. Cognitive dysfunction in early multiple sclerosis: a review. QJM. 111**,** 359-364.
Mealy, M.A., et al., 2018. Vaccines and the association with relapses in patients with neuromyelitis optica spectrum disorder. Mult Scler Relat Disord. 23**,** 78-82.
Messina, S., Patti, F., 2014. Gray matters in multiple sclerosis: cognitive impairment and structural MRI. Mult Scler Int. 2014**,** 609694.
Messina, S., et al., 2021a. The influence of smoking on the pattern of disability and relapse risk in AQP4-positive Neuromyelitis Optica Spectrum Disorder, MOG-Ab Disease and Multiple Sclerosis. Mult Scler Relat Disord. 49**,** 102773.
Messina, S., et al., 2021b. Contrasting the brain imaging features of MOG-antibody disease, with AQP4-antibody NMOSD and multiple sclerosis. Mult Scler. 13524585211018987.
Miller, D.H., et al., 2002. Measurement of atrophy in multiple sclerosis: pathological basis, methodological aspects and clinical relevance. Brain. 125**,** 1676-95.
Miller, H., Simpson, C.A., Yeates, W.K., 1965. Bladder Dysfunction in Multiple Sclerosis. Br Med J. 1**,** 1265-9.
Miller, K.L., et al., 2016. Multimodal population brain imaging in the UK Biobank prospective epidemiological study. Nat Neurosci. 19**,** 1523-1536.
Minagar, A., et al., 2013. The thalamus and multiple sclerosis: modern views on pathologic, imaging, and clinical aspects. Neurology. 80**,** 210-9.
Munot, P., et al., 2010. Congenital fibre type disproportion associated with mutations in the tropomyosin 3 (TPM3) gene mimicking congenital myasthenia. Neuromuscul Disord. 20**,** 796-800.
Nan, D., et al., 2021. Clinical features and management of coexisting anti-N-methyl-D-aspartate receptor encephalitis and myelin oligodendrocyte glycoprotein antibody-associated encephalomyelitis: a case report and review of the literature. Neurol Sci. 42**,** 847-855.

Neil, J.J., et al., 1998. Normal brain in human newborns: apparent diffusion coefficient and diffusion anisotropy measured by using diffusion tensor MR imaging. Radiology. 209**,** 57-66.
Nickerson, L.D., et al., 2017. Using Dual Regression to Investigate Network Shape and Amplitude in Functional Connectivity Analyses. Front Neurosci. 11**,** 115.
O'Connell, K., et al., 2020. Prevalence and incidence of neuromyelitis optica spectrum disorder, aquaporin-4 antibody-positive NMOSD and MOG antibody-positive disease in Oxfordshire, UK. J Neurol Neurosurg Psychiatry. 91**,** 1126-1128.
O'Connor, K.C., et al., 2005. Antibodies from inflamed central nervous system tissue recognize myelin oligodendrocyte glycoprotein. J Immunol. 175**,** 1974-82.
O'Connor, K.C., et al., 2007. Self-antigen tetramers discriminate between myelin autoantibodies to native or denatured protein. Nat Med. 13**,** 211-7.
Obeidat, A.Z., Block, A.N., Hooshmand, S.I., 2021. "Peppering the pons": CLIPPERS or myelin oligodendrocyte glycoprotein associated disease? Mult Scler Relat Disord. 51**,** 102874.
Oertel, F.C., et al., 2019. Cognitive Impairment in Neuromyelitis Optica Spectrum Disorders: A Review of Clinical and Neuroradiological Features. Front Neurol. 10**,** 608.
Ogawa, R., et al., 2017. MOG antibody-positive, benign, unilateral, cerebral cortical encephalitis with epilepsy. Neurol Neuroimmunol Neuroinflamm. 4**,** e322.
Ontaneda, D., Cohen, J.A., Amato, M.P., 2017. Clinical outcome measures for progressive MS trials. Mult Scler. 23**,** 1627-1635.
Ota, M., et al., 2015. Neuromyelitis optica spectrum disorder and multiple sclerosis: Differentiation by a multimodal approach. Mult Scler Relat Disord. 4**,** 515-20.
Pache, F., et al., 2016a. Brain parenchymal damage in neuromyelitis optica spectrum disorder - A multimodal MRI study. Eur Radiol. 26**,** 4413-4422.
Pache, F., et al., 2016b. MOG-IgG in NMO and related disorders: a multicenter study of 50 patients. Part 4: Afferent visual system damage after optic neuritis in MOG-IgG-seropositive versus AQP4-IgG-seropositive patients. J Neuroinflammation. 13**,** 282.
Palace, J., Leite, M.I., Jacob, A., 2012. A practical guide to the treatment of neuromyelitis optica. Pract Neurol. 12**,** 209-14.
Palace, J., et al., 2019. Outcome prediction models in AQP4-IgG positive neuromyelitis optica spectrum disorders. Brain. 142**,** 1310-1323.
Papadopoulou, A., et al., 2019. Attack-related damage of thalamic nuclei in neuromyelitis optica spectrum disorders. J Neurol Neurosurg Psychiatry. 90**,** 1156-1164.
Papp, V., et al., 2018. Nationwide prevalence and incidence study of neuromyelitis optica spectrum disorder in Denmark. Neurology. 91**,** e2265-e2275.
Papp, V., et al., 2021. Worldwide Incidence and Prevalence of Neuromyelitis Optica: A Systematic Review. Neurology. 96**,** 59-77.
Patenaude, B., et al., 2011. A Bayesian model of shape and appearance for subcortical brain segmentation. Neuroimage. 56**,** 907-22.
Patterson, K., et al., 2019. Anti-MOG encephalitis mimicking small vessel CNS vasculitis. Neurol Neuroimmunol Neuroinflamm. 6**,** e538.
Patti, F., et al., 2015. Prevalence and incidence of cognitive impairment in multiple sclerosis: a population-based survey in Catania, Sicily. J Neurol. 262**,** 923-30.
Peschl, P., et al., 2017. Myelin Oligodendrocyte Glycoprotein: Deciphering a Target in Inflammatory Demyelinating Diseases. Front Immunol. 8**,** 529.

Petracca, M., et al., 2021. Neuroimaging Correlates of Cognitive Dysfunction in Adults with Multiple Sclerosis. Brain Sci. 11.
Pichiecchio, A., et al., 2012. Advanced magnetic resonance imaging of neuromyelitis optica: a multiparametric approach. Mult Scler. 18**,** 817-24.
Pisa, M., et al., 2021. Subclinical anterior optic pathway involvement in early multiple sclerosis and clinically isolated syndromes. Brain. 144**,** 848-862.
Pittock, S.J., et al., 2006a. Brain abnormalities in neuromyelitis optica. Arch Neurol. 63**,** 390-6.
Pittock, S.J., et al., 2006b. Neuromyelitis optica brain lesions localized at sites of high aquaporin 4 expression. Arch Neurol. 63**,** 964-8.
Pittock, S.J., et al., 2019. Eculizumab in Aquaporin-4-Positive Neuromyelitis Optica Spectrum Disorder. N Engl J Med. 381**,** 614-625.
Polman, C.H., et al., 2011. Diagnostic criteria for multiple sclerosis: 2010 revisions to the McDonald criteria. Ann Neurol. 69**,** 292-302.
Popescu, B.F., et al., 2010. Absence of cortical demyelination in neuromyelitis optica. Neurology. 75**,** 2103-9.
Popescu, V., et al., 2013. Brain atrophy and lesion load predict long term disability in multiple sclerosis. J Neurol Neurosurg Psychiatry. 84**,** 1082-91.
Porro, C.A., et al., 1996. Primary motor and sensory cortex activation during motor performance and motor imagery: a functional magnetic resonance imaging study. J Neurosci. 16**,** 7688-98.
Ramanathan, S., et al., 2016. Radiological differentiation of optic neuritis with myelin oligodendrocyte glycoprotein antibodies, aquaporin-4 antibodies, and multiple sclerosis. Mult Scler. 22**,** 470-82.
Ramanathan, S., et al., 2018. Clinical course, therapeutic responses and outcomes in relapsing MOG antibody-associated demyelination. J Neurol Neurosurg Psychiatry. 89**,** 127-137.
Rao, S., 1990. A manual for the Brief Repeatable Battery of Neuropsychological Tests in multiple sclerosis. Vol., ed.^eds. Medical College of Winsconsin.
Rao, S.M., et al., 1991. Cognitive dysfunction in multiple sclerosis. I. Frequency, patterns, and prediction. Neurology. 41**,** 685-91.
Reindl, M., et al., 1999. Antibodies against the myelin oligodendrocyte glycoprotein and the myelin basic protein in multiple sclerosis and other neurological diseases: a comparative study. Brain. 122 (Pt 11)**,** 2047-56.
Reindl, M., Waters, P., 2019. Myelin oligodendrocyte glycoprotein antibodies in neurological disease. Nat Rev Neurol. 15**,** 89-102.
Ringelstein, M., et al., 2014. Visual evoked potentials in neuromyelitis optica and its spectrum disorders. Mult Scler. 20**,** 617-20.
Robinson, S., et al., 2009. A resting state network in the motor control circuit of the basal ganglia. BMC Neurosci. 10**,** 137.
Roca-Fernández, A., et al., 2021. Foveal changes in aquaporin-4 antibody seropositive neuromyelitis optica spectrum disorder are independent of optic neuritis and not overtly progressive. Eur J Neurol.
Rocca, M.A., et al., 2004. Magnetization transfer and diffusion tensor MRI show gray matter damage in neuromyelitis optica. Neurology. 62**,** 476-8.
Rocca, M.A., et al., 2012. Large-scale neuronal network dysfunction in relapsing-remitting multiple sclerosis. Neurology. 79**,** 1449-57.
Rocca, M.A., et al., 2015. Clinical and imaging assessment of cognitive dysfunction in multiple sclerosis. Lancet Neurol. 14**,** 302-17.

Rocca, M.A., et al., 2017a. Brain MRI atrophy quantification in MS: From methods to clinical application. Neurology. 88**,** 403-413.
Rocca, M.A., et al., 2017b. Long-term disability progression in primary progressive multiple sclerosis: a 15-year study. Brain. 140**,** 2814-2819.
Rocca, M.A., et al., 2018. Functional network connectivity abnormalities in multiple sclerosis: Correlations with disability and cognitive impairment. Mult Scler. 24**,** 459-471.
Roemer, S.F., et al., 2007. Pattern-specific loss of aquaporin-4 immunoreactivity distinguishes neuromyelitis optica from multiple sclerosis. Brain. 130**,** 1194-205.
Rollot, F., et al., 2021. Cumulative effects of therapies on disability in relapsing multiple sclerosis. Mult Scler. 1352458520980366.
Rombouts, S.A., et al., 1998. Visual activation patterns in patients with optic neuritis: an fMRI pilot study. Neurology. 50**,** 1896-9.
Rosa, M.G., et al., 2009. Connections of the dorsomedial visual area: pathways for early integration of dorsal and ventral streams in extrastriate cortex. J Neurosci. 29**,** 4548-63.
Rose, D.R., Cohen, J.A., 2020. Long-term ocrelizumab in progressive multiple sclerosis. Lancet Neurol. 19**,** 966-968.
Rossi, A., et al., 2012. Super-resolution imaging of aquaporin-4 orthogonal arrays of particles in cell membranes. J Cell Sci. 125**,** 4405-12.
Saji, E., et al., 2013. Cognitive impairment and cortical degeneration in neuromyelitis optica. Ann Neurol. 73**,** 65-76.
Salama, S., et al., 2019a. Radiological characteristics of myelin oligodendrocyte glycoprotein antibody disease. Mult Scler Relat Disord. 29**,** 15-22.
Salama, S., et al., 2019b. MOG antibody-associated encephalomyelitis/encephalitis. Mult Scler. 25**,** 1427-1433.
Salimi-Khorshidi, G., et al., 2014. Automatic denoising of functional MRI data: combining independent component analysis and hierarchical fusion of classifiers. Neuroimage. 90**,** 449-68.
Sastre-Garriga, J., Pareto, D., Rovira, À., 2017. Brain Atrophy in Multiple Sclerosis: Clinical Relevance and Technical Aspects. Neuroimaging Clin N Am. 27**,** 289-300.
Sato, D.K., et al., 2014. Distinction between MOG antibody-positive and AQP4 antibody-positive NMO spectrum disorders. Neurology. 82**,** 474-81.
Savoldi, F., et al., 2020. Functional brain connectivity abnormalities and cognitive deficits in neuromyelitis optica spectrum disorder. Mult Scler. 26**,** 795-805.
Sbardella, E., et al., 2015. Resting-State fMRI in MS: General Concepts and Brief Overview of Its Application. Biomed Res Int. 2015**,** 212693.
Scharfman, H.E., Binder, D.K., 2013. Aquaporin-4 water channels and synaptic plasticity in the hippocampus. Neurochem Int. 63**,** 702-11.
Schmidt, F.A., et al., 2020. Differences in Advanced Magnetic Resonance Imaging in MOG-IgG and AQP4-IgG Seropositive Neuromyelitis Optica Spectrum Disorders: A Comparative Study. Front Neurol. 11**,** 499910.
Schmierer, K., et al., 2004. Magnetization transfer ratio and myelin in postmortem multiple sclerosis brain. Ann Neurol. 56**,** 407-15.
Schmierer, K., et al., 2007. Diffusion tensor imaging of post mortem multiple sclerosis brain. Neuroimage. 35**,** 467-77.
Schneider, T., et al., 2017. Sensitivity of multi-shell NODDI to multiple sclerosis white matter changes: a pilot study. Funct Neurol. 32**,** 97-101.

Schoonheim, M.M., et al., 2014. Changes in functional network centrality underlie cognitive dysfunction and physical disability in multiple sclerosis. Mult Scler. 20**,** 1058-65.
Schoonheim, M.M., Meijer, K.A., Geurts, J.J., 2015. Network collapse and cognitive impairment in multiple sclerosis. Front Neurol. 6**,** 82.
Schulze-Bonsel, K., et al., 2006. Visual acuities "hand motion" and "counting fingers" can be quantified with the freiburg visual acuity test. Invest Ophthalmol Vis Sci. 47**,** 1236-40.
Segonne, F., et al., 2004. A hybrid approach to the skull stripping problem in MRI. Neuroimage. 22**,** 1060-75.
Seiler, A., et al., 2021. Multiparametric Quantitative MRI in Neurological Diseases. Front Neurol. 12**,** 640239.
Senanayake, B., et al., 2019. Seroprevalence and clinical phenotype of MOG-IgG-associated disorders in Sri Lanka. J Neurol Neurosurg Psychiatry. 90**,** 1381-1383.
Sepulveda, M., et al., 2016. Neuromyelitis optica spectrum disorders: Comparison according to the phenotype and serostatus. Neurol Neuroimmunol Neuroinflamm. 3**,** e225.
Sepúlveda, M., et al., 2016. Clinical spectrum associated with MOG autoimmunity in adults: significance of sharing rodent MOG epitopes. J Neurol. 263**,** 1349-60.
Sepúlveda, M., et al., 2018. Epidemiology of NMOSD in Catalonia: Influence of the new 2015 criteria in incidence and prevalence estimates. Mult Scler. 24**,** 1843-1851.
Shaw, B., et al., 2021. 'Cochlear-type' hearing loss as part of aquaporin-4 neuromyelitis optica spectrum disorder. BMJ Case Rep. 14.
Sims, J.R., et al., 2009. ABC/2 for rapid clinical estimate of infarct, perfusion, and mismatch volumes. Neurology. 72**,** 2104-10.
Skucas, V.A., et al., 2011. Impairment of select forms of spatial memory and neurotrophin-dependent synaptic plasticity by deletion of glial aquaporin-4. J Neurosci. 31**,** 6392-7.
Sled, J.G., Zijdenbos, A.P., Evans, A.C., 1998. A nonparametric method for automatic correction of intensity nonuniformity in MRI data. IEEE Trans Med Imaging. 17**,** 87-97.
Smith, A., 2017. Symbol digit modalities test, Vol., Western Psychological Services, Torrance, Calif.
Smith, S.M., et al., 2002. Accurate, robust, and automated longitudinal and cross-sectional brain change analysis. Neuroimage. 17**,** 479-89.
Smith, S.M., et al., 2004. Advances in functional and structural MR image analysis and implementation as FSL. Neuroimage. 23 Suppl 1**,** S208-19.
Smith, S.M., et al., 2006. Tract-based spatial statistics: voxelwise analysis of multi-subject diffusion data. Neuroimage. 31**,** 1487-505.
Smith, S.M., et al., 2009. Correspondence of the brain's functional architecture during activation and rest. Proc Natl Acad Sci U S A. 106**,** 13040-5.
Snaith, R.P., Zigmond, A.S., 1986. The hospital anxiety and depression scale. Br Med J (Clin Res Ed). 292**,** 344.
Song, S.K., et al., 2002. Dysmyelination revealed through MRI as increased radial (but unchanged axial) diffusion of water. Neuroimage. 17**,** 1429-36.
Sormani, M.P., et al., 2009. A reassessment of the plateauing relationship between T2 lesion load and disability in MS. Neurology. 73**,** 1538-42.

Sotirchos, E.S., et al., 2020. Aquaporin-4 IgG seropositivity is associated with worse visual outcomes after optic neuritis than MOG-IgG seropositivity and multiple sclerosis, independent of macular ganglion cell layer thinning. Mult Scler. 26**,** 1360-1371.
Spadaro, M., et al., 2015a. Histopathology and clinical course of MOG-antibody-associated encephalomyelitis. Ann Clin Transl Neurol. 2**,** 295-301.
Spadaro, M., et al., 2015b. Histopathology and clinical course of MOG-antibody-associated encephalomyelitis. Ann Clin Transl Neurol. 2**,** 295-301.
Stroop, J.R., 1935. Studies of interference in serial verbal reactions. Vol., ed.^eds. George Peabody College for Teachers, Nashville, Tenn., pp. 19 p.
Suckling, J., et al., 2014. Are power calculations useful? A multicentre neuroimaging study. Hum Brain Mapp. 35**,** 3569-77.
Sumowski, J.F., 2015. Cognitive Reserve as a Useful Concept for Early Intervention Research in Multiple Sclerosis. Front Neurol. 6**,** 176.
Sun, S.W., et al., 2006. Noninvasive detection of cuprizone induced axonal damage and demyelination in the mouse corpus callosum. Magn Reson Med. 55**,** 302-8.
Suzuki, Y., et al., 2003. Absolute eigenvalue diffusion tensor analysis for human brain maturation. NMR Biomed. 16**,** 257-60.
Tackley, G., Kuker, W., Palace, J., 2014. Magnetic resonance imaging in neuromyelitis optica. Mult Scler. 20**,** 1153-64.
Tackley, G., et al., 2016. Neuromyelitis optica relapses: Race and rate, immunosuppression and impairment. Mult Scler Relat Disord. 7**,** 21-5.
Tackley, G., et al., 2017. Chronic neuropathic pain severity is determined by lesion level in aquaporin 4-antibody-positive myelitis. J Neurol Neurosurg Psychiatry. 88**,** 165-169.
Tackley, G., et al., 2021. An In-vivo 1H-MRS short-echo time technique at 7T: Quantification of metabolites in chronic multiple sclerosis and neuromyelitis optica brain lesions and normal appearing brain tissue. Neuroimage. 238**,** 118225.
Tahedl, M., et al., 2018. Functional Connectivity in Multiple Sclerosis: Recent Findings and Future Directions. Front Neurol. 9**,** 828.
Tajfirouz, D., et al., 2021. Optic chiasm involvement in AQP-4 antibody-positive NMO and MOG antibody-associated disorder. Mult Scler. 13524585211011450.
Takai, Y., et al., 2020. Myelin oligodendrocyte glycoprotein antibody-associated disease: an immunopathological study. Brain. 143**,** 1431-1446.
Takai, Y., et al., 2021. Staging of astrocytopathy and complement activation in neuromyelitis optica spectrum disorders. Brain.
Téllez, N., et al., 2008. The basal ganglia: a substrate for fatigue in multiple sclerosis. Neuroradiology. 50**,** 17-23.
Thompson, A.J., et al., 2018. Diagnosis of multiple sclerosis: 2017 revisions of the McDonald criteria. Lancet Neurol. 17**,** 162-173.
Toosy, A.T., et al., 2005. Adaptive cortical plasticity in higher visual areas after acute optic neuritis. Ann Neurol. 57**,** 622-33.
Tootell, R.B., et al., 1998. Functional analysis of primary visual cortex (V1) in humans. Proc Natl Acad Sci U S A. 95**,** 811-7.
Traboulsee, A., et al., 2020. Safety and efficacy of satralizumab monotherapy in neuromyelitis optica spectrum disorder: a randomised, double-blind, multicentre, placebo-controlled phase 3 trial. Lancet Neurol. 19**,** 402-412.
Tsagkas, C., et al., 2021. Syndrome of inappropriate antidiuretic hormone secretion and hypothalamic hypocortisolism in neuromyelitis optica. Lancet. 397**,** 2194.

van Pelt, E.D., et al., 2016. Neuromyelitis optica spectrum disorders: comparison of clinical and magnetic resonance imaging characteristics of AQP4-IgG versus MOG-IgG seropositive cases in the Netherlands. Eur J Neurol. 23**,** 580-7.
Varela F, C.F., Rojas J, et al., Smoking and Disease Severity in Patients with Neuromyelitis Optica. Neurology.
von Glehn, F., et al., 2014. Structural brain abnormalities are related to retinal nerve fiber layer thinning and disease duration in neuromyelitis optica spectrum disorders. Mult Scler. 20**,** 1189-97.
Vukusic, S., Confavreux, C., 2003. Prognostic factors for progression of disability in the secondary progressive phase of multiple sclerosis. J Neurol Sci. 206**,** 135-7.
Walton, C., et al., 2020. Rising prevalence of multiple sclerosis worldwide: Insights from the Atlas of MS, third edition. Mult Scler. 26**,** 1816-1821.
Wang, J., et al., 2017. Comparison of spontaneous brain activity revealed by regional homogeneity in AQP4-IgG neuromyelitis optica-optic neuritis versus MOG-IgG optic neuritis patients: a resting-state functional MRI study. Neuropsychiatr Dis Treat. 13**,** 2669-2679.
Wang, Y., et al., 2020. Altered resting-state functional connectivity density in patients with neuromyelitis optica-spectrum disorders. Mult Scler Relat Disord. 43**,** 102187.
Waters, P., et al., 2015. MOG cell-based assay detects non-MS patients with inflammatory neurologic disease. Neurol Neuroimmunol Neuroinflamm. 2**,** e89.
Waters, P.J., et al., 2012. Serologic diagnosis of NMO: a multicenter comparison of aquaporin-4-IgG assays. Neurology. 78**,** 665-71; discussion 669.
Weinshenker, B.G., et al., 1989. The natural history of multiple sclerosis: a geographically based study. I. Clinical course and disability. Brain. 112 (Pt 1)**,** 133-46.
Weinshenker, B.G., et al., 2006. NMO-IgG: a specific biomarker for neuromyelitis optica. Dis Markers. 22**,** 197-206.
Whittam, D.H., et al., 2019. Rituximab in neurological disease: principles, evidence and practice. Pract Neurol. 19**,** 5-20.
Whittam, D.H., et al., 2020a. Treatment of MOG-IgG-associated disorder with rituximab: An international study of 121 patients. Mult Scler Relat Disord. 44**,** 102251.
Whittam, D.H., et al., 2020b. Treatment of MOG antibody associated disorders: results of an international survey. J Neurol. 267**,** 3565-3577.
Wingerchuk, D.M., et al., 1999. The clinical course of neuromyelitis optica (Devic's syndrome). Neurology. 53**,** 1107-14.
Wingerchuk, D.M., et al., 2006. Revised diagnostic criteria for neuromyelitis optica. Neurology. 66**,** 1485-9.
Wingerchuk, D.M., et al., 2007a. The spectrum of neuromyelitis optica. Lancet Neurol. 6**,** 805-15.
Wingerchuk, D.M., et al., 2007b. A secondary progressive clinical course is uncommon in neuromyelitis optica. Neurology. 68**,** 603-5.
Wingerchuk, D.M., Weinshenker, B.G., 2014. Neuromyelitis optica (Devic's syndrome). Handb Clin Neurol. 122**,** 581-99.
Wingerchuk, D.M., et al., 2015. International consensus diagnostic criteria for neuromyelitis optica spectrum disorders. Neurology. 85**,** 177-89.
Winkler, A.M., et al., 2014. Permutation inference for the general linear model. Neuroimage. 92**,** 381-97.

Wojcik, C., et al., 2021. Staging and stratifying cognitive dysfunction in multiple sclerosis. Mult Scler. 13524585211011390.
Wong, A.M., Sharpe, J.A., 1999. Representation of the visual field in the human occipital cortex: a magnetic resonance imaging and perimetric correlation. Arch Ophthalmol. 117**,** 208-17.
Woolrich, M.W., et al., 2009. Bayesian analysis of neuroimaging data in FSL. Neuroimage. 45**,** S173-86.
Wu, L., et al., 2016. Altered intra- and interregional synchronization in relapsing-remitting multiple sclerosis: a resting-state fMRI study. Neuropsychiatr Dis Treat. 12**,** 853-62.
Wu, Q., Inman, R.D., Davis, K.D., 2013. Neuropathic pain in ankylosing spondylitis: a psychophysics and brain imaging study. Arthritis Rheum. 65**,** 1494-503.
Yamamura, T., et al., 2019. Trial of Satralizumab in Neuromyelitis Optica Spectrum Disorder. N Engl J Med. 381**,** 2114-2124.
Yang, L., et al., 2020. Quantitative brain lesion distribution may distinguish MOG-ab and AQP4-ab neuromyelitis optica spectrum disorders. Eur Radiol. 30**,** 1470-1479.
Yazbeck, E., et al., 2021. Progressive Leukodystrophy-Like Demyelinating Syndromes with MOG-Antibodies in Children: A Rare Under-Recognized Phenotype. Neuropediatrics.
Yeo, T., et al., 2020. Factors associated with fatigue in CNS inflammatory diseases with AQP4 and MOG antibodies. Ann Clin Transl Neurol. 7**,** 375-383.
Yonezu, T., et al., 2014. "Bright spotty lesions" on spinal magnetic resonance imaging differentiate neuromyelitis optica from multiple sclerosis. Mult Scler. 20**,** 331-7.
You, Y., et al., 2020. Chronic demyelination exacerbates neuroaxonal loss in patients with MS with unilateral optic neuritis. Neurol Neuroimmunol Neuroinflamm. 7.
Young, N.P., et al., 2010. Perivenous demyelination: association with clinically defined acute disseminated encephalomyelitis and comparison with pathologically confirmed multiple sclerosis. Brain. 133**,** 333-48.
Yu, X., et al., 2020. The Role of Antibodies in the Pathogenesis of Multiple Sclerosis. Front Neurol. 11**,** 533388.
Zamboni, G., et al., 2019. Age-dependent association of white matter abnormality with cognition after TIA or minor stroke. Neurology. 93**,** e272-e282.
Zhang, H., et al., 2012. NODDI: practical in vivo neurite orientation dispersion and density imaging of the human brain. Neuroimage. 61**,** 1000-16.
Zhang, H., Verkman, A.S., 2013. Eosinophil pathogenicity mechanisms and therapeutics in neuromyelitis optica. J Clin Invest. 123**,** 2306-16.
Zhang, J., et al., 2020. Gray matter atrophy cannot be fully explained by white matter damage in patients with MS. Mult Scler. 1352458519900972.
Zhang, S., Li, C.S., 2012. Functional networks for cognitive control in a stop signal task: independent component analysis. Hum Brain Mapp. 33**,** 89-104.
Zhang, Y., Brady, M., Smith, S., 2001. Segmentation of brain MR images through a hidden Markov random field model and the expectation-maximization algorithm. IEEE Trans Med Imaging. 20**,** 45-57.
Zhao, D.D., et al., 2012. Diffusion tensor imaging characterization of occult brain damage in relapsing neuromyelitis optica using 3.0T magnetic resonance imaging techniques. Neuroimage. 59**,** 3173-7.
Zhou, D., et al., 2006. Identification of a pathogenic antibody response to native myelin oligodendrocyte glycoprotein in multiple sclerosis. Proc Natl Acad Sci U S A. 103**,** 19057-62.

Zhou, F., et al., 2015. Disconnection of the hippocampus and amygdala associated with lesion load in relapsing-remitting multiple sclerosis: a structural and functional connectivity study. Neuropsychiatr Dis Treat. 11**,** 1749-65.
Zhuo, Z., et al., 2020. Brain structural and functional alterations in MOG antibody disease. Mult Scler. 1352458520964415.

11 Appendix

Supplementary Tables

Table S4.1 Volumetric analysis (not normalised values). Brain volume, white and grey matter fraction are divided by 1,000,000

	NMOSD-AQP4	MOGAD	MS	HC
		Global volume measures		
Mean Brain Volume (dm^3) ± SD	1.07 ± 0.12	1.13 ± 0.13	1.12 ± 0.10	1.17 ± 0.11
Mean White matter Fraction (dm^3) ± SD	0.55 ± 0.07	0.58 ± 0.08	0.58 ± 0.06	0.59 ± 0.06
Mean Grey matter Fraction (dm^3) ± SD	0.51 ± 0.06	0.55 ± 0.06	0.54 ± 0.04	0.58 ± 0.05
Mean 3rd Ventricle (mm^3) ± SD	1443.73 ± 817.42	1206.76 ± 686.57	1426.84 ± 729.75	953.09 ± 197.04
Mean 4th Ventricle (mm^3) ± SD	1932.03 ± 743.80	1809.66 ± 421.51	1969.54 ± 532.16	1906.47 ± 425.36
		Grey matter measures		
Mean Thalamus (mm^3) ± SD	7236.92 ± 760.27	7637.48 ± 1120.65	7230.58 ± 910.4	8310.06 ± 751.59
Mean Caudate (mm^3) ± SD	3363.16 ± 489.16	3452.55 ± 641.71	3104.92 ± 551.6	3982.53 ± 558.95
Mean Putamen (mm^3) ± SD	4470.24 ± 732.75	4591.03 ± 856.76	4543.72 ± 707.31	5163.39 ± 487.03
Mean Pallidus (mm^3) ± SD	1726.53 ± 215.16	1775.30 ± 300.83	1715.86 ±262.77	1907.36 ± 143.62
Mean Hippocampus (mm^3) ± SD	3707.08 ± 541.21	3790.73 ± 586.16	3569.36 ±450.09	4188.56 ± 463.36
Mean Amygdala (mm^3) ± SD	1136.68 ± 203.54	1109.75 ± 233.42	1078.78 ± 189.03	1289.92 ± 198.52
Mean Accumbens (mm^3) ± SD	365.21 ± 111.11	428.43 ± 111.15	384.00 ± 115.69	508.86 ± 86.58
Mean Brainstem (mm^3) ± SD	20662.95 ± 1852.21	21066.15 ± 3413.10	20880.11 ± 2448.66	23009.39 ± 2378.79
Mean Cortex Volumes(mm^3) ± SD	450752.76 ± 73253.72	504018.15 ± 67204.21	504877.19 ± 55520.67	524638.64 ± 54334.01
Mean Cortex thickness (mm^3) ± SD	2.60 ± 0.11	2.65 ± 0.06	2.62 ± 0.09	2.68 ± 0.09
		White matter measures		
Mean Optic Chiasm (mm^3) ± SD	220.06 ± 75.41	203.42 ± 51.06	225.04 ± 38.21	237.38 ± 41.84
Mean Corpus Callosum (mm^3) ± SD	2446.57 ± 408.43	2351.14 ± 371.73	2198.41 ± 413.70	2462.14 ± 310.18
Mean Lesions Volume (mm^3) ± SD	9590.21 ± 13259.46	13100.57 ± 29496.43	27024.88 ± 29125.2	NA

Legend: SD=standard deviation, NA=not applicable.

Table S5.1 Diffusion measures across the four groups.

	NMOSD-AQP4	MOGAD	MS	HC
White Matter diffusion measures				
WML FA	0.41 ± 0.04	0.41 ± 0.09	0.42 ± 0.03	NA
NAWM FA	0.55 ± 0.02	0.57 ± 0.02	0.54 ± 0.05	0.57 ± 0.02
WML MD (x 10^{-3} mm^2 s^{-1})	0.68 ± 0.07	0.70 ± 0.11	0.74 ± 0.07	NA
NAWM MD (x 10^{-3} mm^2 s^{-1})	0.58 ± 0.03	0.57 ± 0.02	0.58 ± 0.04	0.56 ± 0.02
WML RD (x 10^{-3} mm^2 s^{-1})	0.52 ± 0.05	0.51 ± 0.11	0.53 ± 0.05	NA
NAWM RD (x 10^{-3} mm^2 s^{-1})	0.38 ± 0.03	0.36 ± 0.03	0.38 ± 0.05	0.35 ± 0.02
WML AD (x 10^{-3} mm^2 s^{-1})	0.99 ± 0.11	0.98 ± 0.11	1.04 ± 0.07	NA
NAWM AD (x 10^{-3} mm^2 s^{-1})	0.99 ± 0.04	0.99 ± 0.02	0.98 ± 0.02	0.99 ± 0.02
Grey matter diffusion measures				
Cortex MD (x 10^{-3} mm^2 s^{-1})	0.74 ± 0.03	0.73 ± 0.03	0.75 ± 0.04	0.73 ± 0.02
Basal Ganglia MD (x 10^{-3} mm^2 s^{-1})	0.65 ± 0.02	0.65 ± 0.02	0.66 ± 0.05	0.65 ± 0.01

Legend: WML=white matter lesions; NAWM=normal appearing white matter; FA=fractional anisotropy, MD=mean diffusivity, RD=radial diffusivity, AD=axial diffusivity.